Fluoride decontamination of groundwater using exfoliated biochar based sorptive system: A cradle to grave approach through vermitechnology

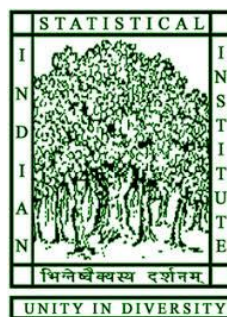*A thesis submitted to*

Jadavpur University

In partial fulfilment of the requirements for the degree of

Doctor of Philosophy (Science)

By

Rupsha Nandi (M.Sc.)

Index No: – 71/22/Life Sc./27

Department of Life science & Bio-technology
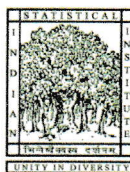
Jadavpur University

And

Agricultural and Ecological Research Unit

Indian Statistical Institute, Giridih

September 2024

INDIAN STATISTICAL INSTITUTE

Pradip Bhattacharyya, PhD
Associate Professor
Biological Science Division
Agricultural & Ecological Research Unit

Rose Villa, New Barganda
Giridih, Jharkhand - 815 301, India
06532-226688 (O), (91) 09859986548 (mobile)
pradip.bhattacharyya@gmail.com

Dated:

Certificate from the supervisor

This is to certify that the thesis entitled **"Fluoride decontamination of groundwater using exfoliated biochar based sorptive system: A cradle to grave approach through vermitechnology"** submitted by **Smt. Rupsha Nandi** who got her name registered on **28.02.2022** for the award of **Ph.D. (Science)** Degree of **Jadavpur University, Department of Life Science and Biotechnology**, is absolutely based upon her work under the supervision of **Dr. Pradip Bhattacharyya** and that neither this thesis nor any part of it has been submitted for either any degree/ diploma or any other academic award anywhere before.

Pradip Bhattacharyya

Pradip Bhattacharyya, Ph.D
Associate Professor
Agricultural and Ecological Research Unit
Indian Statistical Institute
New Barganda, Giridih-815301
Jharkhand, India

Dedications....

To my **Mummum**, who once looked up in awe at a woman pursuing a doctoral degree and dreamt silently of walking in her shoes—this is for you.

To my **Babai**, who envisioned me as a doctor of medicine but has embraced my journey to becoming a doctor of philosophy with pride and love.

To my little **Mistu**, whose unwavering love and emotional support have been my anchor through every challenge.

To my beloved **Sandip**, who saw potential in me when I couldn't see it in myself, and whose steadfast belief kept me going through moments of doubt.

To **Raam**, whose blessings have illuminated my path and given me strength.

AND OFCOURSE !!

To **myself**, for finally conquering procrastination and turning dreams into reality.

DECLARATION OF ORIGINALITY

I, Rupsha Nandi, **Index No.: 71/22/Life Sc./27**, hereby declare that this Ph.D. thesis entitled "**Fluoride decontamination of groundwater using exfoliated biochar based sorptive system: A cradle to grave approach through vermitechnology**" represents my original work carried out as a doctoral scholar at Agricultural and Ecological Research Unit, **Indian Statistical Institute, Giridih, Jharkhand**. The work contained in the thesis is original and has been done by myself under the supervision of my supervisor, **Dr. Pradip Bhattacharyya**. To the best of my knowledge, it does not contain any material previously published by others or written by any other person. The work has not been submitted to Jadavpur University or any other Institute for any other degree or diploma. Any input from sources other than myself or others with whom I have collaborated on this study has been acknowledged. I have given due credit to them by citing them in the text of the thesis and giving their details in the references. When I have used writing from another source, I have always put it in quotation marks and give credit where credit is due by citing the source and providing all necessary information in the references.

Date: (Rupsha Nandi)

Acknowledgements

I would like to express my profound gratitude to my supervisor, Dr. Pradip Bhattacharyya, Associate Professor, Agricultural and Ecological Research unit, Indian statistical Institute, Giridih, for his invaluable guidance, unwavering support, and encouragement throughout my PhD journey. His mentorship has been instrumental in keeping me on track, especially during times when I felt lost. I am deeply appreciative of how he pushed me to overcome my procrastination and adhere to deadlines. His firm yet constructive feedback ensured I met my targets on time, a practice for which I am sincerely thankful. I will always be inspired by his patience in addressing my countless questions before I embarked on any experiment. I am truly grateful for his commitment and the positive impact he has had on my academic growth.

I am thankful to Dr. Abhishek Mukherjee, Associate professor, ISI-Giridih and Dr. Haricharan Behera, Associate professor, ISI-Giridih for the way they have always very gracefully extended every possible facility to benefit my work. Dr. Satya Sundar Bhattacharyya, Tezpur University has helped me extensively by extending his laboratory facilities when required. Dr. Jajati Mandal, School of Sciences, University of Salford, has been the person I have relied on most difficult times in academia. I thank them whole heartedly.

I would like to thank Indian Statistical Institute for providing the financial and infrastructural support required for my work. The illustrious Department of Life science & Biotechnology, Jadavpur University and all its faculty members who have allowed me to register as a Ph.D. candidate deserve my gratitude. I would like to acknowledge Punjab University for providing FESEM-EDX and FTIR facilities

Mondal Mallick and Mrs. Aditi Banerjee, ma'am, in particular, for inspiring my passion for my subject encouraging me to pursue a career in research.

Last but not the least, all my family members deserve my acknowledgements for believing in my dreams and always wishing the best for me. My little munchkins Chonto and Kutti have always been my Bundle of Joy. Mye, bhai mama thank you for being with me on my first day in Giridih. Diya, Dadi, Riya, Ron, Jyatha, Lal, Dadai, Chhotopishi, Pishan, Sunny, Kakai, Kakimoni, Jhilik, Chhotoma, Rishi, Boroma, Mejomami, Didibhai, Boumoni take my love. My new found family, take my love for encouraging me no matter what. All may not be mentioned here, but none is forgotten, I hope I keep receiving such immense love. Mejo mama, boropishi, jhikjyatha, mesho, mashimoni, Guddu dada, I hope you are proud and blessing me from the heavens.

I am forever indebted to my parents (Mrs Suvra Nandy and Mr Ratan Nandy) for getting me this far along in life, for their sacrifices, compromises, presence, trust, support, love and blessings, which have pushed me so far and got me here today. Mistu, my dearest bonui, you have been my bundle of joy, my firefly in the dark. Take my love and keep loving me. Sandip, I mean it when I say, this achievement is equally yours. It would have never been possible without you and your sincere efforts. Be by my side like always. I do not have enough words to express my gratitude for you all. Finally, thank you Raam, you have always guided me through the toughest paths, keep showering me with your blessings.

A Note: EVERYTHING SEEMS IMPOSSIBLE, UNTIL ITS DONE !

Date:

Place:

Rupsha Nandi

ABSTRACT

Index No. 71/22/Life Sc./ 27

Title: Fluoride decontamination of groundwater using exfoliated biochar based sorptive system: A cradle to grave approach through vermitechnology.

Submitted by: Rupsha Nandi

Fluoride (F^-) contamination of underground water table poses substantial threats to human health worldwide including India. This study was designed to investigate the spread and intensity fluoride contamination in lesser explored parts of Jharkhand, India. The Baliapur block of Dhanbad district and Mica mining regions in Giridih district were selected for the study. The fluoride source, spread, intensity and dynamics in the aquifer were evaluated here. Groundwater samples collected from both regions were categorized into F^- safe and F^- unsafe groups based on WHO's permissible F^- limit (1.5 ppm). Significant differences in fluoride concentrations between groups were noted. On analysing physicochemical parameters alkaline pH, high Na^+ and HCO_3^- levels, and extended time of rock-water interaction were found to enhance F^- accumulation. Observations of aquifer chemistry showed silicate weathering and carbonate dissolution to be the primary geogenic sources of fluoride. Logistic regression (AUC: 95.6%) and self-organising maps generated predictive efficiency for F^- in unsampled locations. Health risk assessments indicated non-carcinogenic risks, especially for children and Sobol sensitivity assessment showed concentration of F^- ion and body weight had the highest impact in it. High values of water quality and irrigational indices in F^- rich samples, denied their suitability of use. The application of modelling, machine learning, geospatial analysis and classical chemistry together aided prudent monitoring of water quality in areas impacted by fluoride.

Next, the study addressed F^- removal using an exfoliated biochar (EB) prepared from acid exfoliated water hyacinth (*Pontederia crassipes*). Batch adsorption experiments, and response surface methodology were performed to identify the optimized parameters affecting the process of adsorption. It was found that for pH 6, 30°C, and 20ppm of initial fluoride concentration a 86.08% removal efficiency was noted for a 6.5 gm/ltr of biochar. Monolayer adsorption following Langmuir isotherm ($R^2=0.995$) and chemisorption demonstrated by pseudo-second order reactions ($R^2=0.997$) were reported. Brunauer-Emmet-Taylor analysis suggested successful exfoliation from increased pore volume and surface area. Field emission scanning electron microscopy coupled energy-dispersive X-ray spectroscopy FESEM-EDX confirmed F^- uptake in biochar pores. The surface functional groups responsible for adsorption were identified with FTIR. The generated F^--laden biochars were subjected to remediation using vermicomposting. Temporal studies of compost physico-chemical parameters, microbial activity and F^- fractions were monitored to ensure a safe by-product. This vermi-sanitised biochar was then tested in rice and tomato cultivation, for tracing any F^- bioaccumulation in edible parts of crops and monitoring agronomic parameters. Results supported this vermi-composted product as a viable option for agriculture while simultaneously mitigating the F^- contamination. Overall, a comprehensive study which includes identifying fluoride contamination, producing a sustainable low cost green biosorbent from the otherwise unwanted water hyacinth to combat it and vermi-remediating the spent biosorbent to a valuable agricultural compost, was successfully addressed in this research.

Signature of Student

Signature of Supervisor

Pradip Bhattacharyya, Ph.D
Associate Professor
Agricultural and Ecological Research Unit
Indian Statistical Institute
New Barganda, Giridih-815301
Jharkhand, India

Thesis title: Fluoride decontamination of groundwater using exfoliated biochar based sorptive system: A cradle to grave approach through vermitechnology

<u>**Synopsis**</u>

Groundwater is essential for life, with over 1.5 billion people relying on it for drinking water. However, access to safe drinking water is increasingly challenged by population growth, urbanization, agriculture, and industrial activities, which lead to excessive consumption and pollution. Fluoride (F−), the thirteenth most abundant element in the earth's crust, is a major groundwater contaminant. While low levels benefit dental health, high levels (above 1.5 ppm, per the World Health Organization) cause health issues such as fluorosis, hypocalcemia, kidney disorders, infertility, arthritis, and neurological disorders. Fluoride contamination, often geogenic, arises from natural sources like fluoride-rich minerals and spreads through anion exchange and redox reactions in aquifers, with limited contributions from agricultural and industrial runoff.

Globally, over 200 million people suffer from fluorosis, notably in India, China, and Pakistan. In India, fluoride contamination affects about 276 districts across 20 states, including Rajasthan, Gujarat, Uttar Pradesh, Assam, West Bengal, and Jharkhand. Approximately 40% of India's population lives in fluoride-endemic areas, with concentrations ranging from 0.5 to 48 ppm. Specific regions in Jharkhand also exhibit particularly high fluoride levels.

Examining the spatial distribution of groundwater fluoride concentration in selected blocks of Jharkhand.

Previous studies have noted high fluoride contamination in the Baliapur block of Dhanbad, particularly in Gharbar village, where levels reached up to 14.9 ppm. Studies also reported of fluoride contamination from mica mining. Despite these findings, there is a lack

of comprehensive research at the regional or block level in Dhanbad district, Jharkhand and mica mining regions of the state encompassing the Giridih district. Existing studies mainly address isolated incidents, leaving gaps in understanding the overall extent, sources, and hydrogeochemical characteristics of fluoride contamination. This research aims to fill these gaps by offering a detailed investigation into the spatial distribution and sources of fluoride contamination in Dhanbad and Giridih districts. 283 groundwater samples were collected from 20 Gram Panchayats in the block and analyzed them for fluoride and other major ions. Fluoride concentrations ranged from 0.05 ppm to 15.3 ppm. Of the samples, 23.67% exceeded the 1.5 ppm safety limit set by BIS and WHO, classifying them as 'Unsafe,' while the remaining 76.33% were within safe limits. The average fluoride concentration in the 'Unsafe' group was significantly higher (3.69 ± 0.3 ppm) compared to the 'Safe' group (0.63 ± 0.02 ppm), with a significant statistical difference. A spatial distribution map of fluoride contamination was created, identifying contaminated pockets. The area was classified into five zones based on fluoride levels. About 29.69% of samples had fluoride concentrations below 0.5 ppm, potentially leading to dental caries. In 46.64% of samples, fluoride levels were between 0.5 and 1.5 ppm, beneficial for dental and bone health. However, 16.25% of samples had levels between 1.5 and 4 ppm, which could cause dental fluorosis, and 7.42% had levels above 4 ppm, leading to severe skeletal fluorosis and other health issues. A parallel study carried out in the mica mining regions also generated similar findings of high fluoride in water.

Deciphering the underlying hydrogeochemistry behind the fluoride contamination.

Besides understanding the spread of contamination, assessing the contamination's impact and severity on lives involves the deeper understanding of its sources and health risks. Physicochemical parameters (pH, electrical conductivity, total dissolved solids, total hardness, NO_3^-, HCO_3^-, SO_4^{2-}, Cl^-, Ca^{2+}, Mg^{2+}, K^+, Na^+, and F^-) were measured in every

sample from each group. The findings exhibited that alkaline pH, high concentrations of Na^+ and HCO_3^- ions, prolonged interaction of water with rocks in the aquifer, silicate weathering, carbonate dissolution, low Ca^{2+} levels, and calcite precipitation collectively contributed to elevated fluoride (F^-) levels. The Piper plot indicated that Safe group samples are rich in alkaline earth ions (Ca^{2+} and Mg^{2+}) while Unsafe group samples are dominated by alkali ions (Na^+ and K^+). Examination of three key processes: evaporation, rock-water interaction, and precipitation. Using Gibbs diagrams, the primary mechanisms influencing groundwater chemistry, was observed to be rock-water interaction. A positive correlation between fluoride (F^-) and pH, along with a negative correlation with Ca^{2+} ions, suggested these enhance fluoride dissolution from bedrocks. Health Risk Assessment (HRA), irrigational indices and water quality indices pointed out to the unsuitability of the water in the study area for irrigation and drinking. This analysis informs targeted mitigation and management strategies specific to the study area's characteristics. Machine learning algorithms, including logistic regression (LR), classification and regression trees (CART), and Random Forest (RF), were successfully used to predict and analyze groundwater contamination. Both LR and RF models effectively predicted fluoride presence, providing valuable insights for local water management and public health interventions, especially in resource-limited areas. SOM, Sobol sensitivity analysis were performed too which generated accurate fluoride predictions and pointed out the main contributing factors behind health impacts of fluoride pollution.

Synthesising exfoliated biochar from various feedstocks like sugarcane bagasse, and water hyacinth and assess their fluoride removal efficiency

The high cost of available technologies for fluoride removal from groundwater makes them inaccessible to many. But a sustainable and cost-effective solution for fluoride removal is urgently required for overcoming this growing menace of fluoride contamination. Current methods like reverse osmosis, coagulation-precipitation, and ion exchange are expensive and

have limitations, including secondary waste production and decreased efficiency in the presence of interfering ions. Adsorption, recognized by the WHO as an effective fluoride removal technology, offers a promising alternative. It is both eco-friendly and cost-effective, using various readily available sorbents. Biochar, a porous carbon material created by pyrolyzing organic substances at high temperatures in limited oxygen, could fulfil this need. In this study we investigated, the adsorption potential of exfoliated biochar (EB) derived from different feedstock materials like water hyacinth (*Pontederia crassipes*) using 2(M) HNO_3 acid. Batch adsorption experiments were conducted to assess the impact of factors such as contact time, initial fluoride concentration, adsorbent dose, reaction temperature, and pH of the solution. Response surface methodology was used to determine the optimal conditions for fluoride removal, which were found to be at a pH of 6, a temperature of 30°C, an initial fluoride concentration of 20 mg L−1, and an EB dose of 6.5 g L−1, and resulted in an 86.08% removal rate when replicated in the lab. Kinetic and adsorption isotherm models indicated that the pseudo-second-order model (R^2 = 0.997) and the Langmuir isotherm (R^2 = 0.995) provided the best fits, suggesting monolayer adsorption and chemisorption. Brunauer-Emmet-Teller and Barrett-Joyner-Halenda analyses confirmed the successful exfoliation of native biochar using 2(M) HNO_3, showing increased pore volume (0.037 cc g−1) and surface area (22.291 m² g−1) of EB. Field emission scanning electron microscopy and energy-dispersive X-ray spectroscopy verified the presence of fluoride in the EB, while Fourier transform infrared spectroscopy detected shifts in functional groups on the biochar surface. This research therefore succeeded in highlighting a viable biosorbent for fluoride removal.

Creating vermicompost from the spent fluoride- sorbed exfoliated biochar using *Eisenia fetida*

The subsequent objective of this work was to manage the disposal of saturated biochar. Due to its biodegradability, contaminant-laden biochar cannot simply be discarded as

it may cause new contamination. To address this, we utilized vermitechnology, a sustainable method for environmental pollution mitigation. Earthworms like *Eisenia fetida*, *E. andrei*, *Perionyx excavatus*, *Eudriluseugeniae*, and *Lumbricusrubellus* have shown promise in decontaminating heavy metals (Pb, Zn, Mn, Cu, Cr, Cd) and metalloids (As). These species reduce the bioavailability of contaminants by ingesting them and binding them in their tissues via metal-binding proteins, such as metallothioneins, which sequester toxic metals efficiently.

Feeding habit of surface-dwelling earthworms (*Eisenia fetida*) was utilized to enhance the breakdown of fluoride-laden biochar mixed with cow dung at ratios of 1:1 and 1:2 into high-quality vermicompost. After 90 days, we harvested the end products and measured the physicochemical parameters, microbial and enzymatic activities of the composts at 0, 30, 60, and 90 days to observe changes over time. After 90 days, a three-fold increase in the adult *E. fetida* population with no signs of toxicity was noted. Significant reduction of pH indicated organic matter mineralization, possibly due to the production of HCO_3-, NO_3-, PO_4-, and organic acids. Electrical conductivity (EC) decreased over time due to insolubility, leaching, and microbial immobilization of salts during vermicomposting. The reduction in organic carbon percentage (OC%) suggested enhanced microbe-mediated CO^2 evolution and increased availability of nitrogen (N), phosphorus (P), and potassium (K), supporting effective mineralization. Microbial activity, recorded from basal soil respiration (BSR), substrate-induced respiration (SIR), microbial biomass carbon (MBC), fluorescein diacetate (FDA) hydrolysis, and dehydrogenase (DHG) activity, peaked at 60 days and declined afterward, indicating stabilization in the vermi bed and resource competition at later stages. A decline in the metabolic quotient (qCO_2) and substrate quality index (QR) over time suggested reduced stress on the microflora. Finally, a significant decrease in the water-soluble fraction of fluoride and an increase in the organic-bound form over time assured lower bioavailability of fluoride, making the compost suitable for agricultural use.

Evaluation of the efficiency of produced vermicompost through field demonstration in tomato and rice

A toxicity assessment is crucial to evaluate the impact of experimental compost materials when applied to agricultural fields. In our study, we used these composts at a rate of 10 tons per hectare for submerged rice cultivation. Remarkably, the application did not show any negative effects on soil quality or crop yield parameters. Trace amounts of arsenic were found in the rice after harvest, but the bio concentration factor was much lower than 1 (<0.4), ensuring its safety for consumption. We also tested the impact of these compost materials on Rabi crop cultivation, applying them to tomato plants at the same rate of 10 tons per hectare. Again, no adverse effects were observed on soil quality or crop yield, and no significant bioaccumulation was detected in the roots, shoots, or fruits of the tomato plants. Overall, field studies indicate that the application of arsenic-enriched vermicompost does not adversely affect soil microbiological and biochemical quality indicators. Thus, it can be a viable organic supplement for wetland rice and tomato cultivation. However, long-term field experiments are essential to draw a more definitive conclusion.

Rupsha Nandi
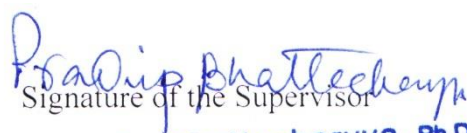
Signature of the Student

Pradip Bhattacharyya

Signature of the Supervisor

Pradip Bhattacharyya, Ph.D
Associate Professor
Agricultural and Ecological Research Unit
Indian Statistical Institute
New Barganda, Giridih-815301
Jharkhand, India

Table of contents

Chapter 3: Methodology and Instrumentation   58-104

Chapter 4: Results and discussions   105-206

List of Tables

List of Figures

Introduction

Chapter 1: Introduction

1. Introduction

1.1. Current scenario of groundwater contamination:

Water is one of the most vital resources of nature that supports life on this planet. While 97% of total earth's water stays confined in the oceans; the rest 3% constituted by surface or ground water plays pivotal role in maintaining livelihood (Khan et al., 2020). Groundwater is the most reliable perennial freshwater source on earth and accounts to be the world's maximum accessed reservoir for fresh water. Groundwater, trapped within the aquifers and pore spaces supplies 100 folds more water than surface water bodies like streams, lakes etc and harbours all groundwater dependant ecosystems. Besides meeting ~69% irrigational, 22% industrial and nearly 8% of the household demands, it acts as the chief source of drinking water in major parts of across the globe (Jha and Tripathi, 2021; Das et al., 2020). According to reports by Adimalla et al., (2019), nearly 1.5 billion lives are dependent on this resource completely for the purpose of drinking. Such being the importance of this life-giving resource, a sincere focus should be laid on regular assessment of its quality. Access to safe drinking water comes among the basic or fundamental right of all beings and is considered among the key indicators of development in country-sides (Kerdoun et al., 2022).

In the present situation; with the booming population, lack of efforts to conserve soil, increasing urbanization, intensified agricultural practices along with its associated irrigational requirements, mining activities without proper approvals and surge in demands within the industrial sectors, consumption of water is growing enormously. This dramatic increase in withdrawals of groundwater to meet these needs lead to significant depletion of the

underground water table (Nandi et al., 2024a). The situation is such intense that many of the aquifers in chief population centres might be on the verge of extinction (Lall et al.,2024).

On the other end, with the clock ticking off, there is increasing pollution of this vital resource from different anthropogenic sources as well. The run-offs from cultivable lands laden with residues of applied chemical insecticides, pesticides, fertilizers etc, leachates from ill-managed dumping sites, leakages from lagoons carrying wastewater, leaking sewers and septic tanks, waste-water from household activities, pharmaceuticals, effluents from industries, pathogens from human waste carried by municipal sewers etc. seep in deep enough through the underlying rock strata to reach the water-table below. Hence, an anthropogenic contamination is encountered which pose a significant threat groundwater quality (Nandi et al.,2024b: Khan et al., 2020; Maheswari et al, 2006). Among emerging contaminants (ECs), antibiotics, pharmaceuticals, personal care products (PCP), dyes, pathogens, microbes etc deserve special mention (Xie et al., 2023).

Moreover, severe evaporation and unpredictable monsoons, scarcity of precipitation, prolonged dry stretches in arid and semi-arid regions further deteriorates the situation as also suggested by Subba Rao et al., in 2017. Longer residence time of groundwater in the aquifers, extended periods of rock water interactions, redox reactions in the aquifer, weathering of bed rocks etc, also shape the groundwater quality (Nandi et al., 2024a; Nandi et al., 2024b). These geogenic factors in union with the anthropogenic ones, have thus posed as a major hindrance in ensuring both quality and availability of this pivotal resource (Maurya et al., 2020).

Depletion and degradation of this vital resource might have extensive impacts on prevailing agricultural value chains and could also be the stimulant for mass migration, endemic diseases, or destruction of existing ecosystem functions. Thus, this increasing loss of balance between demand of groundwater and a sustainable exploitation of the same, puts us on high alert and

demands higher societal awareness on the issue. Framing science-based solutions to sustainable management of groundwater resources and identifying the key issues behind this problem is now a fundamental necessity (Mukherjee, 2022).

1.2. Groundwater contamination from fluoride:

Major contaminants of groundwater include arsenic (As), chromium (Cr), nitrate (NO_3^-), iron (Fe), and fluoride (Jha and Tripathi, 2021; Singh et al., 2022; Nandi et al., 2024a). Among all these, one contaminant which is drawing increasing global attention is Fluoride. Fluoride (F^-) is the ionized form of fluorine. Fluorine, represented with symbol F in the periodic table, is the first element of the halogen group of elements with an atomic number of 9 and atomic weight of 18.99 amu or atomic mass units. Under standard conditions, it exists as a toxic diatomic gas with a pale yellowish appearance. It is highly electronegative and therefore has a tendency of gaining electrons and give rise to the discussed F^- ion in solution (Singh et al.,2018).

Fluoride is a noteworthy trace element abundant in the crust of Earth's, making its primary source geogenic in nature. While fluoride is beneficial at low concentrations, its excessive presence poses severe risks. This duality in the nature of fluoride makes it more concerning (Nandi et al., 2024b). This ion plays a pivotal role in maintenance of bone health and checks dental cavities when taken in minute concentrations (0.5–1.0 mg/L). Conversely, fluoride intake in excess, particularly in concentrations higher than 1.5 mg/L or the permissible safety limit of F^- in drinking water as set by the World Health Organisation (WHO), can lead to fluorosis.

Fluorosis is an incapacitating condition affecting the bones and teeth of the consumer (Singh et al., 2018; Mukherjee et al., 2022). This not only affects dental and skeletal structures giving pain, stiffness, and other debilitating symptoms, it might also lead to complete paralysis. Other than fluorosis, high fluoride levels have been reportedly linked to a diverse range of health

issues, upon chronic exposure, including hypocalcemia, arthritis, myopathy, renal impairments, cognitive degeneration, increased blood pressure, infertility in women , sterility in males, and hampers neurological functions from Alzheimer's disease (Nandi et al., 2024a; Mandal et al., 2021; Yousefi et al., 2018). It has also been linked to digestive and respiratory system disorders (Kerdoun et al.,2022).

Such being the seriousness of impacts of this contaminant on public health and environmental well-being, understanding the sources, spread and intensity of groundwater fluoride contamination becomes crucial. These impacts together underscore the need for efficient management and remediation stratagems to overcome fluoride contamination (Nandi et al., 2024a; Nandi et al., 2024b).

Fluoride contamination of the groundwater table has significant health implications. Addressing this complex issue with such significant implications of public health, is a challenge and facing it sets forth a requirement for a comprehensive understanding of both the geonic and anthropogenic sources of this contaminant. Continued research globally, effectual monitoring, proactive management and tailor-made interventions to mitigate the hazards from fluoride contamination, are the needs of this hour to safeguard communities worldwide and ensure access to safe drinking water (Kerdoun et al.,2022).

The different type of geological rock formations, underlying bed rock conditions of an area, prevailing climatic conditions, groundwater residence time and flow velocity, temperature, pH of the water table, vegetation cover etc, all are key factors in determining the geogenic sources of F^-. Besides, the availability and solubility of fluoride-carrying minerals within the aquifer and bed rock composition, also play crucial roles (Gantait et al., 2022). In arid or semi-arid regions, higher rates of evaporation and scanty rainfall reduce the chances of groundwater recharge, leading to increased dissolution of fluoride-carrying minerals such as fluorite (CaF2),

fluorapatite (Ca5(PO4)3F), biotite, and hornblende from a higher residence time in the aquifer (Singh et al., 2018; Jha and Tripathi, 2021; Nandi et al., 2024a). Other geogenic or natural factors aggravating fluoride levels in groundwater include chemical processes in the aquifers like anion exchange, redox reactions etc. Alkaline pH, lack or abundance of other precipitating ions or complexing ionic moieties like low calcium levels, high bicarbonate and sodium concentrations have also reportedly worsened the fluoride dissolutions (Nandi et al., 2024b; Adimalla et al., 2018; Gantait et al.,2022).

In addition to these natural enrichments of fluoride under the influence of various environmental and geological factors, unchecked human activities also contribute significantly to F$^-$ contamination. These include the use of fluoride-containing pesticides, phosphate-based fertilizers, discharge of sewage-sludge, effluents from glass and ceramic producing industries, as well as activities of mining (Nandi et al.,2024a; Hu et al., 2022; Kashyap et al., 2021). Industrial processes like aluminium and zinc smelting also add to fluoride pollution (Kerdoun et al., 2022).

Fluoride contamination is presently a global concern, with over 200 million people worldwide relying on fluoride contaminated water resources and thus getting affected by different degrees of dental and skeletal fluorosis. It poses significant health threats, particularly in most of the developing and underdeveloped countries. This issue is pervasive, with major contaminated belts found along the East African Rift, Malawi, Turkey, Iraq, Afghanistan, Iran, northern parts of Thailand, China, Japan , some parts of both American continent, Bangladesh and India (Singh et al., 2018; Kashyap et al., 2021). In Asia, people living in arid and semi-arid regions of countries like India (~66 million), China (22-45 million), and Pakistan (~25 million) face notable fluoride exposures (Adeyeye et al., 2021).

In India alone, fluoride contamination impacts 276 districts across twenty plus states of the country. Nearly 40% of India's population lives in regions where fluoride levels exceed the WHO safety limit (1.5 mg/L), with concentrations ranging from 0.5 to 48 mg/L (Dhingra et al., 2021; Naik et al., 2021). Fluoride contamination is particularly severe here because of the extensive fluorite deposits spread across the country. Alluvial aquifers of northwestern states like Rajasthan and Gujarat, limestone-quartzite-shale aquifers of southern states like Karnataka, Andhra Pradesh, and Tamil Nadu , all experience heightened fluoride levels. Major affected districts in the east, include Karimganj, Kamrup, Karbi, Golaghat,. Districts of Gaya, Munger, Naugaon, Bhatinda and Unnao, in the northern part of the country also experience elevated and unsafe fluoride levels. Rajasthan is the most severely impacted among all other staes of our country, with all districts, more than 7,670 habitations and above 4.8 million people affected with fluoride contamination hazards (Singh et al., 2018).

1.3. Fluoride removal techniques

Defluorination of drinking water is essential when alternative sources of drinking water are less accessible in fluoride-hit areas. Different methods for the removal of fluoride from solution has been investigated over the years, and these include adsorption processes, ion-exchange technique, coagulation–precipitation methods, and membrane processes, bioremediation using microbes and plants etc. Nanofiltration, Donnan dialysis, Nalgonda technique, electrodialysis and various electrochemical stratagems like electrocoagulation, electro flotation and electrochemical oxidation have also gained prominence in recent times. All these techniques have their own set of advantages and limitations (Meenakshi and Maheshwari., 2006; Sadhu et al., 2021).

Adsorption methods make use of materials such as activated alumina, activated carbon and other conventional adsorbents like iron, zeolites, titanium, manganese, and ferric phosphates

are among the most commonly employed (Meenakshi and Maheshwari., 2006; Sadhu et al., 2021). The Ion-exchange techniques employ different charged resins to capture fluoride ions, often replace the negatively charged fluoride with anionic chloride, but there activity gets compromised in the presence of other competing and interfering ions (Meenakshi and Maheshwari., 2006; Sadhu et al., 2021). In the coagulation–precipitation technique involving lime and alum, effective removal fluoride is achieved but at the cost of producing the toxic aluminium fluoride complexes which cannot be disposed easily and thereby incur high maintenance and disposal charges. Different membrane processes like reverse osmosis (RO), have very high efficiency in fluoride removal and are having an increasing preference over others for the relative simplicity of use and also remarkable specificity (Meenakshi and Maheshwari., 2006; Sadhu et al., 2021). These RO membranes function under the influence of high external pressure to filter out the desired pollutants, but they are extremely expensive and generate a lot of brine waste as the byproduct. The safe disposal also becomes a hindrance making it less environmentally safe. High operational and treatment cost and regenerative failure of many of these processes discussed above, also sharply elevate the total expense of water defluorination when applied at a large scale. Environmentally safer options like phyto-remediation and bioremediation have also been explored. Phytoremediation involves participation of plants in absorption and accumulation of fluoride from contaminated sites. Whereas, different fluoride-resistant and tolerant bacteria convert fluoride to less hazardous forms and thus play a crucial role in fluoride removal by bioremediation. Combination of multiple available defluorination techniques have often evidently enhanced fluoride removal efficiency. But these also face certain limitation like initial operating and set up costs, maintenance and disposal (Kashyap et al., 2021).

1.4. Biochar as potential adsorbent

Among all the defluorination techniques discussed in the previous section, adsorption has gained the highest popularity. Various materials have been tested for their adsorption potentials. Activated alumina, alum-tagged activated alumina, activated carbons, red mud, zeolite, chitin, chitosan, limestone, biomass and carbonized biomass, bone char, biochar etc have all been tried and tested for the purpose (Mohan et al., 2012). The sorption properties of biochar have drawn attention lately due to their eco-friendly and cost-effective nature.

Biochar can be produced from pyrolysis of easily procurable organic waste including agricultural residues such as sugarcane bamboo, activated rice husk, corn cobs, oil cakes, dried leaves etc and thus has emerged as a low-cost, easily degradable, eco-friendly alternative (Sadhu et al.2021). It can also be made from various other animal-based materials like poultry litter, egg shells and even different types of sludge from industries. Biochar can be produced through a simpler, slow pyrolysis method at lower temperatures making biochar production significantly less expensive, even on a large scale (Akhil et al., 2020). In essence, since, there has been a dire need for sorbents, which would be affordable and would not require additional treatment cost and also would have a steady supply of the raw materials, biochar is growing into the adsorbent of choice with time.

These biosorbents being highly porous offer active sites on their surface for adsorption of target element, fluoride in this scenario. These feature a large surface area and also have specific functional groups on their surface (hydroxyl, carboxyl, carbonyl etc.) and aromatic surfaces, making it effective for removing different pollutants, including toxic heavy metals, dyes, antibiotics, cleaning effluents from sewers, decontamination of municipal waste water etc. These carbonaceous moieties or the biochar are extremely competent for the sequestration and removal of different charged pollutants (Ahmad et al., 2014, Goswami et al., 2016, Mohan et

al., 2014a). In recent times biochar has reportedly been used for both laboratory and large-scale decontamination of ground water, drinking water, synthetic industrial wastewater and the efforts have been successful in a sustainable manner.

However, the advantages of application of native biochar from different agricultural byproduct for removal of contaminants may show limited removal after an extent. In fact, biochar's effectiveness may diminish without additional modifications. The application of pristine or native biochar often suffers from the drawback of diminished specificity, lower adsorption etc. This might stem from the clogging of the available pores or adsorption sites on the biochar surface by the contaminant, presence of insufficient number of functional groups, etc (Tan et al., 2015). Sometimes, the low density and small particle size of the pristine biochar hinder it's application due to difficulty faced during separation of the adsorbed contaminant on its surface without having any magnetic composition attached to it (Tan et al., 2016).

To do away with these drawbacks, surface engineering technique like exfoliation are carried out on the pristine biochar. This facilitates to maximize the decontamination capacity by increasing its porosity, specific surface area, pore volume etc for better binding of adsorbent. This process of exfoliating the native biochar can be performed using different physical, chemical and biological methods (Huang et al., 2022). Chemical exfoliation of biochar which alters the surface chemistry and introduces newer functional groups has been widely practised to increase the adsorption capacity (Akhil et al., 2020). Properties like high surface area, high reactivity and mores specificity transform the chemically exfoliated biochar as excellent adsorbent for large-scale water treatment as well.

1.5. Biochar and its effects on soil health

Biochar has been recognized for its effectiveness as a soil conditioner since older days and dates back to history. When added to soil, biochar has positive effects on different soil physical

properties. It has the potential to modify the aeration status or the oxygen content, water retention capacity, and also the microbial community and their activities in the plant rhizospheric zone. It creates a potent habitat for beneficial soil microorganisms and in turn enhances their growth by improving the availability of nitrogen and phosphorus (Akhil et al., 2020). It reflects in the added fertility of the soil. Additionally, the biochar contributes to increase retention of nutrient retention in its pores bound by different functional groups. The addition of biochar can also improve water permeability and root penetration in dry soils (Mohan et al., 2012). It helps in carbon sequestration and acts as carbon sink of the soil. Overall, incorporating biochar into the soil enhances soil health and increases plant productivity, promoting sustainable agriculture.

1.6. Vermi-remediation of fluoride laden biochar

Vermi-remediation is a low-cost, eco-friendly bioengineering method that involves successful conversion of solid bio-degradable waste material into easily bio-available and nutrient-laden organic fertilizers with help of earthworms and microorganisms. This technique deploys a combined action of the enzymatic activity of microbes and the array of digestive enzymes found within the earthworm gut. These together transform the unwanted contaminants or toxic metals present in the feedstock in their bioavailable forms to less accessible, less toxic, benign, recalcitrant forms within the earthworm's gut. In other words, this is a slow biodegradable progression, deploying the synergistic efficiency of epigeic earthworms and microbes, to covert solid bio-degradable waste materials into useful, aesthetically approved, safer organic fertilizers. In today's world, bio-conversion is preferred over other processes to transform any harmful or hazardous waste material to a benign, energy-rich organic amendment. Vermi-technology aids such bioconversion and accelerated biodegradation and thus is recognised as one of the most efficient way outs for converting various types of solid waste into beneficial

fertilizers and improving the fertility status and health of the soil. It has been reported that application vermicompost also supports the micro-remediation of contaminated soil while also aids plant growth. Vermicompost with its humified nature, is particularly effective at sequestration of different heavy metals, preventing them from creating further pollution to the surroundings. For this ability of converting and stabilising different categories of solid wastes, vermicomposting has gained prominence as a pivotal eco-biotechnological process (Suthar et al., 2012).

The production of vermicompost and the process of decomposition involve various dynamic interactions, where the amount of detritus input poses as the most crucial factor which affects the decomposer community (Yadav & Garg, 2019). Typically, surface-dwelling epigeic earthworms are chosen for the composting phenomenon because of their characteristic ability to ability to uphold a diverse community of microbes, hormones and enzymes. The wigglers consume waste material voraciously, which is then ground into finer particles within their gizzards. This digestion process in turn benefits the intestinal microflora of the earthworms. Together this aids the extraction of nutrients into their mineralized and available forms. This partially digested material or the 'vermicast', is enriched with active microorganisms, mineralised nutrients and several beneficial biomolecules enzymes, hormones, making it a valuable product. It has a peat-like texture, is porous in nature, facilitates aeration, and has high water retention capacity. These qualities of the vermicast enhance its effectiveness as a compost upon its emergence from the vermibeds (Sharma & Garg, 2017). Vermicomposting can also be applied to detoxify wastes containing high concentrations of toxic metals, thanks to the metal-sequestering capabilities of these earthworms. The cysteine-rich protein called metallothionein (MT), present in the intestines of the earthworms, facilitates such metal accumulation. The production of MT isoforms in the intestines of the earthworms increases simultaneously on detecting the presence of metals in the substrate and is ubiquitously present (Maity et al., 2009).

The protein is crucial for maintaining metal ion balance and redox chemistry within cells and facilitates the earthworms to survive the metal stress and continue its detoxification drive. In recent years there have been several instances where vermicomposting technology using suitable earthworms (*Eisenia fetida, Lumbricus rubellus, Eudrillus euginae* etc) have successfully detoxified several industrial wastes, municipal wastes and metal laden wastes and alleviated it (Sahariah et al., 2015, Chakraborty et al., 2022). In this context, we assume vermicomposting could therefore be the potent way of disposing fluoride laden biochars and the created compost could then be deployed for crop trials to ensure its safety.

Review of Literature

Chapter 2: Review of Literature

2. Essence of literatures reviewed for the study:

2.1. Importance of groundwater

Water, an indispensable resource for survival of all forms of life on Earth has almost the vast majority of it locked up in the oceans, unfit for use. Only a small fraction, just 3% of the planet's total water available is fresh water and suitable for use. However little may this fraction be, it is this precious resource that is crucial for sustaining lifeforms, supporting different ecosystems, and catering human needs. Among all the existing freshwater reserves on earth, groundwater plays a pivotal role. Groundwater is a vital element in the global water cycle, and comprises about 30% of the planet's net freshwater reserves. It is almost entirely, approximately 97%, accessible for use by humans in daily lives making it the most generous source of readily accessible fresh water, providing more than all surface water reserves such as lakes, rivers, and streams. It is confiscated within the aquifers and pore spaces below the surface of the Earth and it the supports a plethora of needs. The importance of groundwater extends beyond its role in supplying potable water. Groundwater is crucial not only for the drinking needs but also for irrigation and various industrial processes (Du Plessis, 2017). In other words, in regular lives, household, industrial, and irrigational activities highly rely on groundwater. Significantly integral to diverse human uses, it fulfils approximately 69% of agricultural demands, 22% of industrial requirements, and 8% of household needs. Most importantly, it is the largest drinking water source. 1.5 billion human-lives globally rely on groundwater for meeting their drinking requirements. This resource is vital to safeguarding human health, economic development, and ecosystem balance also. But such heavy reliance on this resource can lead to its scarcity if not maintained sustainably.

2.2. Overexploitation of groundwater

One of the major reasons for scarcity of this resource is unplanned use. The dependence on groundwater has seen a sharp increase in the recent years. If we reflect on its central role in supporting both life forms, human society and ecological systems we could well predict the chances of its shortage in the upcoming years. As per reports from World Health Organization (WHO), approximately 783 million people lack access to basic drinking water supplies, and they have warned of expecting that over half of this world's population is set to face an acute shortage of potable drinking water by the end of 2025 (Lacson et al., 2021). Over the past few decades, the ever-increasing population, the flourishing urbanization, booming industrialization and unregulated extraction and pumping of water resources have ended in reduction in per capita water availability in various developing countries. The society has overlooked the importance of sustainably managing these resources and as a result , groundwater faces this severe challenge that is threatening its quality and availability. Despite its critical importance, degradation of water quality has been reported globally and an additional blow to the society is struck when this situation gets aggravated by water pollution.

2.3. Contamination of groundwater

Due to various ecological factors either natural or anthropogenic the groundwater is being polluted constantly. In other words, groundwater is increasingly threatened by both natural and human-induced pollution.

2.3.1 Contamination of groundwater by geogenic contaminants

Natural or geogenic contaminants such as arsenic, fluoride, chromium etc can severely hamper groundwater quality.

Geogenic factors like evaporation, unpredictable monsoons, long periods of rock-water interactions and pH can alter the chemistry of groundwater and plays a significant role in determining its quality (Subba Rao et al., 2017; Nandi et al., 2024a). Geogenic contamination of groundwater resulting from elevated amounts of arsenic (As)-,fluorine (F)-, and iodine (I), selenium (Se) has been a worldwide public health hazard over the past decades as they bring up devastating endemic fluorosis , iodism, cancer etc. across the continents.

The most discussed geonic contaminants of ground water may be summed up as, cadmium (Cd), iron (Fe), manganese (Mn), arsenic (As), chromium (Cr), fluoride (F$^-$),lead (Pb), nickel (Ni) salinity and alkalinity.

2.3.1.1. Salinity and alkalinity in groundwater

Salinity is a global concern particularly severe in the water deficient semi-arid, arid locations (Pradhan et al., 2023). It is checked by the parameter electrical conductivity of EC. Increased concentrations of different ions in water like sodium, chloride, calcium, magnesium etc can cause increase in groundwater salinity. In simpler words, electrical conductivity (EC) takes note of the salt concentrations present dissolved in groundwater and represents salinity hazard caused to crops (Kouser et al., 2022). Often due to the over-extraction of groundwater by pumping, the water table of the region faces a depletion. This often results in downward dislocation of the surface saline water, the upward shifting of deep-seated saline water, evaporite dissolutions etc (Pradhan et al., 2023). In coastal areas, the intrusion of seawater aggravates salinity which reduces the usability of groundwater. Groundwater with high salinity poses a salinity hazard and are unsuitable for use in plants. Based on the electrical conductivity values, Ayers and Westcott in their report in 1985, categorised the groundwater into 3 types, namely, excellent (EC below 700 µS/cm), good (EC lies between 700 -3000 µS/cm), and fair (EC> 3000 µS/cm). Many regions in our country show elevated groundwater salinity which

often exceed the permissible safety limit for electrical conductivity (EC) or 1500 μS set forth by Bureau of Indian Standards (BIS). According to the reports of Krishan et al., (2017), 14 out of 21 sites studied in the Punjab region exceeded the limit. According to the reports of Castano-Sanchez et al., (2020), Australia has the highest salt-affected soils globally, where the groundwater salt concentration has been recorded to be about 19.32 g/L.

Increased salinity, resulting from elevated chloride levels in underground water table makes the water unfit for both drinking needs and industrial uses. Water with abundant chlorine when used in irrigation might cause leaf burning and defoliation in certain plants (Kim et al., 2005). High sodium ions in water on the other hand lead to high blood pressure and cardiovascular problems (Pradhan et al., 2023). SAR or sodium absorption ratio provides the estimate of accumulation of sodium ions in the soil. It can be calculated from Mg^{2+} and Ca^{2+} ions (Rawat et al., 2018). A high SAR value indicates possible formation of a salt layer in soils irrigated with contaminated water and also clogs pores. This causes an increase in the time required for percolation of the concerned soil (Khan et al., 2020). An alkalinity caused hazard is estimated for the sample with high Kelly's ratio or KR, rendering it unsuitable for irrigation (Gantait et al., 2022). The index is calculated from the ratio of Na^+ ions to sum of Mg^{2+} and Ca^{2+} ions ,which generates values greater than unity when there is higher sodium stress, and is considered unsafe (Gantait et al., 2022; Nandi et al., 2024a; Nandi et al., 2024b). Percent sodium (Na%) reflects the regulation the internal soil drainage capacity, which is found to be extensively hampered by elevated sodium levels (Kouser et al., 2022). According to BIS report in 2012, water with Na% as high as 60% can only be recommended for irrigational activity and when reaches beyond, is considered unsuitable. According to the report of Rao and Latha (2019), elevated concentration of ions like Na^+, Ca^{2+}, Mg^{2+}, and HCO_3, can also impact the permeability of soils. Thus, calculation of the permeability index (PI),calculated from these ions, are necessary to categorise the groundwater quality for irrigation. The PI is calculated

based on an equation used by Doneen in 1964. The groundwater can be classified into three types on basis of PI: class I and II, showing higher than 75% permeability, thus fit to use and class III with permeability as low as 25%(Doneen 1964).

One efficient approach to reducing the soil salinity lies in the cultivation of halophytes that have theability to accumulate salts through various mechanisms. These include, Phytostabilization (e.g., *Carpobrutus rossii*), Phytoextraction by *Tamarix sp*, Phytovolatilization of contaminant (e.g., *Poplar sp.*), Phytodegradation (e.g., *Sarcobatus vermiculatus*) etc. Additionally, different distillation procedures can be employed to remediate salinity effectively. These include solar humidification method, multi-staged flash and membrane- distillation method etc. Membrane technologies, like micro, ultra and nanofiltration, reverse and forward osmosis, electro-dialysis etc, each designed for selectively eliminating a specific contaminant, play a crucial role (Shahid et al., 2020).

2.3.1.2. Iron and Manganese contamination

Iron, an essential mineral for all animals and plants can become harmful for their use when high concentrations of the element accumulate in groundwater. This might arise from the weathering of iron bearing minerals in the bedrock. The solubility of Fe is regulated by the dissolved oxygen in water and pH levels. Iron, usually exists in 2 forms, Fe^{2+} and Fe^{3+}, based on oxygen availability. Fe^{2+} is the soluble form with lower dissolved oxygen, but Fe^{3+} is not soluble. The presence of organic matter can be explored to increase Fe^{2+} solubility as they tend to deplete the available oxygen levels. When water is pumped to the surface, the dissolved iron oxidizes to Fe^{3+} and we experience rusting. It can lead to formation of red oxyhydroxide precipitates which can make water unsuitable for household needs and stain laundry and plumbing fixtures (Pradhan et al., 2023). World Health Organization (WHO) considers the permissible level of iron for drinking water as 0.3 mg/L. Consuming water with higher iron

may cause haemochromatosis which show up as weight loss, fatigue, pain in joints and may also cause potential liver damage, cardiac diseases, and diabetes.

Manganese occurs naturally in earth surface as components of soil, water, and sediments. Its concentration in groundwater is influenced by the mineral types in the aquifer and leaching of manganese ore bearing minerals. It is often found in deep wells and its mobility is affected by the soil acidity, moisture content, organic matter content, and biological activity in the soil. Its solubility increases in acidic soils which lack organic matter. But an opposite picture is encountered under anaerobic conditions, where manganese solubility increases at pH levels above 6.0 (Pradhan et al.,2023). The permissible level of manganese in consumable water is 0.4 mg/L (WHO), while for the Indian subcontinent, it is set at a lower value of 0.1 mg/L by the Bureau of Indian Standards (BIS). Elevated manganese levels can cause neurological issues similar to the Parkinson's disease and can accumulate irreversibly in the brain, particularly in the ganglia's basal region (Pradhan et al.,2023).

Manganese and iron are oxidized first, which makes complexes that are insoluble and then removed by filtration. Common chemical oxidizers include chlorine dioxide, Cl, ozone, and K_2MnO_4. Ion Exchange involving sodium-saturated synthetic resins are also effective for removing small quantities of these ions. Sequestration by polyphosphates also prevent Fe and Mn oxidation (Krishnakumari et al., 2018).

2.3.1.3. Heavy metal contamination

Metallic elements with very high specific density (> 5 g/ml) are called heavy metals. They generally toxic at much low concentrations. Arsenic (As), cadmium (Cd), nickel (Ni), lead (Pb), chromium (Cr), antimony (Sb) are some heavy metals which work as groundwater contaminants. These get into the living bodies via routes of air, drinking water, and food-chain.

They also negatively impact plant health and also ecosystem of the soil when exceed a trace amount. (Srivastava et al., 2017).

Arsenic contamination in groundwater is noticed due to contribution of natural sources like weathered igneous rocks, rocks of sedimentary origin, different fossil fuels, geothermal locations etc. its mobility in groundwater is dependent on different factors such as the adsorption, redox reactions, dissolution and precipitation in the aquifer (Halim et al., 2009; Naik et al., 2010). It is endemic to many countries across the globe like Mexico, Bangladesh, China, Argentina, etc. India is no exception to groundwater pollution by this metalloid and 70.4 million lives approximately are at risk from arsenic levels beyond safe limits. The safe limit of arsenic is 0.01mg/L for groundwater(World Health Organization, 2021). High arsenic levels can lead to serious health issues including gastrointestinal ulcers, abdominal colic pain cardiac arrest, respiratory tract infections, rhinitis, and skin issues like hypopigmentation and hyperkeratosis. In long term use, it is also a potent carcinogen (Pradhan et al., 2023). Adsorptive removal of arsenic using activated alumina-based media is a common practice in India (Kumar et al.,2019). The membrane techniques are used to remove arsenic (Pradhan et al., 2023). *Spirodella (*duckweed) accumulated 175 g/day of arsenic from a pond (Rahman and Ravenscroft , 2003) Microbial remediation is also a potential approach for arsenic remediation as observed by Gupta et al.(2021).

Lead, another important heavy metal, though has mostly anthropogenic sources of occurrence, is also a geogenic contaminant. The lead solubility in groundwater is regulated by factors like pH, concentrations of dissolved salts and minerals types dominating in aquifer. In groundwater, lead mostly exists as precipitates and remains undissolved and precipitates ($PbCO_3$, $Pb(OH)_2$, Pb_2O, and $PbSO_4$). It is also found as adsorbed ions on mineral surfaces, or often it is suspended within organic matter (Pradhan et al., 2023). The WHO in their 2021 guidelines, set

the maximum permissible concentration of Pb in consumable water at 10 µg/L (ppb). Exposure to lead higher than this concentration for long can cause serious health issues like reproductive failures, kidney damage, and hypertension, making it a significant public health concern. Sorption using materials like Bayoxide E33, synthetic hydroxyapatite, pumix perlite mixtures, bioaccumulation, biochar mediated removal, phytoremediation, immobilization by oxidation, reduction, neutralisation techniques have been in use for removing this contaminant (Ramdani et al., 2020; Ranjbar et al., 2017; Dai et al., 2018) **.**

Chromium also draws significant attention in this scenario. Although disposal of chromium containing wastes is the main source for this heavy metal pollution, it is also found naturally. But, in nature it is not found in its elemental form, rathe, it exists as compounds. Under ambient supply of oxygen, chromium is dominant in aquifers at shallow depth as Cr (VI). CrO_4^{2-} or chromate and $Cr_2O_7^{2-}$ or dichromate comprise the principle Cr (VI) species which gets precipitated after reactions with different metallic cations (Ba^{2+}, Ag^+, and Pb^{2+}). It has highest toxic form and has the highest mobility (Pradhan et al., 2023). These free chromium complexes are soluble can leach through the soil and reach the groundwater table contaminating it. The leaching ability of Cr (VI) increases with alkalinity. The World Health Organisation (WHO, 2020) mentioned the maximum permissible limit for this ionic form in drinking water to be 0.05 ppm.

Consuming waters which have Cr concentration higher than the mentioned value slowly bring on several health hazards like immunodeficiency, renal and hepatic problems, skin rashes, ulcers and may even prove fatal on severe exposures (Pradhan et al., 2023). Activated carbon, eucalyptus leaf biochar, ion exchanger filtration, nanomaterials like nanoscopic zerovalent iron, bio-remediation using *Bacillus cereus, Enterococcus sp.* Etc, all have been tested for

removal of Cr (VI) ion (Kumar et al., 2008; Siciliano, 2016, Mtimunye et al., 2017; Choudhary et al., 2017).

Cadmium also creates groundwater contamination scenarios when it exceeds its respective permissible limits of 0.005 ppm set by EPA. . Cadmium (Cd) is found in environment, usually as CdS or $CdCO_3$ form. The commonly found forms of this heavy metal are Cd^{2+}, Cd $(OH)_2$, and cadmium-cyanide complexed moieties (Smith et al., 1995; Hu et al., 2015). A significant portion of this contaminant comes from the by-product generated during the mining activity of the sulfide bearing ores from zinc, lead, copper etc. It is a powerful neurotoxic metal and has a long half-life period of 33 years within the living system. It imbalances the calcium metabolism and causes an array of health concerns like *itai-itai* disease, renal failure, lung cancer, etc (Pradhan et al., 2023). Li et al, used vinegar residue biochar for its successful removal in 2018. Adsorption by nano-metal oxides ZnO, titanium oxides (TiO2) etc is another viable option for Cd removal.

Nickel (Ni) is distributed in nature and found everywhere in the atmosphere, hydrosphere, and the soil system in diverse forms. Although it is a vital element for plants to grow, at minute concentrations, it proves toxic otherwise. The crust of earth typically contains 0.008% of nickel which enters into ground-water table from leaching and dissolution of rocks bearing ores of nickel. The acceptable limit of for this heavy metal in drinking water is 0.1 mg/L as per EPA and 0.02 mg/L according to BIS (Pradhan et al., 2023). Compromised lung function, recurrent allergies, bronchitis, cancer of lungs, and sinus problems are often reported from frequent Ni exposure. In 2010, Hussain et al used water hyacinth *Eichhornia crassipes* to remove Ni from groundwater and the plants removed 24.23 μg Ni/ gram dry weight in this experiment.

2.3.2. Anthropogenic contamination

Human activities further contribute to this growing groundwater pollution. Besides these geogenic sources, urbanization, industrial growth, and intensive agricultural practices have also introduced a diverse range of contaminants into groundwater. Unregulated disposal of industrial effluents, sludges, municipal wastes, pharmaceuticals, and improper management of run -offs from agricultural chemicals aggravate the contamination situation. Additionally, insufficiently treated wastewaters from household sources add up to the range of organic pollutants and pathogens (Nandi et al., 2024a,b).

Extensive use of fungicides, insecticides, pesticides in recent agricultural practices, increase in use of pharmaceutical drugs, cosmetic personal care products (PCPs), plastics, microplastics, endocrine-disrupting chemicals (EDCs), perfluorinated chemicals (PFCs), (PFASs), and even disinfection byproducts (DBPs) are among the many substances that are raising concern. These findings have also been reported by Gogoi et al. in 2018, Tran et al., (2018) and Nawaz and Sengupta (2019)**.** Additionally, households are generating loads of electronic waste (e-waste) due to the sudden surge in use of short- lived electronic devices (Joon et al., 2017). The improper disposal of these discarded electronics prove- hazardous, as these items release heavy metals like , Pb, Hg, and C etc (Houessionon et al., 2021). The list of these emerging groundwater pollutants is lengthy. Agricultural sector contributes some of the major EGCs.

2.3.2.1 Agricultural contaminants

Nitrogen based fertilizers are used in agriculture to boost crop yields, and these release nitrate (NO_3^-) into the soil. Although nitrogen is essential for plant growth, unchecked application can lead to pollution of lithosphere, hydrosphere and atmosphere (Lee et al., 2021)**.** These unabsorbed nitrates leach through the soil during irrigation and with rainwater, ultimately contaminating groundwater. This has become a persistent problem in various regions of India**.**

The European Union's directive sets the threshold for nitrate in groundwater at 50 mg/L. The EPA (USA), marks groundwater with nitrate concentrations higher than 10 mg/L unsuitable for daily use as they pose multiple health risks. Nitrate when solubilises in water creates the toxic and cancer-causing N-nitroso through nitrite formation within the human body (Ghaeminia and Mokhtarani, 2018; Rout et al., 2021a). High levels of NO_3^- cause blue-baby syndrome or methemoglobinemia, prostate and gastrointestinal cancers, oxygen deficiency in developing foetuses causing frequent abortions (Pradhan et al., 2023).To address this issue, adsorption methods, ion exchange, electro-dialysis, reverse osmosis, denitrification catalytic reduction, , and bioremediation are used (Rout et al., 2017a)**.**

Phosphorus, a critical nutrient for plant growth is commonly supplied to crops through phosphatic fertilizers. These fertilisers release various forms of phosphate such as $H_2PO_4^-$, HPO_4^{2-}, and PO_4^{3-} into the soil for uptake by the plants (Rout et al., 2014, 2016a). The unabsorbed residual phosphates leach during rainfall and irrigation into groundwater, causing contamination. These also promote eutrophication. Phosphates have point sources, like industrial activities and discharged from wastewater treating plants, and several non-point sources like the mentioned agricultural field run-off, animal waste etc. weathering of phosphatic rock, erosion, and sedimentation are the geogenic sources of these contaminant. (Rout et al., 2017c). The permissible limit set by EPA for phosphate in drinking water is 5 mg/L. Exceeding this limit calls health risks like kidney damage, destroys cardio vascular health and causes osteoporosis (Vorland et al., 2017). The soil microflora can be appointed for successful remediation of phosphates present in contaminated groundwater. Microbes like *Pseudomonas sp, Coliform sp, Aeromonas sp,Bacillus cereus* etc are used for removing this pollutant (Ying and Wei, 2019).The inorganic phosphate has been reported to be freed of this contaminant by the addition of different coagulants. The elements with multiple valencies l calcium, aluminium, and iron are also generally used (Altaf et al., 2021).

Pesticides are largely used in current agricultural practices to manage growth of weeds, insects, pests, and plant pathogens. They come in different classes like the herbicides, insecticides, nematicides and fungicides. Pest control chemicals, for example DDT or Dichloro-diphenyl-trichloroethane, have extremely low solubility and extensive half-life of about 15 years. These when leach to groundwater along with irrigation water via the macro-pores, channels created by roots, and existing cracks as preferential flow and through small pores as matrix flow cause severe contamination of the underground water table. (Priyadarshini et al., 2021). Organochlorines, Organophosphates, Organonitrogens are the major group of pesticides. Organochlorines have a permissible limit of (0.01–190) μg/L set by BIS, Malathion limit is 190 μg/L (BIS), Chlorpyrifos- 0.03 mg/L (WHO) etc. Long periods of exposure to heavy pesticide doses can prove carcinogenic, induce defects at birth, and damage central nervous system. Systemic poisoning, irritation to skin and eyes, dizziness, nausea, vomiting, fatigue, and abdominal cramps are other concerns (Pradhan et al., 2023). Biochar and surfactants are used for its removal.

2.3.2.2. Contaminants from house-hold and municipality

Flourishing urbanization has contributed to rapid lifestyle changes and has increased waste production worldwide. Household waste including food wastes, leathers, glass, paper, outdated batteries, cardboards, textiles, unused medicines, expired drugs, anionic detergents, insect repellents, personal care products (PCPs), and plastic materials etc are major sources of groundwater contamination. Municipal waste waters carrying human and animal excreta, antibiotics, artificial sweeteners (ASs), PAHs including majority of wastes from households in sewers aggravate the situation. PFASs can trigger cancer and many among these wastes invite health emergencies such as developmental defects of reproductive system, poly cystic ovarian syndrome, infertility, endometriosis, ulcers, thyroid hormone imbalance etc. Bisphenol A, the

microplastic precursor can create blockages in the digestive tract of aquatic animals. Sucralose, an artificial sweetener, can be fatal to marine lives (Tadda et al., 2021). The residues of drugs, antibiotics can get to the soil after their cremation or excretion, which finally leach and contaminate the groundwater (Nawaz and Sengupta, 2019) The current lifestyle involves extensive use of PCPs like dandruff control shampoo, fluoridated toothpaste, moisturizers, body-deodorants, cleansers, and makeup cosmetics, etc. The leachates from landfills containing municipal solid waste also act as a diverse source of pathogens and pharmaceutical contaminants. Wastes from paints, lead containing batteries, mercury thermometers are also a growing menace (Pradhan et al., 2023). Landfill leachate when analysed reported presence of mostly dissolved organic-inorganic salts, metals, ammonia, chloride, iron and fluoride (Jhamnani and Singh, 2009; Samadder et al., 2017). Composting , digestion under anaerobic conditions, EKs or electrokinetic technique, solubilizers like surfactant and cosolvent, micro or nano-bubble methods etc are used to remediate these wastes.

2.3.2.3. Laboratory and healthcare contaminants

Bio-medical wastes are mostly formed from disposal of needles, scalpels, blades for surgery, cotton, outdated drugs, extracted fluids and blood from bodies, tissues, organs etc (Radha et al., 2009). Poor management of wastes produced by laboratories and institutions create problems as they often   contain genetically engineered organisms and cells, infectious microbes, chemicals like ethidium bromide which is a potent carcinogen, radioactive substances for the diagnostic and imaging techniques etc (Rajor et al., 2012, Pradhan et al., 2023). Antibiotics, antifungal drugs, anti-microbial medicines, anti-inflammation medicines, anti-depressant drugs, β-blockers, steroid hormones, UV filters, stimulants of nervous system, plasticizers, insect-repellents, etc., are the chief pollutants from this sector as reported by Tran et al., (2018) and Mohapatra et al.,(2018).

In conclusion, groundwater a fundamental resource is vital for human survival and ecosystem balance. However, the increasing pollution of groundwater from both natural and anthropogenic sources as discussed above present a significant challenge. Implementing effective management strategies and public awareness is essential to preserving this resource.

After reviewing through extensive available literatures on groundwater pollution, its sources and its impacts, we found fluoride (F^-) as one of the major emerging contaminants. It has an interesting duality in its nature. In trace amounts it helps in bone development, whereas, in slightest excess it brings on fluorosis- a global menace. It has both geogenic and anthropogenic sources and is a rising global concern due to its extensive spread and severity. With this, we further move on to gather essence from existing literatures about this contaminant.

2.4. Contamination of Fluoride

Fluorine, the element symbolised by F and has an atomic number of 9, was discovered by French chemist Henri Moissan in 1886. It ranks 13th as the maximum abundant elements in Earth's crust, making more than 0.32% of it (WHO, 1984). As one of the highest reactive electronegative elements of the periodic table, its ionic form fluoride or F^- can easily replace hydroxide ions (OH^-) embedded in minerals because of a striking similarity in their ionic radii (Shaji et al., 2024). Fluoride ion, exists in multiple forms in nature, namely, hydrogen fluoride or HF, which can form the corrosive hydrofluoric acid and is very much soluble in water; the sodium fluoride (NaF) forming the fluorosilicic acid, and (H_2SiF_6) and is moderately water soluble (Shaji et al., 2024). Fluorine is a lithophilic element which has atmophilic affinities, and is prevalent in various rock-forming minerals. Fluoride-rich rocks like amphiboles, muscovites, biotite, volcanic and clay minerals release F^- into groundwater (Mapoma et al., 2017; Shaji et al., 2024). Hydrothermal springs are also potent fluoride sources (Edmunds and Smedley, 2013),

Fluoride levels are typically around 330 mg/kg in soil (Dey and Giri, 2015), 0.9–1.4 mg/L in oceans, 0.1–1.2 mg/L in underground water table, and 0.01–0.3 mg/L in surface water bodies (Shaji et al., 2024). Groundwater usually has elevated fluoride levels than surface water due to prolonged interaction with fluoride-bearing minerals (Edmunds and Smedley, 2012). Anthropogenic activities, such as aluminium and coal production, phosphatic fertilizer use, industrial processes etc contribute to F^- contamination simultaneously (Fordyce et al., 2007).

Fluoride's health impact was taken into note in historical accounts, like 'gaddur' the Icelandic term related to animal disease, dating back 1000 CE, is believed to have links with volcanic fluoride. Fluorosis, the disease from exposure and consumption of fluorinated water, was officially confirmed as an occupational disease in 1930 according to reports of Møller and Gudjonsson, 1932.

2.4.1. Geogenic sources of fluoride

Fluoride (F^-) primarily originates from geogenic sources, as it is commonly found in minerals such as fluorite (CaF_2), fluorapatite ($Ca_5(PO_4)_3F$), biotite ($K(Mg,Fe)_3AlSi_3O_{10}(OH,F)_2$), hornblende ($(Ca,Na)_2(Mg,Fe,Al)_5(Al,Si)_8O_{22}(OH)_2$), sellaite ($MgF_2$), topaz ($Al_2(SiO_4)F_2$), and muscovite ($KAl_2(AlSi_3O_{10})(OH,F)_2$). Extended interaction between rock and water leads to the dissolution of these fluoride-bearing minerals, which contaminates groundwater (Subba Rao et al., 2020). Additionally, other geogenic factors such as exchange of anion between F^- and OH^-, various redox reactions, alkaline pH, lowered calcium levels, and high HCO_3^- concentrations exacerbate fluoride contamination further. Findings from Adimalla et al., (2018), Dehbandi et al., (2017, Hu et al. (2022), Jha and Tripathi (2021), Subba Rao et al. (2017); and Nandi et al., (2024a) bring forth the same. Different soil water and soil gas interactions in the underlying aquifer, the diversity of the bedrocks that interact to the water table and the duration of water rock contact are the chief determining factors (Nandi et al.,

2024b). The weathering and dissolution of fluoride-containing minerals are noticeable especially in areas with pegmatite veins and fractured hard rocks. Alluvial deposits of the plains formed by the river Ganges also show high concentrations of fluoride as a result of being laden with micaceous minerals such as biotite and muscovite. Besides minerals like fluorapatite and topaz, villiaumite and cryolite also contribute to elevated fluoride levels in groundwater. The movement of fluoride in the soil system is dependent to a large extent on the pH of the soil. The presence of different clay minerals and the sorption properties they possess also have a crucial role. (Pradhan et al., 2023). In water bodies created naturally, F exists dominantly as as free F^- or fluoride ions. However, it might also undergo complexation with different elements such as Be, B, Al, and Si under certain set of prevalent conditions (Shaji et al., 2024). According to findings from reports of Liu and Zhu (1991) the trivial factors that affect elevated levels of F^- in water table underground include various climate factors, rates of evaporation, chances of precipitation, geology of the region concerned, geomorphology, and geochemistry of the aquifer. Fordyce et al., in their study in 2007 observed that concentrations of F^- can largely vary from differences in arising in the process of weathering and the obtainability of leachable F^- even for same geological conditions and climatic situations. Previous literatures have recorded a positive correlation within pH and bicarbonate pointing out that alkalinity in the environment may positively influence fluoride leaching from bedrocks. In 2006, Sreedevi et al., observed a remarkable correlation between the total dissolved solids (TDS) in an aquifer and concentration of F^-, showing, high ionic strength might escalate solubility of this ion. Handa (1975) found the correlation between F^- and HCO_3^- to be positive and stated a negative correlation for fluoride to Ca^{2+}. Calcium-poor, alkaline waters show more fluoride concentrations. He et al., in his findings from 2013, estimated the fluoride content of different rocks and found that killas, schist, gneiss, granite, silexite, conglomerate and sandstone have approximately 1873, 1703, 1563, 1043, 982, 963, and 903 mg/kg of fluoride. . Volcanic rocks have the highest fluoride

content at 2000 mg/kg, followed by alkaline igneous rocks with 1300 mg/kg, and limestone with approximately 100 mg/kg (Anazawa 2006, Hem, 1985). Additionally, volcanic activity and active hydro-geothermal vents contribute appreciable amount of fluoride to environment, thus polluting soils, and gases which contain HF simultaneously pollute the air (Vithanage and Bhattacharya, 2015). Marine aerosols also represent a significant natural source of fluoride, and act as the third highest contributor, adding around 20,000 kg of inorganic fluoride to the atmosphere annually (CEPA, 1996, Singh et al., 2018). In 1946, Robinson and Edington reported that high concentration of this ion could be found in clay minerals. As per studies by Umar and Alam in 2012,during the hot, arid pre-monsoons, evaporation rates being higher cause F^- salts to precipitate over the soil surface which then makes a a semi-permanent reservoir of soluble F^-. These then infiltrate the soil along with rainwater, increasing TDS and fluoride to groundwater through. Fluoride enrichment within the aquifers is influenced by various factors, including soil porosity, well depth, soil and rock acidity, temperature, ion exchange processes, and the presence of cations and anions, as well as other chemical reactions (Annaduraia et al., 2014). Evaporation has a crucial role to play in increase of fluoride concentrations in groundwater. It contributes to the phenomenon by raising ionic levels and leading to major mineral precipitations, which in turn reduces Ca^{2+} concentrations and escalates fluoride dissolution (Adam et al., 2001). Atmospheric CO_2 also affects levels of F^-; when -CO_2rich air interacts with rainwater, it creates acidic conditions and acid rain that enhance the release of H^+ causing weathering of silicate rocks and elevating fluoride. Additionally, an increased Na+/Ca2+ ratio, as a result of silicate weathering can further contribute to increasing F^- levels in groundwater (Shaji et al., 2024). Karro and Uppin in 2013 observed powerful association between fluoride and boron in some points of Canada and Western Estonia . That dissolution of fluoride is influenced by clay content, which lowers hydraulic conductivity and thereby extends water interaction time and that there exists a positive correlation between

fluoride concentration and aquifer depth was supported by observation of Kim and Jeong (2005), Vasquez et al., (2006) etc . Additionally, Jacks et al. (2005) observed a positive relationship between F⁻ and Cl⁻ ions.
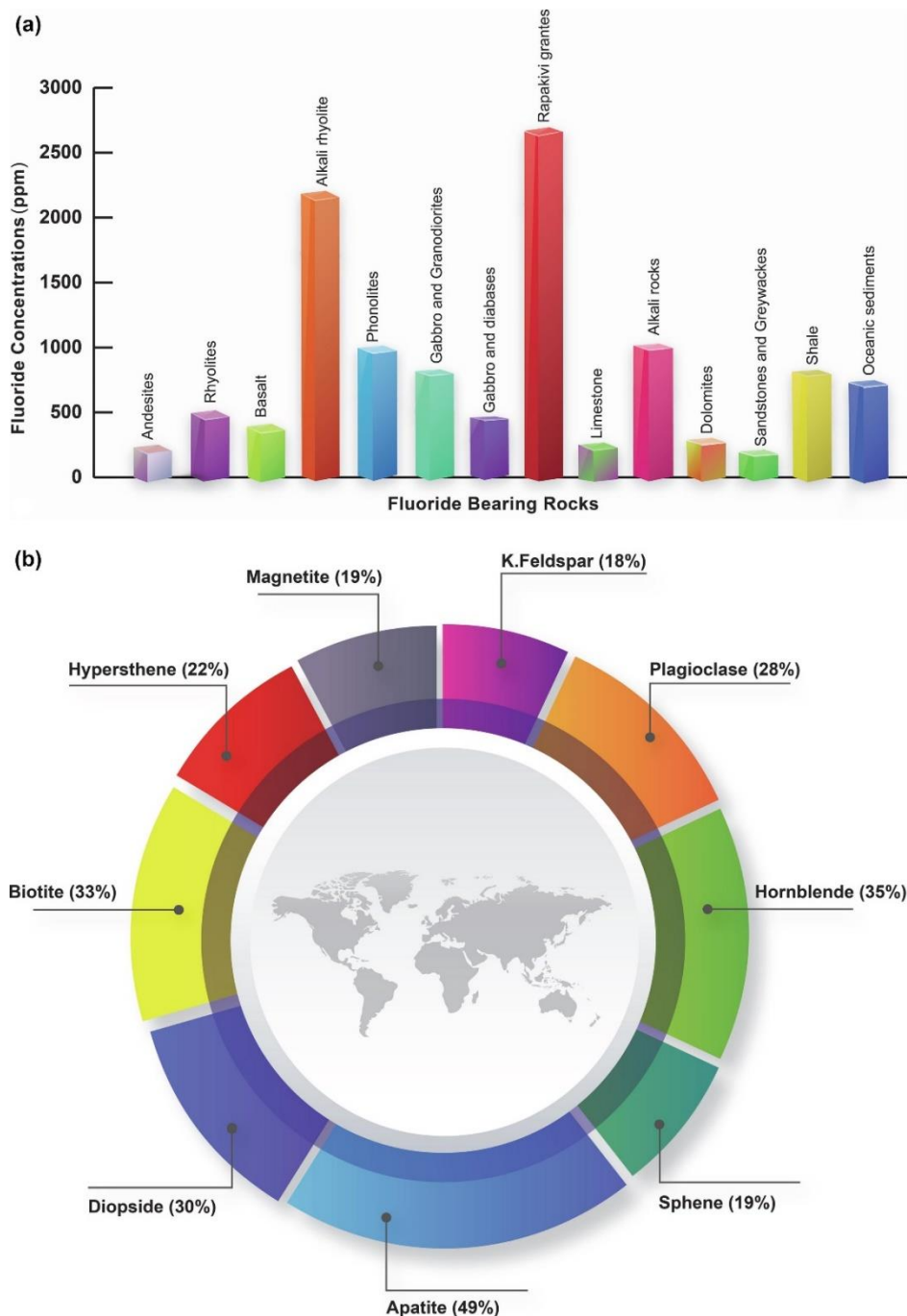
Figure 1: Average fluoride concentrations present in different rocks types and fluoride content in percentage in different minerals

Source: Shaji et al., 2024

Having gained sufficient information about the geogenic sources of fluoride we now move on to study the anthropogenic sources of the same.

2.4.2. Anthropogenic sources of fluoride

The primary anthropogenic source of fluoride is industrial activities. In the US alone, this use for fluoride in processing at industries has increased threefold, from 0.5 million metric tonnes to 1.5 million metric tonnes annually (Singh et al., 2011). Various factors contribute to fluoride emissions, including the extensive use of phosphatic fertilizers in cropping practices, combustion of coal, smelting of aluminium, and cement production (Thapa et al., 2016). Other significant sources include coke production, the manufacturing of glass, production of ceramics, electronics and steel. The use of cryolite as a catalyst in aluminium electrolysis has led to well-documented fluoride contamination around these facilities (Shaji et al., 2024). Cosmetic industries that use mica as an ingredient also act as apotent source. Mica mining itself is an important source of fluoride pollution (Nandi et al., 2024b). Typically, human exposure to fluoride primarily occurs through drinking water. However, fluoride can also enter the body via food, cosmetics, and aerosols. Foods that may contain fluoride include dates, certain types of tea, dairy products, fats and oils, beverages, soups, meat, poultry, fish, and some vegetables (Shaji et al., 2024).

2.4.3. Health hazards from fluoride

Groundwater quality is crucial for drinking water safety. Contamination of this vital resource brings on associated health concerns. Fluoride, a dubious sword can unfold an array of health conditions when exceeds its permissible limit of 1.5 ppm (WHO) in drinking water. While moderate (<1 ppm) F^- levels can take care of dental caries and facilitate bone development, excess of its exposure can bring about health risks. (Kaminsky et al., 1990; Heller et al., 1997;

Li et al., 2001; Subba Rao, 2003; Haji et al., 2021). Aoba in 1997 had shown that this ion can enhance structural stability and simultaneously reduce the solubility of minerals.

The association of fluoride to dental resistance was first observed in 1803 by Morichini upon his discovery of fluoride in the fossil tooth of an elephant (Shaji et al., 2024). The benefits of fluoride in preventing dental caries became evident in the 1930s, when "colourful teeth" of inhabitants of south-western U.S were observed. Afterwards, in the 1950s, determination of optimal fluoride concentrations in drinking water to prevent such dental decay was successful (Shaji et al., 2024).With rising industrialization and extensive population growth, contamination of consumable water by fluoride has become a global issue. The severity of health issues related to fluoride, also depends on additional fluoride sources, physical activity, and dietary habits besides the concentration of the ion in water.

Dental fluorosis is typically caused by consuming water containing fluoride concentrations above 1.5–2 ppm. It begins with white, opaque patches on teeth and later progresses on to brown or black staining. Significant psychological stress is generated in most patients due to tooth deterioration. India reports widespread dental fluorosis in fourteen states and 150,000 villages, with high prevalence in Bihar, Uttar Pradesh, Madhya Pradesh, Rajasthan, and Gujarat, (Pillai and Stanley, 2002). As Fluorine has a highly electronegative property, it shows a strong affinity for positively charged ions like Ca. This characteristic explains the tendency of this ion to harbour in mineralized tissues such as bones and teeth which have abundant calcium. In these tissues, F^- gets incorporated in the form of calcium-fluorapatite crystals. Tooth enamel is primarily composed of crystalline hydroxyl-apatite, which easily changes to fluorapatite after adsorbing fluoride present in drinking water. This fluorapatite is more stable than hydroxyl-apatite. As a consequence, F^- becomes bound in these tissues, liitle is only excreted through sweat, urine, and stool. Dental Fluorosis cause enamel to lose its shine and

lustre and slowly cause significant pitting. Fluoride exposure during formation of teeth, which occurs up to the age of 8–10 is the time that causes most effects. It may not show visible signs of fluorosis in adults who have fully developed teeth (Meenakshi and Maheswari, 2006).

When fluoride concentrations in consumable water increases over 4–8 mg/L, incidences of skeletal fluorosis are noticed. It comes with symptoms such as increased bone density, pain and stiffness of joints, deformities in spine, Arthritis, vertebral fusion and excessive bone growth. This condition affects all ages including children and adults, but symptoms often only become apparent at advanced stages. Accumulation of this contaminant ion in the joints, neck, knees, pelvis, and shoulders make movement restricted. Early symptoms include sporadic pain, stiffness of joint, burning and tingling feeling in the limbs, muscle ,numbness and fatigue. Fluoride levels higher than 8 mg/L can lead to osteosclerosis. Severe cases, with fluoride levels exceeding 10 mg/L, can lead to crippling skeletal fluorosis, characterized by paralysis and neurological disorders (Srivastava and Flora, 2020; Boyle and Chagnon, 1995). In extreme cases, it may cause rare bone cancer, osteosarcoma (Shaji et al., 2024). The condition is classified into mild, moderate, and severe forms based on severity (Mishra et al., 2010).

Besides affecting the bones and teeth primarily, high F^- concentrations can affect other body systems, including the intelligence of an individual, the reproductive organs, digestive systems etc. It may cause significant damage to the pineal gland. Symptoms of fluoride toxicity include gastroenteritis development, excessive salivation, anorexia, muscular weakness, stiffness in the body, restlessness, breathing difficulties, profuse sweating and heart irregularities (Sahu et al., 2017). These issues have been reported in countries like Ghana, India, Canada, China etc (Apambire et al., 1997; Susheela et al., 1993; Gupta et al., 2005; Boyle and Chagnon, 1995). In extreme cases, very high F^- concentrations (>10 mg/L) can not only bring about crippling fluorosis but also severely affect additional organs, including the nervous, hepatic, and renal

systems. Instances of crippling in fluorosis have been observed in some regions of Asia and

Africa according to Rasool et al. (2018). Elevated fluoride exposure can impair brain function
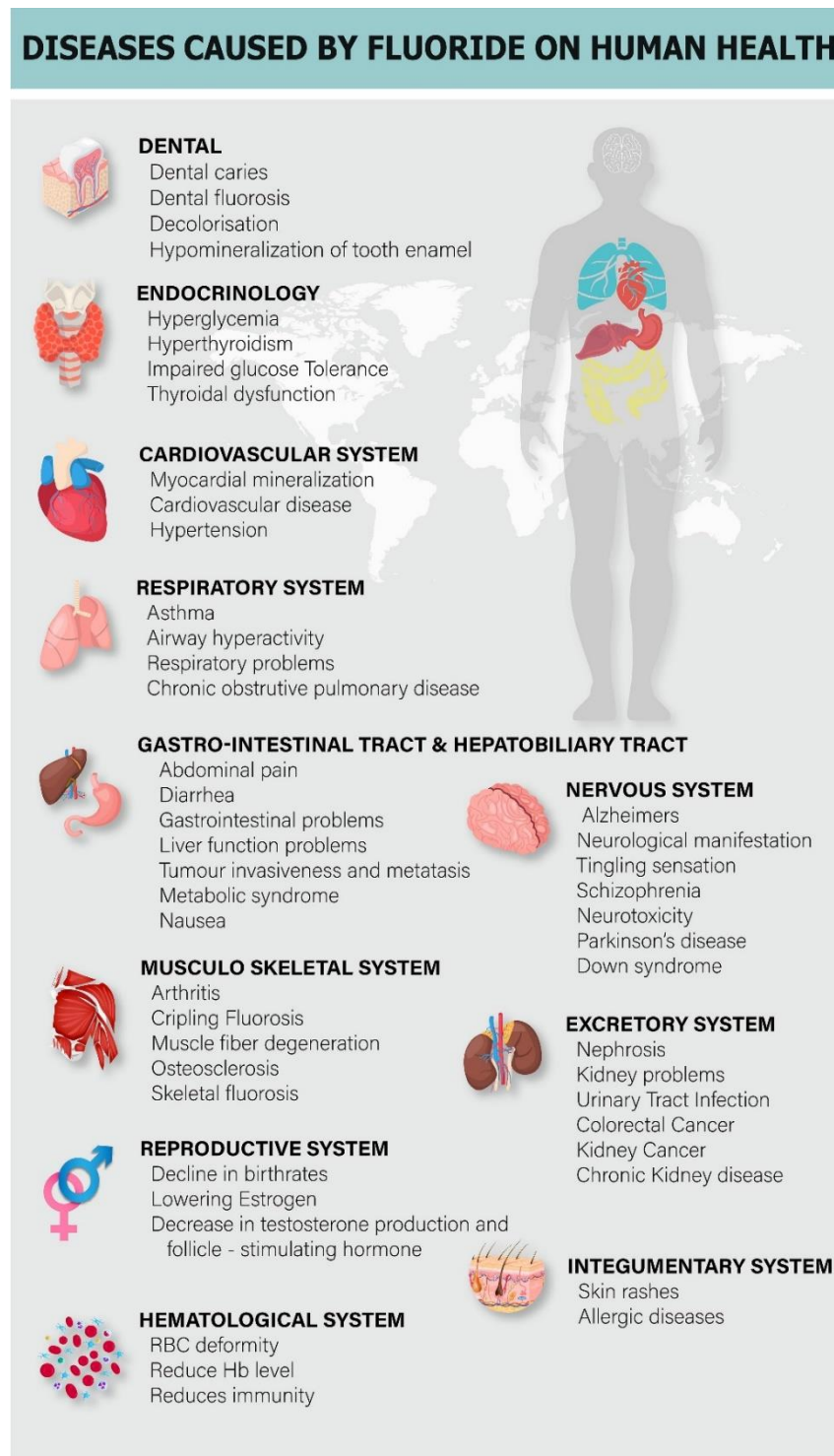
Figure 2: Impacts of F- poisoning on human health

Source: Shaji et al., 2024.

in children, affecting growth hormone production and intelligence as reported by multiple studies like reports of Grandjean and Landrigan in 2006; studies by Choi et al. (2012), Skórka-Majewicz et al., (2020), Onipe et al., 2020. Agalakova and Nadei also brought out a similar report in 2020. It can also impact the energy needs of the central nervous system.

A range of other health problems include muscle-fibre degeneration, low haemoglobin levels, deformations in RBC, excessive thirst, severe headaches, Nephrosis, lowers oestrogen, skin rashes, nervousness, neurological symptoms similar to Alzheimer's disease, gastrointestinal issues, urinary tract dysfunction, nausea, abdominal pain, tingling in limbs, compromission of immunity, recurrent abortions, stillbirths, and male sterility (. Fluoride interferes endocrine sytem and perturbs action of approximately sixty enzymes. The detrimental effects of high fluoride concentrations are similarly observed in animals and can adversely affect plants (Meenakshi and Maheshwari, 2006; Mandal et al., 2021, Shaji et al., 2024).

2.4.4. Fluoride and plants

Fluoride (F^-) intake from diets vary globally, typically ranging from as low as 0.2 to around 2.7 mg/day due to differences in the consumption of crops and vegetables contaminated with F^- (Jolly et al., 1974). Plants generally absorb less than 10 mg/kg of F^- when grown in uncontaminated soils. They can accumulate fluoride, influenced by different factors such as soil type, plant species, and fluoride form (Davidson et al., 1985; Smolik et al., 2011). Soil fluoride is mostly insoluble or tightly bound to particles, with pH and the presence of other ions affecting its uptake. For instance, *Camellia sinensis* absorbs more fluoride with increased soil pH, whereas calcium reduces its uptake (Singh et al., 2018). Plant sensitivity to fluoride varies widely. Tea plants are known for their high fluoride accumulation, correlating with external fluoride concentrations. Fluoride accumulation is higher in plants near fluoride-emitting industrial sites, such as those reported around phosphate fertilizer plants and

geothermal sprinkler-irrigated areas (Devi et al., 2016; Mezghani et al., 2005). Plants like *Brachiaria distachya and Suaeda maritime* have been found to absorb significant fluoride level due to industrial activities.

Fluoride distribution within plants depends on its transport from roots to shoots. It enters plants through apo-plastic transporters and anion channels. Roots are mostly dominated by the first type of transporters (Singh et al, 2018). Stomatal accumulation of fluoride is also possible (Jacobson et al., 1966). Since F^- ions cannot pass freely through the lipid bio-membrane due to polarization, specific proteins known as carrier proteins or channels help their movement into and out of the cell. The 'Fluc' protein or the F^- selective channel has two subunits arranged in an anti-parallel formation (Stockbridge et al., 2013). Intracellular signalling molecules such as Ca^{2+} and abscisic acid (ABA) activate it (Chen et al., 2010; Zhang et al., 2016). Research by Robert (2006) and Zhang et al. (2016) demonstrated that the uptake of F^- in plants is reduced when channel inhibitors such as niflumic acid and NPPB are used (Singh et al., 2018).

Fluoride affects plant physiology and biochemistry, potentially causing significant damage, including cell death and reduced biomass. It also brings on necrosis of leaves and leaf-burns. In contrast, some studies suggest that fluoride-contaminated irrigation water can increase crop yields. Studies mostly show otherwise, it has been reported to negatively impacts photosynthesis and other growth parameters (Singh et al., 2018) . In *Gossypium hirsutum* L., a 73% reduction in root biomass was observed when irrigated with water containing with 1000 mg/L fluoride (Kumar and Singh, 2015). Fluoride interacts with calcium (Ca^{2+}) and magnesium (Mg^{2+}), damaging physiological processes and disrupting enzyme activity in plants (Barbier et al., 2010). This arises from the formation of different complexes such as magnesium-fluoride-phosphate (Lebioda et al., 1993). Fluoride when complexed with Al and Br, can mimic phosphate destroy enzymes involved in phosphoryl transfer (Barbier et al., 2010). Additionally,

fluoride toxicity has been reported to inhibit algal growth by disrupting cell division. It has also has been reported to affect the nucleotide and nucleic acid metabolism by Klut et al., in 1981.

2.4.5. Global spread of fluoride contamination

Analysis of global data indicates that over 100 countries are experiencing fluoride contamination in groundwater levels that exceed the WHO's maximum allowable limit of 1.5 mg/L. The highest number of affected countries is in Africa (38), followed by Asia (28), Europe (23), South America (5), North America (3), and Australia (2) (Shaji et al., 2024). Human lives across the globe, in more than twenty-eight developing and developed nations are affected by the F^- pollution. Countries like France, Germany, China, Holland, Italy, Japan, Sri Lanka, Switzerland, Bangladesh, Pakistan, New Zealand and Thailand all come under the grip of this growing contamination. Countries in South and North America, even the South African nations suffer from Fluorosis (Nandi et al., 2024b). Argentina, Germany, India, and Kenya are the most severely impacted countries in the Americas, Europe, Asia, and Africa, respectively. Over 200 million people globally consume high-fluoride water exceeding safe levels (Kimambo et al., 2019; Podgorski and Berg, 2022). Notably, countries such as China, Sri Lanka, India, parts of Iran, Pakistan, and Jordan face the highest levels of contamination (CGWB, 2018; Kaur et al., 2020; Rashid et al., 2020). For instance, in China, fluoride concentrations in well water were reported to be 21.5 mg/L in 2000 by Wang et al in 2001. Elevated fluoride levels have also been noted in certain regions of Nigeria, the African Rift Valley, Kenya, Iran, and Japan (Hossain et al., 2016; Olaka et al., 2016; Emenike et al., 2018; Qasemi et al., 2019). Geogenic fluoride contamination is a global issue, with the majority of severe cases occurring in Asia and Africa. Countries with significant fluoride pollution include Sri Lanka, India, Pakistan, China, Iran, Jordan, West Bengal, Nepal, Japan, South Korea, North Korea, Libya, Ghana, Sudan, Burundi, Tanzania, Ethiopia, Algeria, Australia, and Chile (Shaji et al., 2024; Nizam et

al., 2022). Many fluoride-prone areas are located in highly metamorphic regions or are linked to alkaline intrusions, hot springs, volcanic activity, arid and semi-arid patches. Additionally, sedimentary rocks such as shales and limestone contribute to contamination.
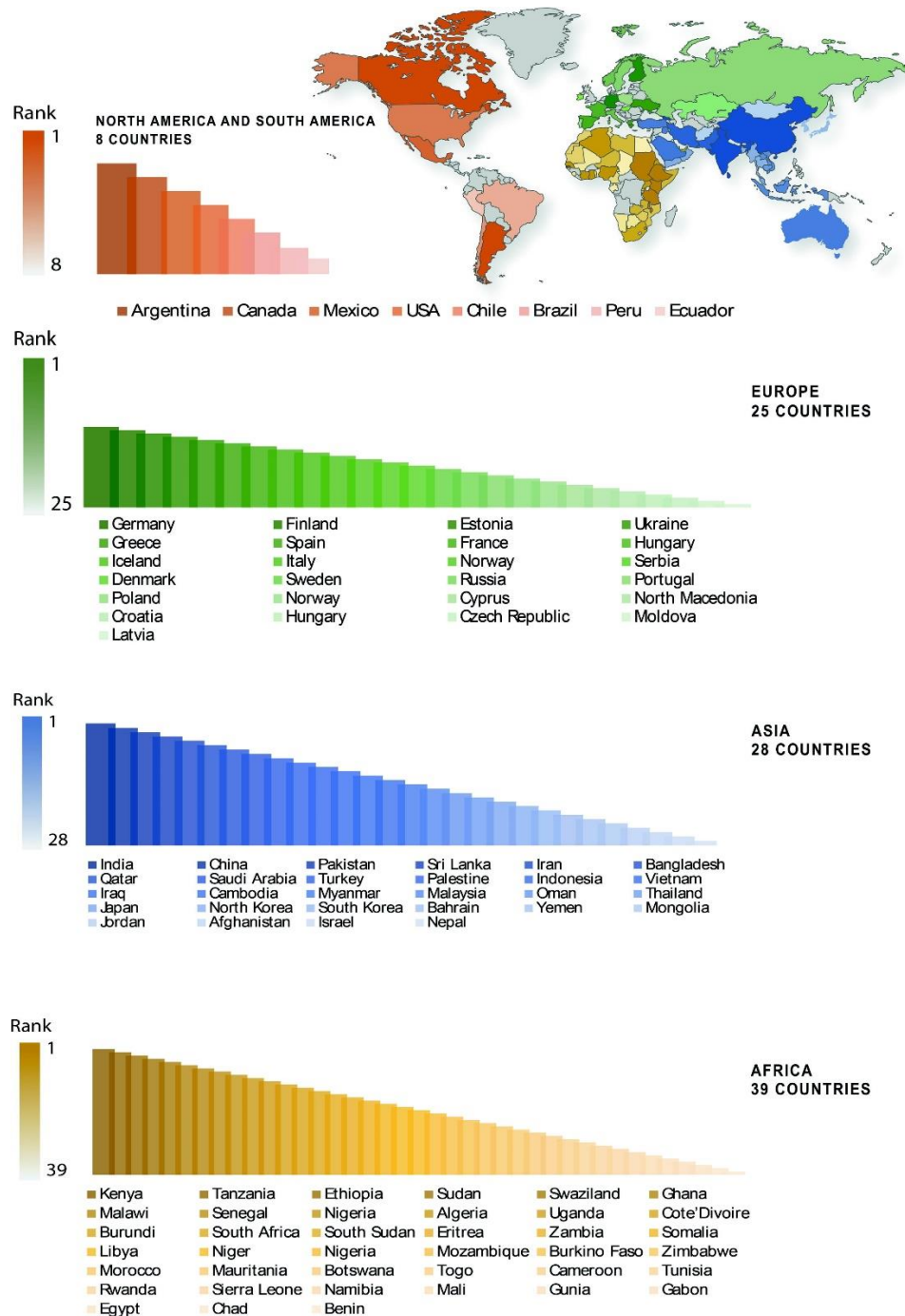
Figure 3: Figure depicting spread of fluorosis across continents and countries globally.

Source: Shaji et al., 2024

2.4.6. Fluoride contamination scenario in India

Fluoride contamination in groundwater in India was first documented in 1937 in Nellore district, Andhra Pradesh, among cattle (Shaji et al.,2024) . India, being no exception, is endemic for fluorosis (Kashyap et al., 2021). More than 22 states, 223 districts including Bihar, Rajasthan, Gujarat, Assam, Uttar Pradesh, Madhya Pradesh, Kerala, Karnataka, Jammu and Kashmir, Punjab, Orissa, West Bengal and Jharkhand come under the fluoride endemic region revealing that fluoride issues persist across various hydrogeological settings (Nandi et al 2024b). Approximately one million people in India are exposed to high fluoride concentrations in their water (Agrawal et al., 1997; Susheela, 1999; Choubisa, 2018; Jha and Tripathi, 2021).

In Andhra Pradesh's Nalgonda region granitic rocks and fluoride levels are notably high here (Brindha and Elango, 2011). Assam's Karbi Anglong and Nagaon districts also have high fluoride concentrations, reaching as high up to 20.6 mg/L from alkalinity (Jacks et al., 2005). In Kerala, Palghat and the Tertiary sediments of Alleppey show contamination as per Shaji et al., (2007) and Raj and Shaji (2017), influenced by factors such as long residence times and low rainfall. Maharashtra's deep aquifers show high fluoride due to extended residence times (Madhnure et al., 2007), while Rajasthan fluoride levels exceeding 8.2 mg/L in some districts as per reports of Maithani et al., in 1998 and Kesari et al. in 2021.

Southern India, including Karnataka, Kerala, Andhra Pradesh, Telangana, and Tamil Nadu, is notably affected. 20 out of 30 districts of Karnataka are primarily in gneissic and granitic areas and face this issue (Shaji et al., 2007; Raj and Shaji, 2017).In Western India, 53 districts across Maharashtra, Rajasthan, Gujarat, and 30 districts in Central India are affected. Rajasthan's contamination is severe, with levels up to 8.2 mg/L in some areas (Suthar et al., 2008; Choubisa, 2018; Coyte et al., 2019) and Central India's Bharatpur district reports 8.7 mg/L (Gupta et al., 2005).Northern India has 51 districts affected. Uttar Pradesh is particularly hard-hit, with

around 50% of its population showing signs of fluorosis, especially in Unnao and Pratapgarh (Srivastava, 2020). Fluoride levels exceeding 6.7 mg/L are reported in Sonbhadra. (Shaji et al., 2024).In Eastern and North Eastern India, 25 districts face fluoride issues, with Odisha experiencing significant contamination due to both geogenic and anthropogenic factors (Routroy et al., 2013; Sahoo et al., 2022). West Bengal, Assam, Jharkhand are also in trouble.
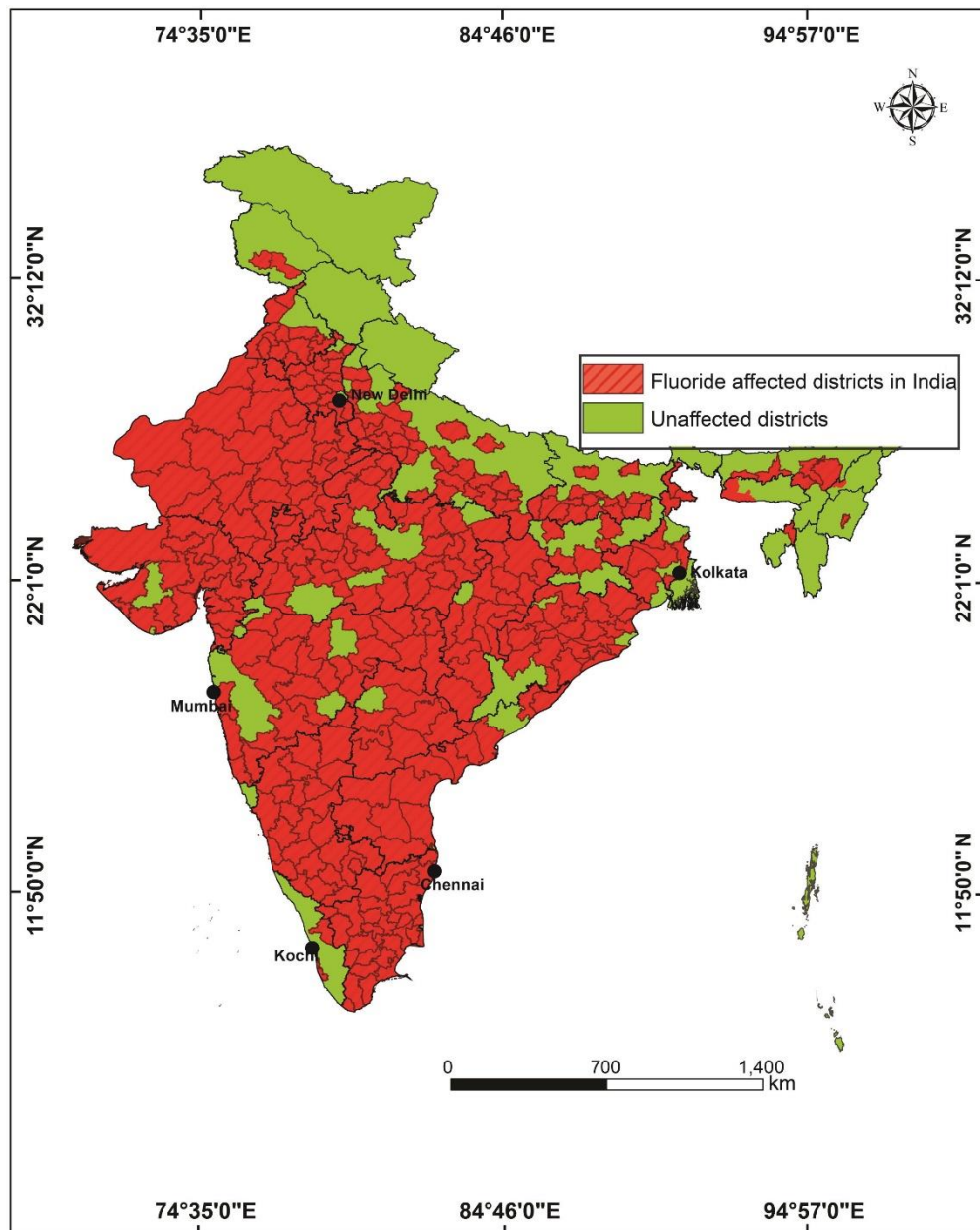
Source: Shaji et al., 2024

Figure 4: Figure showing fluoride-affected states of India, where 22 states are affected.

2.4.7. Fluoride remediation strategies

Fluoride's detrimental effects on human health and plants necessitate effective monitoring and mitigation strategies. Various methods, including physical, chemical, and biological processes, are employed to reduce fluoride levels in drinking water.

Adsorption techniques use materials with active sites to bind F^- ions. Common adsorbents include activated alumina, bone char, and brick pieces. Activated alumina which has found its use in domestic defluoridation plants since 1991, is effective but costly (Daw, 2004). Bone char on the other end economical but culturally sensitive. Alumina-enriched mud pots are both affordable and well-received in rural community (Singh et al., 2018). Ion exchange involves use of synthetic resins to remove F^- ions. Anionic exchange resins (e.g., Deaceodite FFIP, Tulsion A-27) and cationic resins (e.g., sulfonated saw-dust carbon) are popularly used (Suneetha et al., 2015). Modified ion exchangers like poly-acrylamide together with metal salts have also shown remarkably high efficiency in fluoride removal (Singh et al., 2018; Shaji et al., 2024). As per reports of Chubar et al in 2005, two-fold hydrous oxide containing ion exchangers were successful in removing F^- along with associated ions. Precipitation methods convert fluoride into insoluble forms (fluorapatite) for removal (Singh et al., 2018). Techniques include the Nalgonda Technique which uses aluminium salts and lime to form flocs that remove fluoride after sedimentation of the flocs and removing them by filtration. The process derived its name from the place Nalgonda in the state of Andhra Pradesh where it was demonstrated for the first time. It's cost-effective, aesthetically approvable and simultaneously removes other contaminants but has a drawback of generating sludge and may often require desalination when TDS is high in treated water. Its efficiency is also largely dependent on the pH of the solution (Singh et al., 2018). Calcium and phosphate are also useful to precipitate fluoride, which is then filtered using bone char for catalysing the reaction. These procedures fall under the

category of contact precipitation and was developed by WHO in the year 2006. In the popular IISc Method MgO, Ca(OH)2, and NaHSO4 are used for converting fluoride into insoluble MgF2 which are then removed by precipitation (Singh et al., 2018). Membrane techniques are another important aspect of fluoride removal with specific pore sizes are used to filter fluoride. Reverse Osmosis (RO) method applies pressure to a semi-permeable membrane, effectively removing over 90% of fluoride but is costly and less feasible for use by the rural communities (Assefa, 2006). Nanofiltration (NF), a latest membrane technique, has larger pores than RO, thus requiring far less pressure. This helps in preserving essential minerals which were lost earlier due to increased pressure. NF90 has gained immensely popular in this regard after its successful application in Morrocco (Pontie et al., 2008). Finally, Electrodialysis using electric force to enhance ion removal has high efficient across a wide range of TDS. Different biological agents are also being used recently keeping their sustainability in mind. These are eco-friendly options and also are easily available and cost effective (Singh et al., 2018). Biosorbents, derived from agricultural byproducts like sugarcane bagasse, charcoal, rice husk, and neem leaves, offer an eco-friendly alternative for fluoride removal and have been used successfully in previous studies by Mondal et al (2013), Mondal et al (2012), Kumar et al (2008) etc. The functional groups responsible for such adsorption phenomenon may be imidazole group, hydroxyl group, imine group, carboxy group etc. Phenols , phosphodiester groups might also have contributions according to findings by Vieira and Volesky (2000). Various fungal species (e.g., *Aspergillus niger, Fusarium moniliforme*) and algae (e.g., *Spirogyra*) are also used (Singh et al., 2018). The efficiency of biosorbents can be affected by pH and the presence of competing ions, which become a limitation to these methods. Phytoremediation make use of plants to absorb fluoride from contaminated soil and water. Plants such as *Hordeum vulgare, Camellia sinensis,* and *P. juliflora* have shown significant fluoride accumulation and can be relied on for fluoride removal from contaminated sites.

Native plants or arid climatic regions have often been recommended for in-situ remediation of fluoride (Chaudhary and Khan, 2016; Sigh et al., 2018). Several fluoride-resistant bacteria and fungi also have the capacity to bio-transform fluoride into less harmful benign forms. For example, *Acinetobacter* RH5 and *Oscillatoria limnetica* effectively reduce fluoride (Li et al 2013) . Fungal cells loaded with fluoride export proteins (FEX) can expel fluoride ions and thereby mitigate its toxicity. Combining multiple of these available techniques can enhance fluoride removal efficiency**.** For instance, integrating adsorption processes with biosorption or phytoremediation has shown proven efficiency. The SABA process, combining adsorption and bioaccumulation with bacterial assistance, has been reported to achieve significant reductions in levels of fluoride ion (Dwivedi et al., 2016). Addressing both environmental and health concerns associated with fluoride contamination and sustainable removal is the primary goal.

2.5. Biochar

From the literatures reviewed, we found that recent advancements have introduced various chemical, physical, and biological methods for fluoride removal from water, including coagulation, oxidation, adsorption, ion exchange, membrane filtration, and microbial processes (Singh et al., 2018). Among these, adsorption has emerged as the most popular, cost-effective technique for fluoride removal. Traditional adsorbents like aluminum, iron, manganese, titanium, and ferric phosphate, as well as zeolites and fly ash, have been widely studied (Mohan et al., 2012). However, the effectiveness of these adsorbents can be limited by factors such as pH variations and competing anions, and the disposal of waste byproducts remains a challenge (Sadhu et al., 2021). Activated carbon is a commonly used adsorbent due to its efficient metal removal properties, but its high cost and regeneration issues make large-scale treatment expensive and inefficient**.** Therefore, there is a need for more affordable sorbents that do not require costly pre-treatment. Utilizing low-cost adsorbents, such as industrial waste, natural

ores, and agricultural byproducts, is preferable as it ensures a steady supply of materials and reduces overall costs. Recently, biochar has garnered significant interest for its eco-friendly and cost-effective properties. The sorption properties of biochar have been extensively studied. Recently, we reported the effective use of biochar produced from bio-oil for removing arsenic, lead, and cadmium from water (Mohan et al.,2011).

Biochar, an amorphous, highly porous carbon compound produced by pyrolyzing organic materials at temperatures of 350-850°C in the presence of limited oxygen, may fulfil the purpose. In addition to its use in wastewater treatment for a wide range of contaminants including dyes, heavy metals, antibiotics, endocrine-disrupting chemicals (EDCs), pesticides, etc., biochar has demonstrated significant potential in removing fluoride from drinking water (Huang et al., 2022; Akhil et al., 2021; Singh et al., 2018). The feedstock for biochar production can encompass a wide range of diverse and unconventional sources, such as banana peels, rice husks, rice straw, sugarcane bagasse, pinecones, bamboo, agricultural residues, and more (Ganguly et al., 2020). Chemical, physical, or biological modifications to native biochar, feedstock, reaction temperature, pyrolysis conditions etc can also affect contaminant removal by altering the biochar's specific surface area, functional groups, pore size, and adsorptive efficiency. Chemical exfoliation involves treating native biochar with acids, bases, or non-reactive gases (Mahari et al., 2022, Huang et al., 2022). It modifies surface-active functional groups like carboxyl, carbonyl etc present on biochar's surface which act as active sites for adsorption of contaminant (Azeem et al., 2022). High surface-to-volume ratio, thermostability, eco-friendliness, cost-effectiveness, sustainability, porosity, affordability, and technological flexibility have positioned it as the preferred adsorbent.

Biochar, produced from biomass by the process of thermal degradation, has an universe of applications owing to its countless benefits. Key factors which influence biochar's quality

include the type of biomass being selected and pyrolysis conditions being applied, particularly temperature has an important role, which has significant impacts on the biochar's characteristics (Xiang et al. 2020b; Huang et al. 2021). Optimizing the set of pyrolysis conditions is the utmost necessity for maximizing biochar's yield and effectiveness. Pristine biochar or the biochar in its native form without any exfoliation or post treatments, often has only a limited adsorption capacity and takes longer timespan to reach equilibrium, which ultimately can hinder its use in removing different contaminants from aquatic environments (Ling et al. 2017; Son et al. 2018). However, its large surface area, high porosity, and low ash content still keep it in the run of making a promising material out of it for environmental remediation (Balajii and Niju 2019; Kosheleva et al. 2019; Gopinath et al. 2020; Madima et al. 2020). Recent advancements in modifying biochar have extra ordinarily performed in enhancement of its properties, with switching and regulating different factors such as activation temperature, agents, pH, and concentration, thus playing crucial roles in improving their adsorptivity (Heidarinejad et al. 2020). Engineered biochar, with its enhanced surface characteristics and surface chemistry, shows significant benefits in soil improvement, nutritional enhancement, and increased crop productivity (Xiang et al. 2020b; Gunarathne et al. 2019). A study by Chen et al in 2019, showed that a nanoscale zero-valent iron-coated biochar had a 2.2-fold increase in adsorption capacity compared to pristine biochar (Chen et al. 2019a).

Biochar's benefits include its low cost, eco-friendliness, and unlimited versatility of action. It has applications beyond adsorption, including production of valuable chemicals, and clean sustainable fuel production etc (Cai et al. 2020; Lee et al. 2020). For instance, modifying biochar with red mud can reduce extractable arsenic levels by 27% (Zou et al. 2018). Persistent contaminants like antibiotics, pesticides, and dyes can also effectively remove by these novel

engineered biochar (Gopinath et al. 2020; Keerthanan et al. 2020; Madima et al. 2020). These can also work as biochar sensors (Malik et al. 2019).

2.5.1. Methods of biochar production

Pyrolysis is the main step of producing biochar. There are different types of pyrolyzing techniques which largely influence the final produce. The different methods are described briefly hereafter.

Slow pyrolysis produces high yields of biochar. It involves several key steps: Firstly, raw materials or feedstock for production are ground and sieved to sizes smaller than 2 mm. Then they are cleaned by removing soil and dust. Finally, those are air-dried to maintain consistent weight and pyrolyzed with temperature and duration varying on basis of feedstock type. The actual pyrolysis process occurs at temperatures between 300 and 600 °C (Kim et al., 2020, Bandara et al., 2017). Fast pyrolysis is named so because of the speedy completion, characterized by its short residence time, high heating rate, and inert conditions (Ling et al., 2017). Additionally, the use of catalysts, such as zeolite-based materials, also enhance the quality of the biochar. Fast pyrolysis creates produces biochar with a well-developed pore structure thereby improving its performance. The method of co-pyrolysis involves pyrolyzing a mixture of two different raw materials simultaneously. Biochar produced in this method largely help to mitigate heavy metal pollution. By combining materials, the overall quality and environmental safety of the resulting biochar can be enhanced (Zhao et al., 2017). Use of Microwave radiation to heat materials, converting electromagnetic energy into thermal energy is found in microwave pyrolysis. This method offers uniform heating, cost-effectiveness, and enhanced and safety, monitoring, regulation making it a great alternative to traditional pyrolysis method. It typically uses a microwave oven, with key parameters being power output and frequency which is commonly set at 2.45 GHz (Akhil et al., 2021). The process occurs at

temperatures ranging from 400 to 600 °C. Rapidly heats low-grade feedstocks to produce high-quality biochar, with heating rates reaching thousands of degrees per second is done in Flash pyrolysis. When pyrolysis occurs in a vacuum oven, allowing for specific control over the process conditions it is called vacuum pyrolysis. Intermediate pyrolysis relies on three key factors, namely, pyrolysis temperature, vapor residence time, and feedstock residence time and it performs better compared to other conventional methods. It is conducted at moderate temperatures (450 to 550 °C).
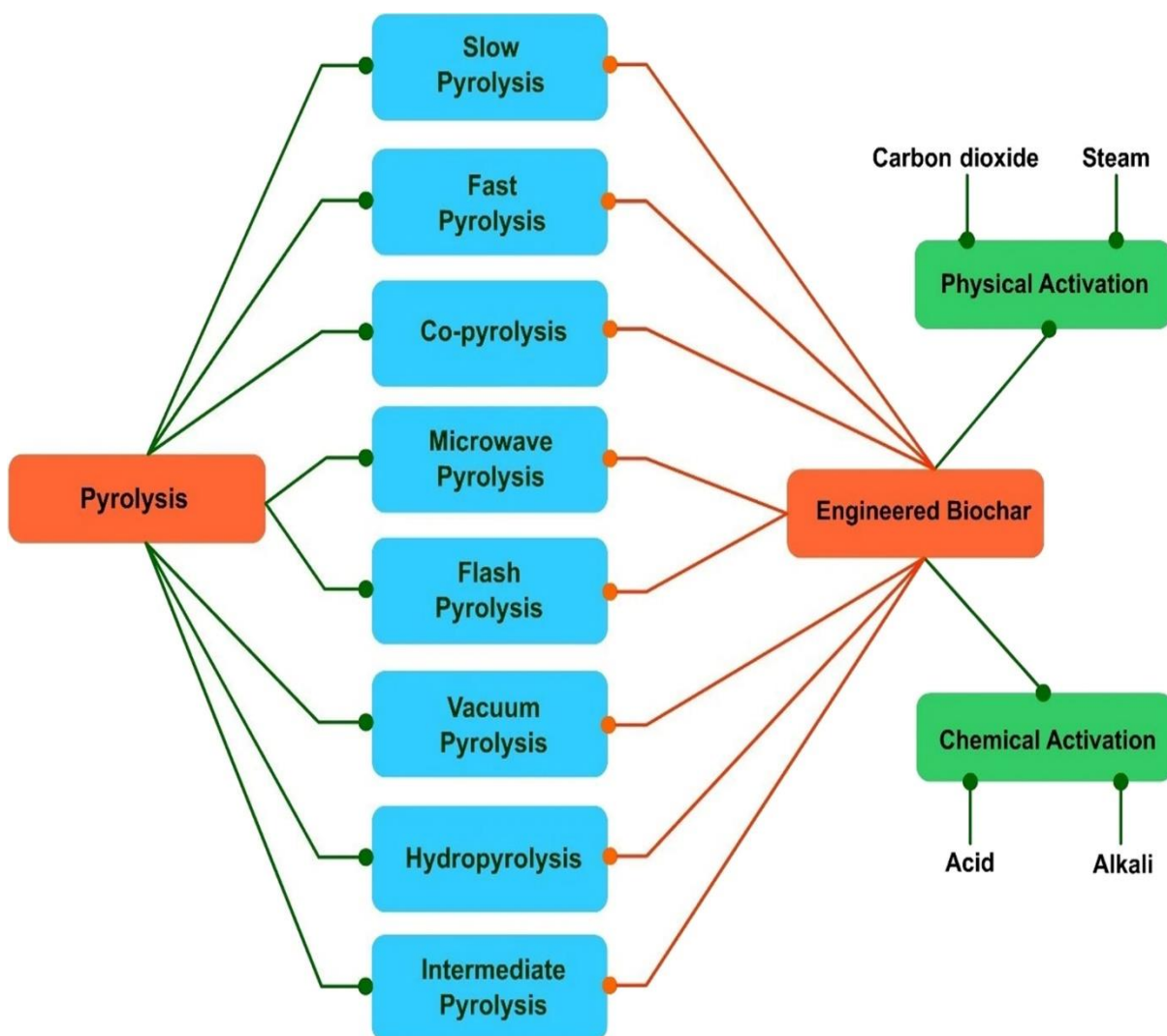
Figure 5: Production of pristine biochar and its further modification to exfoliated biochars

Source: Akhil et al., 2021

2.5.2. Exfoliation methods of biochar

Exfoliating biochar means the process of expanding the native structure to enhance its adsorption by increasing the surface area and porosity, etc. This is achieved through diverse methods- physical, chemical, and engineering techniques mainly. Physical exfoliation includes treatments like steam or carbon dioxide for activation, which create pores by gasifying the carbon and altering internal structure. Chemical exfoliation involves acids and alkalis or often both, to remove non-volatile substances and tar, thus creating new pores and improving or adding surface functional groups. Engineering methods are also largely used, such as ultrasonication and ball milling. These modern-day methods, further refine the properties of native biochar by breaking the previous structure into small, finer particles, which thus help in improving dispersion, and simultaneously increase formation of the nanopores. Each of these methods, mentioned above affects the properties of native biochar differently, but the ultimate goal is to increase its sorption efficiency for removal of contaminants in environment.

2.5.3. Key features of biochar composition

Biochar's effectiveness in removing heavy metals and its various applications depend on multiple key characteristics. Higher surface area enhances biochar's capacity to adsorb, improving its pollutant removal ability. This surface area is influenced by factors such as temperature, duration, and feedstock type. Study by Son et al. (2018) depicted that biochar with increased surface area can significantly increase removal of copper compared to previous methods. The pore properties of biochar are affected by temperature. For instance, earlier study by Yakout et al in 2017 depicted how increasing the temperature from 400 to 500 °C raises the total pore volume from 0.5 to 0.6 cc/g due to pore melting. Biochar can be acidic or basic, with diverse pH values from 4.0 to 12.0. Higher pyrolysis temperatures tend to increase the pH towards basic range. As higher pH levels generate more negative charges, its performance

increases. Biochar mainly contains carbon, hydrogen, and oxygen, with minute amounts of sulphur and nitrogen. Pyrolysis temperatures increase carbon from the release of volatiles but lower the H and O from the weaker bonds breaking (Yakout 2017; Jia et al. 2018). This results from combined action of multiple processes like polymerization, aromatization, and carbonization. The stability of biochar is influenced by the feedstock used, pyrolysis method, and pH conditions (Akhil et al., 2021). Higher pyrolysis temperatures generally enhance biochar's stability. Overall, these factors determine the efficiency and applications of biochar.

2.5.4. Biochar in agriculture

Soil salinization is harmful crop growth as it increases the osmotic pressure of soil. This can be undone by biochar application. Biochar helps eliminate soil salinity and promotes plant growth on saline soils (Akhil et al.,2021). It improves the soil's physical and chemical properties and increases the adsorption capacity of soil, helping in better adsorption of nitrogen, phosphorus, potassium, and organic matter (Brassard et al. 2019; He et al. 2020a). Biochar also reduces the movement of pollutants (Huang et al. 2021).Studies have shown that biochar positively affects growth parameters (He et al. 2020a). Recent research, involving biochar from coconut husk in combination with manure inhibited nitrate leaching and reduce nitrifying bacteria during monsoons (Plaimart et al. 2020).

2.5.5. Biochar in pollution remediation

Biochar can effectively adsorb a wide range of pollutants, including heavy metals, antibiotics, endocrine-disrupting chemicals (EDCs0, and carbon dioxide. (Vieira et al. 2020; Bandara et al. 2020). This efficiency is regulated by the type of feedstock used, pyrolyzing temperature, its morphology, composition, porosity, and chemical attributes (Boostani et al. 2019). Modified biochar has been reported to effectively adsorb rare heavy metals like rhenium, cerium, and lanthanum also (Wang et al. 2016; Lou et al. 2018; Hu et al. 2019; Keshtkar et al. 2019). It has

also found its use in degrading antibiotics, either alone or in combination with materials like titanium dioxide TiO2 (Akhil et al., 2021). Studies have demonstrated significant removal efficiencies, such as 90% degradation of 2,4-dichlorophenol using eggshell-based biochar in sulfate radical-based processes (Liu et al. 2020c). Additionally, biochar combined with TiO2 has shown higher efficiency in removing dyes like methyl orange compared to TiO2 alone (Lu et al. 2019). Biochar has also been effective in capturing carbon dioxide in soils (Wang et al. 2020c; Xu et al. 2020) and reducing nitrous oxide emissions from bamboo-growing soils. Endocrine-disrupting chemicals, for example, 17β-estradiol was removed by potassium ferrite activated graphene-like biochar (Akhil et al.,2021).

Biochar is useful in wastewater treatment. Phosphorus recovery from agricultural wastewater can be done by modified biochar treated with Fe^{3+} or Ca^{2+} (Maroušek et al. 2020).It removed thallium from industrial wastewater. Textile manufacturing wastewater often contains dye pollutants. Biochar combined with photocatalysts, such as TiO2, has successfully degraded dyes like methylene blue as per Mudhoo et al. (2019).

Studies by Mukome et al. (2020) have investigated the use of biochar from different feedstocks for degrading petroleum hydrocarbons in crude oil-affected soils. Recent reports of biochar include its efficiency as a catalyst in biodiesel production. (Balajii and Niju 2019; Buentello-Montoya et al. 2020). Biochar also exhibits high electrical conductivity, making it valuable in the electrochemistry industry. It has been applied in energy storage devices, such as batteries, and also function as electrodes (Kalderis et al. 2020).

2.6. Eichhornia in pollution remediation

Water hyacinth or *Eichhornia crassipes* now called *Pontederia crassipes* is an aquatic plant originally indigenous to the Amazon Basin but it has spread globally. Its high growth rate and adaptability has contributed to its invasive nature. It is a free-floating, perennial aquatic plant

and has the ability to form dense mats that cover water bodies. Reaching heights of nearly three feet, these invaders can cause ecological and economic concerns (Galgali et al., 2023). Despite it being infamous as an invasive aquatic species, several recent studies have highlighted its potential in pollutant removal and treatment of wastewater.

Water hyacinth has become a significant tool in phytoremediation. This plant's extensive root system and prolific growth are key reasons behind its efficiency. Malik (2007) emphasized the plant's role as a biosorbent for toxic metals, other studies also gave indications metals like cadmium, zinc, and mercury in its root system (Rezania et al., 2015). The large surface area and the chelating properties of its tissues contribute to its efficiency in heavy metal removal. Several studies have reported of removing heavy metals like Cu, Zn, Ni, Pb and Cd using water hyacinth. In wastewater treatment, water hyacinth has crucial role. Valero et al. (2007) reported that it could significantly reduce solids, calcium, magnesium, and total hardness in swine wastewater. Jianbo et al. (2008) found that it effectively reduced chemical oxygen demand (COD) and excess nutrient in wastewater from farms rearing ducks. The plant has also been shown to remove up to 79% of total nitrogen and 69% of total in combination with duckweed (Tripathy & Upadhyay, 2003). This aquatic weed has been extensively used in removal of heavy metals, dyes, pharmaceuticals, potentially toxic elements, organic compounds like phenol, nitrogen, phosphorus etc. It has found ex tended application in biofuel industries as well. Treatment of wastewater from various industries, including sugar mills, tanneries, textile mills, paper and pulp industries etc have also been achieved (Galgali et al., 2023). It could be potentially used beyond pollution control also by processing it into various byproducts including animal feed, fish feed, compost, biogas etc (Rezania et al.,2015). In addition, it also has explored medicinal properties. Oudhia (1999) reviewed several traditional uses of the plant in treating various ailments. But very little literatures have explored its fluoride removal efficacy.

Despite its advantages, water hyacinth presents significant challenges too. Its rapid growth, large biomass causes ecological disruptions, obstructs waterways and impacts aquatic ecosystems (Gopal, 1987; Malik, 2007). It prevents sunlight and oxygen from penetrating the water, disturbing the photosynthesis and creates hypoxic conditions which causes death of fish and other aquatic organisms spoiling ecological balance (Galgali et al., 2023).Additionally it serves as a breeding ground for disease vectors such as mosquitoes. It also increases evapotranspiration, reducing the availability of irrigation waters in arid and semi-arid regions. It also blocks ship movement and disturbs fishing practices. While there are various existing control methods, including physical, chemical, and biological approaches, to manage its proliferation, each has limitations and drawbacks. Effective management of water hyacinth requires a integrated approach that is sustainable, cost-effectiveness and simultaneously uses its positive potentials. Exploring its potential as a biochar, also needs more attention.

2.7. Vermi-technology

Vermicomposting, is an advanced method for accelerating the decomposition of resistant organic matter. This technique is dependent on the symbiotic relationship between earthworms and microbes and is more effective than traditional composting methods (Piearce et al., 1990; Bouche, 1977; Bhattacharya and Kim, 2016). Besides turning waste into valuable fertilizers, it improves soil conditions, offering a cost-effective and environmentally friendly solution to waste management and soil fertility (Bhattacharya & Kim, 2016). Vermicomposting can enhance compost quality and adjust the carbon-to-nitrogen ratio (Tognetti et al., 2007). Earthworms also contribute to mucus, excretory products rich in nitrogen, enzymes etc improving quality of the compost (Hobson et al., 2005; Suthar, 2006). The end product of vermicomposting, is rich in essential nutrients like nitrogen, phosphorus, and potassium, and has huge potential a valuable soil amendment (Edwards et al., 1998; Kaushik et al., 2008).

Earthworms belong to the phylum Annelida. These invertebrates, which originated around 600 million years ago during the Pre-Cambrian era, are integral to various ecological processes and have been harnessed in vermi-technology for waste management and soil improvement. Aristotle famously described earthworms as "the intestine of earth and restoring agent of soil fertility," highlighting their crucial role in soil health and fertility. Earthworms thrive in moist, dark conditions and can significantly speed up composting by breaking down organic waste faster. They improve soil structure and nutrient status of soil and enhancing microbial activity (Singh and Suthar, 2008; Sinha et al., 2010). Their activities help maintain soil-water balance and improve soil structure as well. Earthworms can thrive in an extended temperatures range (5°C to 29°C), with optimal conditions being 20°C to 25°C and 60%-75% moisture content in vermi-bed. They have a high reproductive rate, with potential to multiply approximately 28 times within a span of six weeks (Sinha et al., 2010). They can house diverse microbial community in their gut. The gut dwellers include bacteria that enhance nutrient content and aid pollutant transformation during vermicomposting procedure (Hussain et al., 2016; Medina-Sauza et al., 2019). The earthworms process organic waste by grinding it in their gizzard and breaking it down within their gut (Sharma et al., 2005). Earthworms also contribute to soil sanitation by detoxifying heavy metals. They also reduce pathogen loads. Their chloragogenous tissue helps in metal detoxification through mechanisms like cation exchange and protein binding, which immobilizes harmful metals such as Cd, Cu, Mg, Zn, As (Stürzenbaum et al., 2013; Santana et al., 2019). The increased expression of metallothioneins and other metal-binding proteins in earthworms aids in this detoxification process (Goswami et al., 2016; Hussain et al., 2021).

Earthworms are classified based on their habitat and feeding habits. Bouche (1977) categorized them into epigeic (surface-dwelling), anecic (deep-burrowing), and endogeic (horizontal-burrowing) species. Lee (1995) further classified them based on their feeding strategies into

detritivores (litter feeders) and geophages (soil feeders). Epigeic earthworms, such as *Eisenia fetida, Eudrilus eugeniae,* and *Perionyx excavatus*, are particularly valued in vermicomposting due to their efficiency in decomposing organic waste. In contrast, endogeic and anecic species, like *Metaphire posthuma* and *Lampito mauritii*, are less commonly used in composting due to their different ecological roles (Ismail, 1997; Sahariah et al., 2015).

The efficiency of vermicomposting is examined through various quality control parameters of the finished product like its texture, odour, colour, bulk density, particle size, porosity, water holding capacity, and nutrient content (C:N ratio, nitrogen, phosphorus, potassium). Key benefits of vermitechnology include its cost effectiveness, low maintenance, speedy detoxification, and compost production suitable for agricultural use (Chang & Chen, 2010; Lim et al., 2011).Various industrial wastes, such as paper mill sludge and textile sludge etc have been successfully converted into vermicompost and has been demonstrated to enhance soil fertility (Ravindran et al., 2008; Das et al., 2016). However, there has been no research on using vermicomposting to process fluoride-conjugated biochar and also its subsequent use in agriculture.

2.8. Identifying Research Gaps, Defining Problem, Framing Solutions:

Fluorosis a global menace has equally affected India. More than twenty Indian states including Bihar, Rajasthan, Gujarat, Assam, Uttar Pradesh, Madhya Pradesh, Kerala, Karnataka, Jammu and Kashmir, Punjab, Orissa, West Bengal and Jharkhand come under the fluoride endemic belt. Extensive studies have been conducted in other states including studies by Ali et al., (2018), Adimalla & Venkatayogi, (2018); Singh et al., (2018), Gantaint et al., (2022) etc. But Jharkhand continues to lack enough supporting studies for establishing its fluoride contamination status. Former studies across the nation have reported instances where dissolution of micaceous mineral and silicate weathering as the chief source of F^- in

groundwater in areas with granitic rocks (Giri et al., 2023). There also have been reports which established that upon interaction of alkaline waters with rocks containing fluoride-bearing minerals, the dissolution of fluoride begins along with precipitation of calcite (Adimalla & Qian, 2019a, 2019b; Kashyap et al., 2021). Additionally, some other reports have highlighted secondary sources of fluoride pollution from agricultural and industrial activities (Gantait et al., 2022). A key section of the Great Mica belt known for its high-class mica, encompasses the state of Jharkhand with active mica mining prevalent in the Giridih district (Chakraborty et al., 2024). During the processing of raw mica blocks, the waste generated is often not disposed of properly which might lead to a potentially F^- contamination of groundwater table on seeping. Thus, the lack of studies on fluoride contamination in Jharkhand demands attention. Though sporadic fluoride contamination has been reported across the state and previous reports of the Central Ground Water Research Board (CGWB) have also shown elevated levels of F^- in different parts of the region, a detailed study on the contributing factors to this sporadic distribution is yet to be addressed. There exists a substantial gap in understanding the overall extent, sources, and hydrogeochemical facies of F^- contamination in the state. A comprehensive and systematic study at the regional level (Dhanbad district, Jharkhand, India) and at the mica mining regions (Khijri, Tisri) has thus been targeted in this research, aiming to explore the distribution, intensity, spread and dynamics of fluoride hydro-geochemistry in the area.

After this, the next gap that needs to be mended is to find out a cost-effective, environment-friendly, sustainable yet efficient adsorbent for removing fluoride from water. All existing defluorination methods have certain limitations. They often suffer from high operational and maintenance costs and generate sludge which are difficult to dispose. Although, biochars could be an alternative, availability of an easily available, cheap feedstock needs to be assured. Here, water-hyacinth being an unexplored alternative, to design an exfoliated biochar from this aquatic weed was targeted next. Thus, next major hypothesis of this study thus posits that

biochar derived from *Pontederia crassipes*, or water hyacinth, when exfoliated, can serve as an efficient, sustainable, and cost-effective sorbent for the removal of fluoride from water. This hypothesis is grounded in the need to address the limitations of conventional defluorination techniques and the potential of biochar, specifically from an abundant aquatic weed, to provide a viable solution to fluoride contamination in drinking water. While previous studies have demonstrated the successful removal of heavy metals such as Cd and Cr, as well as dyes like methylene blue, using water hyacinth-derived biochar, its potential for fluoride removal remains relatively unexplored to the best of our knowledge assuring the novelty (Fito et al., 2023).

The next gap that needs to be sealed is finding an efficient remedial technique which could successfully handle the waste generated from defluorination. Biochar being biodegradable, though are greener and eco-friendly adsorbents, they suffer from a potential drawback. If not disposed properly, pollutant laden biochar may pose serious threat and pollute further upon decomposition. Vermi remediation has proven efficiency in transforming toxicants to their benign forms. Given the extensive detoxification potential of vermicomposting besides its eco-friendly, low-cost nature, with an added advantage of enhancing nutrient bioavailability, it emerges as an interesting option and pushes us to assume it as a strong candidate for clean disposal of fluoride-laden biochar resulting from our experiments. To the best of our knowledge, no literature records an attempt to vermi-remediate spent fluoride saturated biochar. Our next hypothesis thus is to use vermi-technology to remediate spent fluoride laden biochar to a good quality compost.

 Finally, a toxicity assessment is crucial to evaluate the impact of the experimental compost materials when applied to agricultural fields as there are no prior experiments like this in

literatures so far. With this plan of research, we thus conducted our experiments to attain a cradle to grave transition.

2.9. Objectives of study:

1. To examine the spatial distribution of groundwater fluoride concentration in selected blocks of Jharkhand.

2. To decipher the underlying hydrogeochemistry behind the fluoride contamination.

3. To synthesise exfoliated biochar from various feedstocks like sugarcane bagasse, and water hyacinth and assess their fluoride removal efficiency

4. To create vermicompost from the spent fluoride- sorbed exfoliated biochar using *Eisenia foetida*

5. To evaluate the efficiency of produced vermicompost through field demonstration in tomato and rice

Methodology and Instrumentation

Chapter 3: Methodology and Instrumentation

3.1. Orientation of the work:

The present thesis enlightens the fluoride aquifer chemistry, the extent of fluoride contamination, the successful fluoride mitigation by an exfoliated biochar and finally, the agricultural prospects of using a compost prepared from vermi-remediation of spent fluoride laden biochar. To reach the goal, the entire work has been divided into four phases. This chapter gives a quick review of the experimental planning and procedures used to achieve success for the proposed aim of the study.

In the first phase, the first two objectives were taken care of simultaneously. The spatial distribution of groundwater fluoride concentration was examined for selected areas of Jharkhand and attempts were made to decipher the underlying geochemistry behind the contamination.

The second phase covers the third objective of research. It involved attempts to prepare an exfoliated biochar for fluoride removal. The biochar was then characterized, assessed for fluoride removal efficiency and the most efficient biochar (Water hyacinth-based acid exfoliated biochar) was studied to unveil the chemistry behind its adsorption potential.

The fourth objective was taken care of in the third phase. The epigeic earthworm *Eisenia fetida* was used to evaluate the potential of vermicomposting technology for converting hazardous fluoride saturated biochar into sanitized vermicompost with high nutrient value and low toxicity, thus providing a sustainable way of disposal of defluorination end products. The produced compost was analysed by constant monitoring of physico-chemical parameters and microbial activity in vermi-beds periodically.

In the final phase, in an attempt to meet the final objective, the vermicompost prepared consisting of various combinations of spent fluoride saturated biochar and cow dung (CD) were used in two distinct crop trials (Pot experiments in tomato and rice under field conditions). The agronomic and soil parameters in crops treated with experimental vermi-composts were compared against same from crops treated with recommended fertiliser doses to check the efficiency of the produced compost. Fluoride content in agricultural produces were also measured to ensure safety of consumption.

3.2. Deciphering the spatial distribution of fluoride contamination and exploring the underlying aquifer chemistry.

3.2.1. Study area selection and geomorphology

For this thesis, we have chosen two distinct regions in the state of Jharkhand based on existing literature and potential for groundwater fluoride contamination. Previous research by Thapa et al. (2019) highlighted alarmingly high levels of fluoride in drinking water in Gharbar village in Baliapur block, Dhanbad. However, after this, there have been no similar reports from nearby regions. This thus prompts us to select the Baliapur block of Dhanbad district as the primary study area and investigate whether the contamination is isolated or if it reflects broader regional fluoride pollution issues. This block-level study will help us determine the scope of fluoride contamination in this area and identify possible causes if it is indeed sporadic in nature.

The second study area we chose is located within a mica mining region- the Tisri and Gawan blocks of Giridih district. This selection has been driven by concerns about the potential impacts of mining activities in the region on aquifer chemistry, and whether it could contribute to fluoride pollution. Micas are great source of fluoride as stated by previous literatures therefore can be a potential pollution source. By studying this area, we aim to understand how mining practices might impact levels of fluoride ion in the groundwater.

In summary, our selection of two different sampling locations, allows us the privilege of exploring both known instances of F⁻ contamination and potential new sources, providing a comprehensive view of fluoride pollution dynamics in Jharkhand.

3.2.1.1. Dhanbad District: Study location and geomorphology

Topographically, Dhanbad, is located midway between the Damodar basin, in the Chhota Nagpur plateau and shares borders with districts of Purulia and Paschim Bardhhaman, in West Bengal. Baliapur is one of the ten blocks in the district with a total area of 151.17 km^2 extending between 23° 40′ 30″ N to 23° 49′ 43″ N latitudes and 86° 26′ 6″ E to 86° 31′ 26″E longitudes (Fig. 6). Groundwater from twenty Gram Panchayats of Baliapur block, Dhanbad district and surrounding areas have been extensively sampled in this study. The average topographic elevation of the area is 150 metres above mean sea level. Barakar and Damodar are the major drainages of the region with general slope being southwards. It enjoys a humid subtropical climate to tropical wet and dry climate. The average summer and winter temperatures here are about 44.5 °C and 20 °C respectively with an average annual rainfall of 1300 mm (Thapa et al., 2019). Rainfed rice (*Oryza sativa L.*) is the principal crop grown in Kharif season due to unavailability of irrigation facilities during other seasons. The fairly copious rain in monsoons and high summer temperature lead to the formation of infertile lateritic type of soil in the district. Ultisols (red and yellow soils) and Alfisols (Red sandy soils) constitute the major soil types. Dissected pediments, denudational hills and piedmont alluvium occupy the most of this area and Chhota Nagpur Gneissic Complex (Archean to Proterozoic age)formed of quartz-biotite, granite gneiss, hornblende gneiss, felspathic gneiss, augen gneiss schist, amphibolite, phyllite makes the principal aquifer. Within this complex, the groundwater mobility and storage depend on the abundantly present fissures, fractures, weathered rocks etc. Ground water occurs under phreatic/ unconfined to semi-confined conditions presented by weathered granite-

gneiss zone (CGWB, 2021; CGWB, 2022). These rocks contribute to the abundance of fluoride bearing minerals in the region. In deep seated fractures, with no connection to the top weathered zone, water is found in semi-confined to confined conditions (Patolia and Sinha, 2017; Thapa et al., 2019).
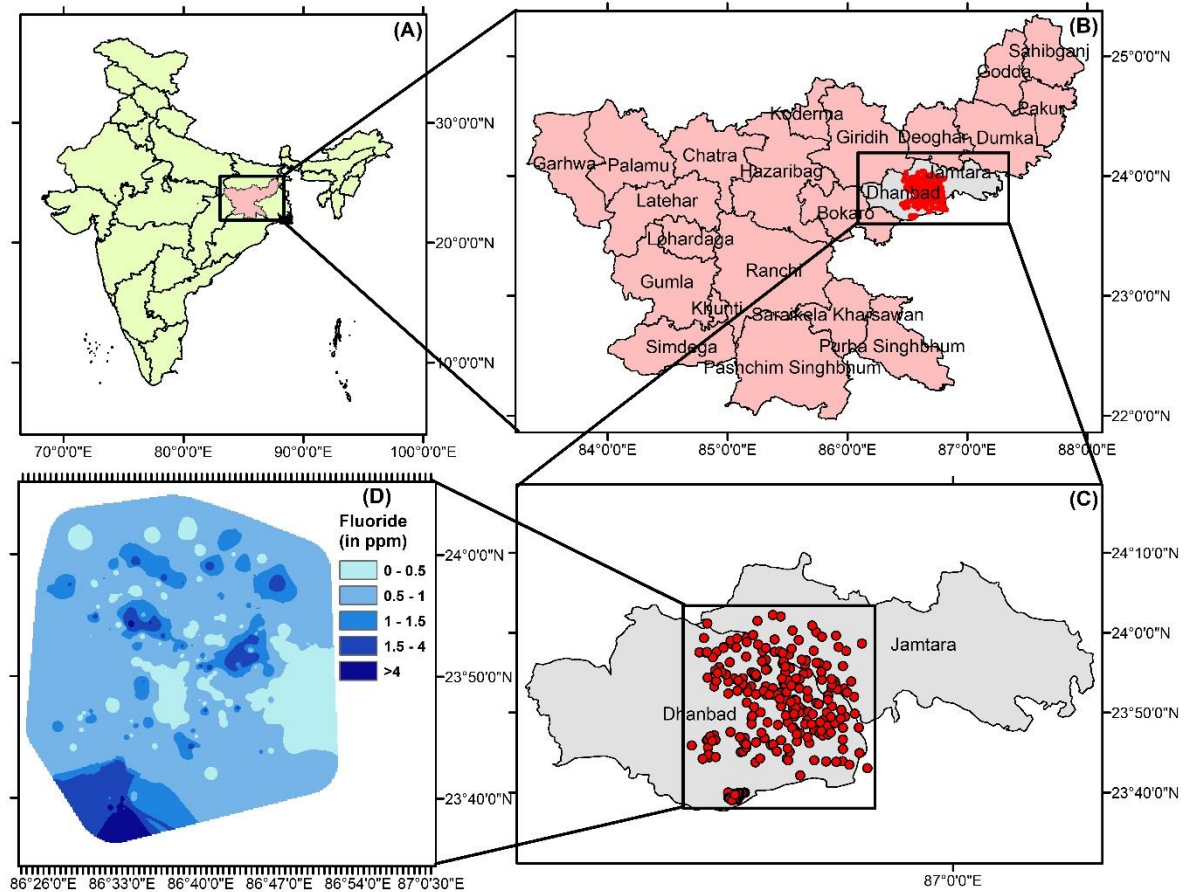
Figure. 6. Study area map of groundwater collection in and around Baliapur block, Dhanbad district of Jharkhand (B), India (A). The majority of the samples were collected from twenty Gram Panchayats of Baliapur block, Dhanbad (C). A spatial distribution map (D) of fluoride concentration was prepared using the inverse distance weighting (IDW) interpolation method, where darker colours represent higher fluoride concentration.

Source: Nandi et al., 2024 a

3.2.1.2. Giridih District: Study location and geomorphology

Giridih district loacted in the central part of North Chhotanagpur Division shares its borders with Jamui and some region of Nawada district of Bihar to its north, while Dhanbad, Jamtara, and Deoghar districts of Jharkhand defines its eastern boundaries. To the south, it is bordered Bokaro and some part of Dhanbad district borders Giridih southwards, and by Hazaribag and Kodarma district on the western end. The abundance of hillocks in the area has earned this district its name. Two of its thirteen blocks, Tisri and Gawan, famous for its mica reserves have been selected for this study and areas near the mining zone have been sampled for groundwater. The extent of the sampled area lay between 24° 32′ 16″ N to 24° 34′ 27″ N latitudes and 86° 4′ 16″ E to 86° 7′ 15″E longitudes (Fig. 7). The mean elevation of the region is around 250 meters above the mean sea level. Sakri river drains the region. The region has three marked seasons, the scorching summer with temperature shooting up to 45°C in the month of May, the monsoon where the district receives maximum of 1300 mm rainfall and the pleasant winter. Alfisols, Ultisols and Entisols are the major types of soil in the area (CGWB, 2013, Nandi et al., 2024a). The district's oldest geological formation dates back the Archaean-age creating dense and solid crystalline metamorphics. Above this layer, lay rocks from the Proterozoic-era or the Chota Nagpur Granite Gneissic complex, made of biotite, quartz biotite, gneiss, granite gneiss, hornblende, schist etc. The top most covering is provided by lower Gondwana sedimentary rocks. The top layers lack natural openings and groundwater is found in the secondary spaces like fractures and joints. Structural disruption governs the flow of groundwater in the area. For areas with weathered mantle, it occurs in unconfined state and semi confinement to confinement is notice for deeper seated fissures. The post monsoon water level varies within 2- 5 m below the ground level (CGWB, 2013).
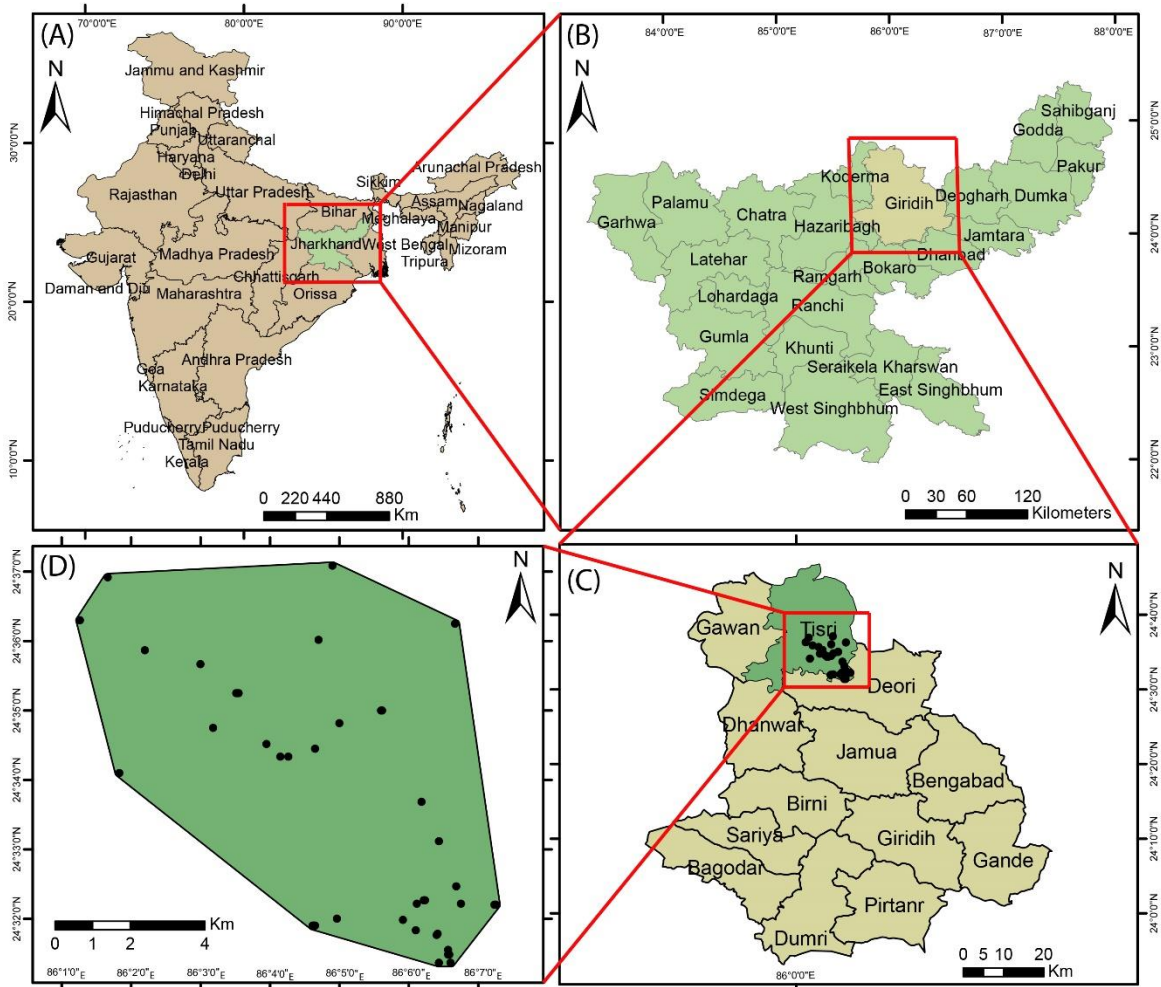
Figure 7. Study area map for groundwater collected in and around Tisri block (C) of Giridih district, of Jharkhand (B), India (A).

Source: Nandi et al., 2024 b

3.2.2. Sample collection and preservation

Groundwater samples (n = 283) were collected in total during the winter season (November-December) of 2021. A random sampling pattern was followed during collection of samples from 20 Gram Panchayats of Baliapur block, in Dhanbad district, Jharkhand, India

Similarly, a total of forty water samples were collected after the monsoons (September-October) of 2021, following a random sampling design from villages around the mica mining areas of Tisri block of Giridih district, Jharkhand, India.

For a better understanding of the sampling plan, grid maps was created for the entire blocks before sampling. The sampling points were not uniformly distant from each other but were decided based on the availability of existing pumps and wells. The sampling depth ranged between 2-10 m below ground level (bgl) for shallow tube wells and 100-120 m bgl for deep tube wells (bore wells) (CGWB, 2022). A minimum gap of 200 meters between two points were allowed. Samples were collected in 100ml airtight high-density polyethylene (HDPE) bottles in triplicates. The bottles were pre-cleaned by soaking in dilute HNO_3 overnight and thoroughly washing in distilled water to remove any traces of the acid. Samples were collected from wells, borewells and handpumps with varying depths. Handpumps were pumped and wells were purged for several minutes before collecting samples to remove stagnant water. The bottles were filled up to the neck and sealed with inner cap to avoid any air gap. Once sealed and labelled properly, the precise latitudinal and longitudinal coordinates of the sampling location were recorded using a handheld GPS meter. The collected samples were transported to the analytical laboratory keeping in ice baskets at the earliest and refrigerated at 4°C with addition of 0.1% v/v of concentrated nitric acid to one replicate of each sample bottle, as preservative for further analysis. All guidelines (APHA 2012) were maintained during the sampling to prevent any contamination. The water quality parameters of the collected samples considered for the study were namely pH, total dissolved solids (TDS), electrical conductivity (EC), total hardness (TH), K^+, Na^+, Mg^{2+}, Ca^{2+}, SO_4^{2-}, Cl^-, HCO_3^-, NO_3^- and F^-.

3.2.3. Studying abundance and spatial distribution of Fluoride

The concentration of F^- was detected using an ion selective electrode (Orion star a 214 pH/ISE Benchtop meter, Thermo Scientific, USA). Total Ionic Strength Adjustment Buffer TISAB-III in the ratio 1:10 (TISAB: sample; Orion® 940911) was added to each sample and standard 100 ppm fluoride solution (Orion® 940907) was used for preparing calibration standards. All

readings were taken in triplicates and the average of those were noted. Based on the same, the groundwater samples were categorised as 'Safe' (F^-<1.5 ppm) and 'Unsafe' (F^->1.5 ppm) (WHO, 2011) for samples collected in Baliapur block. The collected samples were grouped as 'Fluoride contaminated' (FC, F^- ion >1.5 ppm) and 'Fluoride uncontaminated' (FU, F^- ion <1.5 ppm).

A spatial distribution map of fluoride contamination was created using the Inverse Distance Weightage or IDW method. The IDW interpolation is a geospatial statistical technique where concentration of unsampled locations can be explained based on the weighted average of known sampling points in the neighbourhood. A point closest to the point to be predicted is assigned the maximum weight and weightage decreases with increasing distance from the point of interest, that is assigned weights are inversely proportional to the power of distance and hence the name. IDW prediction surface map of Fluoride distribution was prepared using ArcMap 10.2, ESRI with graduated colour symbols; where lighter colour represents lower fluoride concentrations (Mondal et al., 2020).

3.2.4. Ion analysis, quality control (QC) and quality assurance

The samples from each group were tested for major ions in laboratory as per standard methods (APHA 2012) and previous research works (Kouser et al., 2022; Gantait et al., 2022). Analytical grade chemicals and double distilled water were used throughout the study. Glassware used for the experiments were pre-soaked in 10% HNO_3 solution (Merck, India) overnight and rinsed thrice with double distilled water before use. All instruments used for the study were calibrated regularly. In-situ physical parameters like EC, pH etc. were measured with the help of a digital pH meter-335 (Systronics, India) and EC meter-307 (Systronics, India). Na^+, K^+ and Ca^{2+} were determined through flame photometry (Type 130, Systronics, India). The mother stock for the standard preparations (1000ppm) of the same were prepared

using sodium chloride (NaCl), potassium chloride (KCl) and calcium chloride (CaCl$_2$) salts (Merck, India). Mg^{2+}, was determined by Atomic Absorption Spectrophotometry (AAS-816, Systronics, India) and standard stock solution of 1000 ppm (Sigma-Aldrich grade) was used for preparing calibration standards. An 1ml aliquot of 0.1% Lanthanum chloride was added to 10 ml of each sample (previously acidified with 1% HNO$_3$) prior to magnesium analysis. The same was maintained for preparing the standard solutions. The flame type was Air-Acetylene with a lowest detection limit of 0.001 ppm. This was additionally done to avoid any interferences from phosphorus, aluminium, titanium etc. The standard argentometric titration method using silver nitrate (Merck, India) and potassium chromate (Merck, India) indicator was used to determine Cl$^-$. Available sulphur as SO$_4^{2-}$ was used by standard turbidimetric procedure in a UV-Vis spectrophotometer (Type 117, Systronics, India). HCO$_3^-$ ions was measured using titrimetric method involving methyl orange, phenolphthalein indicator and sulphuric acid (Merck, India). Fluoride (F$^-$) and NO$_3^-$ was measured using ion selective electrodes (Orion star a 214 pH/ISE Benchtop meter, Serial no:X49554, Software version: 3.04, Thermo Scientific, USA). Nitrogen Interference Supressor Solution (NISS, Orion® 930710) and Nitrate standard of 1000 ppm (Orion® 920707, Thermo Scientific, USA) was used. After initial calibration for all experiments, a continuous calibration verification (CCV) was done after every 10 samples with known spiked solutions to assure the reliability. To ascertain the precision of the ionic measurements carried out, the ionic balance equation (IBE) or charge balance equation (CBE) was calculated by equation below . The value for the same being within the desirable limit of ±10% (Thapa et al., 2019), the calculations were found to be precise. Total dissolved solid (TDS) and the total hardness or TH were evaluated using formulas as per previous literatures.

$$IBE/CBE = \frac{\sum cations - \sum anions}{\sum cations + \sum anions} \times 100$$

$$TH = 2.5 \times Ca^{2+} + 4.1 \times Mg^{2+}$$

$$TDS = EC \times 0.65$$

3.2.5. Deciphering the hydrochemistry from ionic abundance studies

Relationships amongst the major cations and anions as observed in both groups (Safe -Unsafe and FC-FU) were represented as bivariate scatter plots (Nasher and Ahmed, 2021). Pipers trilinear diagram was used to understand the water type and dominance of ions. Gibbs diagram was used to identify the natural processes and mechanisms responsible for regulating the ionic abundance in water samples (Kouser et al., 2022; Onipe et al., 2021). Spearman's correlation analysis was carried out to explore the pattern of the interrelationship between various water quality parameters (Gantait et al., 2022). Saturation indices were calculated for each group considering the mean values for all parameters from each group using software Visual MINTEQ 3.1 (Bhattacharyya et al., 2011; Gantait et al., 2022; Thapa et al., 2019). A PCA biplot constructed in this study helps to reduce the dimensionality of the study data (Batabyal et al., 2017).

3.2.6. Calculating Irrigation indices

Several irrigation indices, namely, residual sodium carbonate (RSC), sodium absorption ratio (SAR), percent sodium (%Na), Kelly's ratio (KR), magnesium hazard (MH), permeability index (PI) and total hardness (TH) were calculated using the formulas listed in Table 1 (Rao et al.,2021; Rawat et al., 2018). Spatial distribution maps using the IDW method were created for the better visualisation of the classifications generated against analysed irrigation indices, for samples collected in the study area. The Doneen diagram, Wilcox diagram and USSL diagrams were also plotted.

Table 1. Equations describing TH, TDS and the different irrigation indices used in this study. All ion concentrations were expressed in milli-equivalent/litre (meq/l)

Irrigation index	Equation
Sodium Absorption Ratio (SAR)	$SAR = \dfrac{Na^+}{\sqrt{\dfrac{Ca^{2+}+Mg^{2+}}{2}}}$
Percent Sodium (%Na)	$\%Na = \dfrac{Na^+}{Ca^{2+}+Mg^{2+}+Na^++K^+} \times 100$
Residual Sodium Carbonate (RSC)	$RSC = (HCO_3^{2-} + CO_3^{2-}) - (Ca^{2+} + Mg^{2+})$
Kelly's ratio (KR)	$KR = \dfrac{Na^+}{Ca^{2+}+Mg^{2+}}$
Permeability Index (PI)	$PI = \dfrac{Na^+ + \sqrt{HCO_3^-}}{Ca^{2+} + Mg^{2+}} \times 100$
Magnesium Hazard (MH)	$MH = \dfrac{Mg^{2+}}{Ca^{2+}+Mg^{2+}} \times 100$
Total Hardness (TH)	$TH = 2.5 \times Ca^{2+} + 4.1 \times Mg^{2+}$
Total Dissolved Solids (TDS)	$TDS = EC \times 0.65$

3.2.7. Water Quality Index (WQI)

Water quality index (WQI) can estimate the suitability of groundwater for drinking purposes, at a particular location, at a given point of time, by measuring the qualitative nature of water with a single number based on the water quality parameters. It is easily usable by public (Adimalla et al., 2019; Ravindra et al., 2022). For the calculation of WQI for drinking purposes, the standards set by WHO 2011 and BIS 2012 are considered. Weighted arithmetical index method is used to calculate the WQI. Here, 12 water quality parameters had been taken into account for the calculation, namely pH, TDS, TH, K^+, Na^+, Mg^{2+}, Ca^{2+}, SO_4^{2-}, Cl^-, HCO_3^-, NO_3^- and F^- (Gantait et al., 2022). The unit weights (W_i) for each of these parameters were calculated and used for the study (Table 2) to calculate WQI with the help of equations below.

Table 2. Unit weight of water quality parameters

used in this study calculated from BIS standards

Parameters	Unit weight (W_i)
pH	0.089
TDS	0.001
Na^+	0.003
K^+	0.076
Ca^{2+}	0.010
Mg^{2+}	0.025
Cl^-	0.003
SO_4^{2-}	0.0038
HCO_3^-	0.002
NO_3^-	0.016
F^-	0.762
TH	0.003
ΣW_i	1.00

$$WQI = \sum_{i=1}^{n} \frac{W_i Q_i}{W_i}$$

Where, Q_i = quality rating of ith parameter and W_i= unit weight of ith parameter

$$Q_i = \frac{V_o - V_i}{V_s - V_i} \times 100$$

Where, V_o = observed value, V_i= ideal value of ith parameter for a particular sample (for pH = 7.0 and 0 for other parameters) and V_s = standard value of the ith parameter

$$W_i = \frac{K}{S_i}$$

Where, K = relative constant and S_i = standard value of the ith parameter

$$K = \frac{1}{\sum_{i=1}^{n}\frac{1}{S_i}}$$

Based on these calculated WQI values, drinking water samples were classified into five classes, viz; Class-I or Excellent (<50), Class-II or Good (50–100), Class-III or Poor (100-200), Class-IV or Very poor (200-300) and Class-V or Unsuitable (>300) (Ganguli et al., 2022).

3.2.8. Human Health Risk Assessment (HHRA)

Human health is largely reactive any contaminant present in the surrounding and it might pose a severe threat to their health. To estimate the health hazards, the human health risk assessment (HHRA) can be performed based on the guidelines provided by United States Environmental Protection Agency (USEPA) and are being undertaken by researchers worldwide (Ghahramani et al., 2020; Liu et al., 2022; Panaskar et al., 2016; Taloor et al., 2022).

The health risk can be classified into two classes, i.e., the non-cancer or non-carcinogenic risk and cancer or carcinogenic risk. In this study, the non-carcinogenic risks posed by the contaminant Fluoride has been addressed (Adimalla et al., 2019; Das et al., 2020; Rao et al., 2021). The calculated hazard quotient (HQ) for a parameter may vary with the routes of exposure (oral, dermal and inhalation) and the target group considered for the calculation. For this current study, the oral route and two age groups were considered; children below age of 12 years and adults (≥12 years).

The estimated daily intake (EDI) or chronic daily intake (CDI) of the afore mentioned age groups to fluoride (F⁻) in groundwater was assessed using equation below.

$$CDI = \frac{C * ED * IR * EF}{BW * AT}$$

Where, chronic daily intake for fluoride via oral route (CDI) is expressed in unit mg/kg/ day; C is content of F in the tested groundwater samples; ED is exposure duration (adults: 58 years, children: 12 years) (Hanse et al., 2019); IR is daily ingestion rate (adults: 4 L/day, children: 1.5 L/day) (Kadam et al., 2021); EF stands for exposure frequency (365 days/year for all individuals); BW reflects body weight (adults: 57.5 kgs, children:15 kgs) (Hanse et al., 2019; Mukate et al., 2022); and AT stands for average lifetime (ED*EF).

Next, the hazard quotient (HQ) for F- was determined from the ratio of CDI values to its reference dose (RfD) 0.06 for each age group separately (Das et al., 2020; Kadam et al., 2021).

$$HQ = \frac{CDI}{R_f D}$$

The HQ for children ($HQ_{Children}$) and adult (HQ_{Adult}) in both 'safe' and 'unsafe' groups were calculated separately and compared with each other to evaluate the human health risk. A value greater than 1 for the same makes the sample unsuitable for use and poses subsequent non carcinogenic threats to human health (Adimalla et al., 2019; Kadam et al., 2021).

3.2.9. Multi Criteria Decision Making model: Fuzzy TOPSIS

The Dhanbad district study site having a good number of samples was suitable for applying different machine learning models. Fuzzy TOPSIS was used particularly in this location for better understanding. A great solution for multi criteria decision making is provided by Fuzzy-TOPSIS (Technique for Ordering Preference by Similarity to Ideal Solution). It is potent in alleviating ambiguities resulting from different results achieved by different assessments. In this study it has been used to rank the two study groups based on their overall performances in different fields like WQI, HRA and irrigation indices It is calculated as follows;

Step 1: construction of decision matrix (D_{ij})

Step 2: normalising the constructed matrix ($D_{ij}{}^*$)

$$D_{ij}^* = \frac{D_{ij}}{\sqrt{\sum_{j=1}^{n} D_{ij}}}$$

Where i= no of criteria compared, j= alternatives available

Step 3: Weight calculation of each criterion

$$\omega = \frac{\omega_i^*}{\sum_{i=1}^{n} \omega_i^*} \quad \text{where, } \sum_{k=1}^{s} \omega_i = 1, \omega_k \in [0,1]$$

Step 4: Evaluating the normalised matrix.

$$D_{ij} = D_{ij} \times \omega_i$$

Step 5: Finding the ideal best and ideal worst values

M^+= Max (x_{ij}) for beneficial criterion, M^+= Min (x_{ij}) for non-beneficial criterion

M^-= Min (x_{ij}) beneficial criterion and M^-= Max (x_{ij}) for non-beneficial criterion

Where j = 1,2, …., n

Step 6: Calculating Euclidean distance of each alternative from the ideal best ($d_i{}^+$) and ideal worst ($d_i{}^-$) solutions

Step 7: Calculation of performance score

$$P_i = \frac{d_i^-}{d_i^+ + d_i^-}$$

Where, p_i is the performance score.

Step 8: Allotment of ranks based on the performance scores.

The alternative with the highest performance score is ranked first or is considered closest to the ideal solution.

3.2.10. Statistical analysis and machine learning models

All the univariate descriptors (i.e., major ions concentrations in water, irrigation indices and health risk assessment) were tested for normality distribution and homogeneity of variances using Shapiro-Wilk and Bartlett's test respectively. If normality assumptions were not met, the Welch t-test was conducted to analyse variations among the safe and unsafe groups of water. Spearman correlation analysis was performed using the 'GGally' package in R to visualize the relationships between the concentrations of fluoride and other ions in the water samples. The relationships between the safe and unsafe group of water were visualized using a Principal component analysis (PCA)-biplot using 'Factoextra' and 'FactoMineR' packages (Peter et al., 2022).

The Dhanbad district study site having a good number of samples was suitable for applying different machine learning models. Additionally, in this study site, three machine learning approaches, namely LR, CART and RF were used to predict the fluoride contamination using other ions present in the water samples using 'modelr', 'rpart' and 'caret' packages respectively. Machine learning have been used successfully in several groundwater contamination studies (Lopez et al., 2020; Nafouanti et al., 2021). The classification tree was visualized using the 'rpart.plot' package. 80% of the entire dataset were used for training phase while the remaining 20% constituted the testing phase for each model. The receiver operating characteristic (ROC) area under the curve (AUC) was taken into consideration to evaluate the best fit model. All of the graphs used in this study were prepared using the 'ggplot2' package in R.

3.2.11. Self-Organising Maps

Although the second study location could not benefit from application of LR, ML and CART due to its small sample size, another interesting approach was selected for this region for getting proper predictive technologies- the SOM. The Self Organising Maps (SOM) or the Kohonen maps are a form of artificial neural network, consists of adjacently connected neighbourhood neurons (Kohonen, 2001). The appropriate number of neurons or m is determined by a heuristic equation (= 5 × √n), where 'n' is the number of input parameters. Initialization of map prototype was determined based on PCA method. Finally, processed training data, initial map prototype along with other parameters were used for training using '*som*' function of '*kohonen*' package in R. Quality of the map was determined using quantization error, percentage of explained variance, topographic error and Kaski-Lagus error.

To identify the superclass, we used clustering algorithm following k-medians approach (PAM). The optimum number of super-classes were determined using both scree plot and Silhouette methods respectively. Finally, observations cloud map and respective parameters using bar plots within the SOM map were visualized to understand their relationships.

3.2.12. Sobol Sensitivity Index

The samples from the Giridih district or the mica mining regions were additionally subjected to a sensitivity index study. The sensitivity indices by Sobol (Sobol, 2001) in combination with Monte Carlo approach has been widely used to find the most important input parameters and perform the evaluation of their contributions towards the variances of the outcome. The ratio of a particular variable to total variables are referred to as the sensitivity indices (SIs). The very first type of SI , called the First Order Sensitivity Index (FOSI), is nothing but the impact of a particular input parameter on variance of the model outcome. The SOSI or Second Order Sensitivity Index arises from the interaction between parameters and ultimately, the overall

impact of interaction among all parameters is described by the TOSI or Overall Order Sensitivity Index. Any value exceeding 0.1 is termed 'highly sensitive'. For values lying between 0.01-0.1, the term 'sensitive' is used and 'insensitive' are ones with sensitivity indices value being lower than 0.01. These three types advocate for the significantly relevant, prominent and inputs with no response respectively (Mukherjee and Singh, 2021). This analysis was performed using the 'EnvStats', EnviroPRA' ,'sensobol', 'EnviroPRA', 'ggplot2' packages in R software.

3.3. Exploring targeted fluoride removal with exfoliated biochar

3.3.1. Preparation of biochar

The feedstock used for this study, were sugarcane bagasse and common water hyacinth. *Pontederia crassipes* or water hyacinth was collected from the local ponds around Panchra, Birbhum, (23.76° N and 87.316° E)West Bengal, India. It was sun-dried for 15 days to reduce the water content substantially, ground to a powder form using a high-speed mixer grinder and pyrolyzed to make native biochar (NB). The bagasse collected from a local vendor were cleaned, washed and sun dried too. The pyrolysis was conducted in a muffle furnace for two hours, at 500°C temperature with at constant heating rate 25°C/ min (Fito et al., 2023, Ganguly et al., 2020). The initial pH of the native biochar produced from pyrolysis was recorded at 9.96 (Water hyacinth) and 10.4 (sugarcane bagasse) To exfoliate this native biochar, chemical modification was carried out using 2(M) HNO_3 (Merck, Purity: 69%) and 2(M) NaOH for both biomass through the contact process in an orbital shaker at 120 rpm for 24 hours (Ahmad et al. 2022; Qin et al., 2023; Kasera et al., 2022.). Acid modification of the biochar helps in generating more oxygen bearing functional groups like hydroxyl and carboxyl groups. Additionally, it might also help in generating positive charges on the biochar surface which in turn would work to improve electrostatic attractions between the negatively charged target ion

(F⁻) and cationic charges on surface of the biochar(Xu et al., 2020). Alkaline modification also alters the functional groups altering its adsorption potential. To wash of the traces of excess acid and alkali from the biochar, repeated distilled water washes were applied until the pH of the wash water reached a near neutral range (6-6.5) followed by overnight heating at 100 °C in a hot air oven (Systronics, India), for further use. Once dried, the powdered exfoliated biochar or EB was kept in airtight containers for future uses. The final pH of the acid exfoliated biochar after exfoliation were noted for 1: 10 biochar to water ratio (digital pH meter-335, Systronics, India).

3.3.2. Selection of biochar

Four different exfoliated biochar were prepared initially -the sugarcane bagasse acid exfoliated biochar (SB -Acid), sugarcane bagasse alkali exfoliated biochar (SB-Alkali), water hyacinth acid exfoliated biochar (WH-acid) and water hyacinth alkali exfoliated biochar (WH-Alkali). They were tested for their fluoride removal potentials. 10 ppm fluoride solutions were exposed to these biochar in 10gms/ltr dosage for 3 hours. At the end of three hours the remaining fluoride in the solution was estimated using a fluoride ion selective electrode. As, no significant removal was noticed by SB -Acid, SB-Alkali and WH-Alkali biochar, they were discarded. WH-Acid showing more than 98% removal was further explored in the study. Henceforth, all experiments were limited to WH-Acid and it has been referred to as EB from this point onwards.

3.3.3. Materials, reagents used & quality control

Unless otherwise mentioned, double distilled water was used during chemical preparation, pH adjustment and other necessary operations throughout this experiment. Aqueous solutions with a fluoride concentration of 1000 mg L^{-1} (adsorbate) were prepared from ammonium fluoride (NH$_4$F) salt (Merck, India). All required working solutions were then derived from this stock.

Measurement of fluoride (F⁻) concentration was taken using ion selective electrode (Orion star a 214 pH/ISE Benchtop meter, Serial no:X49554, Software version: 3.04, Thermo Scientific, USA). Prior to each measurement, an initial calibration for the meter was performed, and after every 10 samples measured, a continuous calibration verification (CCV) was carried out for enhanced reliability. Total Ionic Strength Adjustment Buffer (TISAB-III) was added to every sample in the ratio 1:10 (TISAB: sample; Orion® 940911) and standard F⁻ solution (Orion® 940907, 100 mg L⁻¹) was used as the mother stock for standard preparation. All readings were noted as the mean of triplicates.

3.3.4. The batch adsorption study

The batch adsorption study was designed to investigate the impact of varying adsorbent doses (3, 6.5, 10 g L⁻¹), adsorbate concentrations (10, 20 and 30 mg L⁻¹), pH of adsorbate (4, 6 and 8), temperature (20°C, 30°C and 40°C) on fluoride removal efficiency over four-time intervals (1, 2, 3 and 4 hours) keeping other parameters constant. The adsorbate solutions were prepared from mixing ammonium fluoride salt (Merck, India) in distilled water, and they were adjusted to the desired pH using 0.1 N HCl/ NaOH. The experiments were conducted in a BOD incubator shaker at 150 rpm. At each time interval, samples were centrifuged at 10,000 rpm for 10 mins to precipitate the biochar from the adsorbate solution and tested for fluoride ion concentration as mentioned earlier. The removal percentage was calculated following equation as mentioned below.

$$\%Removal = \frac{C_i - C_f}{C_i} * 100$$

Where C_i and C_f are the initial and final concentrations of the fluoride solution respectively.

3.3.5. Statistical optimization using response surface methodology

Response surface methodology (RSM) was used for the optimization of parameters influencing fluoride removal efficiency. This approach constructs empirical models, identifying the individual and interactive effects of the most significant parameters, resulting in an accurate and optimized operational process (Banerjee et al., 2016a). RSM based on the Box-Behnken design matrix has been used for optimization analysis. Initially, a second-order polynomial model was used to fit the observation as mentioned below.

$$Y = \beta_0 + \sum \beta_i x_i + \sum \beta_{ii} x_{ii}^2 + \sum \beta_{ij} x_i x_j$$

Where Y is the response variable i.e. the F$^-$ removal capacity of biochar, β_0 is the intercept; β_i is the ith linear coefficient of the input parameter x_i; β_{ii} is the ith quadratic coefficient of the input parameter x_{ii}; β_{ij} is the different interaction coefficient between input parameter x_i and x_j. The model was further simplified based on the statistical significance of each parameter. The goodness-of-fit of the model was determined using both multiple and adjusted R^2. The predicted fluoride removal % by the model was also compared against the removal under experimental conditions. Musa et al., 2024; Banerjee et al., 2017; Banerjee et al., 2016b and many others have widely used this method in prior studies with efficient model performances.

3.3.6. Adsorption kinetics

Different kinetic models were studied to define the reaction kinetics of adsorption process, namely, linear forms of pseudo-first-order (PFO) and pseudo-second-order (PSO) models. According to Lagergren (1898), in PFO the reaction rate depends only on one of the components. It is based on the concentration of the adsorbate for single adsorbate systems. The mechanism here involves a process of diffusion which serves as the rate limiting step and follows physisorption (Agbovi and Wilson, 2021).

$$\ln(q_e - q_t) = lnq_e - k_1 t$$

Where, q_t= adsorption capacity (mg g^{-1}) at time t, q_e= adsorption capacity (mg g^{-1}) at equilibrium and k_1=equilibrium rate constant (min^{-1})

On contrary, it is found from reports by Ho and McKay (1998), PSO is laid on the assumption that chemisorption serves for the rate limiting stage. Here, unlike PFO, the rate of reaction depends on the adsorption capacity instead of adsorbate concentrations (Sahoo and Prelot, 2020).

$$t/q_t = (1/k_2)(1/q_e^2) + 1/q_e$$

Where, k_2=equilibrium rate constant for second order (min^{-1}).

3.3.7. Adsorption isotherms

For the present study, different isotherm models namely, Langmuir, Freundlich, Temkin Elovich and BET isotherms were studied to assess the interaction between the water hyacinth biochar molecules and the fluoride ions.

3.3.7.1. Langmuir isotherm

Langmuir isotherm model speaks for the homogenous distribution of active sites on the adsorbent surface and physical adsorption with high energy of sorption for solutions with high concentrations (Langmuir, 1918; Ganguly et al., 2020; Charan et al., 2024). Four different linear forms of the isotherm, first, second, third and fourth were tested for the best fit in the study.

$$\frac{C_e}{Q_e} = \left(\frac{C_e}{Q_m}\right) + \left(\frac{1}{K_l Q_m}\right) \qquad \text{(first form)}$$

$$\frac{Q_e}{C_e} = (K_L Q_m - K_L Q_e) \qquad \text{(second form)}$$

$$\frac{1}{Q_e} = \left(\frac{1}{K_L Q_m}\right)\left(\frac{1}{C_e}\right) + \left(\frac{1}{Q_m}\right) \qquad \text{(third form)}$$

$$Q_e = Q_m - \left(\frac{1}{K_L}\right)\left(\frac{Q_e}{C_e}\right) \qquad \text{(fourth form)}$$

Here, C_e Concentration of fluoride at equilibrium (mg L^{-1})

Q_e Adsorption capacity at equilibrium (mg g^{-1})

Q_m=Maximum monolayer coverage (mg g^{-1});

K_L= Langmuir isotherm constant (L mg^{-1})

The K_L value which is related to the adsorption capacity shares correlation with porosity and surface area of the adsorbent. The dimensionless constant named R_L or the separation factor can be calculated from the R_L value.

$$R_L = \frac{1}{1+K_L C_o}$$

Where, C_0 = initial adsorbate concentration (mg g^{-1});

R_L>1 signifies an unfavourable adsorption, R_L=1 shows a linear adsorption, 0<R_L<1 speaks of favourable and R_L=0 of irreversible adsorption conditions (Ayawei et al., 2017, Charan et al., 2024).

3.3.7.2. Freundlich isotherm

The Freundlich isotherm, developed by Freundlich (1906), brings forth a concept of multilayer adsorption and shows the physicochemical adsorption on layers of heterogeneous nature (Wang and Guo, 2023). In simpler terms, it applies to biosorption in heterogenous systems where

molecular interactions occur. In its equation (provided below), 'n' or the heterogeneity factor acts as an indicator of the characteristics of adsorption. A value of n greater than 1 signifies adsorption in cooperative manner (Musa et al., 2024). When, 1/n is unity, it becomes a linear model and irreversible in nature, $0 < 1/n < 1$ means a spontaneous adsorption process and a value of $1/n > 1$ makes the process difficult to proceed (Zhang e t al.,2019).

$$\log Q_e = \log K_F + \left(\frac{1}{n}\right) \log C_e$$

Where, C_e = Concentration of sorbate at equilibrium (mg L^{-1})

Q_e =Adsorption capacity at equilibrium (mg g^{-1})

K_F = constant for Freundlich isotherm (L mg^{-1})

1/n = heterogeneity factor

3.3.7.3. Temkin isotherm

Adsorption involving intermolecular attractions within adsorbate-adsorbents complexes and heat of adsorption is represented by the Temkin isotherm model (Temkin, 1941; Ganguly et al., 2020; Musa et al., 2024). The Temkin isotherm has been represented by following equation (Musa et al., 2024; Benmessaoud et al., 2020).

$$Q_e = B_T \ln C_e + B_T \ln K_T$$

Where, Q_e =Adsorption capacity at equilibrium (mg g^{-1}),

C_e = Concentration of sorbate at equilibrium (mg L^{-1})

B_T = Adsorption coefficient of heat of adsorbent (J mol^{-1})

3.3.7.4. Elovich isotherm

As per the Elovich isotherm model by Elovich and Larinov (1962), the sites of adsorption increase exponentially with chemical reactions during the adsorption process (Batool et al., 2018) This model is based on a kinetic principle which implicates adsorption in multiple layers (Benmessaoud et al., 2020) and can be expressed by following equation.

$$\ln\frac{Q_e}{C_e} = \ln K_E Q_{mE} - \frac{Q_e}{Q_{mE}}$$

Here, Q_e =Adsorption capacity at equilibrium (mg g^{-1}),

C_e = Concentration of sorbate at equilibrium (mg L^{-1})

K_E = Elovich equilibrium constant (L mg^{-1}) and

Q_{mE} = Elovich maximum adsorption capacity (mg g^{-1}).

3.3.7.5. Brunauer Emmet and Teller (BET) isotherm

BET isotherm developed by Brunauer et al. (1938) is widely used for multi-layer adsorptions. It is most often used for determining the multi-layer adsorption process of gas systems, but can also be used for solid-liquid ones. It assumes a process of physical adsorption and establishes the binding between layers under the influence of charges of surrounding molecules (Charan et al., 2024). According to this, the initial layer adsorbed, acts a surface for further adsorption and it can be expressed as equation 13 (Paixão et al., 2022).

$$Q_e = \frac{Q_{BET} K_{BET} C_e}{(1 - K_u C_e)(1 - K_u C_e + K_{BET} C_e)}$$

Where, Q_{BET} =adsorption capacity for first layer (mg g^{-1}),

K_{BET}= Equilibrium constant for first layer (L mg^{-1}) and,

K_u = Adsorption equilibrium constant for upper layers (L mg^{-1}).

3.3.8. Deciphering the morphological characteristics of biochar

3.3.8.1. Estimation of pore size and surface area using BET analysis

Surface properties of the native and chemically exfoliated biochar BET surface area, pore volume and pore size) were assessed (ASiQwin™ ,Quantachrome Instruments version 5.21) and compared to prove evidences for exfoliation.

3.3.8.2. Field emission scanning electron microscopic analysis (FESEM) coupled Energy-dispersive X-ray spectroscopy (EDS)

The changes in the surface of the chemically exfoliated adsorbent upon biosorption were studied with the help of field emission scanning electron microscopic analysis or FESEM (Model: SU8010, Hitachi, Japan). When coupled to Energy-dispersive X-ray spectroscopy or EDS, variations in elemental peaks were noted to find differences in compositions of the biochar after and before fluoride adsorption (EDS, INCA 250, UK).

3.3.8.3. Fourier transform infrared spectroscopy (FTIR)

The changes in presence of the surface-active functional groups of the biosorbent was monitored using FTIR method. The resulting spectra of biosorbent in its native, chemically exfoliated and fluoride saturated forms were noted within wavenumber range of 400-4000cm^{-1}. A Shimadzu, Model: IRPrestige-21 FT-IR Spectrometer was used for the study.

3.3.9. Statistical analysis for Biochar characterisation

The comparison of fluoride removal efficiency across different dosages of the adsorbent, concentrations of the adsorbate, pH of the adsorbate, and surrounding temperature over time

was analysed using repeated measures of ANOVA. The mean comparison test was conducted using the Student-Newman-Keuls (SNK) test. For this analysis, the '*agricolae*' package was employed in the R statistical software (Version R-4.3.2) (de Mendiburu., 2019). The '*ggplot2*' package was utilized to visualize the fluoride removal percentage across these parameters over time using group bar plots (Wickham., 2011). Response surface methodology (RSM) using Box-Behnken design was performed using the '*rsm*' package in R (Lenth et al., 2015). The optimized model was then used to visualize the relationship between these influencing parameters through colour-gradient contour plots.

The "PUPAIM" (version 0.3.1) package in R software was used for finding the best fit model for our study (Ostan et al., 2022). The "PUPAK" (Version 0.1.1) package in R software was used for finding the best fit kinetic model for our study (Magalong et al., 2022). The accuracy for each of the models were tallied based on the linear regression coefficient values (R^2). comparing the theoretical value of adsorption capacity obtained from the batch adsorption studies.

3.4. Vermi-remediation of fluoride saturated biochar

3.4.1. Procurement of cow dung, Fluoride saturated biochar (FSB), and earthworm species

Urine-free cow dung (CD) used in this experiment was obtained from a local cowshed of Giridih. 40 to 50 days old ciliated adult epigeic species of earthworm *Eisenia fetida*, weighing approximately 200-300 mg were procured from institutional vermiculture unit at Giridih, Jharkhand. FSB was prepared by incubating prepared exfoliated biochar (acid treated water hyacinth biochar) with fluoride solution (60ppm) at 10gms/ltr biochar dose for 24 hours at 30°C with continuous shaking for allowing complete adsorption of fluoride ions into micro/ meso porous structures of biochar. After the procedure, the fluoride-saturated biochar was

recovered by filtration, dried at 60°C, overnight and sieved well to remove clots. This prepared FSB was mixed with collected cow dung in two different ratios- 1:1 or equal parts of CD and FSB (V1) and1:2 or one part FSB to two parts CD (V2) and left to settle down for 10 days. Finally, epigeic earthworms *Eisenia fetida* were introduced to these respective vermibeds @ 10 worms/ Kg substrates, and they were subjected to vermicomposting. Another vermicompost (V3) was prepared with only CD as a control for the experiment.

Round shaped, broad mouthed, perforated, properly washed mud vessels (0.80 m diameter and 0.5 m height) were taken to monitor entire vermi-remediation study and used as vermiveds.4.5 kg of each mixture, in triplicates, was poured into the vessels inoculated with earthworm and incubated for 90 days. 50-60% moisture content was maintained in the vermibeds throughout the study. During the entire incubation period, the mixtures were churned daily for 30 minutes to maintain adequate aeration. The treatment combination used during entire vermi-conversion procedure are tabulated as follows (Table 3):

Table 3: Vermicompost combinations used in the study

Treatment	Combination used
V1	FSB:CD (1:1) + *Eisenia fetida* (10 worms/ Kg substrate (90 days)
V2	FSB:CD (1:2) + *Eisenia fetida* (10 worms/ Kg substrate (90 days)
V3	Only CD + *Eisenia fetida* (10 worms/ Kg substrate (90 days)

Samples were collected periodically from each replicate of each vermicompost combination at 0, 30, 60 and 90 days of the experiment and different parameters of the collected samples were analyzed as described in the upcoming section (Sahariah et al. 2015). An earthworm count was taken at each interval.

3.4.2. Analysing the earthworm growth, physico-chemical properties, microbial activity and fluoride fate

3.4.2.1. Earthworm count

Earthworms were handpicked and taken out periodically at interval of every 30 days and counted by the existing standardized protocol by Goswami et al., (2016). To sum up, feedstocks were poured out on aluminium trays, and earthworms in them were sieved via a mesh, handpicked, counted manually, and reintroduced to the native vessel along with the vermi-bed feedstock. Finally, at the 90th day the final product, the vermi-processed feedstock or the prepared compost was sieved and the final count of juvenile and adult earthworms were noted.

3.4.2.2. Evaluating the physico-chemical properties

The physico-chemical dynamics of vermi-feedstock were examined using the methods outlined by Page et al. (1982). Analysis was conducted for attributes such as pH, electrical conductivity (EC), easily mineralizable nitrogen (N), phosphorus (P), potassium (K), and total organic carbon (TOC) at initial and final day of vermicomposting. All measurements were carried out following standard quality control procedures and utilized analytical grade chemicals with a purity exceeding 90%. The methodology for each analysis has been outlined in following sections.

3.4.2.2.1. Evaluating pH

To determine the pH of the vermi-bed samples collected temporally, a 1:5 solution was created by combining 10 grams of the sample with 50 millilitres of distilled water. The mixture was stirred well intermittently with a pre washed glass rod for a period of 30 minutes to ensure uniform mixing. Then, the pH of the suspension was measured using a calibrated digital pH meter from Systronics, India (Page et al., 1982).

3.4.2.2.2. Evaluating EC

To measure the electrical conductivity (EC), a 1:5 solution was prepared by preparing as solution of 10 grams of the sample with 50 ml of distilled water in a properly washed, 100-ml glass beaker. The mixture was stirred uniformly with a glass rod initially and then it was allowed to stand for 30 minutes, unperturbed. The suspension was left as it is until all particles had fully settled down to the bottom. Finally, the electrical conductivity was recorded using a calibrated digital conductivity meter from Systronics, India (Model- Conductivity Meter 307) (Page et al., 1982).

3.4.2.2.3. Evaluating Total Organic Carbon (%) or TOC

Modified Walkley Black Method (1934) was followed for this analysis.

0.5 g of sample was taken in a prewashed conical flask of 250 ml, to which 10ml potassium dichromate (1N) was added quickly followed by 20ml of conc. H_2SO_4 (containing 1.25% Ag_2SO_4). After this, the flask was kept aside without being disturbed for about thirty minutes in a dark place. After completion of this dark incubation period, 30 ml of distilled water was added to it along with 1 ml of 85% orthophosphoric acid (H_3PO_4). Afterwards, 4-6 drops ferroin indicator was added to the flask just before final titration with 0.5 N ferrous ammonium

sulphate solution {FeSO$_4$. (NH$_4$)2SO$_4$.6H$_2$O}. The end point was obtained at reaching a baff pink colour.

Calculation:

Total organic carbon (%) = $Vk \times (1 - Vs/Vb) W \times Sk \times 0.3$

Where, Vk: Volume of K$_2$Cr$_2$O$_7$; Vs: Titrant reading; Vb: Blank reading; Sk: Strength of K$_2$Cr$_2$O$_7$ solution; W: Weight of sample

3.4.2.2.4. Evaluating mineralizable nitrogen (Avl N)

To begin, 2.5 g of air-dried sample was placed in a distillation tube of Kjeltech-N-analyzer. To it 40 ml 0.32% KMnO$_4$ solution, 40 ml of 2.5% NaOH solution, and 20 ml normal distilled water was added one after the other. Then the digestion tube was fitted well in the distillation unit for 6 minutes. Simultaneously, 20 ml of N/50 H$_2$SO$_4$ was taken in a 250ml conical flask. To it with 4 drops of methyl red indicator (0.3 g of bromocresol green + 0.2 g of methyl red dissolved in 400 ml of 90% ethanol) were added and the flask was kept for collecting distillate fitted to the ammonia exhaust pipe. After completion of distillation, N/50 NaOH was used to titrate the collected ammoniacal solution to original straw yellow colour. A blank without any sample was performed following the exact steps.

Calculation:

Total N mg/kg = W (Vb −Vs)×0.28×1000

Where, W= sample weight; Vb = Volume of N/50 NaOH consumed for blank titration; Vs = N/50 NaOH Volume consumed for sample titration.

3.4.2.2.5. **Evaluating available potassium (Avl K)**

The estimation was carried out using Flame photometric method. First, 50 ml of 1N ammonium acetate (CH$_3$COONH$_4$) pH adjusted to 7 by acetic acid, was taken in a conical flask containing 5 grams of desired sample. The flask was then left on a mechanical shaker for thirty minutes at room temperature. Afterwards, the supernatant was filtered by passing through Whatman No. 1 filter paper and the collected filtrate was examined in flame photometer for available potassium content. A calibration curve was prepared using standard solutions with known concentration of potassium before taking the readings.

Calculation: Available K (mg/kG) = derived concentration × dilution factor (if any)

3.4.2.2.6. **Evaluating available phosphorus (Avl P)**

The estimations of available phosphorus content were carried out following the study of Jackson (1973)

Depending on the pH and nature of samples, there exist two methods for available phosphorus determination. Namely, the Bray and Kurtz method (pH < 6) and the Olsen's Method is (pH> 6). The samples were processed in either of the two methods depending on their pH (Black, 1965)

3.4.2.3. **Evaluating the microbial dynamics**

3.4.2.3.1. Microbial Biomass Carbon (MBC)

Microbial biomass carbon (MBC) was analysed following Jenkinson, 1988.

Chloroform fumigation of experimental samples (soil and vermicompost) results in the death and subsequent lysis of microbial cells, which releases cellular cytoplasm into the solution.

Using this protocol, cell material can be extracted by 1 N KCl from the test samples. The microbial biomass carbon per gram of dry sample can be calculated by dividing the difference in ninhydrin-reactive nitrogen between fumigated and unfumigated samples by the calibration factor (KEC), which is 0.38.

Reagents required

1. Ninhydrin reagent : prepared fresh.0.8 g ninhydrin and 0.12 g hydrindantin were dissolved in 30 ml of dimethyl sulfoxide (DMSO).To it 10 ml lithium acetate buffer was added.

2. Lithium-Acetate Buffer: 168 g of lithium hydroxide (LiOH·H_2O) in 500 ml distilled water was stirred to dissolution. Then, add 293 ml of glacial acetic acid was added and volume was made up with distilled water. Then, the pH was adjusted to 5.2 with acetic acid or lithium hydroxide.

3. Ethanol-Water Solution

4. 2M KCl

5.Chloroform HPLC-grade

6. Nitrogen Standards: 47 milligrams was dissolved in 2M KCl and made up to 50 ml, resulting in a concentration of 100 μg N/ml. Then serial dilutions were made to achieve concentrations of 0, 2, 4, 8, and 16 μg N/ml with 2M KCl.

Procedure:

10 grams of moist sample is required for both fumigated and unfumigated carbon analysis.

Unfumigated Sample Analysis:

10 grams sample was taken in 250 ml conical flask and 40 ml 2M KCl was added to it followed by a shaking period of 30 mins on a mechanical shaker. Next, it was filtered and 1 ml of the filtrate was transferred to a fresh test tube. To it 0.5 ml of the freshly prepared ninhydrin reagent was added and the tubes were then placed in a hot boiling water bath for next 25 minutes. Once heated, the tubes were taken out and kept to cool down. 9.5 mL of ethanol-water solution was added to them in the next step and mixed thoroughly. A bluish colour was developed and the absorbance was measured at 570 nm using a spectrophotometer, keeping KCl solution as the blank. Here we get the values for ninhydrin reactive nitrogen.

Fumigated Soil Analysis:

10 grams of moist sample were placed in a vacuum desiccator containing 10 grams of soda lime and 25 ml chloroform along with glass boiling chips in a beaker. The desiccator was lined with wet tissues and was sealed shut after greasing to avoid air gaps. Evacuation of air was done using a motor run pump for 2 minutes until chloroform came to boiling. The desiccator was then placed in an incubator set at 25 C for the next 24 hours. Next day, the beaker with chloroform was removed by opening the desiccator, and repeated evacuations were carried out to remove any residual chloroform vapour from the desiccator chamber. Once it has been achieved, next the soil was transferred to a fresh 250-milliliter conical flask and the same extraction procedure was carried out like the unfumigated samples. All other steps were repeated hereafter.

Standard Curve:

Determination of Ninhydrin-Reactive Nitrogen was carried out using the leucine standards prepared and a calibration curve- absorbance versus nitrogen concentration was generated before calculation.

Calculations

MBC (µg/g) = [(Fumigated – Unfumigated concentration) × DF] Difference in oven-dry soil weight.

For example, if the moist weight is 10 grams and the oven-dry weight is 9.23 grams, the difference is 10 – 9.23 = 0.77 grams.

Microbial Biomass Carbon (µg/g oven-dry soil) = 31 × ninhydrin-reactive N

Microbial Biomass Nitrogen (µg/g oven-dry soil) = 4.6 × ninhydrin-reactive N

3.4.2.3.2. Basal Soil Respiration (BSR) and Substrate Induced Soil Respiration (SIR)

The procedure used for estimating soil respirations were reported by Alef in 1995 for soils and Epstein in 1997 for composts.

Principle:

The carbon dioxide evolved during the sample incubation within a closed system is estimated here by trapping it in a NaOH solution and subsequent titration by HCl.

Procedure outline:

10g moist sample (soil or compost) was weighed in incubation flasks in triplicates and 1ml 0.5 % glucose(for substrate induced respiration)/ 1ml of distilled water (for basal respiration) was added it.   5ml of 0.1 (M) NaOH solution was poured into the hanging tube placed within the closed system and the mouth of the flask was sealed properly to avoid any exchange of air. Blanks having no soils were also performed (triplicate) similarly. The flasks as well as the blank flasks were incubated at 22 degrees for 5 hours (SIR) and 24 hours (BSR)After completion of incubation, the hanging tubes with NaOH solution were taken out of the flask and the remaining

contents were then transferred to a fresh 100ml conical flask after rinsing with 5ml distilled water. Next 5ml BaCl2 solution and 3 drops phenolphthalein indicator solution were added to the flask. Finally, titration with 0.05 (M) HCl (drop wise) under continuous stirring was performed until the color turned colorless from the initial bright pink hue.

Calculation

mg CO_2/kg oven dry soil/hour = $\{(Vo - V)*S* 22*1000 \}/(M* d_{wt}* t)$

Here,

V_0= HCl (ml) required for titration of blank (mean of all three replicates);

V= HCl required for titrating sample (mean of all three replicates);

S = strength of HCl expressed in normality;

t= time for incubation expressed in hours;

M= sample weight in grams;

d_{wt} = oven dry weight for 1gm used sample in grams

and 22 comes from the equivalent weight of CO_2 is 22 of 1g sample.

3.4.2.3.3. Fluorescein diacetate hydrolysing activity ((Schnurer and Roswall 1982 ;Alef, 1995)

Principle

This method estimates fluorescein levels by measuring the fluorescein released after incubating soil with fluorescein diacetate (FDA) for 3 hours at 24°C.

Reagents

1. Sodium orthophosphate buffer (60mM, pH 7.6)- Adjusted to 7.6 with HCl

2. Acetone- analytical grade

3. Fluorescein diacetate solution (2mg/ml)

4. Fluorescein standard solution (5mg/ml) - stored at -20°C

Procedure

1 gram of sieved, field-moist soil was placed into a beaker. And 24 millilitres of sodium phosphate buffer and 1 millilitre of FDA solution (240 µg/ml) were added to it. The FDA solution was not added to the control flasks. All the beakers were then incubated on an incubator shaker set at 24°C for 3 hours. After incubation, 25 millilitres of analytical grade acetone were added to each vessel to aid the reaction termination. For control, the remaining 1 ml of FDA solution was added at this point, to replicate the reaction conditions to samples. The suspensions were then filtered and measured at 490 nm.

Standard Curve Preparation

Standard solutions were prepared by diluting the fluorescein stock solution to concentrations of 10, 20, 40, 80, 100, and 150 µg/ml. For each standard concentration, 1 millilitre of the diluted solution was added to 24 millilitres of sodium orthophosphate buffer and 25 millilitres of acetone. The solutions were then filtered to take readings at 490 nm. The absorbance values were plotted against the fluorescein concentrations to create a standard curve which was then used to determine the unknown fluorescein concentration in prepared soil samples.

It has to be ensured that all reagents are freshly prepared and stored properly. The experiment was conducted in triplicate sets for accuracy.

Calculation:

FDA activity (μg p-fluorescein released/g oven dry sample/h at 37^0C)

$$FDA = \frac{C * V}{d_{wt} * SW * T}$$

Where, C = fluorescein concentration measured (μg/ml filtrate);

d_{wt} = Oven dry weight/g of sample;

V = Total volume of the sample (50ml);

SW = weight of sample used (1g);

t = The incubation time (3hour).

3.4.2.3.4. Dehydrogenase activity or DGH (Casida et al., 1964)

Principle of the method:

The method is based on estimation of triphenyl formazan (TPF) released after the incubation of soil with triphenyl tetrazolium chloride (TTC) for 24hr at 37∘C.

Reagents

1. Calcium carbonate

2. 2,3,5, - triphenyl tetrazolium chloride or TTC

3. Triphenyl formazan or TPF

4. Methanol

Procedure

10g moist sample was placed in a 100 ml conical. A pinch of $CaCO_3$ about 0.1 gm was mixed to it thoroughly and it was kept aside overnight at room temperature. The following day, 1 ml of 3% TTC was added to it along with 2.5 ml of distilled water. The apparatus was sealed shut and incubated at 37◦C for 24 hours. The TPF which was by then extracted was filtered ot next day by repeated washes with methanol in a 100 ml. volumetric flask till the orangish red colour disappeared. The colour intensity was recorded as estimate of TPF produced at 485nm spectrophotometrically.

Calibration curve

A 100µg/ml mother stock of TPF was prepared in methanol and stored in freezer in dark. It was then diluted to working standards of 5, 10, 20, and 40 µg/ml using methanol. The absorbance of the individual dilution was noted and standard was prepared by taking OD.

Calculation:

Dehydrogenase activity (µg TPF/g oven dry sample/h at 37◦C) $= \frac{C*V}{d_{wt}*SW*T}$

Where, C = Measured concentration of p-nitrophenol (µg/ml filtrate);

dwt = Oven dry weight of 1g sample;

V = Total volume of sample (100ml);

SW = The weight of the sample used (10g);

t = The incubation time (1day).

3.4.2.4. Exploring the fate of Fluoride

One major question that could be faced was regarding the fate of fluoride in the vermi processed samples, whether there was any change in fluoride concentration during the experiment and if any change had occurred, what was the existent form of fluoride ion after vermicomposting. To find the answers, total fluoride content in samples were estimated at the zeroth and ninetieth day. The available forms of the ion were investigated using sequential fraction method. Both methods are underlined below.

3.4.2.4.1. Estimation of total fluoride -Alkali Fusion (McQuaker and Gurney, 1977)

McQuaker and Gurney described a method for the determination of total fluoride in 1977 which is also called the alkali fusion method. In this study, the total fluoride content in different samples, in this case, vermi samples of zero and ninety days, were estimated abiding the procedure described by them. Initially, the samples were dried in an hot air oven maintained at $50 \circ C$, ground to powder form in a mortar pestle, sieved through mesh and then 0.5 grams of the sample were placed in 50 ml nickel crucible. Moistened with 5 ml of distilled water, 6 ml of 17 M NaOH solution was added to it, and the mixture was heated in an oven set at $150°C$ for 1 hour. Following this, the samples were transferred to a muffle furnace preheated to $600°C$ and left for 30 minutes. After cooling to room temperature 20 ml distilled water was then added to the crucibles for dissolving the formed NaOH fusion cake and heated on a hot plate. The solutions were then transferred to pre washed 50 ml centrifuge tubes, pH adjusted to 8-8.5 using concentrated HCl, mixed well by shaking, centrifuged, and the supernatant was collected for analysing fluoride using a fluoride ion-selective electrode.

3.4.2.4.2. Sequential fractionation of Fluoride

Sequential extraction of species of fluoride were carried out following a procedure reported by Chen et al. (2013) and Moirana et al.,(2021).

2.5 g of dried soil sample was sieved using 0.2 mm mesh and placed in 50 ml centrifuge tubes. All the different fractions of fluoride were extracted then by adding 25 ml of the extracting solutions as summarized in table below (Table 4).

Table 4: Extraction processes of various species of fluoride

Fluoride fraction	Extractants used
Water-soluble fluoride (Ws-F)	Shaking for 30 min at 60 ∘C with 25 ml distilled water, centrifuged, supernatant collected
Exchangeable fluoride (Ex-F)	25 ml of 1mol/l $MgCl_2$ added to previous pelleted soil and shaking for 1 hour at 25 ∘C, centrifuged, supernatant collected
Fe/Mn bound fluoride (Fe/Mn-F)	25 ml of 0.04 mol/l NH4.HCl mixed and shaking for 1 hour at 60 ∘C, centrifuged, supernatant recovered
Organic matter bound fluoride (Or-F)	First step: 3 ml of 0.02 mol/l HNO3 + 10 ml 30 % H2O2 added to tubes with previous round soil pellet, mixed well Second step: 12 ml of 3.2 mol/l NH4 acetate added to same tube and put on shaker for 30 min at 25 ∘Cs
Residual fluoride (Res-F)	Total F from alkali fusion minus all above for species of fluoride summed together

Calculation:

Fluoride amount = C x (V/1000) x (1000/W)

Where; C = measured reading in mg/l

 V = Total volume

W = Sample weight

3.4.2.5. Statistical analysis of vermicomposting parameters

All the descriptors were tested for normality distribution and homogeneity of variances using Shapiro-Wilk and Bartlett's test respectively. If normality assumptions were not met, non-parametric Kruskal-wallis test was conducted to analyse variations among the groups. Post hoc Tukey tests were done. Two-way ANOVA was performed on meeting normality. All plots were generated using 'ggplot' package in R software.

3.5. Agronomic trials

The Green Revolution revolutionized agriculture by introducing modern techniques, high yielding varieties, chemical fertilisers, pesticides etc to increase the overall productivity. This lead to an increasing reliance on inorganic fertilizers. But this practices over the years has led to nutrient depletion in cultivable soils, reduced their fertility and added to environmental pollution due to agrochemicals getting accumulated and extensively harming soil health. This meant loss of beneficial microorganisms in rhizosphere and a steady reduction of soil biodiversity. Recently, a growing awareness has been noticed regarding the same and a growing need for sustainable and eco-friendly practices is being noticed. Besides, organic supplements, such as cow dung, farm yard manure etc vermicompost also offers a viable solution. Numerous reports have been published on their benefits. So, it was important to ascertain, that the vermicompost created in the course of this research from fluoride saturated biochar keeps up to the expectation. Thus, enhancement of soil organic carbon, available N, P, K content, the other physico-chemical parameters, microbial activity of the soils where this

compost was applied, needed to be recorded. Additionally, it was necessary to check if there were chances of any fluoride accumulation in edible plant parts of crops grown in biochar-vermi-amended soils.

Hence, Agronomic trials on two crops, namely, tomato and rice were conducted in the experimental farm of Indian Statistical Institute Giridih, Jharkhand, India.

3.5.1. Pot experiment on tomatoes

Tomato is one of the major cultivated crops worldwide and a model system to study plant response to the changing environmental conditions. In this study, pot experiments were carried out on tomatoes (*Solanum lycopersicum* L.) for two consecutive Rabi seasons of 2021-2022 and 2022-2023 at the Agricultural and Experimental Farm, Indian Statistical Institute, located in Giridih, Jharkhand in completely randomised design (CRD). Arka Vikas Variety of seeds marketed as Sonal 21 by Sardar Grow Seeds were used for both seasons. Temporal variation in soil microbial and enzymatic activities were recorded along with physico-chemical parameters of the soil were recorded in the study period along with the fluoride content in both crop and pot soil. Agronomic data was collected during harvesting of the fruit. Round mud vessels (1.0 m diameter and 0.75 m height) with soil holding capacity of 10 kgs, were used. Each vessel was filled up with soil which was amended with various experimental vermi-composted samples at the dose 10 tons per hectare. Pots for total of eight treatments (T1- T8) replicated thrice were prepared. Pre-germinated seedlings were transferred to them and were maintained for next 90 days in a net house. The treatment details are tabulated below (Table 5).

Physico-chemical analysis (pH, EC, TOC%, Available N,P,K) of soil parameters for each treatment pot were performed at 0 days and 90 days or post-harvesting. The microbial activity (MBC, BSR, SIR, FDA, DGH) in the pot soils were also checked temporally over the period at 0, 30, 60 and 90 days to study soil health. Soil total fluoride and fluoride fractionation studies

were also done at the start and end of the experiment (0 and 90 days). The harvested plant and the tomatoes produced were also checked for presence of fluoride toxicity and fluoride accumulation. Finally, the agronomic prospect was analysed by checking parameters like the lycopene content and total yield from different treatments with respect to the recommended fertiliser dose amended treatment.

Table 5: Treatments used in pot experiment of tomatoes to test efficacies of experimental vermicomposts.

Treatment	Details of amendments
T1	50% V1 +50% RDF
T2	100% V1 (10 t/ha)
T3	50% V2 +50% RDF
T4	100% V2 (10 t/ha)
T5	50% CD vermi (V3) +50% RDF
T6	100% Cow dung vermi (V3) (10 t/ha)
T7	Absolute Control (no amendment)
T8	100% RDF

Where RDF= Recommended dose of fertiliser

CD Vermi (V3)= Cow dung vermi

V1= vermicompost (Fluoride saturated biochar: Cow dung = 1:1)

V2= vermicompost (Fluoride saturated biochar: Cow dung = 1:2)

The methodology used for physicochemical, microbial and fluoride estimations involved in the study have been discussed in earlier sections (3.4.2.2 to 3.4.2.4). The statistical analysis were performed following methods mentioned in section 3.4.2.5.

3.5.2. Field trials on monsoonal rice (*Oryza sativa*)

Over half of the worldwide population depends on rice as a staple food. Our country India is a major producer of this essential crop. Due to such increased the demand for rice production, a greater reliance on inorganic fertilizers is observed for increasing productivity. In the lateritic zones, soils are often acidic, lack organic matter, and deficient in available nutrients. These soils are often gravelly, coarse-textured. Due to a lack of enough surface water sources, cultivation also depends solely on rainfall. Consequently, farmers have turned to excessive use of chemical fertilizers to enhance crop yields here. Therefore, in such a scenario, a need for an effective organic amendment is being created to counter these chemical fertilizer use. The vermicompost produced from sanitising fluoride saturated biochar in this research was thus tested for its efficiency.

In this study, field experiments were carried out on rice (*Oryza sativa*) for two consecutive Kharif seasons of 2021-2022 and 2022-2023 at the Agricultural and Experimental Farm, Indian Statistical Institute, located in Giridih, Jharkhand in a randomised block design (RBD). Sita variety of seeds were used for both seasons. Temporal variation in soil microbial and enzymatic activities were recorded along with physico-chemical parameters of the soil were recorded in the study period along with the fluoride content in both crop and field soil. Agronomic data was collected during harvesting of the fruit. Three plots of 1 square meter plots were allotted for each treatment out of ten (T1-T10) total treatments used in the study. The treatment details are tabulated below (Table 6).

A total of 30 plots were thus prepared. Each plot' soil was amended with various experimental vermi-composted samples at the dose 10 tons per hectare and left for 15 days at the beginning to allow mixing. The plots were irrigated as required. Pre-germinated seedlings were transplanted to them and were maintained for next 90 days. Fertilizer was applied at the time

Table 6: Treatments used in field experiment of rice to test efficacies of experimental vermicomposts.

Treatment	Details of amendments
T1	Absolute Control
T2	100% V1 (10 t/ha)
T3	50% V1 +50% RDF
T4	100% V2 (10 t/ha)
T5	50% V2 +50%RDF
T6	100% V3 (10 t/ha)
T7	50% V3 +50% RDF
T8	100% FSB (10 t/ha)
T9	50% FSB +50%RDF
T10	100% RDF

Where, FSB = fluoride saturated biochar

RDF = recommended dose of fertiliser

V1= vermicompost (Fluoride saturated biochar: Cow dung = 1:1)

V2= vermicompost (Fluoride saturated biochar: Cow dung = 1:2)

V3= cow dung vermi

of transplanting. During wet season cultivation, soil received applications of N fertiliser in three split doses (transplanting, tillering, panicle initiation) and complete application of P_2O_5, K_2O at transplanting date. All of the treatments were applied consistently using agronomic management practises including irrigation, pesticide application, etc. For every treatment during cultivation, other control managements including weeding, cleaning, and crop protection were also carefully maintained. soil samples required for analysis at different time

points of the study were collected by cutting a slice that covered a depth of 0 to 15 cm, sectioned in two, air dried one at room temperature, grinded it, sieved in two fractions with two mesh sizes of 2mm and 0.2mm, and then stored in plastic containers for further examination. The other section was maintained moist for performing microbial analysis. soil samples required for analysis at different time points of the study. Physicochemical attributes viz., pH, EC, TOC, and available NPK, fluoride content etc were analysed before and after cultivation (0 and 90 days), while microbial parameter viz, microbial biomass carbon, and soil respiration were carried out temporally viz, 0 days, 30 days, 60 days, and 90 days. Agronomic parameters were recorded during harvesting of crop. The produced grains were also tested for presence of any traces of fluoride.

The methodology used for physicochemical, microbial and fluoride estimations involved in the study have been discussed in earlier sections (3.4.2.2 to 3.4.2.4). The statistical analysis were performed following methods mentioned in section 3.4.2.5.

Results and Discussions

Chapter 4: Results and Discussions

4. Investigating the spatial distribution, impacts and contributing factors behind fluoride contamination of groundwater

As discussed in section 3.2.1, two sites were selected for this study and ground water water samples were collected from these two sites for further analysis. For the ease of understanding, the results of all the analysis performed will be discussed in separate sections for each study site (Dhanbad district study area- Section 4.1; Giridih district study area- Section 4.2).

4.1. Findings from the study area in Dhanbad district

The study plan ahead has been explained with a graphical abstract (Figure 8)
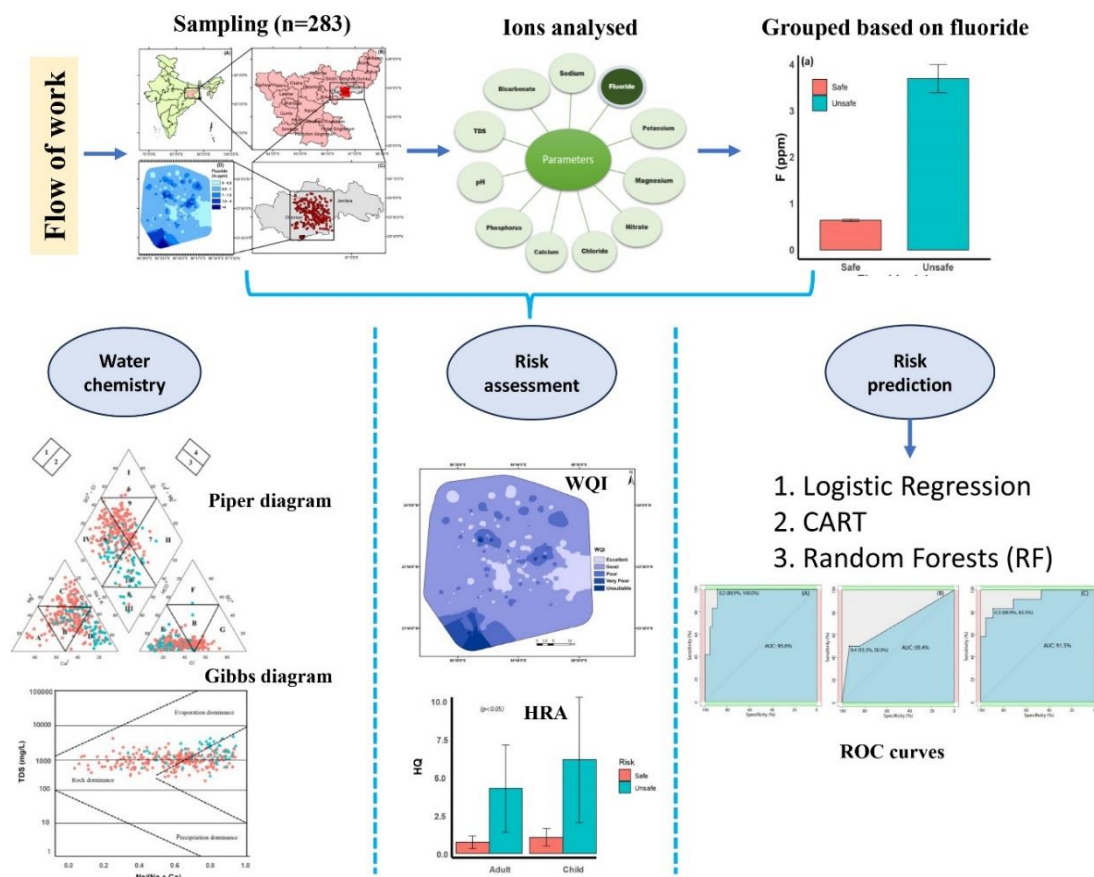
Figure 8: Graphical outline of workflow in analysis of samples from Dhanbad district

Source: Nandi et al., 2024a

4.1.1. Evaluating the ionic composition and physical parameters

4.1.1.1. Fluoride abundance and spatial distribution

Fluoride concentration in samples of the area ranged between 0.05 ppm to 15.3 ppm. Among 283 of the collected samples, 23.67% of samples ('Unsafe' group) were beyond the permissible limits of 1.5 ppm as set by BIS and WHO, while the remaining 217 samples were categorized as Safe (F^-<1.5 ppm). Mean fluoride concentration in Safe (0.63±0.02 ppm) and Unsafe (3.69 ± 0.3 ppm) groups showed significant (t-value = -10.04, p< 0.05) variations (Fig. 9a).

Fig. 6D shows the spatial distribution of fluoride contamination in the study area. Based on fluoride concentration, the study area was classified into five zones using graduated colour symbols. Among total, 29.69% of samples had fluoride concentration below 0.5 ppm, which might cause dental carries formation. While, in 46.64% of samples it ranges between 0.5-1.5 ppm, promoting good bone and teeth health. 16.25% of samples had Fluoride concentration between 1.5 to 4 ppm, which could result in the development of dental fluorosis. However, 7.42% of samples showed alarming levels of fluoride (>4 ppm) which might cause skeletal, crippling fluorosis and other adverse health issues in the population (Mridha et al., 2021; WHO, 2004).

4.1.1.2. Other major ions and physical parameters of groundwater

The pH is mostly affected by the composition of the underlying bedrock, the total residence time of water in the aquifers and the geogenic mineralogy (Gantait et al., 2022). The mean pH of the Safe (7.48 ± 0.02) and Unsafe (7.29 ± 0.06) groups showed statistically significant (t-value = 2.93, p <0.05) variation (Fig. 9b). However, most of the samples have pH within the permissible range as framed by WHO (2011) and BIS (2012). Electrical conductivity (EC) also showed significant (t-value = -5.78, p <0.05) variation among the Safe and Unsafe groups of

water. Almost 50.74% of water samples belonging to the Unsafe group had EC values beyond the permissible limit of 1500 µS (Khan et al., 2020). While only ~15.27% of Safe water crossed the threshold limit. The highest EC of 5600 µS was documented from the study area and also belongs to the Unsafe group of water. Total dissolved solids (TDS) largely affect the taste of water. While the acceptable limit of TDS ranges between 1500-2000 ppm according to WHO (2011) and BIS (2012); ~9.18% of total water samples were found to exceed the threshold limit of 1500 ppm. Average TDS in Safe and Unsafe group of water was found to be 711.53 ± 26.06 and 1241.79 ± 87.86 ppm respectively, showing significant (t-value = -5.78, p <0.05) variation among two groups (Fig. 9g). Higher TDS in unsafe water group might be from the improper sewage systems, agricultural run-offs and other anthropogenic sources (Gantait et al., 2022). TDS was categorized into four groups following Khan et al., (2020) on the basis of suitability of usage. According to this classification 23.5% of the total samples were best suited for drinking (<500 ppm), 54% were within the 'permissible for drinking' category (500-1000) and 22.5% were suitable to be used in agriculture (>1000 ppm). However, none of the samples fell in the category 'unfit' (>10000 ppm). The total hardness (TH) of the collected water samples largely depends on the abundance of calcium and magnesium ions in the area. While the BIS (2012) consider 500 ppm as a threshold limit of TH, ~40.6% of total water samples of the study area (19.45% of the Unsafe group, 47.2% of the Safe group) were unsafe for drinking. Significant (t-value = 6.52, p <0.05) variation in TH was observed among both groups (Safe and Unsafe) of water (Fig. 9h). Samples may also be categorised as 'soft' when TH <75 ppm (0.92% of Safe group), 'moderately hard' if TH ranges between 75-150 ppm (2.31% of Safe group, 11.9% of Unsafe group), 'hard' between 150-300 ppm of TH (12% and 32.83% of Safe and Unsafe group respectively), and 'very hard' with TH values exceeding 300 ppm. 84% of fluoride safe samples,55.35% of Unsafe ones were very hard (Khan et al., 2020). Hard water

might cause health issues and therefore the water samples from most of the region, remarkably the Safe group, were found unsuitable for daily use.

The cations (Ca^{2+}, Mg^{2+}, Na^+, K^+) in the collected samples have been measured to understand the basic cation chemistry of groundwater in the region of interest. The source of calcium in groundwater may be traced back to the underlying bedrock (shale, limestone etc.) laden with calcium-bearing minerals like amphibole and plagioclase (Kouser et al., 2022). The average Ca^{2+} concentration in Safe (86.53± 5.68 ppm) and Unsafe (45.88 ±3.63 ppm) water categories showed significant (t-value = 6.02, p <0.05) variation (Fig. 9c) indicating a markedly higher concentration of the ion in group Safe. Na^+ ions in groundwater come from continuous evaporation phenomenon, silicate weathering and cationic exchange processes (Kouser et al., 2022). The permissible limit for this ion is 200 ppm. The concentration for this ion exceeds this value for both groups and are hence considered unsuitable for drinking purposes in this regard. The mean of values for group Safe (144.25 ± 8.51) and Unsafe (203.16 ± 15.27) differ significantly from each other (Fig. 9e). The group Unsafe showed greater abundance of sodium hinting at silicate weathering (Gantait et al., 2022; Kouser et al., 2022). The presence of magnesium (Mg^{2+}) may be attributed to both geogenic (underlying bedrock) and anthropogenic sources (e.g., industries and mining) also showed significant (t-value =3.63, p <0.05) variation among Safe and Unsafe groups (Kouser et al., 2022). However, the average Mg^{2+} concentration was higher in the Safe (74.24 ± 2.5) category than Unsafe (56.03 ± 4.3). The concentration of potassium (K^+) in water samples ranged between 1 to 52.5 ppm. However, no significant variation was observed between the two groups. From the mean of these ion concentrations in both groups, the observed order of abundance of cations was $Na^+ > Mg^{2+} > Ca^{2+} > K^+$ for Unsafe and $Na^+ > Ca^{2+} > Mg^{2+} > K^+$ for Safe group.

Among anions other than fluoride, bicarbonate (HCO_3^-) shows the highest abundance followed by chloride (Cl^-), sulphate (SO_4^{2-}) and nitrate (NO_3^-) indicating carbonate dissolution as an underlying mechanism in the aquifer chemistry a potential reason for the alkalinity of samples (Gantait et al., 2022; Nasher and Ahmed, 2021). The mean value of HCO_3^- ion varies significantly (t-value = -5.27, p <0.05) across Safe (348.77±11.48) and Unsafe (601.98±46.6) groups of water (Fig. 9d). Higher abundances of HCO_3^- in Unsafe water also indicates silicate weathering (Nasher and Ahmed, 2021) besides carbonate dissolution (Zhang et al., 2020). It also agrees with the idea of a positive correlation of fluoride to HCO_3^- in prior studies (Gantait et al., 2022; Subramaniyan et al., 2022). Both Cl^- and SO_4^{2-} showed no significant difference in abundance across both water types. All the samples were within the permissible Cl^- limit of 600 ppm. However, only 0.3% of the samples exceeded the permissible SO_4^{2-} limits of 400 ppm. The NO_3^- concentration ranges between 1.23 to 151 ppm with no significant (t-value = 0.27, p = NS) differences between the two water types. Only ~9.8% of total samples fall beyond the permissible limits of 45 ppm as suggested by WHO (2011) and BIS (2012). A statistical summary of water quality parameters has been provided later (Table 7 and 8).

Table 7. Summary statistics for Group Unsafe (F->1.5 ppm)

Parameters	Mean	Standard Error	Median	Mode	Standard Deviation	Kurtosis	Skewness	Range	Minimum	Maximum
pH	7.30	0.06	7.12	6.93	0.50	0.13	0.76	2.20	6.55	8.75
F^-	3.69	0.30	3.01	4.80	2.48	8.50	2.64	13.73	1.57	15.30
Cl^-	143.59	17.20	85.20	42.60	140.79	3.95	1.98	639.00	28.40	667.40
HCO_3^-	601.99	46.60	463.60	439.20	381.47	0.18	0.99	1573.80	73.20	1647.00
Ca^{2+}	45.88	3.64	34.60	16.96	29.78	-0.80	0.59	123.73	5.99	129.71
NO_3^-	18.35	3.56	5.98	1.88	29.17	8.97	2.92	142.77	1.23	144.00
Na^{2+}	203.17	15.27	195.35	234.42	125.03	-0.53	0.67	443.45	44.93	488.38
SO_4^{2-}	51.99	6.75	40.21	35.54	55.25	34.56	5.26	430.12	1.81	431.93
K^+	3.15	0.20	3.00	3.00	1.62	-0.85	0.32	6.00	0.50	6.50
Mg^{2+}	56.04	4.30	48.63	20.87	35.21	2.10	1.32	178.30	0	178.30
EC	1.91	0.13	1.51	1.70	1.11	1.58	1.28	5.29	0.31	5.60
TDS	1241.79	87.86	981.50	1105.00	719.17	1.58	1.28	3438.50	201.50	3640.00
TH	344.47	19.94	315.16	275.60	163.25	-0.02	0.75	675.39	113.01	788.41

Table 8. Summary statistics for Group Safe (F⁻<1.5 ppm)

Parameters	Mean	Standard Error	Median	Mode	Standard Deviation	Kurtosis	Skewness	Range	Minimum	Maximum
pH	7.48	0.02	7.46	7.44	0.31	2.41	-0.40	2.41	6.03	8.44
F^-	0.63	0.02	0.60	1.01	0.35	-0.68	0.43	1.48	0.005	1.49
Cl^-	141.61	5.50	132.06	142.00	80.95	1.79	1.03	468.60	28.40	497.00
HCO_3^-	348.77	11.48	317.20	244.00	168.74	9.01	2.41	1244.40	73.20	1317.60
Ca^{2+}	86.53	5.68	76.50	84.81	83.58	12.35	3.06	596.68	1.99	598.68
NO_3^-	19.38	1.36	13.35	20.80	20.03	9.19	2.31	149.72	1.28	151.00
Na^+	144.25	8.51	96.69	117.21	125.17	15.03	3.21	928.89	8.79	937.68
SO_4^{2-}	40.42	1.47	38.09	34.88	21.69	2.65	1.11	132.76	2.90	135.67
K^+	3.19	0.30	2.00	1.00	4.53	65.58	6.68	52.50	0.00	52.50
Mg^{2+}	74.24	2.57	73.21	6.89	37.87	3.59	1.08	268.93	0.00	268.93
EC	1.09	0.04	0.97	1.10	0.58	9.29	2.16	4.78	0.22	5.00
TDS	711.53	26.06	633.75	715.00	383.14	9.29	2.16	3107.00	143.00	3250.00
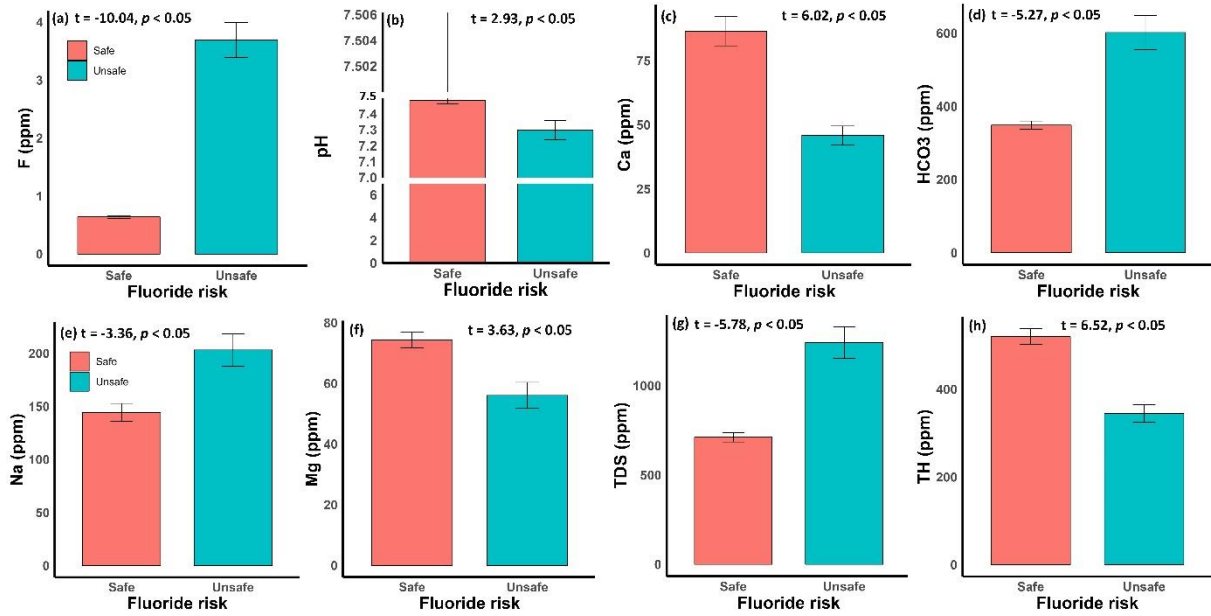
Figure. 9. Bar plots showing differences in physicochemical parameters between Safe (n = 216) and Unsafe (n = 67) groups of water samples. The bars in the graph represent the mean ± SE of respective parameters.

Source: Nandi et al., 2024a

4.1.2. Assessing the hydrogeochemistry

4.1.2.1. Dissolution of minerals and ion exchange processes in the aquifer

Different scatter plots were used to elucidate the weathering status and responsible chemical reactions controlling the hydrogeochemical profile of the groundwater of the study area.

The bivariate plot of (Ca^{2+} + Mg^{2+}) Vs (HCO_3^- + SO_4^{2-}) (Fig. 10a) shows majority of the Unsafe samples lie below the equiline (1:1) giving an indication of silicate weathering and carbonate dissolution, whereas, the samples from Safe group gather above the equiline giving evidences for carbonate weathering and reverse ion exchange mechanisms (Chowdhury et al., 2021; Gantait et al., 2022).The plot of (Ca^{2+} + Mg^{2+}) Vs HCO_3^- (Fig. 10b) supports the results by

showing the presence of Unsafe group samples below the 1:1 line, which confirms that cation exchange mechanism and silicate weathering is responsible for the abundance of Na^+ ion in groundwater (Nasher and Ahmed, 2021). If the samples lie near or on the equiline, it signifies congruent, incongruent dolomite or congruent calcite dissolution (Jia et al., 2020), and when they lie above it, gypsum dissolution, carbonate weathering and reverse ion exchange methods are held responsible for the ionic abundance, just like the case of Safe group of samples here. A similar scenario is encountered in the $(Ca^{2+} + Mg^{2+})$ Vs Na^+ plot corresponding to the current results (Fig 10c) (Ganguli et al., 2022; Prasad et al., 2018). $(Ca^{2+} + Mg^{2+})$ when plotted against TC (total cations) (Fig. 10d), shows Unsafe group of samples lying higher above the equiline (1:1) than the Safe samples, showing greater abundance of silicate weathering and less correlation between TC and $(Ca^{2+} + Mg^{2+})$. The linear spread of a large majority of Safe group of samples along the equiline speak for the greater dependence for total cations on Ca^{2+} and Mg^{2+} ions (Nasher and Ahmed, 2021). The exact opposite picture is encountered in the $(Na^+ + K^+)$ vs TC plot (Fig. 10e) (Jandu et al., 2021). When $(Cl^- + SO_4^{2-})$ is plotted against HCO_3^- (Fig. 10f), the Unsafe ones clearly appear above the 1:1 line, showing bicarbonate as the principle anion and dissolution of feldspar mineral and silicate weathering by carbonic acid (Singh et al., 2020). In Fig. 10g, the bivariate plot of Mg^{2+} vs Ca^{2+} show very few samples around the equiline. This points out to the fact that there is no significant common source (dolomite dissolution) for the release of these two ions (Jandu et al., 2021). The ones which lie below the equiline, have a higher abundance of calcium ion probably from the calcite dissolution. Most of the Unsafe group samples lie above the 1:1 line indicating silicate weathering. When Ca^{2+} is plotted against Na^+ (Fig. 10h), almost a similar trend is observed. The Unsafe group of samples mostly lie much the equiline, showing a greater abundance of Na^+ ion than the other study group establishing the dominance of silicate weathering again (Jandu et al., 2021). The ratio of Na^+ to Cl^- ion is very important in identification of these ionic sources. This ratio is

unity when these ions are derived from dissolution of halites. The ratio when plotted (Fig. 10i) show that samples below equiline ($Na^+/Cl^- > 1$) have a non-halite source, forward ion exchange and silicate weathering (albite and montmorillonite) (Jia et al., 2020). Samples along the equiline (most Safe ones) come from halite dissolution and very few samples which fall above the equiline, have higher Cl^- abundance (Wagh et al., 2020).
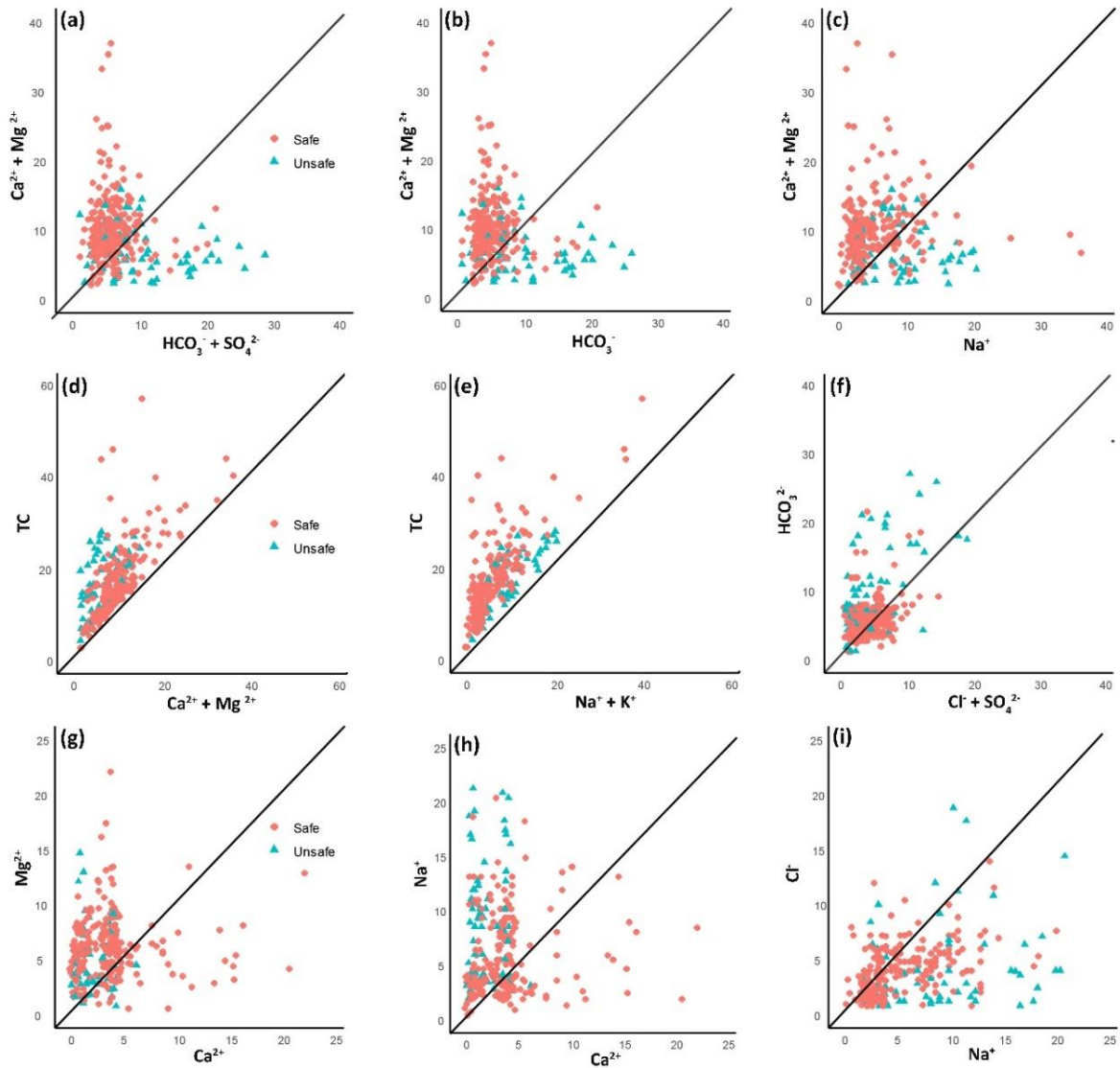
Figure. 10. Assessment of bivariate plots of major ions (meq/l) to identify the underlying solute acquisition processes in the aquifer.

Source: Nandi et al., 2024 a

4.1.2.2. Identifying the hydrogeochemical facies of groundwater using the Piper's trilinear diagram

The Piper Trilinear diagram (Fig. 11) assists in identifying the dominant facies in the samples collected, based on their ionic constitution. With the help of this diagram, we get to know the dominant hydrogeochemical facies from the 4 established facies namely; Ca^{2+}-Mg^{2+}-Cl^--SO_4^{2-} facies (I) or the zone of permanent hardness, Na^+-K^+- Cl^--SO_4^{2-} facies (II) or the saline zone, Na^+-K^+-HCO_3^- or the zone of fluoride dissolution and finally the HCO_3^- zone or the zone of temporary hardness (Gantait et al., 2022; Singh et al., 2020). From the Fig. 11, we find, the dominant facies for group Safe and group Unsafe are IV>I>II>III and III>IV>II>I respectively. That the dominant facies of the group Unsafe is facies III correctly points out to the reason behind the fluoride abundance. Majority of the samples from group Safe are plotted in the zone A (calcium type) and zone C (Magnesium type) whereas zone D (Sodium type) is occupied by the samples from group Unsafe, thus throwing light on the dominant cation in those study groups (Ganguli et al., 2022; Khan et al., 2020). From the triangle of anions, it was recorded that samples from both study groups gather in the zone E or have a bicarbonate type of water. On investigating the water type, it was found that the Safe group samples lie in zone 1 and share Ca^{2+}-Mg^{2+}> Na^+-K^+ type of water. For the samples of the Unsafe group the positions of the samples were restricted largely to the zone 2 or shared the Na^+-K^+> Ca^{2+}-Mg^{2+} water type. Overall, the inference which can be drawn from the piper plot is that the samples from the safe group show a dominance of the alkaline earth ions (Ca^{2+}-Mg^{2+}) and fall under the zone of temporary hardness. The alkali ions (Na^+-K^+) are dominant in the samples from Unsafe group and fall in the alkali carbonate zone, mixing zone and the zone of temporary hardness.
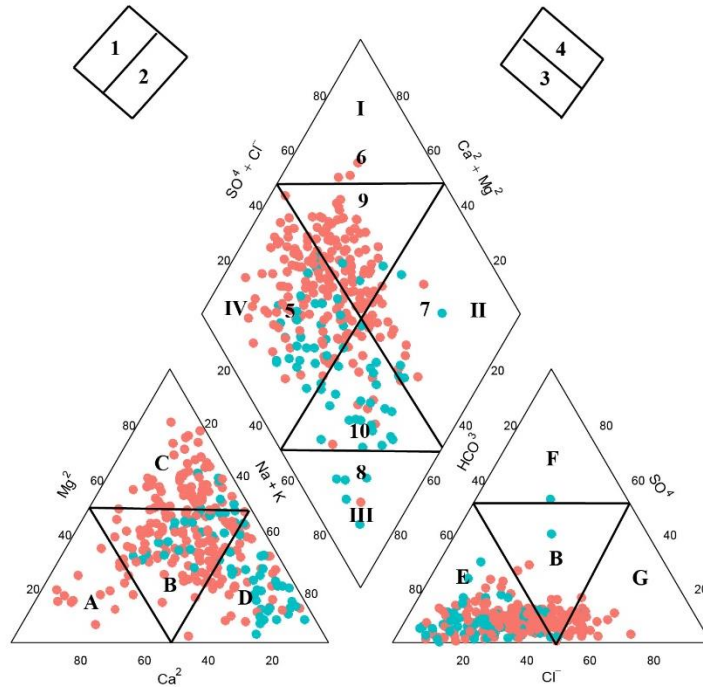
Figure 11. Identification of hydrogeochemical facies of groundwater from both Safe (n = 216) and Unsafe (n = 67) groups of water samples using the Piper trilinear diagram. Source: Nandi et al., 2024a

4.1.2.3. Identifying the dominant mechanism responsible for the existing hydrochemistry

Multiple processes in combination shapes the final water chemistry of the study area. Three major mechanisms namely, evaporation, rock water interaction and precipitation, have the control over the groundwater composition (Gantait et al., 2022; Khan et al., 2020). To identify the dominance of any of these three mechanisms, the Gibbs diagram or the scatter plots of TDS versus $Na^+ / (Na^+ + Ca^{2+})$ (Fig. 12a) and $Cl^-/(Cl^-+HCO_3^-)$ (Fig. 12b) are drawn. We can infer from the diagrams that in both the study groups, rock dominance has been the chief contributor of the groundwater chemistry.
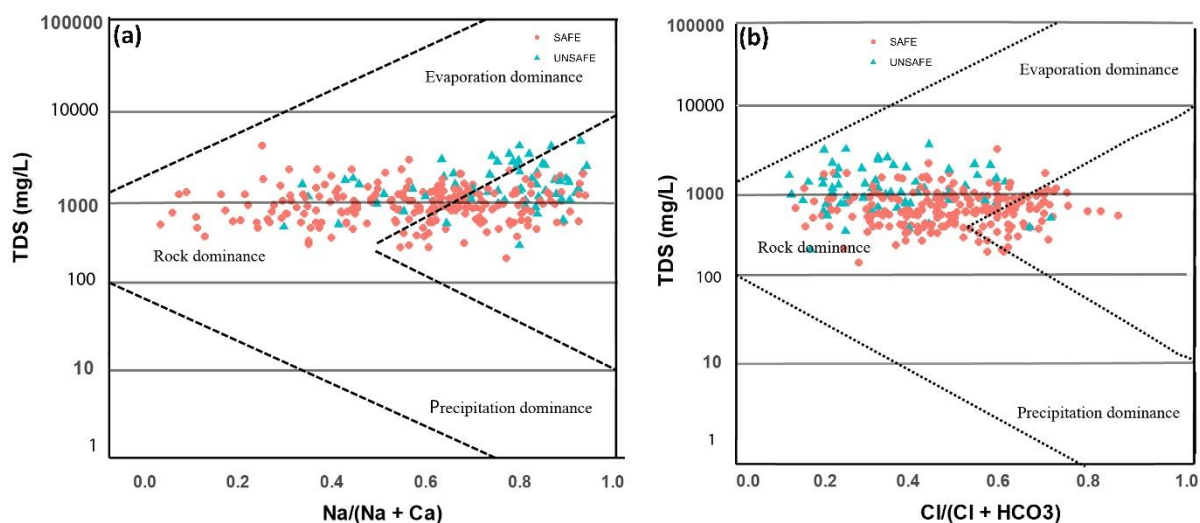
Figure 12. Gibbs diagram of (a) TDS vs. Na^+/ (Na^+ + Ca^{2+}) and (b) TDS vs. Cl^-/ (Cl^- + HCO_3^-) showing rock dominance as the chief contributor of hydrogeochemical evolutionary mechanism.

Source: Nandi et al., 2024a

4.1.2.4. Correlation among the participating ions

The relationships among the different ions of the collected water samples from both study groups were studied using the Spearman's correlation analysis. In this study, when a correlation analysis was performed with the samples of the 'Safe' and 'Unsafe' group (Fig. 13). The correlation between ions of group Unsafe were studied keenly to understand the keys to higher fluoride abundance. It was observed that F^- shares a significant ($p<0.05$) positive correlation with pH in Unsafe groups (r_{unsafe}= 0.270) and HCO_3^- (r_{unsafe}=0.132) (Gantait et al., 2022; Maurya et al., 2020). Both these cases have similarity with earlier reports (Maurya et al., 2020; Subramaniyan et al., 2022). This suggests that at higher alkaline conditions, an ion exchange might have occurred between F^- and OH^- due to a similarity in ionic radii between the two. Fluoride ions have the lowest solubility in pH ranging between 5-6.5 (Chen et al., 2021). At

higher pH more F^- ions are adsorbed by the clay particles, which get replaced by OH^- ions resulting in fluoride dissolution in water (Singh et al., 2020). Chowdhury et al., (2021) also stated that alkaline conditions promote dissolution of fluoride bearing minerals like CaF_2.

$$CaF_2 \leftrightarrow Ca^{2+} + 2F^-$$
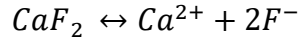
But this dissolution increases the abundance of Ca^{2+} ion the study area which results in calcite precipitation upon reaction with HCO_3^-, thereby ultimately removing the Ca^{2+} ions from solution. Earlier reports by Adimalla et al., (2017), Maurya et al., (2020) and Gantait et al., (2022), supports this phenomenon and thereby justifies the significant negative correlation status between F^- and Ca^{2+} (r_{unsafe}=-0.307). The other study group shows a weaker correlation status for the mentioned ions(r_{safe}=-0.151).

$$Ca^{2+} + 2HCO_3^- = CaCO_3 + CO_2 + H_2O$$
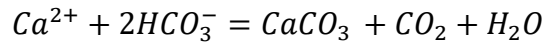
The CO_2 produced as an end product of this reaction, now reacts to Na^+ bearing feldspars to release more Na^+ and this has been reflected by a positive correlation between F^- and Na (r_{unsafe} = 0.218) in this Unsafe study group (Gantait et al., 2022). It also increases the HCO_3^- pool and keeps the calcite precipitation process continuous (Patolia and Sinha, 2017).

$$4NaAlSi_3O_8 + 4CO_2 + 22H_2O = Al_4(Si_4O)(OH_8) + 8H_4SiO_4 + 4Na^+ + 4HCO_3^-$$
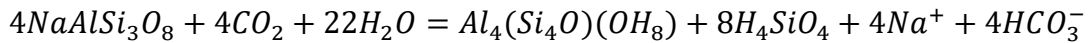
Mg^{2+} shows a similar negative r value like Ca^{2+} which might be due to the precipitation of dolomite (r_{unsafe}=-0.277, $p<0.05$).

$$Mg^{2+} + 2HCO_3^- + CaCO_3 = CaMg(CO_3)_2 + CO_2 + H_2O$$
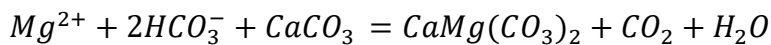
Other possible fluoride dissolution mechanisms in the area might follow the following reaction (Patolia and Sinha, 2017; Zhang et al., 2020).

$$CaF_2 + Na_2CO_3 \rightarrow CaCO_3 + 2Na^+ + 2F^-$$
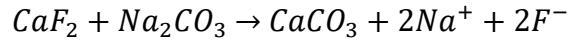
EC is significantly ($p<0.05$) positively correlated to Na^+($r_{unsafe} = 0.553$), showing signs of a major impact of these ions on water chemistry and the existence of weathering processes, precipitations of minerals and rock dominance as major phenomenon in the aquifer (Kouser et al., 2022).The positive correlation of EC to NO_3^- (0.57, $p<0.05$) being statistically significant hints at anthropogenic sources of contamination (Maurya et al., 2020; Singh et al., 2020).
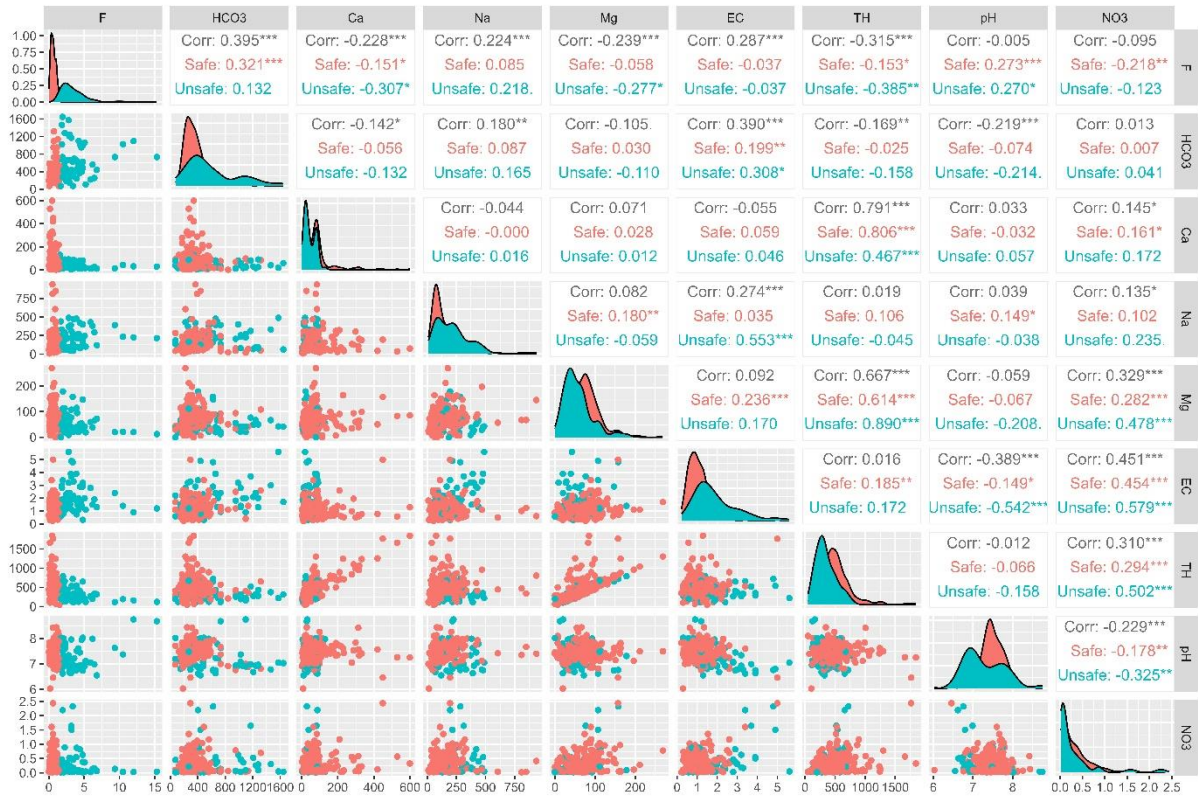
Fig. 13. Rank correlation between different physiochemical parameters of the safe and unsafe group of water samples.

Source: Nandi et al., 2024a

For the group Safe, HCO_3^- shows differences in correlations it shares with other ions. It shows a lower positive correlation ($r_{safe}= 0.087$) with Na^+, thus showing reduced chances of silicate weathering and reduced Na^+, HCO_3^- content (Fig. 9d and Fig. 9e). The lower degree of

correlation of these ions to EC also supports the evidence. A reduction in this ion, also causes a possible disruption in the calcite and dolomite precipitation process, thus increasing the abundance of Ca^{2+} and Mg^{2+} ions (Fig. 9c and 9f) in water. Scarcity of Ca^{2+} in water is one important factor which drives Fluorite dissolution (Mandal et al., 2021). In this scenario, the abundance of this ion therefore nullifies the need for the same and has a lower F^- concentration than the other study group. Figure 13

4.1.2.5. Principal Component Analysis

Thirteen parameters, namely (pH, K^+, Na^+, Mg^{2+}, Ca^{2+}, SO_4^{2-}, Cl^-, HCO_3^-, NO_3^-, EC, TDS, TH and F^-) were used for creating a PCA biplot (Fig. 14a). First five axes (or dimensions) had eigen value greater than 1, explaining ~71.4% of the total variation. While first two axes explained ~44.1% of the total variance of the dataset with eigenvalues of 3.25 (conserved ~25% variations) and 2.48 (conserved ~19.1% variations) respectively. For component 1, the contributors responsible for the positive loading were K^+, Na^+, SO_4^{2-}, Cl^-, HCO_3^-, NO_3^-, EC, TDS, TH and F^- whereas pH and Ca showed negative loading. The primary contributors to Dim-1 were TDS and HCO_3^- (Fig. 14b). While, in case of Dim-2, TH, Mg^{2+}, Ca^{2+}, NO_3^- and F^- showed maximum contributions (Fig. 14c). The positive loadings by TH, Mg^{2+}, Ca^{2+}, NO_3^- and negative loading by F^- also reflects of a negative correlation of these ions to fluoride as established in the correlation analysis (Fig 13). The poor correlation of F^- and NO_3^- nullified the possibility of anthropogenic contamination from fertilizer sources (Chen et al., 2021). It also sheds light upon the rock water interactions and geogenic dominance in groundwater chemistry. The positive correlation of fluoride to HCO_3^- is also supported by the negative loading of HCO_3^-. Though two ellipses of Safe and Unsafe group overlapped with each other, the mean points (larger coloured circle) were separated widely, reflecting remarkable differences in ionic composition between these two groups.
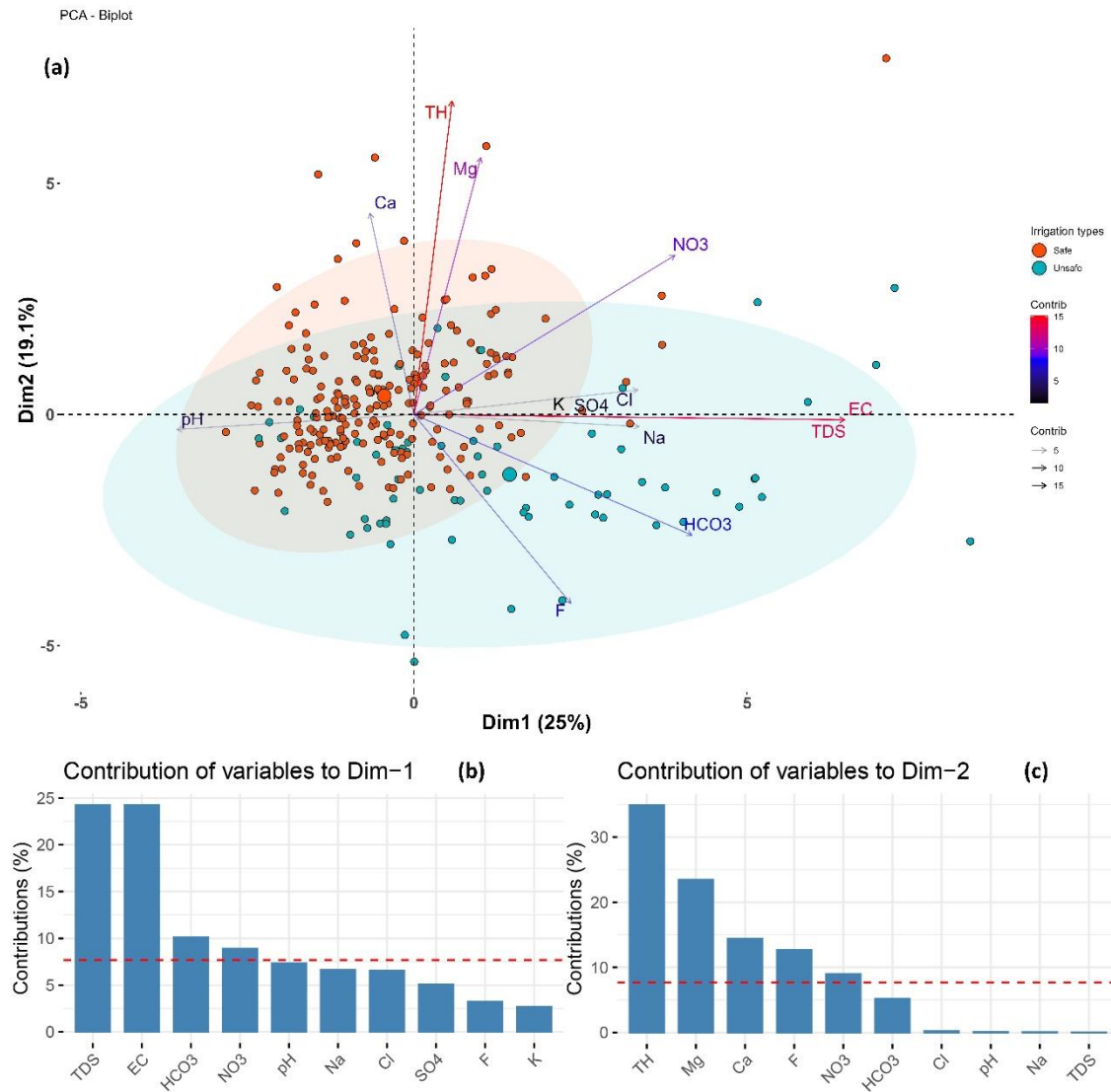
Fig. 14. Principal component analysis of physicochemical parameters of collected groundwater samples across safe and unsafe groups

Source: Nandi et al., 2024a

4.1.2.6. Saturation index (SI)

The saturation index helps us to get a picture of the aquifer's existing reactive mineralogy with no need of actual analysis of the studied aquifer. An idea of the precipitation and dissolution of minerals present can be achieved (Gantait et al., 2022). Software Visual MINTEQ version

3.1 has been used to study the saturation indices of two study groups and the input data for each group consisted of the group mean values for each parameter (pH, K^+, Na^+, Mg^{2+}, Ca^{2+}, SO_4^{2-}, Cl^-, HCO_3^-, NO_3^- and F^-). A negative value for the index hints at a undersaturation of the mineral in water and higher potential of the mineral dissolution. On contrary, a positive SI value achieved speaks for oversaturation, abundance, sustained rock-water contact and a potential to get precipitated. A value between 0.005 to -0.005 speaks of equilibrium condition for the mineral.

$$SI = \log IAP - \log Ks$$

Here, Ks represents the temperature-corrected solubility constant, and IAP stands for Ion Activity Product. From Table 9, we find both groups have positive values of SI for calcium and magnesium bearing minerals (calcite, dolomite and hydroxyapatite), showing a possibility of precipitation and subsequent removal of these ions from groundwater.

Table 9. Values for Saturation Indices of some minerals in study groups Safe and Unsafe

Mineral	Group Safe value	Group Unsafe value
Calcite	0.565	0.103
Dolomite	0.873	0.1
Hydroxyapatite	3.28	0.92
Fluorite	-1.664	-0.392

On contrary to this finding, we have encountered a different scenario earlier, where group Safe samples show an abundance of these ions (Fig 9c and 2f). HCO_3^- ions are important for this precipitation to occur, but significantly lower lev9ls of Na^+ and HCO_3^- ions are found in this group (Fig. 9d and 9e). A possible lack of silicate weathering in this group as discussed earlier (Fig. 10c and Fig. 10h) may explain the scarceness of these ions. This now explains how, unlike the Unsafe group, Ca^{2+} and Mg^{2+} ions in group Safe do not precipitate and remain in solution despite having a positive SI for Ca ang Na bearing minerals in the aquifer. The dissolution of Fluorite, causing an abundance of F^- ion particularly in group Unsafe can also be elucidated from here. Though, both groups have a negative SI value for fluorite, the Safe group has an abundance of Ca^{2+} ions, thereby limiting CaF_2 dissolution (Gantait et al., 2022).

4.1.3. Assessing the suitability of groundwater for irrigational and drinking purposes

4.1.3.1. Irrigation indices

Due to the scarcity of rain in this region in the summer months, farmers largely rely on groundwater for providing necessary irrigation to their fields. Therefore, testing the suitability of the water in agricultural operations should be an important aspect.

Residual sodium carbonate (RSC) represents the alkalinity hazards of the test water samples. A higher abundance of Na^+ ions in groundwater results in the precipitation of Ca^{2+} and Mg^{2+} ions in the soil, thereby making soil infiltration difficult to achieve (Subramaniyan et al., 2022). The value of RSC is calculated from Table 1 and based on those values, Aravinthasamy et al, classified samples as suitable (RSC, 1.25 – 2.5) and 'unsuitable' (RSC > 2.5), based on the suitability of water in agricultural usages. In this study, ~81%, ~3.55% and 15.1% of total samples belonged to 'safe', 'permissible' and 'unsuitable' categories respectively. Significant (t-value = -7.64, $p < 0.05$) variation in RSC was observed between the Safe and Unsafe group of water (Fig. 15a). Moreover, the average RSC of the Safe group was -4.68, while in the

Unsafe (2.98) group it exceeded the range of the 'unsuitable' category. Fig. 16a depicts the spatial variation map of RSC, where the southern part of the study area belonged to the unsuitable category. Moreover, small, dispersed pockets were also observed across the study area. Interestingly, higher RSC was observed in high fluoride-contaminated areas, showing a strong relationship between them.
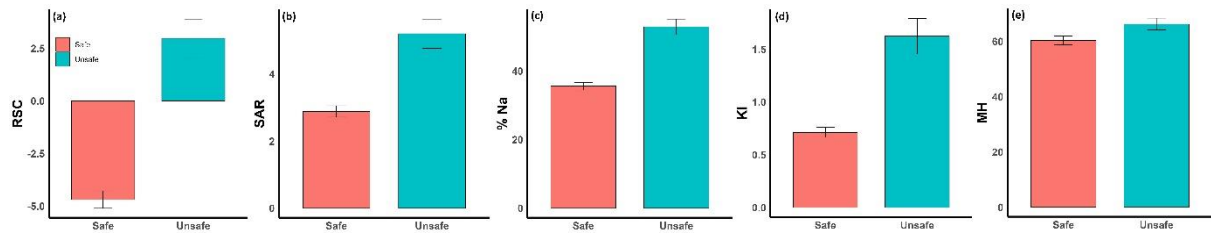
Figure 15. Bar plots showing differences in values of irrigation indices between Safe (n = 216) and Unsafe (n = 67) groups of water samples. The bars in the graph represent the mean ± SE of respective indices.

Source: Nandi et al., 2024 a

Sodium adsorption ratio (SAR) is an estimation of the accumulation potential of Na^+ ions in the soil with respect to magnesium and calcium ions (Table 1) (Rawat et al., 2018). It defines the alkali hazard in sample area. The water percolation time increases with increasing SAR as a result of salt layer formation and soil clogging (Khan et al., 2020). Average SAR values in Safe (2.88) and Unsafe (5.20) groups showed significant (t = -4.93, $p < 0.05$) variation (Fig. 15b). The calculated SAR and EC values are plotted in the United State Soil Laboratory Staff (USSLS) diagram (Fig. 17b). Here, S1 to S4 on the y-axis depicts increasing sodium hazard, while C1 to C4 in the x-axis represent increasing order of Salinity hazard. Very few samples were found in the S4-C4 zone (high sodicity-high salinity zone). A majority of the samples from the safe group fall in the S1-C2, S1-C3 Zone or the low sodicity-moderate salinity zone and the Unsafe group samples flock in the S2-C3, S2-C4, S3-C4 (moderate sodicity-moderate

to high salinity) zones. Therefore, according to the USSL diagram, the safe group of samples are more suitable for irrigation. When classified according to Richards (Kouser et al., 2022), 95% of total samples belonged to the 'excellent' or S1 category (SAR<10); 4.24% in the 'good' or S2 category (SAR < 18); ~0.34% in 'suitable' or S3 category and no sample was found in the 'poor' category (SAR>26) (Subramaniyan et al., 2022).
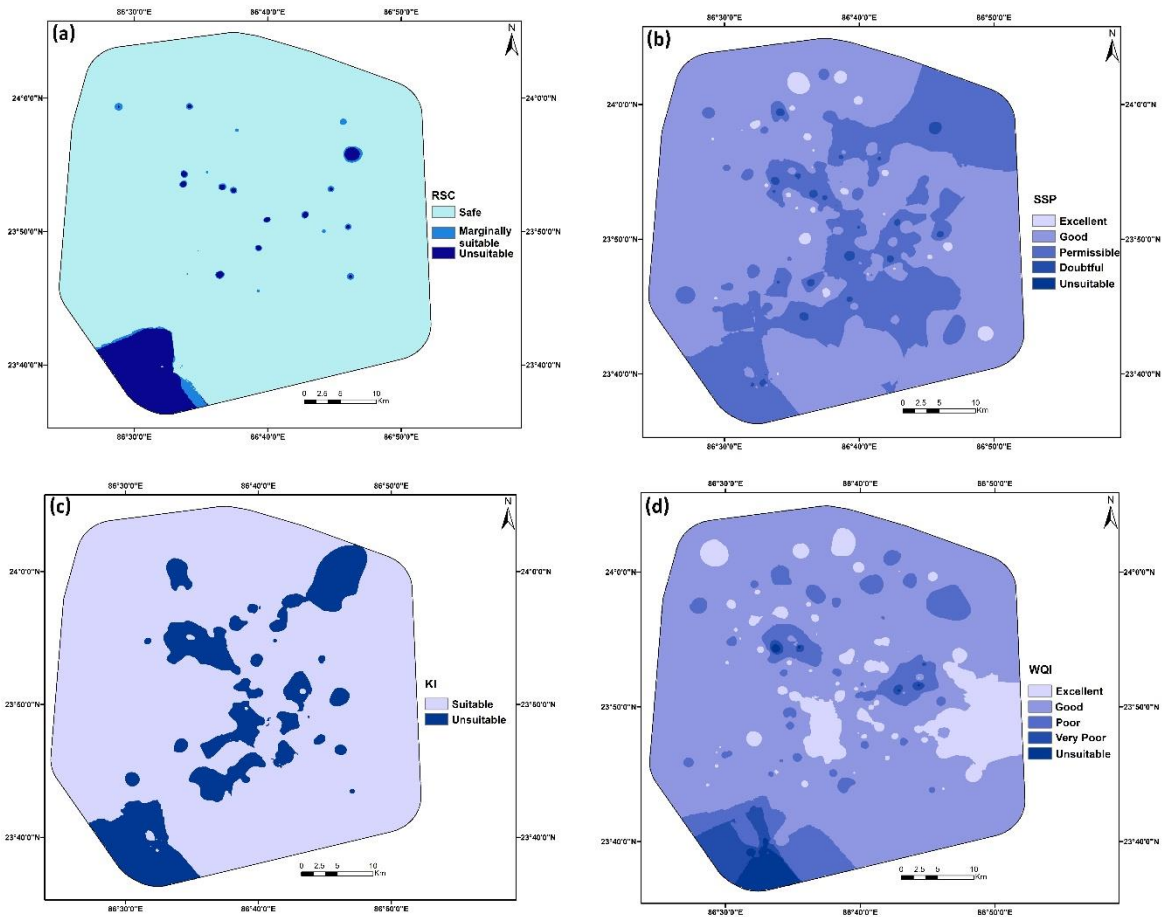
Fig. 16. Spatial distribution maps of (a) residual sodium carbonate (RSC); (b) Soluble sodium percentage or % Na; (c) Kelly's index (KI) and (d) water quality index (WQI) have been prepared using the inverse distance weighting (IDW) interpolation method, where darker colours represent higher values of respective parameters.

Source: Nandi et al., 2024a

Soluble sodium percentage (SSP) or Na% is another important index for evaluating the suitability of irrigation water. Higher SSP in groundwater might reduce the integral soil drainage capability (Kouser et al., 2022). Significant (t-value = -6.84, $p < 0.05$) variation in % Na was observed across safe and unsafe group of water type (Fig. 15c). It has been classified into five categories; Excellent (0-20), Good (20-40), Suitable (40-60), Doubtful (60-80) and Unsuitable (>80) for irrigation usages (Kouser et al., 2022). In our study area, 13.42%, 41.69%, 28.62%, 13.78% and 2.47% of the total collected samples belonged to the respective classes as mentioned earlier. The Fig. 16b depicts the spatial distribution map of these water types. Moreover, the Wilcox diagram (Fig. 17a) has been plotted with the calculated % Na (Table S1) and EC values from both groups (Kouser et al., 2022; Subramaniyan et al., 2022). Unlike the samples from group Safe, a large majority of Unsafe samples lie in permissible to doubtful and doubtful to unsuitable zones.

Kelly's ratio (KR) is based on the ratio of Na^+ ions to the sum of Ca^{2+} and Mg^{2+} ions (Table 1). A ratio greater than 1, depicts alkalinity hazard and is considered unsuitable for agricultural uses (Gantait et al., 2022). The average KI in Safe group was found to be 0.71, while in unsafe (1.62) water; it exceeded the threshold limit of 1 (Fig. 15d). Significant (t-value = -5.20, $p < 0.05$) variation in KI was observed among two groups of water. 25% of samples were found 'unsuitable' and had KI >1 showing excess alkalinity due to sodium. As per expectation. more samples with high KI belonged to Unsafe group (Fig. 15d) or regions of higher F^- concentrations as they have a greater abundance of Na^+ ions as already evident from (Fig. 9d) and the IDW map for this index (Fig. 16c) shares a striking similarity with the map depicting fluoride levels (Fig. 6D).
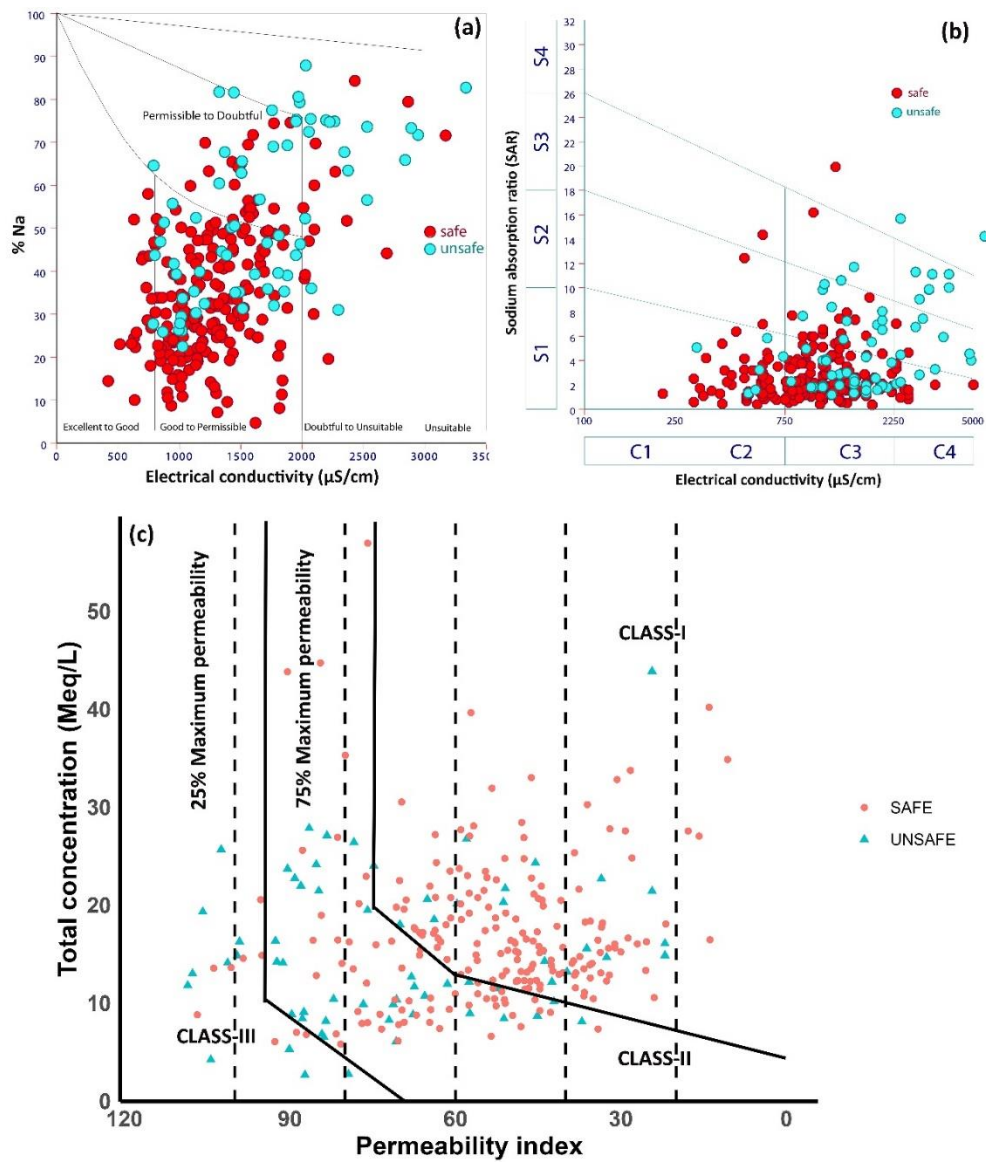
Figure 17. Assessing the suitability of water samples for irrigational purposes and comparing both study groups (Safe and Unsafe) on this basis. (a) Wilcox diagram; (b) USSLS diagram; and (c) Doneen diagram.

Source: Nandi et al., 2024a

Permeability index (PI) represents the degree of its impact on soil permeability. With continuous use of irrigation water laden with ions like Na^+ Ca^{2+} Mg^{2+} and HCO_3^-, the permeability of soil decreases over time (Rawat et al., 2018). The data of both study groups were plotted in the Doneen plot (Fig. 17c). The mean PI of group Unsafe (75.5) deviated

significantly (t=-8.15, *p*<0.05) from the mean PI (53.09) of Safe group. Following the classification by Doneen (Gantait et al., 2022), majority of the Safe samples fell into Class I (Suitable) of permeability index and Class II (Good) showed a mixed population of samples from both groups. Water samples from both these classes can be used for irrigation but, water samples in class III which mostly come from group Unsafe are considered unsuitable for agricultural activities.

Excess magnesium abundance in irrigation water increases soil alkalinity and deteriorates crop production (Kouser et al., 2022) and can be estimated with the help of Magnesium hazard (MH). Significant (t-value = -2.22, *p* < 0.05) variation of MH was observed between safe and unsafe group of water (Fig. 15e). Group Unsafe with a higher mean MH can therefore be considered more unsuitable than the other study group.

4.1.3.2. Water Quality Index (WQI)

The WQI values for the collected water samples from both study groups are presented in Table 10, where we find, a large majority of the samples (34%) from the group Unsafe were unfit for drinking and none were found in the good or excellent category. Whereas the group Safe had no samples with WQI >200 and were safer for drinking. The mean WQI of Unsafe group (294.09) was significantly (*p*<0.05) higher than the same for group Safe (64.22) indicating unsuitability of the former study group. The geospatial map showing the distribution of WQI in the study area was also constructed (Fig. 15d) for better understanding of its distribution. It shows a remarkable similarity with the spatial distribution map of fluoride (Fig. 6D) and shows 'Unsuitable' class of WQI in zones with greatest fluoride abundance.

Table 10. Classification of samples according to WQI values

WQI	Water type	Group Safe (no of samples)	Group Unsafe (no of samples)
<50	Excellent	78	0
50-100	Good	114	0
100-200	Poor	24	25
200-300	Very poor	0	19
>300	Unsuitable	0	23

4.1.3.3. Health Risk Assessment (HRA)

The noncarcinogenic effect of an element poses threatens human lives after the hazard quotient (HQ) value for the same crosses the value of unity. This HQ value is largely dependent of CDI. In this study a range of CDI values from 0.00833 mg/kg/day to 25.5 mg/kg/day are observed in children, while the range of CDI values for adults lies between 0.0058 to 17.73 mg/kg/day. On comparing the HQ for children ($HQ_{F.Children}$) and HQ for adults ($HQ_{F.Adult}$) between the two study groups we find group Unsafe samples pose significantly ($p<0.05$) higher noncancerous risk to both age groups considered (Fig. 18). Unlike all samples of group Unsafe, 47% and 27.3% Safe group samples pose threat to children and adults respectively. The variation of HQ according to changes in study area are in proportion to the changes in abundance of F^- ions across study groups. Group Unsafe having a higher fluoride concentration in the samples also show higher HQ. Lower bodyweights might be the main factor behind greater impacts on children in both study groups (Kadam et al., 2021; More et al., 2021).
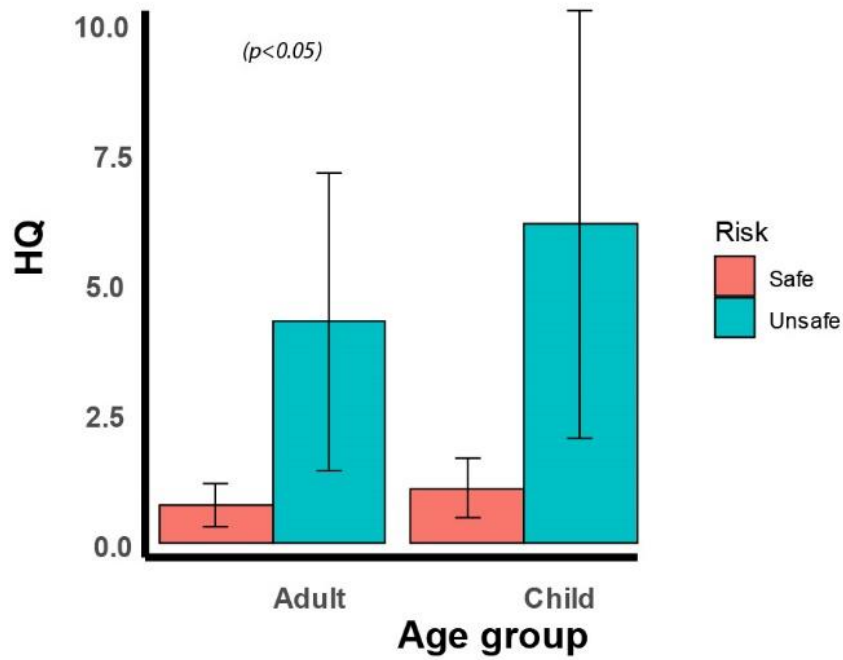
Figure 18. Bar plots showing differences in values of non-carcinogenic health risks (HQ) of fluoride on different age groups (child below 12 years and adults) between Safe (n = 216) and Unsafe (n = 67) groups of water samples. The bars in the graph represent the mean ± SE of respective indices.

Source: Nandi et al., 2024a

4.1.4. MCDM (Fuzzy TOPSIS)

The Fuzzy-TOPSIS model was used to find the closest match to the ideal solution between the samples from two study groups. Their mean values of the considered criteria (WQI, HRA in children, HRA in adult, SAR, %Na, KI, PI, F⁻ and MH) were used for the study. The calculated weights for the former mentioned criteria were 0.111, 0.114, 0.114, 0.100, 0.099, 0.10, 0.09, 0.114 and 0.04 respectively. From the performance scores, Safe samples were ranked 1 (score = 1) and therefore were better alternatives and closer to the ideal solution (Table 11).

Table 11. The ranking based on performance scores as calculated by Fuzzy TOPSIS

Groups	Euclidean distance from ideal best	Euclidean distance from ideal worst	Performance score	Rank
Safe	0	0.1979	1	1
Unsafe	0.1979	0	0	2

4.1.5. Predicting fluoride contamination using machine learning

Earlier studies have already established the importance of machine learning models in predicting fluoride contamination. To compare the importance of predictor variables across different models, it is crucial to utilize a normalized measure where the relative importance is measured on a scale of 0 to 100. Before conducting LR, CART and RF models, we performed feature selection with 'boruta'; and removed P and B and SO_4^{2-} from further analysis as their importance value was less than the shadowMax (Fig.19). For each of the above-mentioned models, 10-fold cross-validation was performed with 5 repetitions.

In the case of logistic regression, when the groundwater parameters (pH, Cl^-, HCO_3^-, Ca^{2+}, NO_3^{--}, Na^+, K^+, Mg^{2+} and EC) were used as predictors, HCO_3^-, Na^+, Ca^{2+}, Mg^{2+} and EC showed statistically significant contributions. This model had an Akaike's Information Criterion (AIC) value of 180.4, with and accuracy of 83%. EC was found to be the most important variable, followed by Na^+, HCO_3^-, Mg^{2+}, Ca^{2+}, Cl^-, NO_3^-, K^+, and pH (Fig. 20A). The AUC of this model was 95.6%, which also suggests a good accuracy of the model. ROC curve was generated for visualization of the accuracy of the model (Fig. 22A).
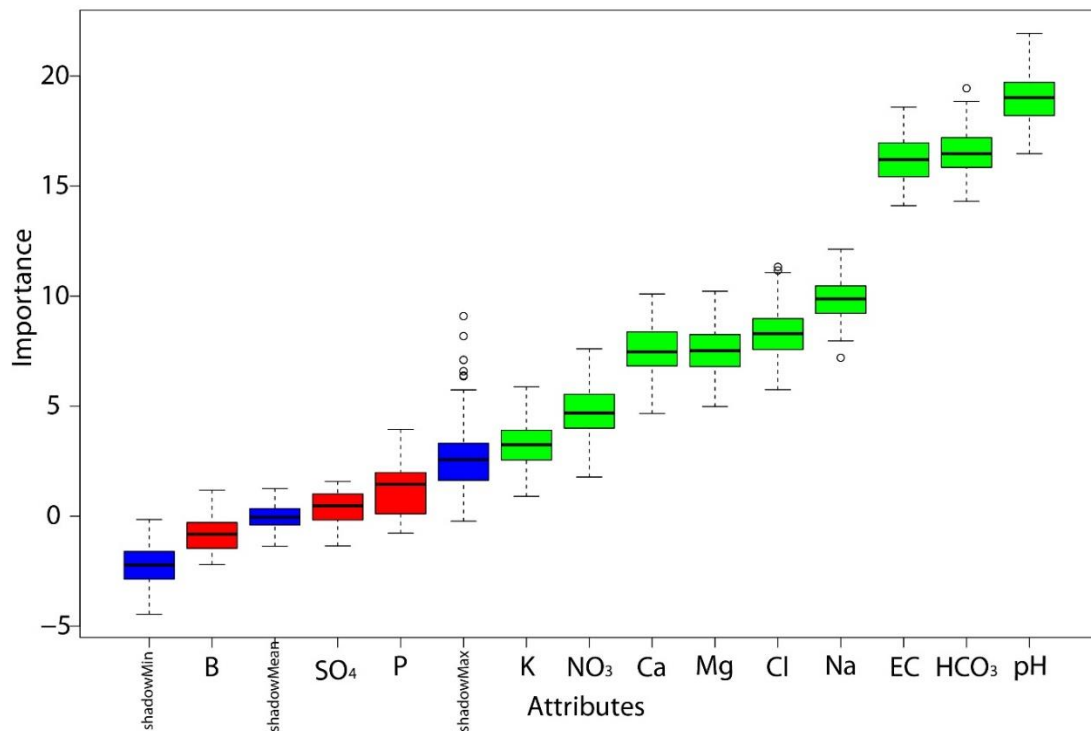
Figure 19. Boruta variable selection selecting variables with significant contributions towards the studied models (LR, CART and RF). P, B and SO_4^{2-} with values lesser than shadow max got eliminated in the process.

Source: Nandi et al.,2024a
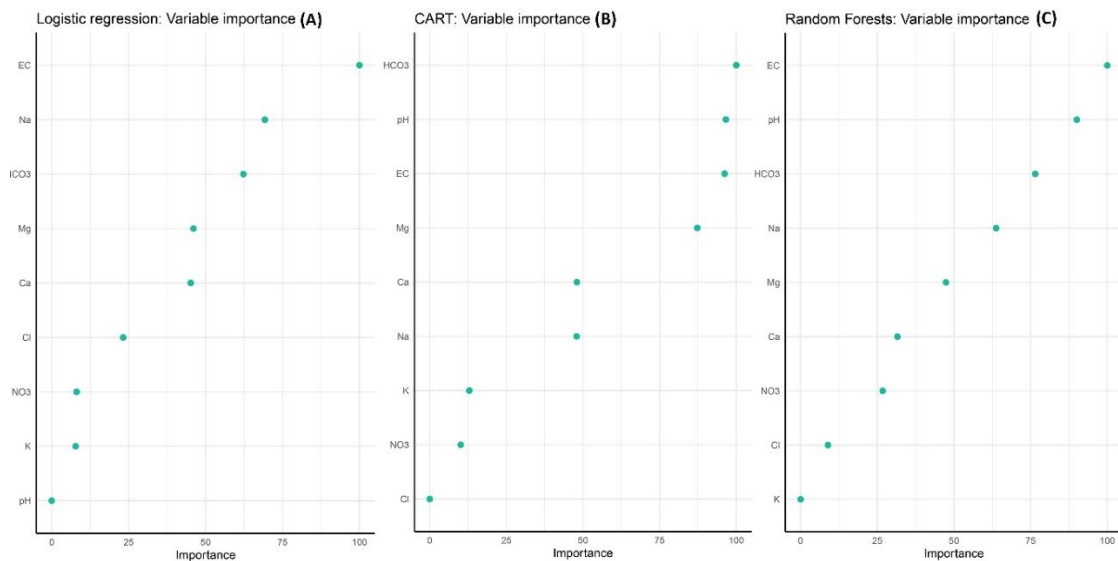
Figure 20. A comparison between the order of variable importance for fluoride prediction among (A) logistic regression (LR) (B) CART and (C) Random-forest (RF) model.

Source: Nandi et al., 2024 a

For the CART model, the best cp of 0.05 was selected based on the highest accuracy of 0.77 to develop the optimal model. EC was found to be in the root node of this optimally developed tree, where an EC value of 2.7 was decided as a critical value (Fig.21). Further classification of the tree was based on HCO_3^- and Ca^{2+} with their respective critical values of 470 and 64. During model evaluation on testing data, it showed an accuracy of 84.21% with a sensitivity of 0.93 and specificity of 0.50. The variable importance plot (Fig.20B) depicts the importance of HCO_3^-, pH, EC, Mg^{2+}, Ca^{2+}, Na, K, NO_3^- and Cl^- in predicting fluoride risk. The AUC of this model was 69.4%, which implies that logistic regression performed better than the CART approach (Fig. 22B).
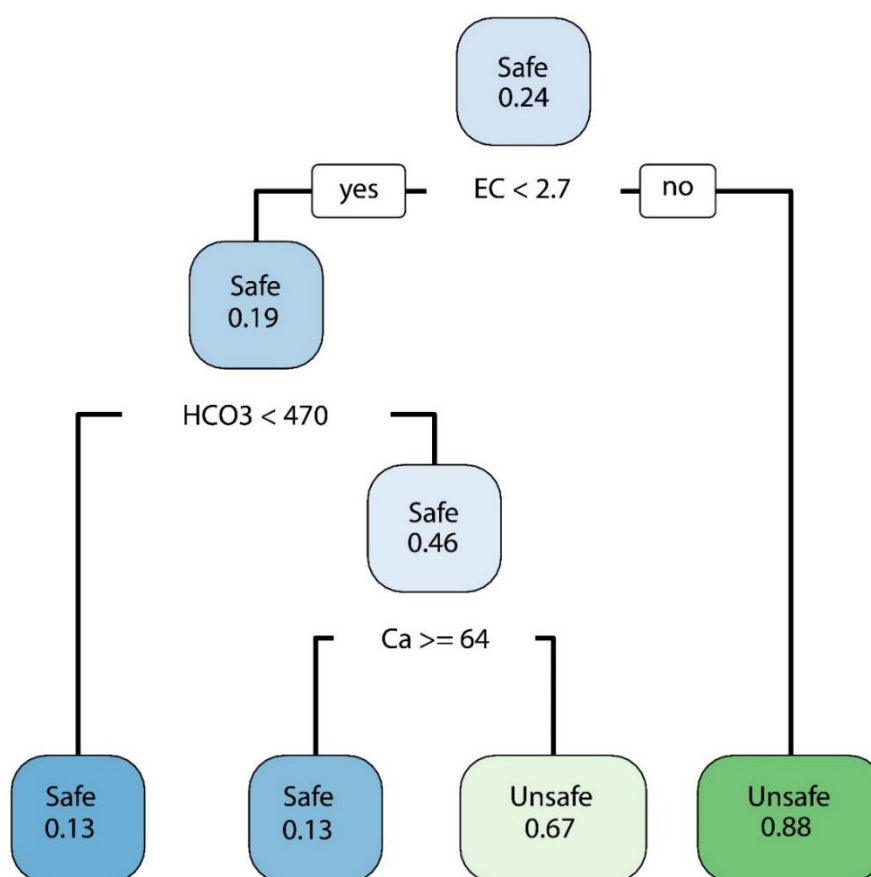
Figure 21. The tree developed by Classification and regression tree (CART) model showed EC to be in the root node, with as a critical value of 2.7. other classifying factors for the tree were HCO_3^- and Ca^{2+} with their respective critical values of 470 and 64. Source: Nandi et al., 2024a

In the case of the Random Forest model, 10-fold cross-validation was used to optimize the 'mtry', which represents the number of variables to randomly sample as candidates at each split. The final 'mtry' value of 2 was chosen based on the highest accuracy of 0.835. During model evaluation on testing data, this model showed an accuracy of 89.47% with a sensitivity of 0.97 and specificity of 0.58. However, the AUC of this model was 91.5% (Fig. 22C). In RF model, EC was the most important variable, followed by pH, HCO_3^-, Na^+, Mg^{2+}, Ca^{2+}, NO_3^-, Cl^- and K^+ (Fig. 20C). Therefore, logistic regression has been found to be the best prediction model. Though RF is an excellent machine learning model, in comparison to LR, it showed poor probability calibration (Niculescu-Mizil and Caruana, 2005). Models like RF are more data hungry, therefore the data could be simply insufficiently expressive. In a study by Mandal et al., (2022) also found better performance of logistic regression than other machine learning approaches like Random Forest and gradient boosting machine (GBM) while predicting the bioavailable arsenic (AS) concentration in paddy soil.
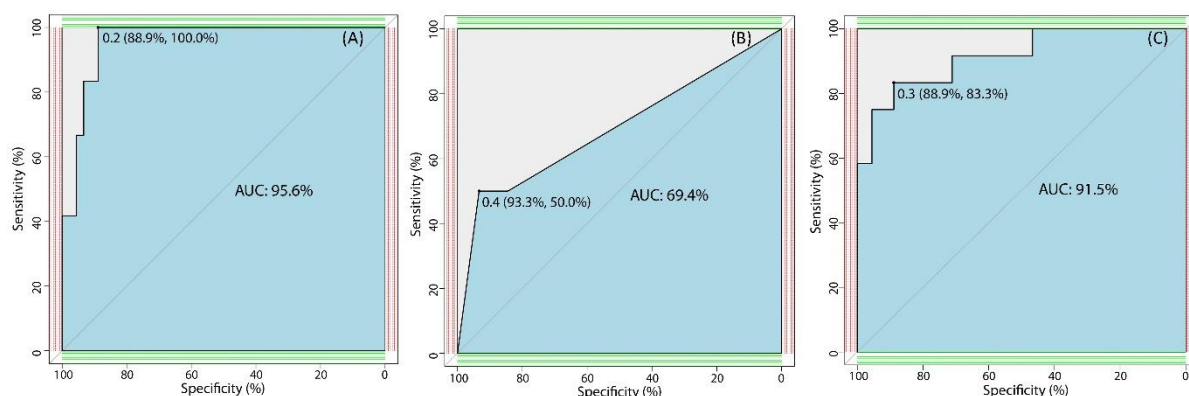
Figure 22. Comparison between ROC curves of three different models depicting model accuracy, namely; (A) Logistic regression (AUC: 95.6%), (B) Classification and regression tree (AUC: 69.4%) and (C) Random-forest (AUC: 91.5%). Model accuracy was performed on the testing data set and plotted with sensitivity vs (1- specificity). LR is the best-performing model with the highest AUC score.

Source: Nandi et al., 2024a

4.2. Findings from samples of Giridih District

4.2.1. Evaluation of general water quality

4.2.1.1. Abundance and spatial distribution of Fluoride

Fluoride level of the samples collected from the area studied varied between 0.34 ppm to 2.8 ppm. Out of those 16 (40%) samples were recorded to have F$^-$ levels higher than the permissible limit of 1.5 ppm) set by World Health Organisation (WHO) and were grouped under 'FC' (fluoride contaminated) group. The other study group 'FU' had the remaining 26 samples with fluoride levels below 1.5 ppm.
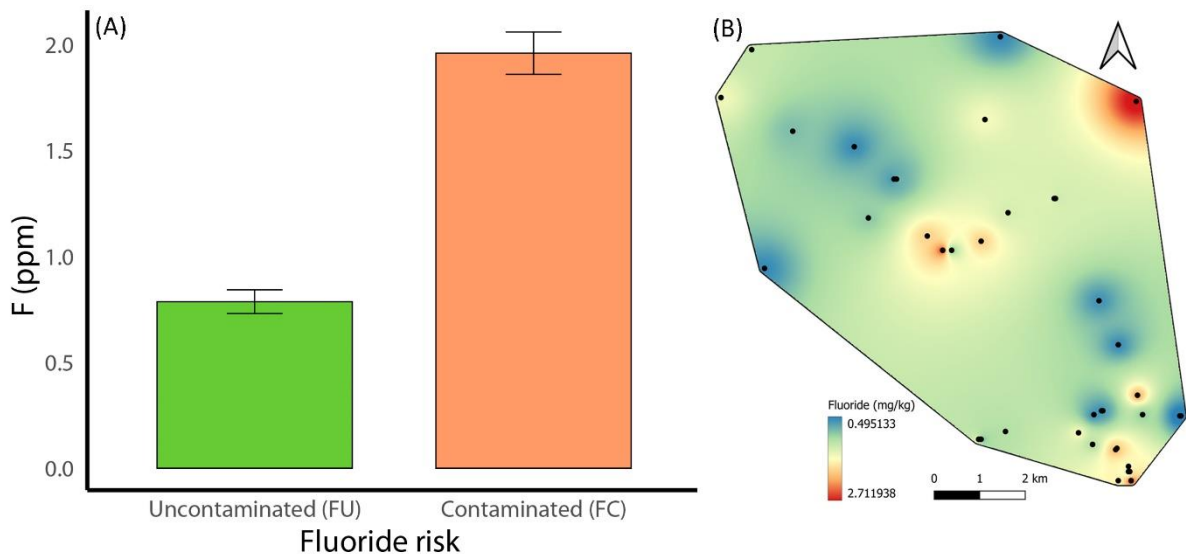
Figure 23. (A) Bar plots showing differences between mean fluoride concentration of Fluoride contaminated (FC) and Fluoride uncontaminated (FU) group of collected water samples. The bars in the graph stand for the mean ± SE of respective parameters. (B) A spatial distribution map of fluoride concentration in the study area created using the inverse distance weighting (IDW) interpolation method.

Source: Nandi et al., 2024b

A sharp contrast was evident when the mean of F^- concentration of the two groups were compared and a *p* value of less than 0.05 (t = -10.236) was encountered proving the means to be significantly different from each other (Fig. 23A). The mean F^- concentration in the FC and FU groups were 0.786 ± 0.59 ppm and 1.959 ± 0.09 respectively. Fig. 23B elucidates distribution of the F^- ion in the study area with an IDW map. Based on the F^- concentration, the area studied was categorised using graduated colour symbols, with the areas of highest fluoride abundance appearing red and the ones with least F^- ions taking up blue colour.

4.2.1.2. Comparison of physical parameters and major ions between study groups

The bedrock composition of an area, the areas geogenic mineral abundance and total residence of water in largely determines the ionic abundance in groundwater table. Its physico-chemical properties like pH , TDS, EC are also affected by the same. Significant differences in the mean pH of the 2 study groups FC (7.15 ± 0.02) and FU (7.06 ± 0.01) were not found (*p* >0.05). However, the scenario was different when we compared the group means of EC and TDS (Table 12 ,Fig. 24A and B). In both cases, there existed a significant variation (*p* < 0.05, t = -5.22 and t = -5.23 respectively). Three samples from the group FC were beyond the permitted limit of 1500 µS for EC (Khan et al., 2020). TDS values can classify samples in four groups based on suitability of use, namely 'best fit' (<500 ppm), 'permissible for drinking' (500-1000 ppm), 'suitable for agriculture' (>1000 ppm) and 'unsuitable' (>10000 ppm) (Khan et al., 2020). 61.53% samples from group FU fell under the best fit type and all others came in the permissible for drinking category. On the other end, merely 6.25% samples of group FC qualified for the best fit type, and 18.75% from the group were suitable for irrigation only. However, none of the samples were from the unsuitable type. Another important parameter, the TH of water, is dependent on the concentration of magnesium and calcium ions in the aquifer has a threshold limit of 500 ppm put forward by the BIS or Bureau of Indian Standards

in 2012. Although none of the samples in the current study exceeded the limit, on comparing the mean TH of the two study groups it was evident that the group FU (139.66 ± 13.52 ppm) had a significantly (t-value = 2.19, p <0.05) higher value than the other group (98.39 ± 13.03 ppm) concerned (Fig. 24C). Hard (150-300 ppm) and very hard (>300 ppm) water might be threatening to the human health and are unsuitable for household needs (Khan et al., 2020). 56.25% of samples from the group FU come under this type.

Table 12. Summary statistics of water-quality parameters in the study groups.

Parameters	Fluoride uncontaminated	Fluoride contaminated
	Mean ± SE	Mean ± SE
pH	7.15 ± 0.02	7.36 ± 0.01
F^- (ppm)	0.78 ± 0.55	1.95 ± 0.09
Cl^- (ppm)	80.18 ± 13.36	101.17 ± 17.09
HCO_3^- (ppm)	250.00 ± 13.19	319.61 ± 22.76
Ca^{2+} (ppm)	22.99 ± 2.48	11.39 ± 1.77
Na^+ (ppm)	34.59 ± 3.91	60.08 ± 4.53
SO_4^{2-} (ppm)	19.39 ± 6.73	21.28 ± 4.05
K^+ (ppm)	4.71 ± 1.17	2.18 ± 0.37
Mg^{2+} (ppm)	20.04 ± 2.14	17.04 ± 3.23
EC (µS/cm)	652.08 ± 63.03	1198.12 ± 83.23
TDS(ppm)	423.85 ± 40.97	778.78 ± 54.10
TH (ppm)	139.66 ± 13.52	98.39 ± 13.03

The major cations (Na^+, Ca^{2+}, Mg^{2+}, K^+) in groundwater samples can be measured to get an overview of the aquifer chemistry in the study region. No significant differences were noted when the means of the two concerned groups were compared against each other for the Mg^{2+} and K^+ ions (Table 12). But the results of the Welch test showed sharp differences for the other two cations. The mean Ca^{2+} ions of the group FU (22.998 ± 2.48 ppm) were significantly more ($t = 3.79$, $p < 0.05$) as compared to the other group (Fig. 24D), whereas, the group FC had significantly higher levels of Na^+ ions (60.08 ± 4.53 ppm, $t = -4.25$, $p < 0.05$, Fig. 24E). The abundances of Na^+ ions may be attributed to the silicate weathering (Gantait et al., 2022) and the source of calcium ions, might be from the calcium bearing minerals (plagioclase, amphibole etc) in the underlying bed rocks.
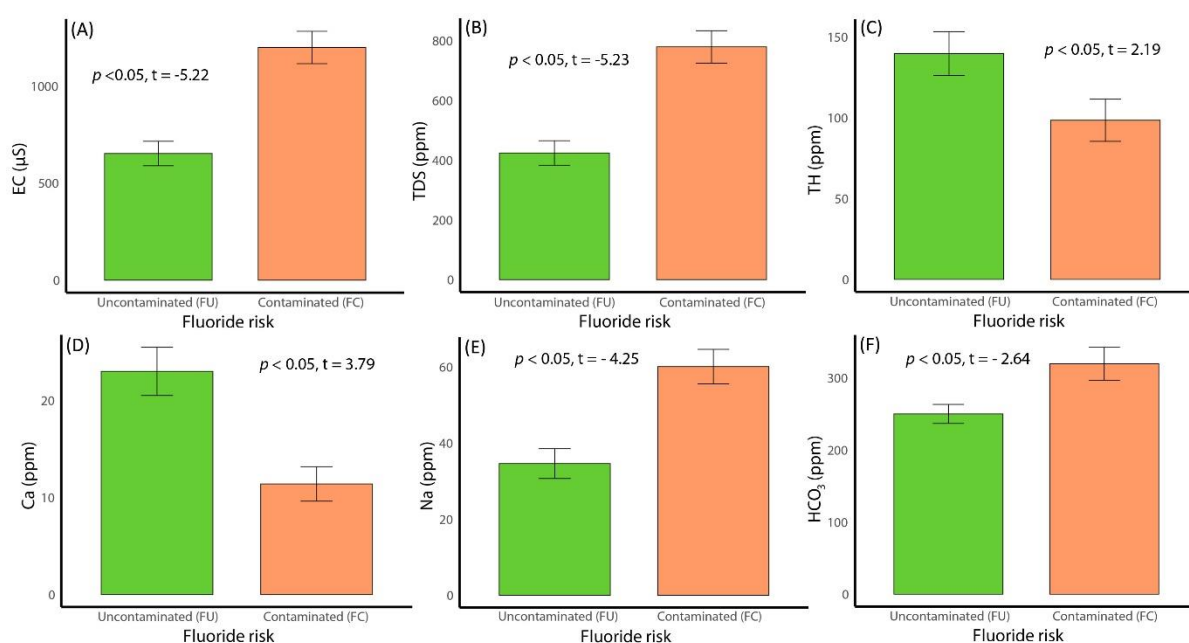
Figure 24. Bar plots showing significant differences in physicochemical parameters between Fluoride contaminated (FC) and Fluoride uncontaminated (FU) groups of water samples. The bars in the graph represent the mean ± SE of respective parameters. Source: Nandi et al., 2024b

Among the anions, chloride (Cl^-) and sulphate (SO_4^{2-}) did not show any significant difference in their means when comparison was drawn between FC and FU groups. But HCO_3^- was

present more abundantly in the fluoride contaminated group (FC). The mean HCO_3^- ion concentration of the FC group was 319.612 ± 22.76 ppm and significantly abundant ($t = -2.64$, $p < 0.05$, Fig. 24F) when tallied against the mean HCO_3^- ionic concentration (250 ± 13.19 ppm) of FU. As per previous reports, Fluoride shows a positive correlation to this ion and carbonate dissolution along with silicate weathering is the major source for this ion (Gantait et al., 2022). These findings agree to the same.

4.2.2. Calculating indices to evaluate suitability of collected samples

4.2.2.1. Assessing suitability for drinking needs (WQI)

Table 10 shows the different categories where each collected sample belong based on WQI values calculated for them. We found, majority of samples (~54%) of group 'FU' or uncontaminated with fluoride were 'good' for drinking, 37.5% were 'excellent' and only two were 'unfit'. Whereas, the group FC or samples with unsafe fluoride score had only 'unfit' samples.
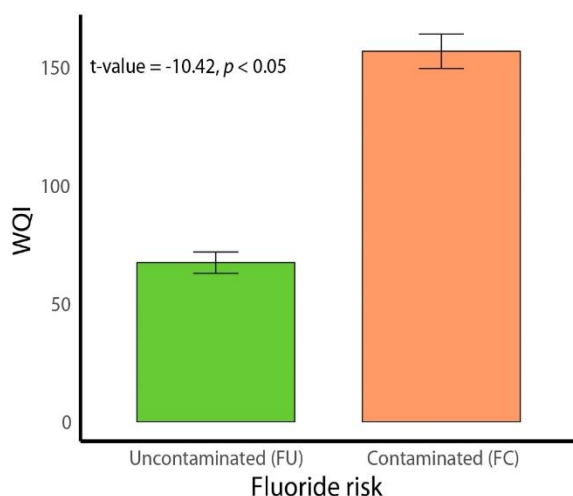
Figure 25. Bar diagram showing differences (p < 0.05, t = -10.42) in values of water quality index between two considered groups of water samples. Source: Nandi et al., 2024b
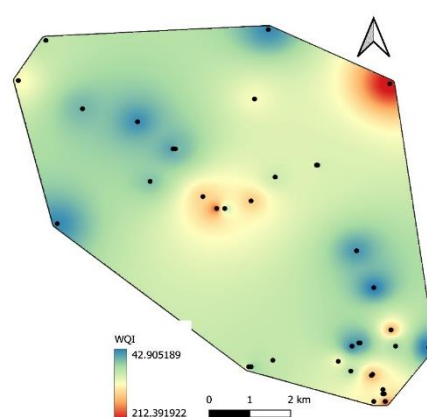
Figure 26. IDW map showing spatial distribution of WQI across the study area with the highest value of WQI in areas of highest fluoride ion occurrences.

139

The mean WQI of FC group (156.76 ± 7.30) was significantly different) (t = - 10.42, p <0.05,) and dangerous (p<0.05) than the same for group FU (67.34 ± 4.49) indicating the former group more unsuitable for use (Fig. 25). The IDW maps showing geospatial distribution of the WQI within the study area (Fig. 26) aids clear visualisation. The striking similarity of this map to the fluoride spatial distribution map (Fig. 23B) shows a potential contribution of the F^- ion in dictating the water quality.

4.2.2.2. Evaluating risks to irrigation

As discussed earlier, SAR provides estimate of sodium ion accumulation in the soil. It is calculated from magnesium and calcium ions (Table 1) (Rawat et al., 2018). Formation of salt layer and clogging of pores in the soil due to high SAR leads to an increase in percolation time of the concerned soil(Khan et al., 2020). Mean SAR values in 'FU' (1.34) and 'FC' (2.77) groups in the study significantly (t = -4.98, $p < 0.05$) varied (Fig. 27A). IDW map generated to look into the spatial distribution of this parameter shows areas with highest SAR in red colour (Fig. 27B).

Alkalinity hazards from the test samples can be well represented by RSC. As per Rawat et al., 2018, it can be grouped in 3 categories on basis of suitability in agricultural needs; 'good' where RSC < 1.25, 'permissible' with RSC ranging between 1.25 – 2.5 and 'unsuitable' where RSC exceeds 2.5. In this study, ~21%, of total FU samples and ~63% from FC belonged to the 'unsuitable' category. Variation in RSC was significant (t-value = -3.27, $p < 0.05$) between two studied sample groups (FC mean = 3.26 ± 0.47, FU mean = 1.29 ± 0.37) (Fig. 27C). The spatial variation map of RSC (Fig. 27D), where red coloured regions with highest RSC were found in dispersed pockets around the boundaries of the study area. Higher RSC was found in areas with higher fluoride concentration , showing a positive relationship between them.

One very crucial index for evaluating irrigation water quality is percent sodium (Na%). Value of Na% regulates the internal soil drainage capacity (Kouser et al., 2022). Significant (t-value = -5.62, $p < 0.05$) variation in was observed on comparing mean values of this parameter between fluoride safe (FU, 34.43 ± 2.88) and fluoride unsafe (FC, 56.78 ± 2.73) groups.
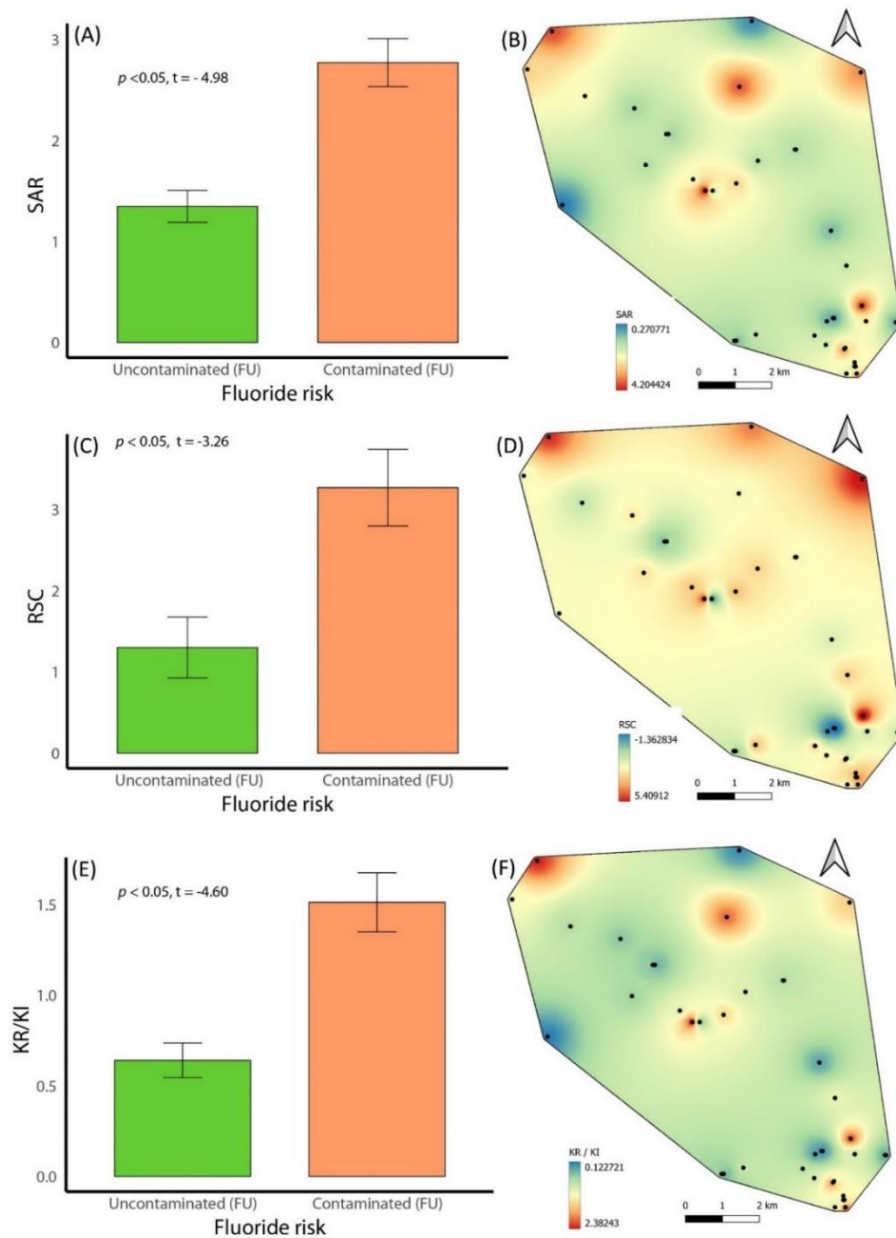
Fig. 27. Assessing the suitability of water samples for irrigation using major irrigation indices by comparing their mean between both study groups using bar plots and visualising their spatial distribution across the study area using IDW maps for the respective indices. Source: Nandi et al., 2024b

The index, KR, created on the basis of the ratio of Na^+ ions to sum of Mg^{2+} and Ca^{2+} ions (Table 1) when generates values greater than unity, an alkalinity hazard is predicted for the sample making it not so suitable for irrigation (Gantait et al., 2022). The average value of KR in 'FU' was 0.64 ± 0.95, while 'FC' samples had the mean KI value of 1.51 ± 0.16 water (Fig. 27E) and was significantly higher (t-value = -4.60, $p < 0.05$). This excess alkalinity was from sodium and as expected, most of them came from the fluoride contaminated group. Regions of high F^- also have more Na^+ ions due to positive correlation between them. The generated IDW map for KR (Fig. 27F) thus shares remarkable similarity with fluoride IDW map.

4.2.3. Geochemical evaluations in the light of classical approach

4.2.3.1. Mineral dissolution and ionic exchanges

Scatter plots have been created in this study to illuminate the weathering profile and pivotal chemical reactions monitoring the hydro-geochemistry of the area of study. In the bivariate scatter plot of $(Ca^{2+} + Mg^{2+})$ Vs HCO_3^- (Fig. 28A) all the samples from the FC group lie below the equiline (1:1) and further away from it when compared to the samples from the FU group. Most of the samples from the latter group lie closer to the equiline signifying dissolution of dolomite or calcite. Some are even located above the line hinting at the possible gypsum dissolution (Nandi et al., 2024a). This indicates the abundance of HCO_3^- ion from silicate weathering and carbonate dissolution in the FC group (Gantait et al., 2022). Similar findings were previously encountered in the results of the Welch test. The plot for $(Ca^{2+} + Mg^{2+})$ Vs $(HCO_3^- + SO_4^-)$ (Fig. 28B) similar trend and supports the findings. The gathering of FU samples above the 1:1 line or equiline speak not only for carbonate weathering, but also for reversed ion-exchange mechanisms. When we plotted $(Ca^{2+} + Mg^{2+})$ Vs Na^+ (Fig. 5C), we found almost all of the samples from group 'FU' flocked above the equiline showing the abundance of Ca^{2+} and Mg^{2+} in them. However, the samples from FC clearly indicated an excess presence of Na^+,

thus strengthening former interpretations. From the Ca^{2+} Vs Na^+ scatter (Fig. 28D) we could elucidate the same. The scatter diagram for $(Na^+ + K^+)$ Vs TC (Fig. 28E) showed the samples from FC groups lie closer to the equiline than samples from the second group. It described that FC has a higher Na^+ ion content. $(Ca^{2+} + Mg^{2+})$ Vs TC (Fig. 28 F) put forward the exact opposite scenario.
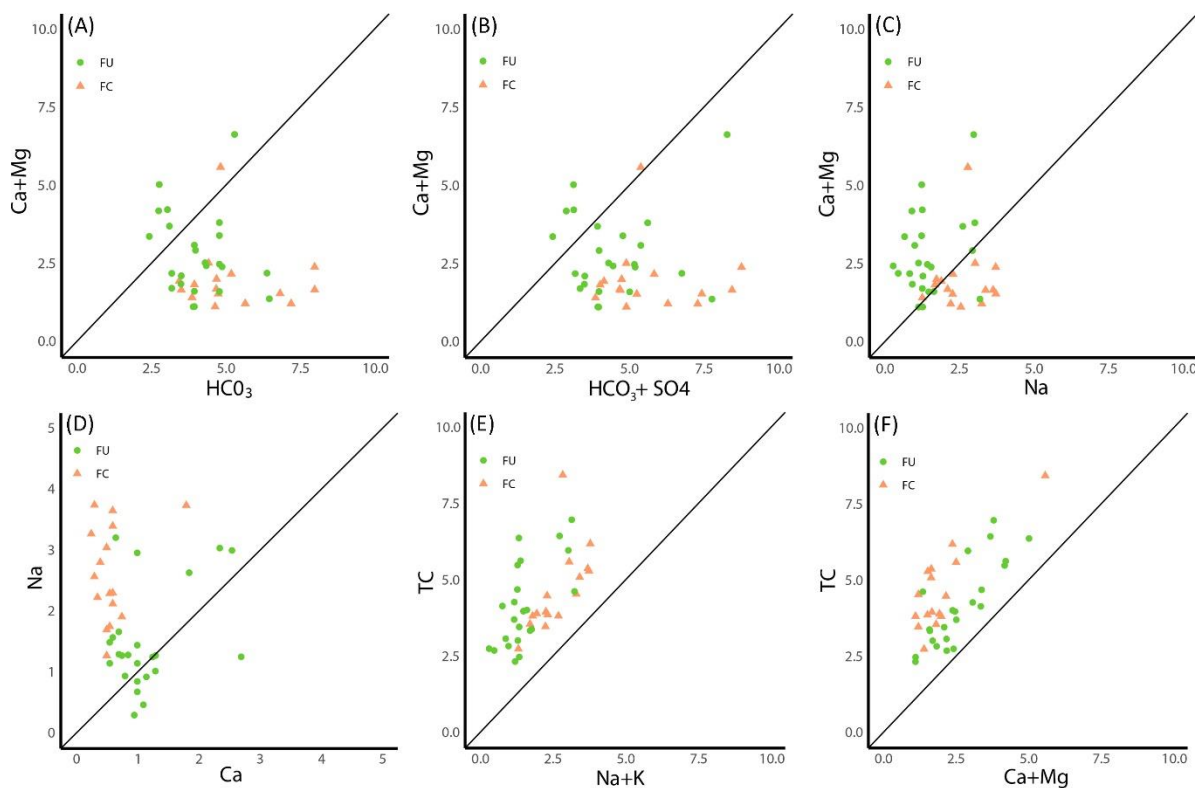
Figure 28. Bivariate scatter plots of major ions to elucidate the underlying chemical processes in the aquifer.

Source: Nandi et al., 2024b

4.2.3.2. Identification of hydrogeochemical facies

The Piper Trilinear Diagram (Fig. 29) aids in identification of primary facies of the collected samples, based on composition of their ions. Through the diagram, the prevailing hydrogeochemical facies is discerned among four established categories: the Ca^{2+}-Mg^{2+}-Cl^--

SO_4^{2-} facies (I) which denoting permanent nature of hardness; the Na^+-K^+-Cl^--SO_4^{2-} - facies (II) or the facies indicating salinity; the representative of fluoride dissolution Na^+-K^+-HCO_3^- facies (III); and finally, the HCO_3^- or type IV facies , suggesting temporary hardness. Gantait et al., (2022) also followed this classification to find the exact water type. The FC group samples were mostly found in the type III facies, well explaining the fluoride abundance. Type IV is the most dominant water type for FU group.
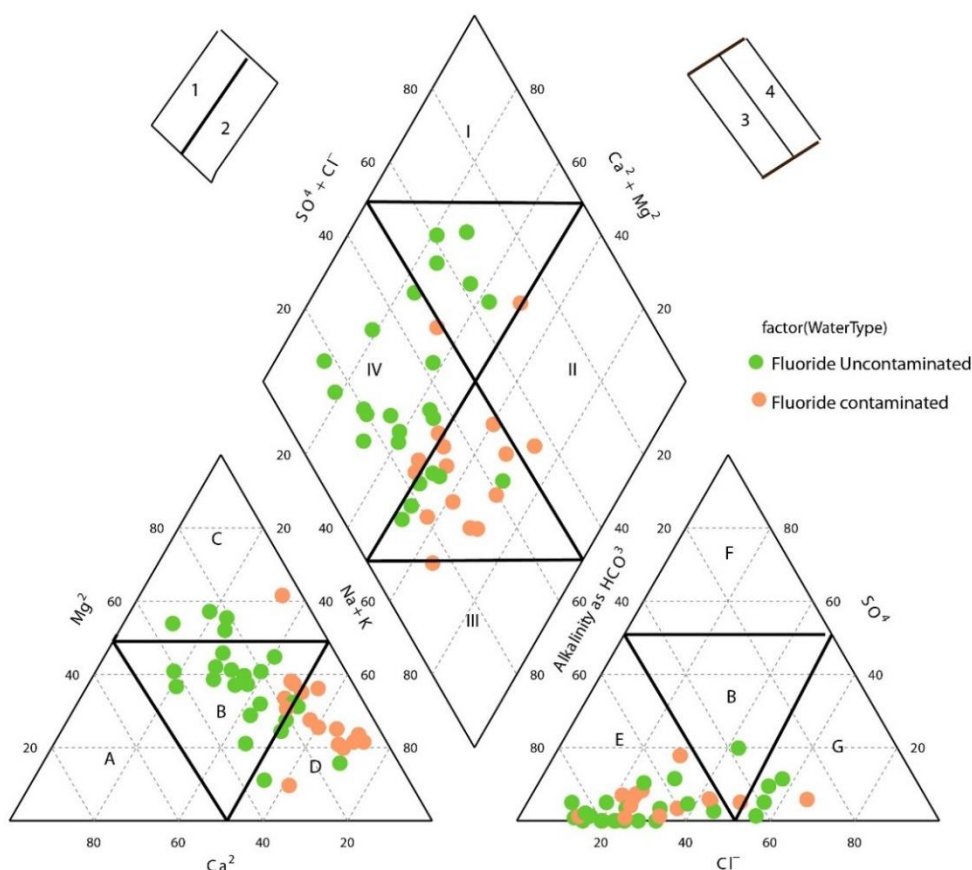
Figure 29. Piper trilinear diagram to aid identification of hydrogeochemical facies of groundwater from both study groups FC or fluoride contaminated and FU or fluoride uncontaminated.

Source: Nandi et al., 2024b

Most samples from group FU fall in zone B (mixing zone) in the triangle of cations, whereas, the sodium type (zone D) houses samples from fluoride contaminated group (FC) (Khan et al.,

2020). It was evident from the triangle of primary anions, that most water samples from FU and FC group were present in zone E or bicarbonate-type water zone. The Zone 1 where Ca^{2+}-$Mg^{2+} > Na^+$-K^+, housed 75% of the fluoride safe (FU) water samples. In contrary, the FC samples were mostly confined to the Zone 2 and exhibited the domination of alkali ions (Na^+-K^+) (Gantait et al.,2022) as already noted from the results of the welch tests and scatter diagrams earlier in the manuscript.

4.2.3.3. Identification of dominant mechanisms shaping aquifer-chemistry

The three primary mechanisms shaping the ionic composition of an aquifer are precipitation, evaporation and rock-water interaction (Gantait et al.,2022). The Gibbs diagram can efficiently pinpoint the most dominant mechanism amongst the three. It uses two different scatter diagrams of $Cl^-/(Cl^-+HCO_3^-)$ Vs TDS (Fig. 30) and $Na^+ / (Na^+ + Ca^{2+})$ Vs TDS (Fig. 30) to identify the principal contributor. It could be well inferred from these figures that for both study groups, rock dominance bags the largest share of contribution towards the existing aquifer chemistry.
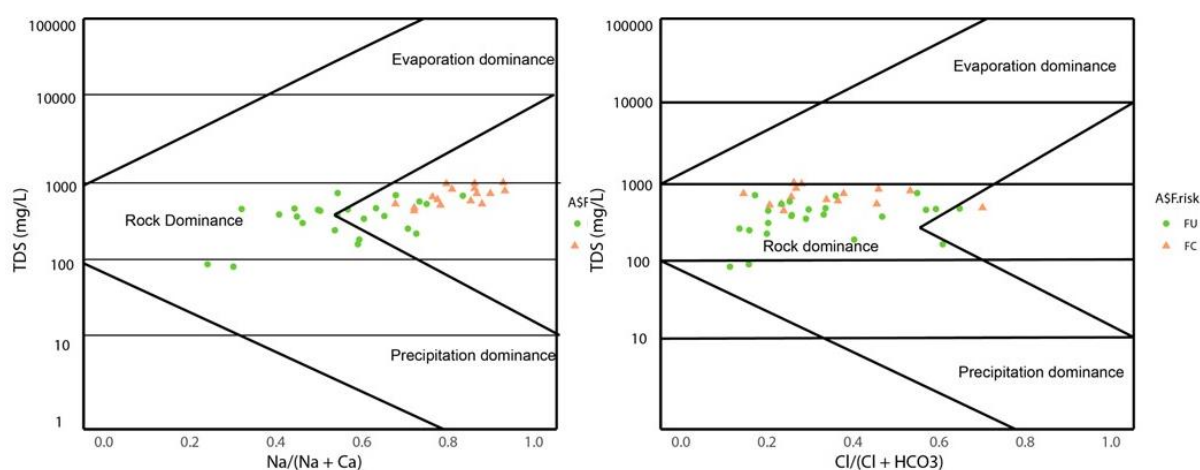
Figure 30. Gibbs diagram of TDS vs. $Na^+/ (Na^+ + Ca^{2+})$ and TDS vs. $Cl^-/ (Cl^- + HCO_3^-)$ depicting the contribution of rock dominance to be pivotal in regulation of hydrogeochemical evolutionary mechanism. Source: Nandi et al., 2024b

4.2.4. Statistical dimensions to fluoride dissolution

4.2.4.1. Correlation analysis among participating major ions

The correlation analysis of collected water samples from 'FU' and 'FC' groups revealed substantial insights (Fig. 31). In group FC or fluoride contaminated group, F^- ions showed a significantly positive ($p<0.05$) correlation with HCO_3^- (r = 0.750) as reported in earlier studies by Gantait et al., (2022) and Maurya et al., (2020). Previously, this group had exhibited a significantly greater abundance of bicarbonate and a bicarbonate water type from the piper diagram. Higher HCO_3^- can contribute to increased alkalinity and conditions promote fluoride dissolution from minerals like CaF_2. Additionally, due to a striking similarity in the ionic radius of F^- ion to OH^-, the later replaces F^- bound to clay particles at alkaline conditions (Chowdhury et al., 2021). The released Ca^{2+} ions then react to HCO_3^- ions present in the aquifer and get precipitated. This was reflected from the significant ($p<0.05$) negative correlation of F^- and Ca^{2+} in all collected samples (r = -0.429). Gantait et al., (2022) reported a similar finding. The samples from 'FC' also exhibited higher positive correlations between F^- and Na^+ (r = 0.517), indicating silicate weathering. The CO_2 formed as a by-product of calcite precipitation reaction, reacts to silicates like feldspar releasing Na^+ (Gantait et al., 2022)

$$Ca^{2+} + 2HCO_3^- = CaCO_3 + CO_2 + H_2O$$

$$4NaAlSi_3O_8 + 4CO_2 + 22H_2O = Al_4(Si_4O)(OH_8) + 8H_4SiO_4 + 4Na^+ + 4HCO_3^-$$
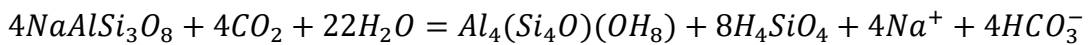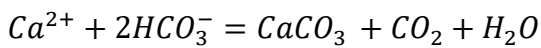
Conversely, in the 'FU' group, comparatively lower correlations of the F^- ion to Na^+ (r = 0.458, $p<0.05$) and HCO_3^- (r =0.316) suggested reduced rate of silicate weathering.
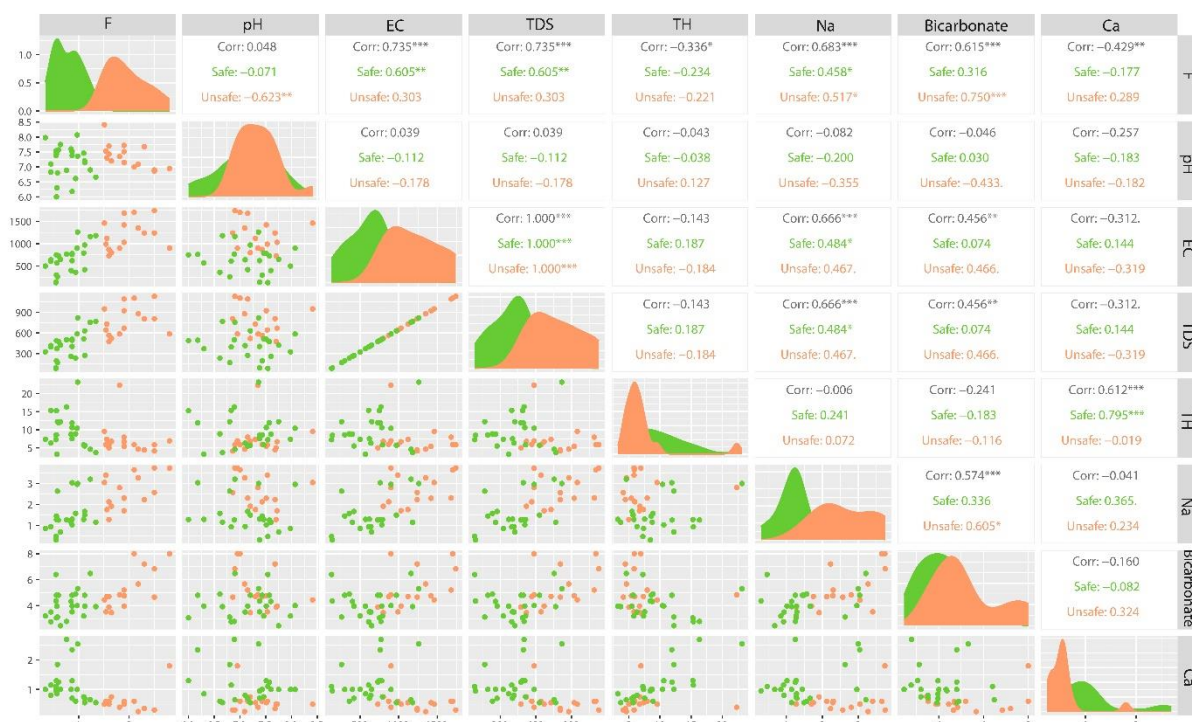
Figure 31. Spearman's rank correlation between different physiochemical parameters of the FC (unsafe) and FU (safe) group of water samples. Source: Nandi et al., 2024b

4.2.4.2. Reducing dimensions by Principal Component Analysis

PCA- biplot a dimension reduction technique was created using different parameters, namely pH, TDS , EC, TH, K^+, Na^+, Ca^{2+}, Cl^-, HCO_3^- and F^- to elucidate the contrasts in responses of these parameters between two study groups (Fig. 32). The first five dimension showed eigen values higher than unity and could explain 73.46% variation in total. The chief contributors to dimension 1 were F^-, TDS, EC, Na^+ and HCO_3^- which showed positive loadings with respect to the dimension along with Cl^-. It indicated a positive correlation between the parameters. All other parameters gave negative loadings to it. A positive loading for F^- and negative for Ca^{2+} to the same dimension again threw light on their negative correlation. For dimension 2 all parameters except pH showed positive loadings. Remarkable distinction between two study groups were evident from the widely separated large coloured circles or mean points.
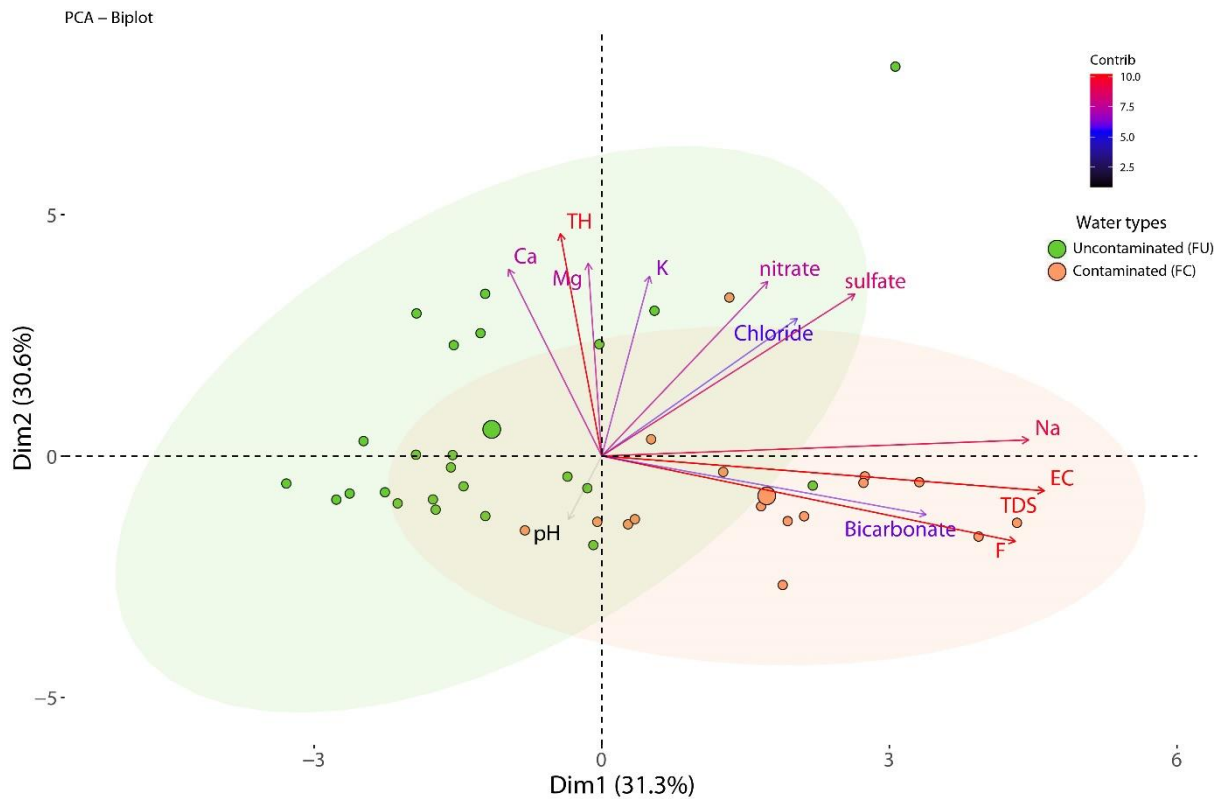
Figure 32. Principal component analysis of physicochemical parameters of collected groundwater samples across Fluoride contaminated and fluoride contaminated groups Source: Nandi et al., 2024b

4.2.5. Predicting fluoride dynamics and distribution by SOM

By generating the SOM using 10 parameters, we found that the optimal number of neurons was 16. In the observation cloud map (Fig.33), 5 points were misclassified, indicating a model accuracy of 80%. Both the scree plot and Silhouette methods identified the optimal number of super-classes as two, with an average silhouette width of 0.22. The model explained 77.92% of the total variance, with a quantization error of 2.15. Topographic error measures the preservation of the topographic structure of the map, calculated as the proportion of observations where the best-matching node is not adjacent to the second-best matching node on the map.
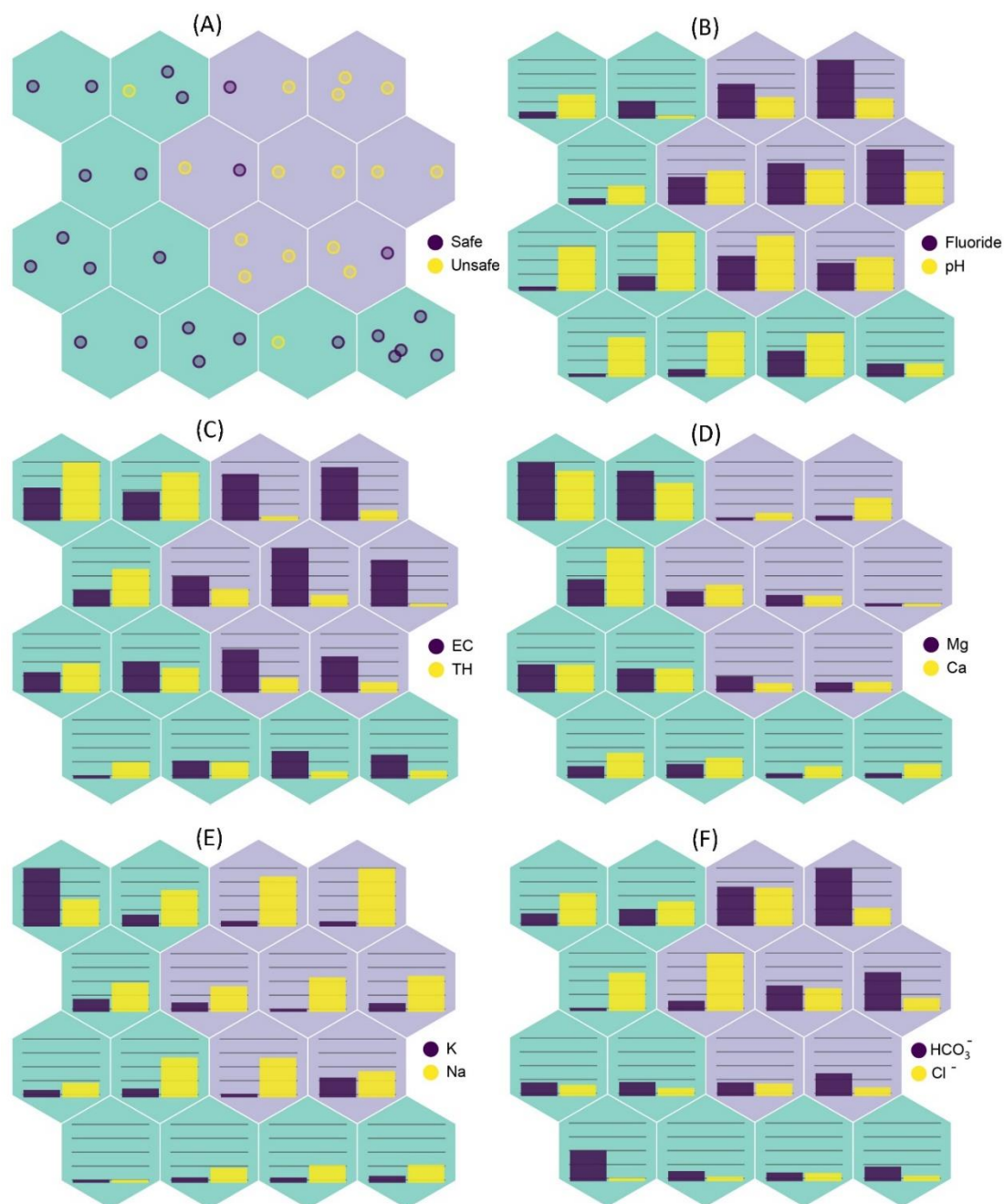
Figure 33. Observation cloud maps created using the supervised Kohonen mapping or Self Organising Maps (SOM) aiding in visualisation of the nodes occupied by the two super-classes or categories (FU or Safe and FC or unsafe). Number and type of samples in each node and the accuracy of the classification have also been elucidated in (A). From B to F, the mean concentration of other major ions and physico-chemical parameters in each node has been depicted as coloured bars. Source: Nandi et al., 2024b

Both a low topographic error (0.12) and Kaski-Lagus error (3.63) demonstrate the quality of the SOM model. From the cloud maps (Fig. 33B-F) it is visible that the nodes 5, 6,10,11,12,13 and 14 which come under the fluoride unsafe category or the FC group, show very low levels of Ca^{2+}, Mg^{2+} and TH, proving the derivations so far. On the other end, the highest of these values can be found in the fluoride safe nodes. The positive correlation of F^- with HCO_3^- and Na^+ established in former sections can be validated from the higher and prominent bars for those ions. These ions possibly shared a homogeneity in their sources (Nakagawa et al, 2017 and 2019).

4.2.6. Analysing the potential health hazards from fluoride by health risk assessment (HRA)

The various non-carcinogenic effects from any element can have the potential to pose substantial threat to human health if the calculated hazard quotient (HQ) value for it exceeds unity. This HQ value is regulated by the CDI. In this study, the mean CDI values for the two age groups studied (children and adults) are 1.31 ± 0.09 mg/kg/day and 0.911 ± 0.064 mg/kg/day respectively for the fluoride safe group (FU). While, mean CDI in group FC are 3.26 ± 0.16 mg/kg/day and 2.27 ± 0.11 mg/kg/day for children and adults respectively. Fig.34 elucidates samples from group FC pose significantly higher health risks to both age groups considered and provides indication towards the contribution of higher fluoride to increased health risks. For both groups 'FU' and 'FC', the children seemed to be at greater risk, possibly because of their lower bodyweights (Kadam et al, 2021). Thus, to predict the sensitivities of different interacting parameters to the accumulated health risk, SSI was taken into consideration.
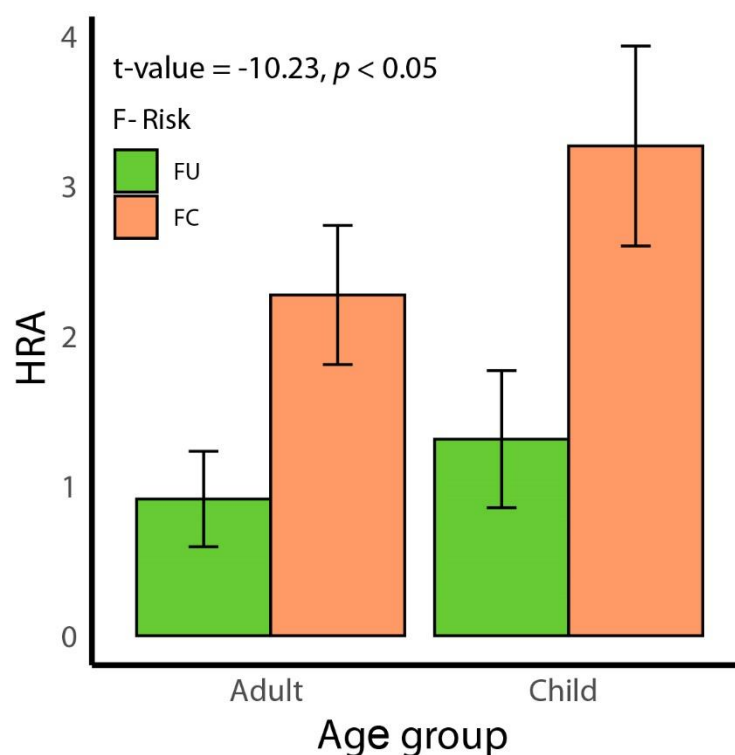
Figure 34. Bar diagram showing differences in values of HRA based on non-carcinogenic threats of fluoride ion between two considered study groups (Fluoride contaminated or unsafe and Fluoride uncontaminated or safe). The bars in the graph represent mean ± SE of HRA. Source: Nandi et al., 2024b

4.2.7. Identification of the chief contributor with the Sobol Sensitivity Indices

To estimate the impact of different input variables on the non-cancerous health risks caused by the F^- ion present in collected drinking water samples, the Sobol Sensitivity analysis was conducted for two concerned study groups (adult and children). Four different factors, namely Fluoride concentration (C_w), weight of body (BW), frequency of exposure (EF), and rate of ingestion (IR), previously encountered for calculation of HQ in HRA were used as input variables for the analysis. A total of 17000 runs were conducted. Fig. 35 depicts the results from the analysis. For children the most impactful parameter was C_w (0.48), followed by BW (0.21), IR (0.19) and EF (0.001). A similar trend was observed for the other group as well. In

adults the values for FOSI were 0.65, 0.05, 0.22 and 0.001 for C_w, BW, IR and EF respectively. The value of FOSI for EF being less than 0.01 in both groups, this parameter was considered insignificant in terms of response. In both groups, for all included parameters the TOSI was greater than the FOSI showing the presence of interactions within the parameters themselves. In the diagram showing interaction between parameters in children, the highest accountable interaction was noted between C_w-BW (0.036), followed by C_w-IR (0.035) and IR-BW (0.02). For adults the important among interactions were C_w-IR (0.038) and C_w-BW (0.096). These SOSI scores bring forward the impact of pairwise interactions and therefore we conclude that the outcome could be appropriately appraised only by taking all these interactions into account along with fluoride concentration itself (Rajabi et al., 2022, Mukherjee and Singh, 2021).
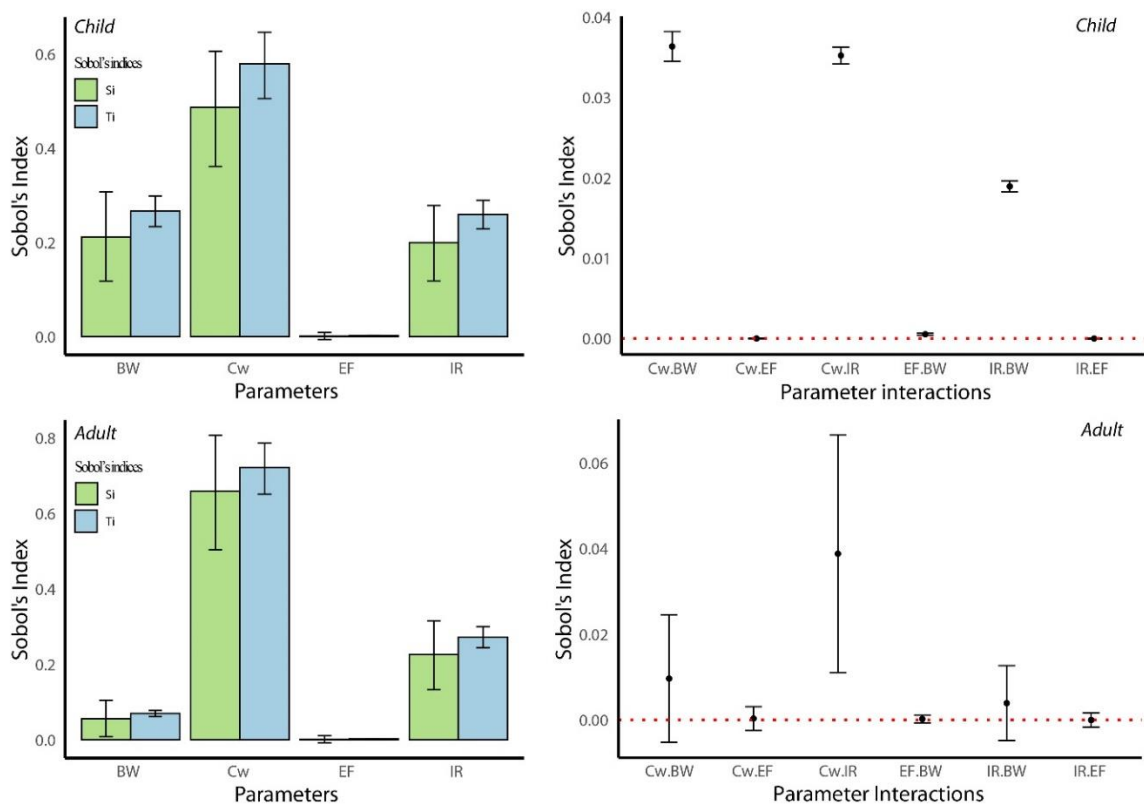
Figure 35. Sobol sensitivity analysis based on oral HQ ingestion model with four input parameters (Cw, BW, IR and EF) for two age groups showing the first-order (Si) and total (Ti) effects and also pair-wise secondary interactions between parameters.

Source: Nandi et al., 2024b

4.3. Evaluating targeted fluoride removal with exfoliated biochar

4.3.1. Selection of biochars based on efficiency

Among the four different types of exfoliated biochar prepared, the biochar with the highest sorptive efficiency was selected first before proceeding further. The sorptive efficiencies of the four different biochar prepared were compared based on their removal percentages calculated from the formula given below.

$$\%Removal = \frac{C_i - C_f}{C_i} * 100$$

Where, Ci = Initial concentration of fluoride solution

 Cf = Final concentration of fluoride solution.

On comparison, the sorptive efficiencies differed significantly amongst the biochars ($p < 0.01$, ANOVA: $F_{3,8} = 2799$) and the highest removal efficiency was shown by the 2(M) HNO_3 exfoliated water hyacinth- based biochar or WH-Acid (Fig. 36) and the further studies were carried out with it. Hence forth, it has been denoted as EB.
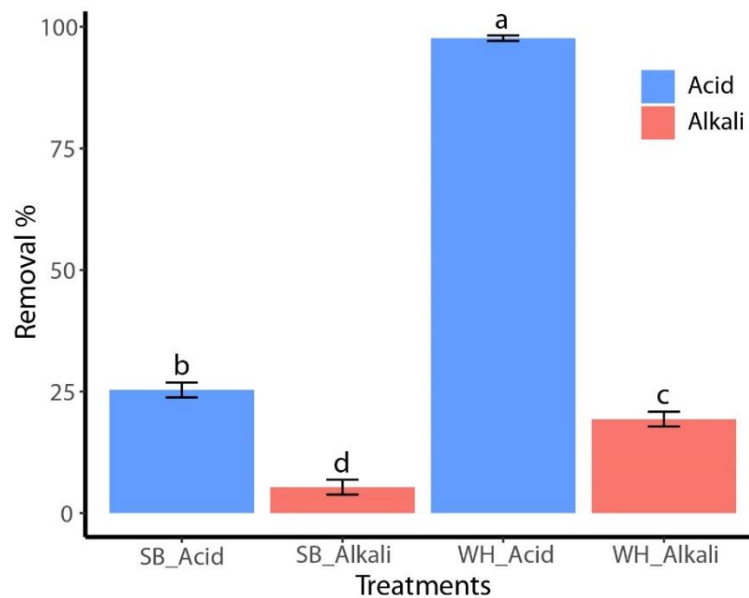
Figure 36: Comparisons between adsorptive efficiencies of biochars based on removal percentage.

4.3.2.1. Batch Adsorption studies

4.3.2.1.1. Effect of biochar dose on percentage removal of fluoride

To find out how the dosage of biochar affects the final removal efficiency experiments were carried out in batches. In every batch the dose of the adsorbent or the nitric acid exfoliated water hyacinth-based biochar (EB) was varied as 3, 6.5 and 10 gm L^{-1} respectively. In each set, the other reaction conditions like the reaction pH (pH 6), the surrounding temperature (30°C) and initial fluoride concentration in the adsorbate solution (10 mg L^{-1}) were kept constant. Under such conditions, when remaining fluoride from the solutions was measured at different time intervals (1hr, 2hr, 3hr and 4 hr), it was found that on increasing the biochar dose, a significant increase takes place in percentage removal of fluoride. From the results of the two-way ANOVA performed we found the biochar dose ($F_{2,12}$= 319.543, p <0.01), varied significantly with the highest removal in 10gm L^{-1} biochar doses (Fig.37A). Our findings were in line with reports of Ganguly et al. (2020) where they noted an increased removal of malachite green dye with increasing the concentration of the biochar and showed maximum removal at the highest biochar dose of 2 gm L^{-1}. The increased number of active sites for adsorption from the abundance of biosorbent as the dosage increases, facilitates higher adsorption of fluoride. In this case, the time ($F_{3,12}$= 8.88, p<0.01) of contact and biochar dose-time interaction ($F_{6,12}$= 3.54, p <0.05) also showed significant variations across the experimental sets.

4.3.2.1.2. Effect of pH on percentage removal of fluoride

The sensitivity of percent fluoride removal to pH alterations (pH 4, 6 and 8) in the reaction solution was estimated by conducting a batch sorption experiment keeping all other reaction parameters constant (Reaction Temperature = 30°C, Biochar dose=10 gm L^{-1}, Initial fluoride concentration =10 mg L^{-1} fluoride). In Fig.37B, the results of the batch study have been represented across time (1- 4hrs) where the fluoride removal capacity is found to be maximised

at pH 4. At alkaline conditions (pH 8) there was a decrease in removal efficiency of fluoride by the exfoliated biochar. As evident from the ANOVA, there were significant differences for removal percentage of fluoride with alteration of adsorbate pH ($F_{2,12}$= 32.619, $p<0.01$). The acidic pH was best suited for removal of negatively charged fluoride ion because it was easily attracted to the biochar surface which shows a tendency to become protonated under such acidic conditions. The results from studies by Chakraborty and Das, 2023, corroborates with the current study. They reported more efficient removal of negatively charged Cr (VI) ion in acidic pH. Another study on removal of a cationic dye (MG) using activated char adsorbent (Ganguly et al., 2020) pointed to the altered efficiency of dye removal due to the increased abundance of H_3O^+ ions under acidic conditions.
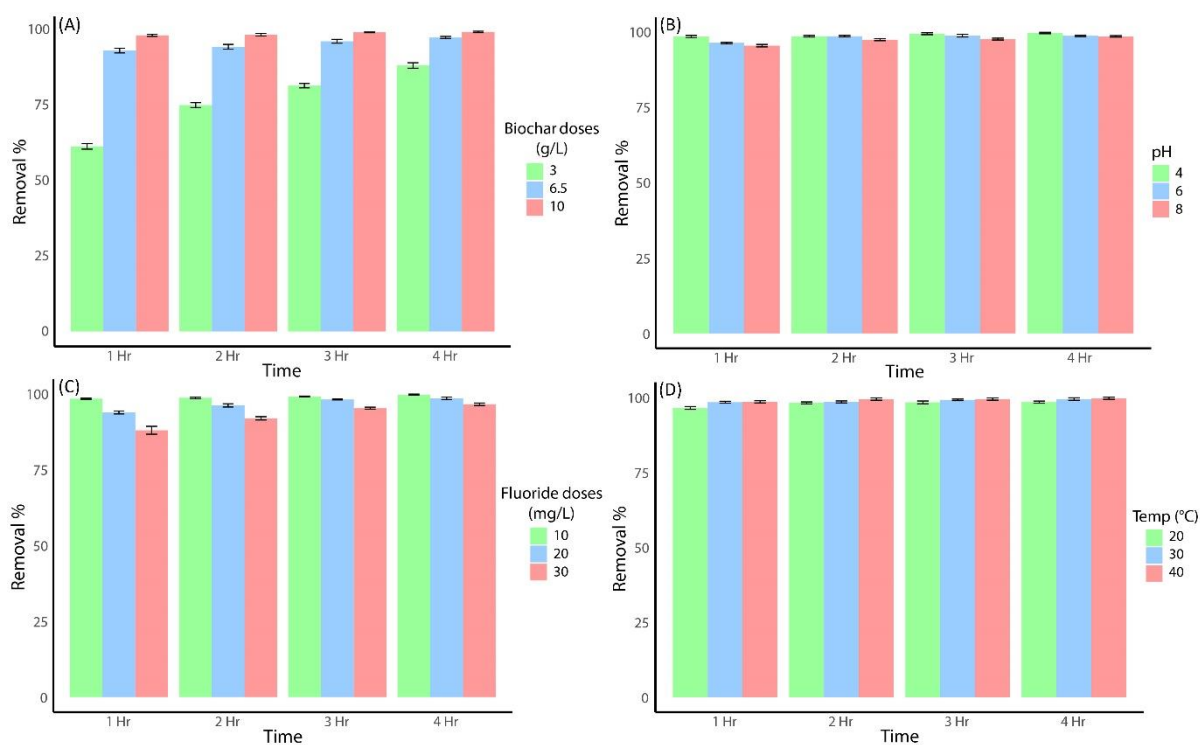
Fig 37. Bar plots showing effects of (A) Biochar dose (gm L^{-1}) (B) pH of adsorbate solution (C) Initial fluoride concentration (mg L^{-1}) and (D) reaction temperature (∘C) on removal % of fluoride by nitric acid exfoliated water hyacinth biochar (EB). The bars in the graph represent the mean ± SE of respective parameters.

With a shift of pH to the alkaline range, a negative environment gets created from the deprotonation of carboxyl and hydroxyl groups on adsorbent surface hindering the removal of negatively charged fluoride from the solution (Ganguly et al., 2020). Probably, the similar mechanisms occur in our case. The time of contact ($F_{3,12}$= 5.043, $p<0.05$) also had created significant variations in removal percentage of adsorbate under altered pH conditions.

4.3.2.1.3. Effect of initial fluoride concentration on percentage removal of fluoride

Fluoride removal efficiency of the prepared biochar was tested based on the percentage fluoride removal under conditions of varied initial fluoride concentrations (10, 20 and 30 mg L^{-1}) in batch experiments. The data generated was noted across different intervals of time. A BOD incubator was used for the purpose like other set of batch experiments to maintain constant reaction temperature (30°C). A constant dose of biochar (10 gm L^{-1}) was added to the reaction mixtures set to pH 6 and samples were read at time intervals of 1 hour, 2 hours, 3 hours, and 4 hours. Fig. 37C represents the results of the study. The best performance was observed with the minimum initial fluoride dose (10 mg L^{-1}) and decreased simultaneously with increasing initial adsorbate concentration in the experimental reactions. A high initial adsorbate dosage takes up room for further adsorption by utilising free active sites. It adds up to the competition between adsorbate moieties for availability of sites of adsorption as also pointed out by Ganguly et al., 2020. The study reported similar findings for removal of malachite green dye. The changes in the removal were significantly different. The performed two-way repetitive ANOVA, resulted in significant p values for effects of initial fluoride dose ($F_{2,12}$= 40.093, $p<0.01$) and the contact period ($F_{3,12}$= 3.87, $p<0.05$). The initial fluoride concentration-time interaction however had no significant (($F_{6,12}$=0.689, $p>0.05$) contribution to make in this regard. The reasons for the incidence might be the increasing competition for the unchanged number of active sites resulting from a constant biochar dose.

4.3.2.1.4. Effect of reaction temperature on percentage removal of fluoride

A series of batch experiments were set to assess the impact of reaction temperature on fluoride removal, similarly, keeping all other parameters constant. For the set of experiments the solution pH was maintained at 6 and 10gm L^{-1} biochar was applied to remove 10 mg L^{-1} fluoride from test solutions over various intervals of time likewise. On performing a two-way repetitive ANOVA, a significantly high ($F_{2,12} = 5.1$, p<0.05) percent removal of fluoride ion was seen for reactions set at temperature 40°C with 20°C giving the least removal efficiency (Fig.37D). An increased reaction temperature may favour attraction between the adsorbate and adsorbent molecules as previously reported by Roy et al., (2018).

From the batch adsorption experiments the best removal performance for fluoride by the biochar of interest was recorded at pH 4, 40°C reaction temperature, a biochar dose of 10 gm L^{-1} and initial fluoride concentration of 10 mg L^{-1}. To identify the optimum influencing factors a statistical optimisation was carried out using RSM.

4.3.2.2. Optimisation using Response Surface Methodology

To optimize the response variables of fluoride removal, response surface methodology (RSM) using BBD approach was used. Validation of the optimized model was achieved using ANOVA test. Table.13 depicts the results of the finally optimized model parameters. Initially the full model showed a multiple and adjusted R-squared value of 0.9 and 0.82 respectively. Though the model was significant ($F_{20,27} = 12.21$, $p < 0.01$), it showed negative lack-of-fit value, which signifies lack of adequacy of the fitted model. Time showed no significant contribution in fluoride removal, and furthermore, no interaction was observed among the variables. Finally, a reduced model was ran using those variables which showed significant contribution during the initial model. The final model showed a multiple R-squared of 0.83, and an adjusted R-squared of 0.81 ($F_{5,42} = 42.06$, $p < 0.01$). Moreover, the differences between R^2 and R^2_{adj} was

less than less than 0.2, which demonstrate higher accuracy and reliability of the selected model (Rasoulzadeh et al., 2020).Insignificant lack-of-fit value of reduced model shows its support of adequacy of the fitted model. The mean square value of the lack-of-fit error is close to the pure error, which also reflect the reliability of the selected model. The predicted value of fluoride removal from the model (85.20%) was also very close to the experimental fluoride removal (86.08%) under the optimised conditions (pH= 6, biochar dosage=6.5 gm L^{-1}, initial F$^-$ concentration=20 mg L^{-1} and a reaction temperature=32.98°C).

Table 13. ANOVA test for BBD modelling and result of process optimization.

Estimate	Estimate	Std. Error	t value	Pr (>|t|)	Sig
Parameter statistics					
Intercept	84.3519	1.1669	72.2851	< 2.2e-16	***
pH	-8.9444	1.6503	-5.4199	2.698e-06	***
Temperature (Temp)	5.7369	1.6503	3.4763	0.001195	**
Biochar dosage (BD)	15.9394	1.6503	9.6585	3.133e-12	***
Fluoride dosage (FD)	-12.0056	1.6503	-7.2748	5.895e-09	***
Temp * Temp	-9.6113	2.0212	-4.7552	2.347e-05	***
	Df	Sum Sq	Mean Sq	F value	Pr (>F)
Model Statistics					
FO (pH, Temp, BD, FD)	4	8177.8	2044.45	46.9174	5.810e-15
PQ (Temp)	1	985.3	985.35	22.6124	2.347e-05
Residuals	42	1830.2	43.58		
Lack of fit	27	1454.3	53.86	2.1493	0.06151
Pure error	15	375.9	25.06		
		Value		Unit	
Optimization process					
pH		6			
Temperature		32.98		°C	
Biochar dosage		6.5		g/L	
Fluoride dosage		20		Ppm	
Predicted efficiency by the solver		85.2		%	

The quadratic equation corresponding to the BBD model for fluoride adsorption on biochar can be defined as:

Y= 84.35 – 8.94 (pH) + 5.73 (Temp) + 15.93 (BD) – 12.005 (FD) – 9.61 (Temp * Temp)

Where Y is the fluoride removal %; Temp: temperature; BD: biochar dosage; and FD: fluoride dosage.
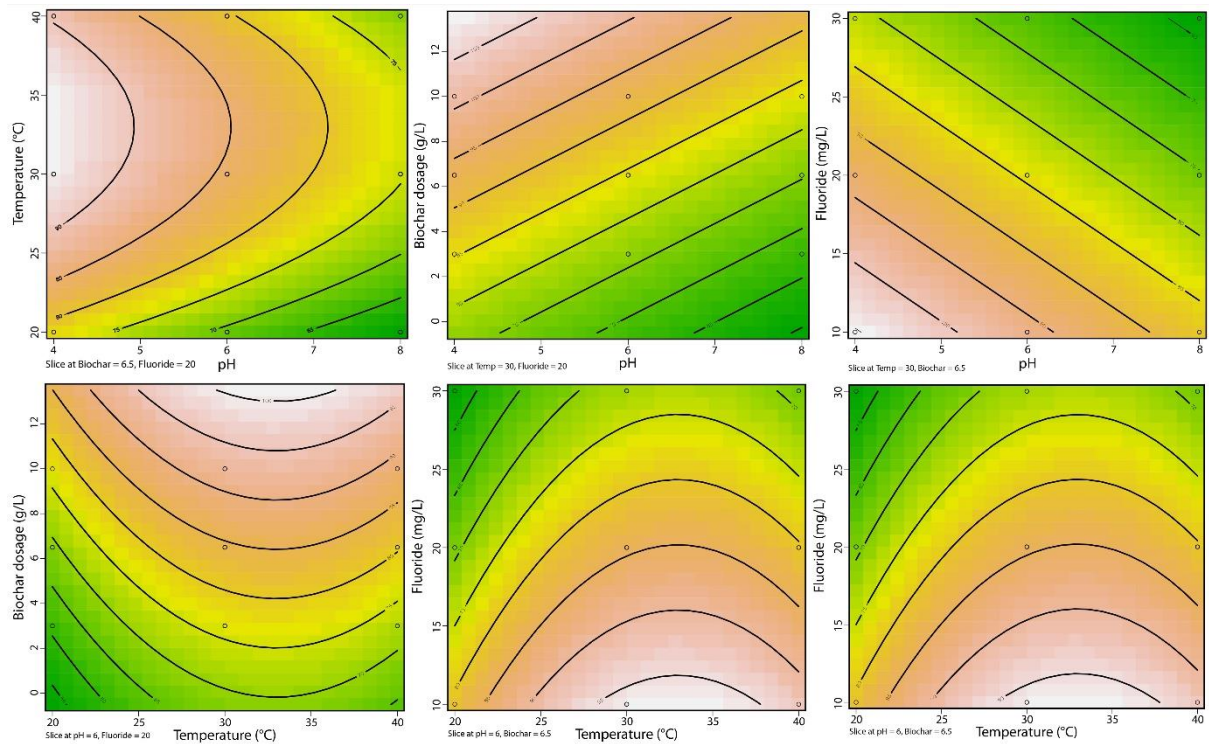
Fig 38. Contour plots by RSM elucidating the interactive effects of a pair of variables on the fluoride removal % by biochar of interest, keeping the third parameter constant. An array of six different combinations from four parameters, namely, temperature (○C), biochar dose (g L⁻¹), pH and initial fluoride concentration (ppm) were created.

Contour plots were used to visualize the impact of those variables on fluoride removal (Fig. 38). RSM has been used in several studies to optimize the response of variables of fluoride removal. In a study by Hashemkhani et al., (2022), central composite design of RSM approach was used to optimize pH level, doses of adsorbent, time and concentration of fluoride on

removal of fluoride (%) by seashell. The author observed a negative relationship of pH and fluoride concentrations level, and a positive relationship of adsorbent doses on fluoride removal % corroborate with our observation. The study also confirms that slightly acidic to neutral pH is optimum for fluoride removal and supports our findings from batch adsorption study (Section 4.3.2.1).

4.3.2.3. Adsorption kinetics

In this study, the recorded data for biosorption share the best fit with the pseudo second order model (PSO) as obtained from analysis using the PUPAK package in R software. A high regression coefficient (R^2=0.9970) supported the finding (Fig.39). Further, the difference between the values of calculated adsorption capacity ($Q_{e.calculated}$=0.985) and that from experiment ($Q_{e.experimental}$ =0.994) was also negligible. On the other hand, the pseudo first order model (PFO) was rejected for depicting the best fitting model for the current study due to its relatively poor R^2 value of 0.8200 (Fig. 39 H).
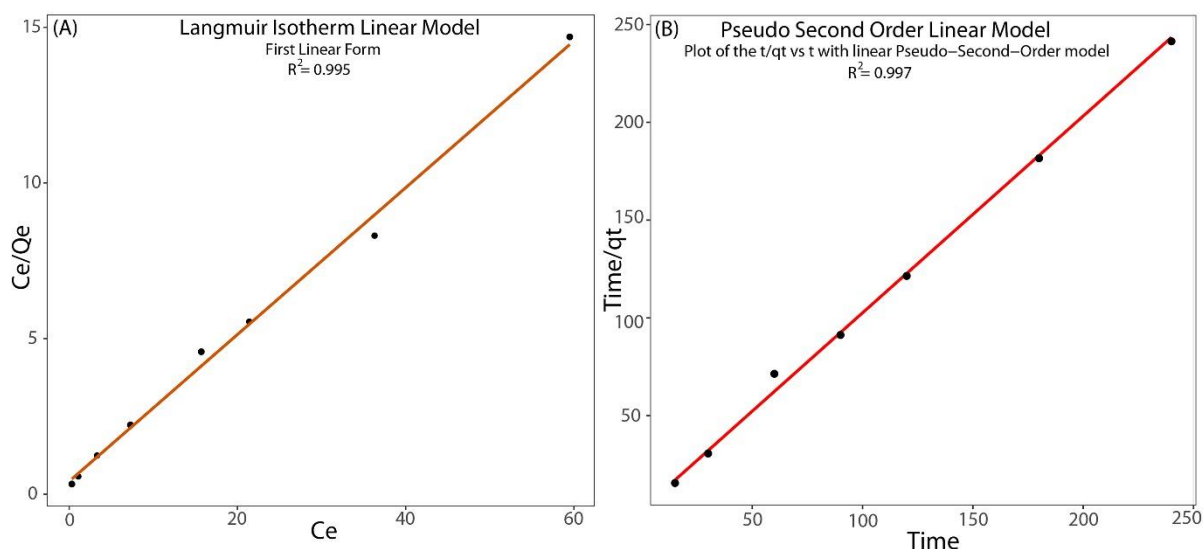
Fig 39. The plots for (A) First linear form of Langmuir isotherm model followed by the biochar during fluoride sorption (C_e/Q_e Vs Ce) and (B) Pesudo second oder linear model (time/q_t Vs time) are elucidated.

It might be deduced that the chemo-sorptive valence force which arise from the coordination, chelation, complexation, and exchange or sharing of electrons within the biochar and the fluoride ion served as the rate limiting step (Charan et al., 2024). In simpler words, and surface biosorption is probably the rate determining step. Sadhu et al., (2021); Kumar et al., (2023) also landed up with similar results. Here, we may deduce that kinetic rates show positive correlations to availability of binding sites (Kumar et al., 2023).

Table. 14 houses the different parameters of the applied kinetic models.

Table 14. Kinetic Model Parameters for adsorption of fluoride with Exfoliated Water Hyacinth Biochar

Kinetic model	Parameters	Values
Pseudo First Order Linear	K_1	0.039
	$Q_{e.calculated}$	0.993
	$Q_{e.experimental}$	0.994
	R^2	0.820
Pseudo Second Order Linear	K_2	0.504
	$Q_{e.calculated}$	0.985
	$Q_{e.experimental}$	0.994
	R^2	**0.997**

4.3.2.4. Adsorption isotherms

On assessing various isotherm models (Langmuir, Freundlich, Temkin, Elovich and BET) as discussed earlier, it was found that the first linear form of Langmuir isotherm generated the best fitting curve (R^2=0.995, Adjusted R^2=0.994) compared to other isotherm models (Table.15, Fig. 39).
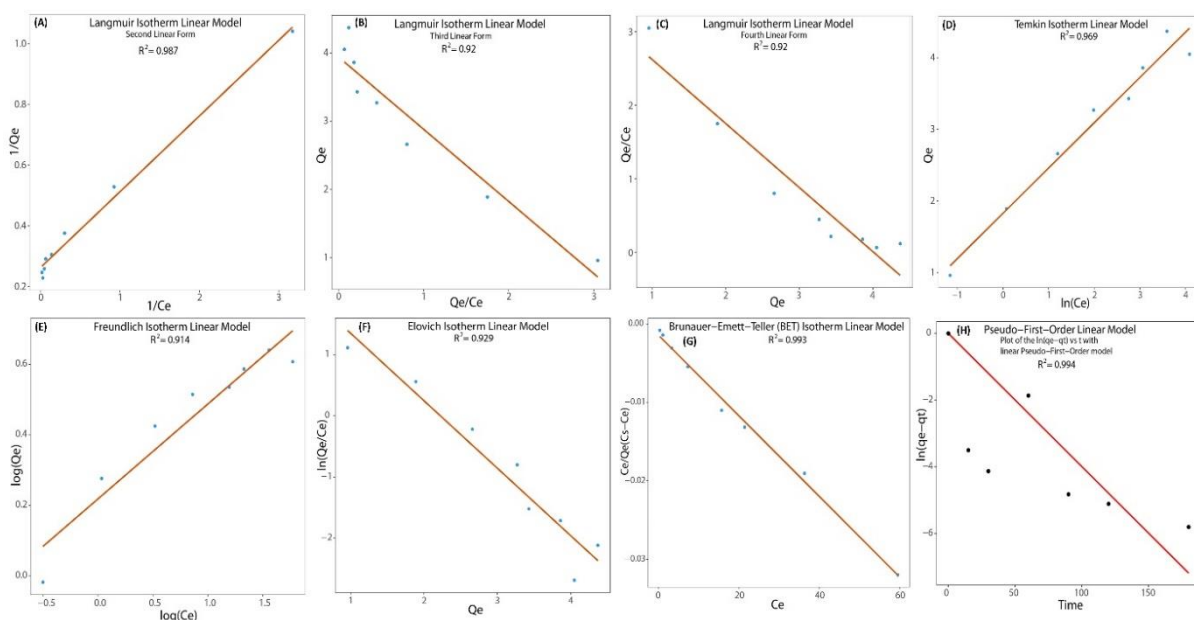
Fig 40. The plots for (A) Second linear form of Langmuir isotherm model (B) Third linear form of Langmuir isotherm model (C) Fourth linear form of Langmuir isotherm model (D) Temkin isotherm model (E) Freundlich isotherm model (F) Elovich isotherm model (G) BET isotherm model followed by the biochar during fluoride sorption and (H) Psesudo first order kinetic model (time/q_t Vs time) are elucidated.

All other models showed lower R^2 values and were thus considered unsuitable choices to explain the adsorption mechanism (Fig. 40A-G). The Q_m or maximum monolayer coverage value was 4.240 (mg g^{-1}) and the Langmuir isotherm constant (K_L) was 0.567 L mg^{-1}. The combination of these parameters provided a quantitative measure of the biochar's capacity to adsorb F$^-$ and the strength of interaction between the biochar and the F$^-$ ions. A high Q max value is desirable as it indicated a high adsorption capacity, making the biochar an effective material for fluoride removal. Meanwhile, a strong affinity (indicated by a high K_L value) suggested that the biochar can effectively adsorb F$^-$ ions even at low concentrations, which is beneficial for treating water with varying levels of F$^-$ contamination. The adsorption mechanism, considering these parameters, involved the physical or chemical interaction of F$^-$ ions with the available sites on the biochar surface as previously discussed (Ahmad et al.,

2014). The process is likely to be a combination of physisorption (physical adsorption due to van der Waals forces) and chemisorption (chemical bonding), with the exact mechanism depending on the nature of the biochar's surface and the properties of the F- ions (Inyang et al., 2016). The R_L upon calculation generated a value of 0.149 which pointed to the favourable adsorption.

Table 15. Isotherm Model Parameters for adsorption of fluoride with Exfoliated Water Hyacinth Biochar

Isotherm model	Parameters	Values
Langmuir Isotherm (First Linear form)	Q_{max} (mg/g)	**4.240**
	K_L (L/g)	0.567
	R^2	**0.995**
	Adjusted R^2	**0.994**
Langmuir Isotherm (Second Linear form)	Q_{max} (mg/g)	3.79
	K_L (L/g)	1.05
	R^2	0.987
	Adjusted R^2	0.986
Langmuir Isotherm (Third Linear form)	Q_{max} (mg/g)	3.93
	K_L (L/g)	0.946
	R^2	0.920
	Adjusted R^2	0.906
Langmuir Isotherm (Fourth Linear form)	Q_{max} (mg/g)	4.01
	K_L (L/g)	0.870
	R^2	0.920
	Adjusted R^2	0.906

Freundlich Isotherm (Linear form)	K_F (L/g)	1.65
	n	3.72
	R^2	0.914
	Adjusted R^2	0.900
Temkin Isotherm (Linear form)	A_t (L/g)	17.91
	B_t	3978.96
	R^2	0.969
	Adjusted R^2	0.964
Elovich Isotherm (Linear form)	Q_{max} (mg/g)	0.906
	K_E (L/g)	12.84
	R^2	0.929
	Adjusted R^2	0.918
BET Isotherm (Linear form)	C_{BET}(L.mg^{-1})	0.006
	R^2	0.993
	Adjusted R^2	0.992

4.3.2.5. BET analysis

The specific surface area of an adsorbent plays a key role in deciding its adsorbate removal performance. The BET surface area analyser was used to assess the specific surface area (m^{2}g^{-1}) at multiple points of an analyte's surface by adsorption-desorption studies of an inert gas like nitrogen in this case. Here in this research, BET specific surface areas of the native biochar (NB) and the nitric acid exfoliated biochar (EB) were compared to find evidence of exfoliation. An increased surface area facilitates better adsorption, so the exfoliated biochar with a surface area of 147.722 m²/g was a better adsorbent against the native biochar with a specific surface area of 51.385 m²/g as reported from the multi point BET analysis. Another important factor in

predicting the biochar performance lies in its pore size, pore volume and distribution. Barett-Joyner-Halendar (BJH) analysis using desorption method helps to determine the pore area, specific volume of pores and distribution of pore size independent of outer area because of the particle size of an analyte. With the help of BJH desorption study, we found that the exfoliated biochar prepared had greater surface area (22.291 m²/g) and pore volume (0.037 cc/g) when compared to the native biochar with surface area and pore volume of 12.406 m²/g and 0.023 cc/g respectively. Pore Radius however was almost same for both analytes (19.211 Å). These findings assured the successful exfoliation of the native water hyacinth biochar by using nitric acid. Yapo et al., (2022) also used this method to check the increase in surface area of the sorbent.

4.3.2.6. FESEM- EDS analysis

FESEM images of exfoliated biochar (EB) before fluoride adsorption (Fig. 41 A, B and C) and fluoride saturated biochar or FSB (Fig. 41 D, E and F) showed several differences to point out to the successful fluoride adsorption by the biochar. The microscopic images of EB showed
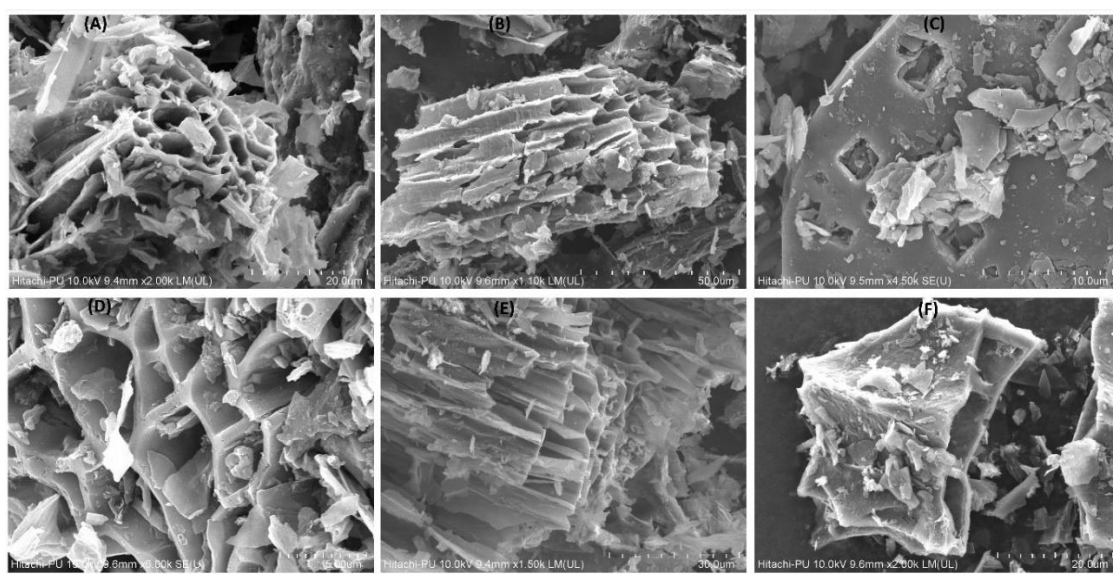
Fig 41. Morphologies of nitric acid exfoliated water hyacinth biochar (EB) before fluoride adsorption (A, B, C) and fluoride saturated biochar (FSB) after adsorption (D, E and F) as evident from FESEM analysis under different magnifications.

(A)

Spectrum: test 17639

Element	Series	unn. C [wt.%]	norm. C [wt.%]	Atom. C [at.%]	Error (3 Sigma) [wt.%]
Carbon	K-series	68.67	68.67	73.97	32.50
Oxygen	K-series	25.09	25.09	20.29	19.12
Fluorine	K-series	0.13	0.13	0.09	0.83
Nitrogen	K-series	6.12	6.12	5.65	11.47
	Total:	100.00	100.00	100.00	

(B)

Spectrum: test 17638

Element	Series	unn. C [wt.%]	norm. C [wt.%]	Atom. C [at.%]	Error (3 Sigma) [wt.%]
Carbon	K-series	67.74	67.74	73.61	24.66
Oxygen	K-series	22.59	22.59	18.43	10.71
Fluorine	K-series	4.24	4.24	2.91	2.77
Nitrogen	K-series	5.42	5.42	5.05	4.90
	Total:	100.00	100.00	100.00	

Fig 42. EDS spectral representations of exfoliated biochar before (A) and after (B) adsorption of fluoride. The composition and percentages of the elements present in them are displayed alongwith.

presences of pores which could act as adsorption sites, having a rough, rugged and flaky appearance. As previously reported that a heterogeneity in surface has a positive effect on the

adsorption process (Belhassan et., 2023) The pores here appeared to be brighter when compared to the pores on FSB in Fig. 41D. The later showed filled pores with flaky depositions. The Fig. 41E also appeared to be clouded as against the Fig. 41B. Fig. 41F showed some crystal-like depositions on the surface. A clarity is provided by the EDS spectra for both EB and FSB (Fig. 42 A and B respectively). The adsorption spectra in Fig. 42B showed more intense fluoride peak than Fig. 42A and the weight % of the ion increased from 0.13 to 4.24 % confirming the uptake of fluoride by FSB.

4.3.2.7. FTIR analysis

The FTIR sorbent spectrum of native, exfoliated and fluoride saturated biochar (FSB) samples are given in Fig 43. From the spectrum, different peaks have been identified for all three samples. -OH stretching vibrations have been recorded in all samples in the range of 3750-3100 cm^{-1}. Elongation vibrations of N-H groups also result in peaks in the region. Two peaks in the spectrum of EB at 2991 and 2895 cm^{-1} respectively arise from the elongation vibrations of aliphatic alkyls, C-H groups (Belhassan et al., 2023) But there is a shift of the peak to 2906 cm^{-1} in the FSB spectrum after fluoride absorption, which might hint at the involvement of methyl and methylene groups (Sadhu et al., 2021). The peak at 1707 cm^{-1} in EB, which denotes elongation vibrations of the carbonyl group (C=O), slightly shifted to 1701 cm^{-1} after fluoride adsorption. The peaks 1585, 1587,1589 cm^{-1} in NB, EB and FSB spectrum denote elongation vibration of C=C aromatic phenols, aromatic C=O and deformations in N-H plane (Belhassan et al., 2023; Sadhu et al., 2021). Only NB displayed a peak at 1440 cm^{-1}. According to literature, it might have stemmed from the asymmetric elongation vibrations of the C-O group of $CaCO_3$ (Belhassan et al., 2023) or also might be from C-H methyl out of plane bending vibrations (Vazquez-Vuelvas et al., 2020). Pyrolysis may have affected the presence of this structure, as no peaks were noticed in this region in spectra of EB and FSB. However, EB showed a peak

around 1344 cm^{-1} which shifted to 1332 in FSB and both stand for the presence of CO_3^{2-} group of bicarbonate (Yapo et al., 2022; Sarma and Rashid, 2018). A peak was evident at 1085 cm^{-1} in the exfoliated biochar, unlike the FSB spectrum. C-O-H stretching vibrations, C-O-C out of plane stretching vibrations and cyclic ring like structures often cause such patterns(Vazquez-Vuelvas et al., (2020). Also, as per reports from Yapo et al., (2022) a peak around 1083 cm^{-1} might be from the formation of hydroxyapatite. Instead, the FSB spectra showed a peak at 1101 cm^{-1}.which might have been due to the presence of exocyclic glycosidic bonds, C-O-C and C-O-H stretching vibrations (Vazquez-Vuelvas et al., 2020). According to Sadhu et al., (2021), presence of peaks in the range of 1000-1200 cm^{-1} is regular in materials containing cellulose and hemicellulose structures. All three biochar have shown peaks in the region. Out of plane deformation of aromatic C-H can be predicted from peaks around 871 cm^{-1} in NB (Belhassan et al., 2023). A shift in peak was noticed on comparing EB spectrum to FSB from 893 to 891 cm^{-1} respectively and from reports of Vazquez-Vuelvas et al., 2020, these stemmed from presence C-O-C and C-O-H stretching vibrations, cyclic rings and exocyclic glycosidic bonds. A special peak at 810 cm^{-1} was noticed in EB which might be due to aromatic C-H groups (Banerjee et al., 2016b) which was lost after fluoride adsorption. Fe-O stretching vibrations were evident in all three spectra of NB, EB and FSB, though at positions different from the other, at 680, 671 and 678 cm^{-1} respectively (Vazquez-Vuelvas et al., 2020). The process of fluoride adsorption gave the FSB spectra two unique peaks at 781 cm^{-1} and 466 cm^{-1} which show the presence of out of plain C-O deformations and Si-O-Si bending (Belhassan et al., 2023; Hsu et al., 2011) and might have arisen from various complexations during adsorption process. The shifts in peaks at different points in the spectra and changes in their intensities upon variation of conditions fairly support the involvement of those functional groups in the process and establish adsorption. Similar findings have been reported by Charan et al., (2024) and Belhassan et al., (2023).
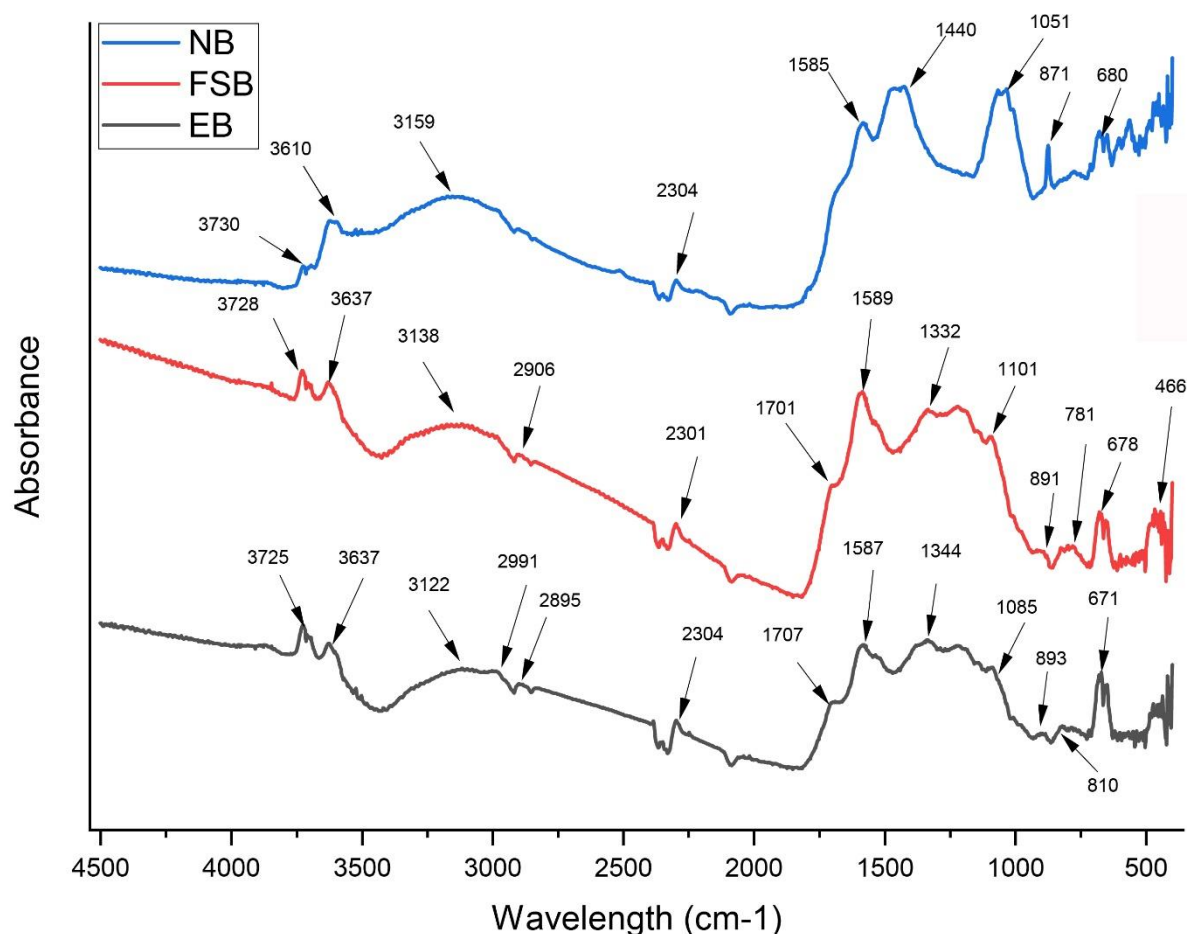
Fig 43. FTIR spectra of native water hyacinth biochar; NB(blue), nitric acid exfoliated water hyacinth biochar; EB (black) and fluoride saturated biochar;FSB (red) showing the peaks representing different surface functional groups.

4.4. Vermi remediation of spent fluoride saturated biochar

Biochar being easily biodegradable, the disposal of it in a contaminant laden form, in this case, stirs up a controversy. Fluoride saturated biochar if disposed without any post treatment may subsequently contaminate the surroundings with fluoride upon decomposition. To prevent this from happening during the course of our research we selected to perform vermi-sanition of the spent adsorbent. To check the efficacy of the vermicomposting process several analyses were performed during the entire span of 90 days. The figures below, Fig 44 and 45, provide a quick sneak peek into the process discussed in earlier section (Section 3.4)
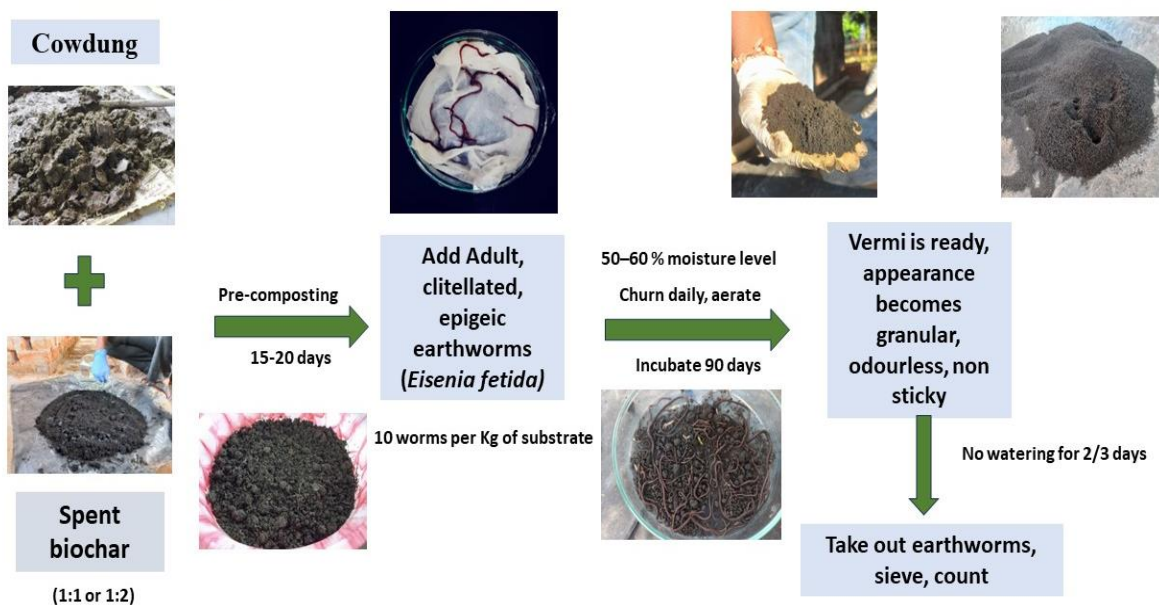
Fig 44. A flow diagram depicting the process of praparing vermicompost from fluoride saturated biochar
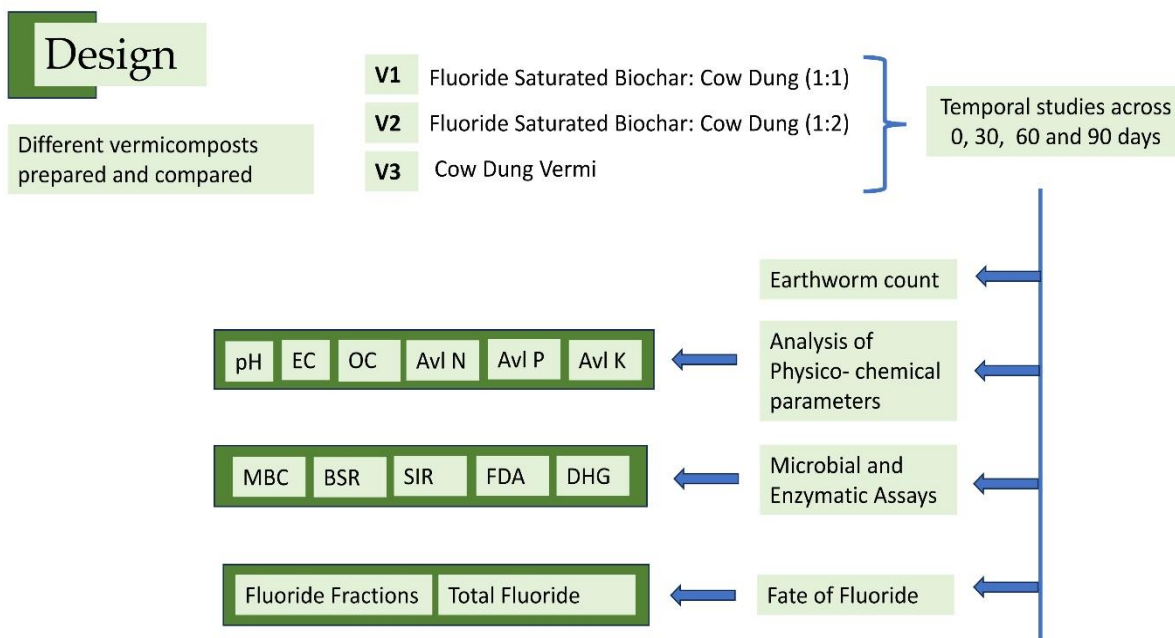
Fig 45. The outline of different analysis carried out during vermiprocessing

We now move into evaluating the results of the experiments mentioned in the outline of work (Figure 45).

4.4.1. Temporal variation in the earthworm count during the process of vermicomposting

The dynamics of adult earthworm population serves as a good indicator of feedstock's compatibility in the biochar-cow dung composting processes according to Dominguez and Edwards (2011). The results obtained from the temporal earthworm count taken during the course of our vermicomposting study indicated that the effect of three different compost systems namely, V1, V2 and V3 on earthworm growth and reproduction rate significantly varied across the treatments ($F_{2,24} = 266.06$, $p < 0.001$) and days of composting ($F_{3,24} = 858.66$, $p < 0.001$). The interaction of treatment and days also had significant changes ($F_{6,24} = 55.27$, $p < 0.001$) as evident from the results of two-way repeated ANOVA performed in the R software. Higher than three-fold increases in adult *E. fetida* population after 90 days was observed in V2 and V3. V1 although showed increase, it was limited two a two-fold growth. Chakraborty et al.,(2022), Jha et al., (2024), Charan et al. (2024) reported how addition of cow-dung in composting contaminant bearing feedstock could reverse the hazards on earthworms from composting those alone and support earthworm growth. However, earthworm count declined sharply in the initial days of composting (0-30 days), they showed greater tolerance and adaptability in the upcoming days of trial and thrived in the vermi-beds. After the initial shock they received from a sudden change in their surrounding environmental conditions, they stopped showing any further signs of lethality. Although another decline in count was noticed as the vermicomposting period was coming to an end, which was reflected in the 90 days earthworm count. This could have been resulted from the decline in availability of food, overcrowding, accumulation of excreta etc. Charan et al., (2024) and Paul et al., (2020) also faced similar observations and conclude that the vermicomposting process had reached maturity by that point cause the lack of available degradable food source. We might therefore say, that in our experiments, the maturity of compost had been achieved prior to 90 days.
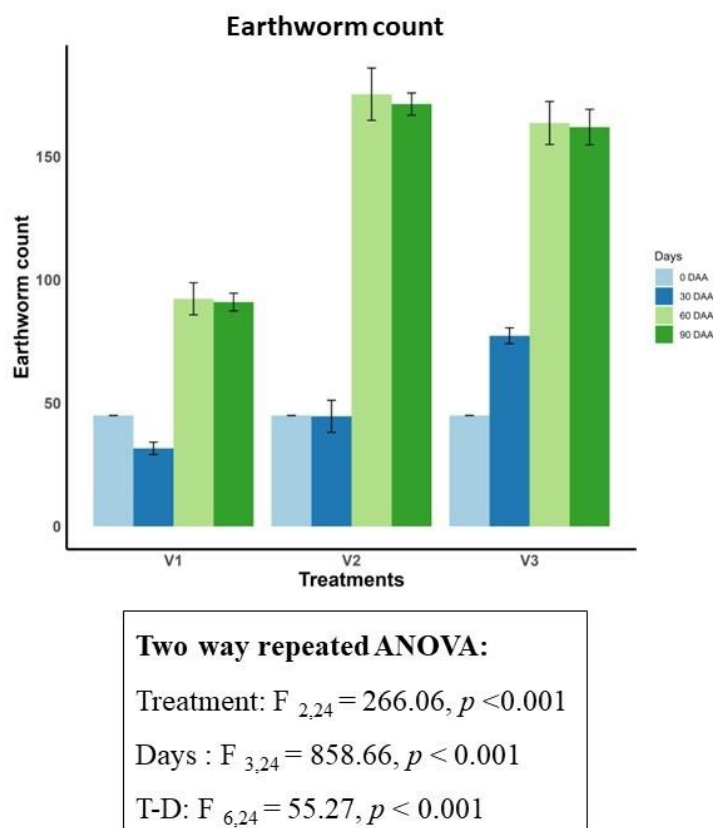
Fig 46. The temporal variation in number of adult earthworms during the vermicomposting period

4.4.2. Observable changes in physico-chemical properties during composting

4.4.2.1. Temporal alteration in pH

In the initial stage of incubation, pH of different ratios of exfoliated biochar-cow dung mixture (V1 and V2) was observed to be near neutral (Figure 47) whereas V3 prepared solely from cow-dung showed a near alkaline pH. As reported by Yuan et al., (2011, biochars from the pyrolysis of feedstock at temperatures near 400°C and above, tend to show basicity and thus are often used to enhance the pH of acidic soils. This was an exception in V1 and V2, probably because of the pH of the biochars prepared from acid exfoliation, had an acidic pH near 5. This on mixing with alkaline cow dung resulted in the near neutral pH of these vermicompost

mixtures. But in all cases, a significant reduction in pH (F $_{1,12}$ = 221.74, p < 0.001) across the days was noted. This could have probably stemmed from the production of ions like HCO_3^- , NO_3^- , PO_4^- and organic acids. Sahariah et al., (2015) also concluded similarly in his study. Such production of organic acid provides an indication of accelerated organic matter decomposition which has been reported to reduce pH of substrate by Yuan et al., (2011). In case of biochar-cow dung mixture pH change was found to be significant with incubation time. In case of cow dung vermi-conversion of cow-dung based V3, pH drop was lesser and was maintained at near neutral ranges. This could be explained by the possible formation of alkaline humates and formation of Al^{3+} and Fe^{3+} complexes, as stated by Paul et al.,(2018). As evident from the results of Two-way ANOVA, there were significant variation in Ph across treatments (F $_{2,12}$ = 337.92, p< 0.001). The interaction between days of occurrence and treatments was also found to be significant (T-D: F = 9.57, p < 0.01).

4.4.2.2. Temporal variation in Electrical Conductivity (EC)

Electrical conductivity is a reflection of availability of mineral, ions etc within a soil-system that might have been generated from the process of vermi-sanitation, feeding of earthworms and subsequent excretion. Previous reports have pointed out that any evident increase in EC during the process of composting presumably provides indication of the accumulation of soluble salts of sulphates, phosphates of different base-forming positive ions (Deka et al., 2011). On contrary, any decrease in the parameter was previously attributed to the immobilisation of different salts assisted by microbial activity. Leaching was also mentioned as the probable cause (Plaza et al., 2008). **From figure 47,** we could see, that all three vermibeds had shown a sharp significant (Days : F $_{1,12}$ = 29.85, p < 0.001) decline in EC over time from 0 days to 90 days, Hence, pointing out to a satisfactory vermi-stablisation process

(Charan et al., 2024). The EC also varied significantly across treatments ($F_{2,12} = 7.99$, $p < 0.01$) as observed from the findings of a two-way ANOVA performed in R software.
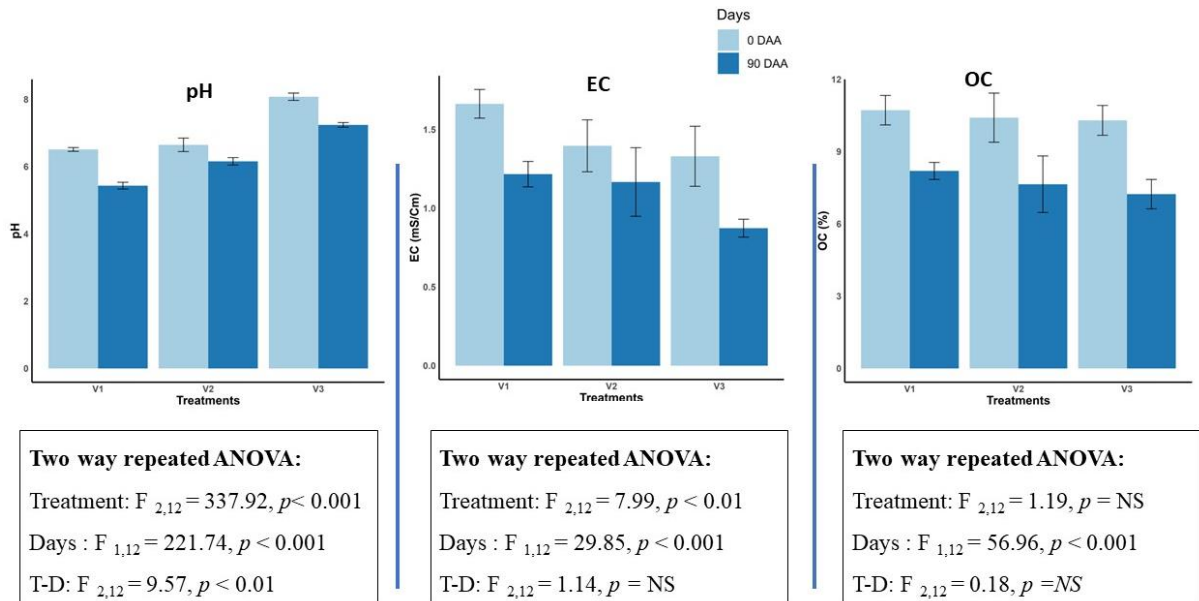
Fig 47. Analysis of physico-chemical attributes (pH, EC and TOC%) at the beginning (0 days) and end (90 days) of vermicomposting

4.4.2.3. Noticeable alterations in TOC%

Reduction in TOC with time was evident in all three vermicomposting units (V1, V2 and V3). This significant reduction ($F_{1,12} = 56.96$, $p < 0.001$) of TOC possibly implied a successful mineralization of organic matter in the vermibeds with subsequent loss of carbon in the form of CO_2 which supports efficient decomposition and vermi-stabilisation in agreement to earlier findings by Deka et al., (2011) and Paul et al., (2018). On performing a two-way ANOVA, no significant variation (Treatment: $F_{2,12} = 1.19$, $p = NS$) was found in the TOC value across different treatments (Figure 47).

4.4.2.4. Temporal changes in the content of available N, P, K

Considerable increase in the available forms of major nutrients like N, P and K was observed with time. The matured vermicompost at 90 days was found to have greater abundance of

mineralizable nitrogen (N), available phosphorus (P)and available potassium (K). The results from the two-way ANOVA performed supported significant increase in N, P and K across days in all treatments (V1, V2, V3). Earthworms involved might have contributed directly to this increase by excretion and secretory activities and indirectly by aiding mineralisation of organic matter and modifying the microclimate of substrate during the process. This additionally prompted the promotion of microbial activity in vermibeds which again participated in organic matter mineralisation. The already prevalent nitrogen fixer community of microbes in the system speeds up the process further aiding this significant increase ($F_{1,12} = 110.31$, $p < 0.001$) in mineralizable N across days of processing. Earlier reports by Chakraborty et al., (2022) and Charan et al., (2024) reported similar findings in their studies and supported the hypothesis. The highest mineralizable N content at the end of 90 days was reported from V1, followed by V3 and V2, although there existed significant variations in N content across treatments ($F_{2,12} = 59.57$, $p < 0.001$). The activity of alkaline phosphatase (AP) enzyme present within the gut of the earthworms accelerates mineralisation of phosphate when the feedstock passes through the worm gut, resulting in a vermicast with abundant available phosphorus. The worm gut also harbours a diverse population of beneficial microbes, out of which the phosphate solubilisers also aid this mineralisation (Sarariah et al., 2014). The difference in available P content of three types of compost were significant ($F_{2,12} = 16.75$, $p < 0.001$) and V2 showed the highest bioavailable P among all. The observed increase in content of available P of V1, V2 and V2 over the days was found to be significant ($F_{1,12} = 17.67$, $p < 0.01$) from the results of two-way ANOVA. The combined action of gut microbes and gut enzymes of earthworms might have also enhanced the concentration of available potassium in the mature vermicompost. Another potential reason behind this significant increment ($F_{1,12} = 1047.64$, $p < 0.001$) of available K, may be the reduction in total volume of the substrate over the period of time and the increase

of net surface area due to the grinding action on substrate within the worm gizzard after ingestion and subsequent release as vermicast (Charan et al.,2024).
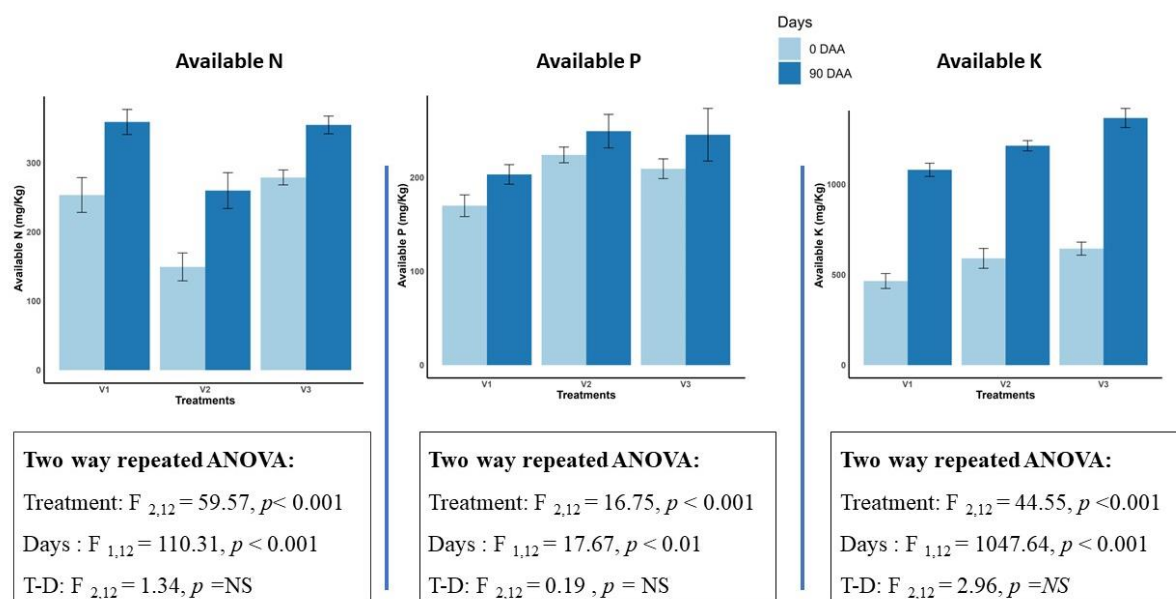
Fig 48. Analysis of physico-chemical attributes (Available N, P and K) at the beginning (0 days) and end (90 days) of vermicomposting

4.4.2.5. Temporal changes in the microbial activity during vermi-processing

Microbial biomass carbon (MBC) measures the weight of total carbon content of microbes inhabiting analysed soil. Unlike all physico-chemical parameters of the composting bed, which were studied at the beginning (0 days) and end (90days) of analysis, the microbial dynamics of the bed were observed temporally at 0, 30, 60 and 90 days of vermi-processing. This study, recorded a significant ($F_{3,24} = 254.022$, $p < 0.001$) increase in soil MBC across all the treatments over time till 60 days. According to earlier reports by Pramanik et al., (2000), the germination of microbial spores is facilitated in the worm-gut and their abundance in vermicast enriches the vermicompost with a diverse population of microbes. This is subsequently reflected in the increased MBC over time in composting systems. The parameter also varied significantly ($F_{2,24} = 3.680$, $p < 0.05$) across treatments and V2 showed the highest MBC among

all three treatments enlisted. But, an interesting finding from the study was the sudden decline in microbial biomass carbon or MBC after 60 days. Similar findings were reported by Charan et al., (2024) and it was held as an implication of attainment of vermi-stabilisation after 60 days of processing.
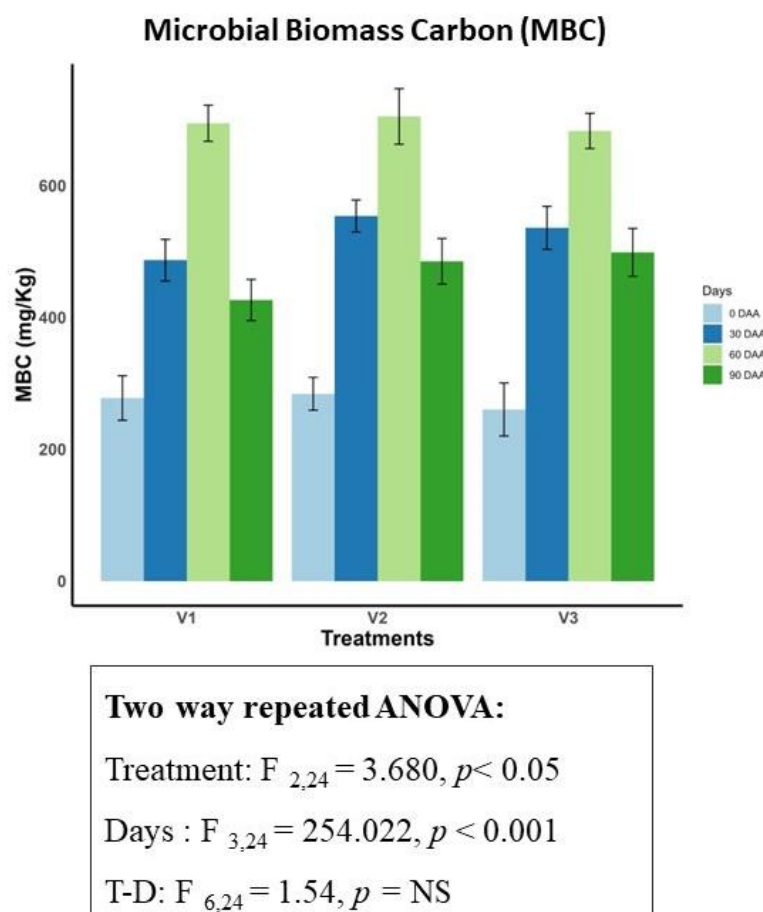
Fig 49. Temporal monitoring of microbial biomass carbon (MBC) at 0, 30, 60 and 90 days of vermicomposting

Basal soil respiration usually reflects the metabolically dormant population of inhabiting microorganisms. It is dependent on the population dynamics of K strategist microbes or the autochthonous microbes, which are usually slow growers by nature. On the other hand, substrate-induced respiration reflects the metabolically active, resident microbe populations of a sample. It depends on the fast-growing zymogenous population or the r-strategist micro-organisms (Dilly, 2005; Jha et al., 2024). A gradual increase in both these types of respiration,

177

namely, BSR and SIR, was observed in all three vermi beds till the 60th day of processing. On approaching the 90th day of incubation, there was a sharp decline in this parameter, which might possibly be indicative of compost maturity (Goswami et al., 2016). There existed significant variation of BSR ($F_{2,24}$ = 58.40, p< 0.001) values across different treatments. Both BSR ($F_{3,24}$ = 131.35, p < 0.001) and SIR (: $F_{3,24}$ = 33.06, p < 0.01) values varied significantly across days of processing as well.

Two way repeated ANOVA:
Treatment: $F_{2,24}$ = 58.40, p < 0.001
Days : $F_{3,24}$ = 131.35, p < 0.001
T-D: $F_{6,24}$ = 3.74, p < 0.01

Two way repeated ANOVA:
Treatment: $F_{2,24}$ = 1.119, p = NS
Days : $F_{3,24}$ = 33.06, p < 0.01
T-D: $F_{6,24}$ = 1.63 , p = NS
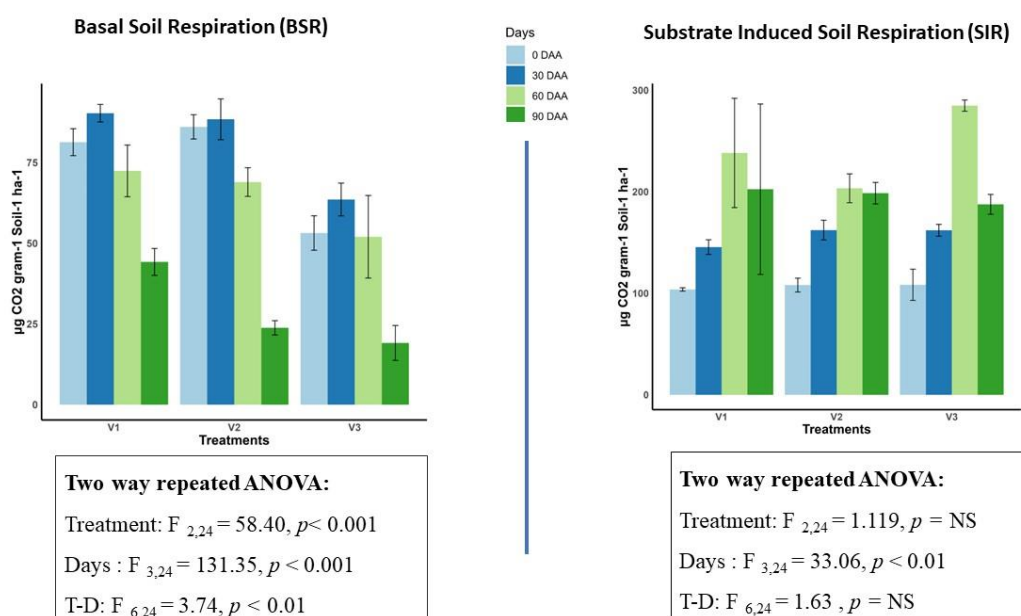
Fig 50. Analysis of basal soil respiration (BSR) and substrate induced respiration(SIR) temporally at 0, 30, 60, 90 days of vermicomposting

According to Nannipieri et al., (1990), the different microbial activities reflect the complexities of several metabolic processes. The relationship, between different metabolic processes can thus reveal a lot of secrets of any organic system. For example, the ratio of BSR to MBC also known as the microbial metabolic quotient or qCO_2 provides an accurate measurement of different responses by microbes to perturbations faced. An increase in this value can point out towards increasing stress factors in the system because of which the microbial biomass tends to divert their energies from the process of proliferation and growth to customary cellular

maintenance to assure their survival amidst the odds (Tripathy et al., 2014; Charan et al., 2024). This faster rate of respiration and reduction in the effectiveness of incorporating substrate to generate biomass has been reported by Chander et al., (2001) and Tripathy et al., (2014) earlier in stressed conditions. Thus, q CO_2, , whose increase reflects shift of energy in catabolic processes, shares a positive correlation with induced stress in any system. However, in our study, a significant (F $_{3,24}$ = 215.28, p < 0.01) decline in this parameter temporally was observed, which therefore stands for a declining stress in the substrate as the maturity of compost reaches the endline. This supported the idea of successful mineralisation and contaminant immobilisation in the vermibeds over the time. This parameter however did not vary significantly within the three composting mixtures (F $_{2,24}$ = 31.7, p= NS). V3 or cow dung vermicompost with no added pollutant source scored the lowest, proclaiming itself to be the least stressed system in the run.

Respiratory Quotient (QR)

Two way repeated ANOVA:
Treatment: F $_{2,24}$ = 45, p< 0.001
Days : F $_{3,24}$ = 224.82, p < 0.001
T-D: F $_{6,24}$ = 9.57, p < 0.05

Metabolic Quotient (qCO$_2$)

Two way repeated ANOVA:
Treatment: F $_{2,24}$ = 31.7, p = NS
Days : F $_{3,24}$ = 215.28, p < 0.01
T-D: F $_{6,24}$ = 2.58 , p <0.01
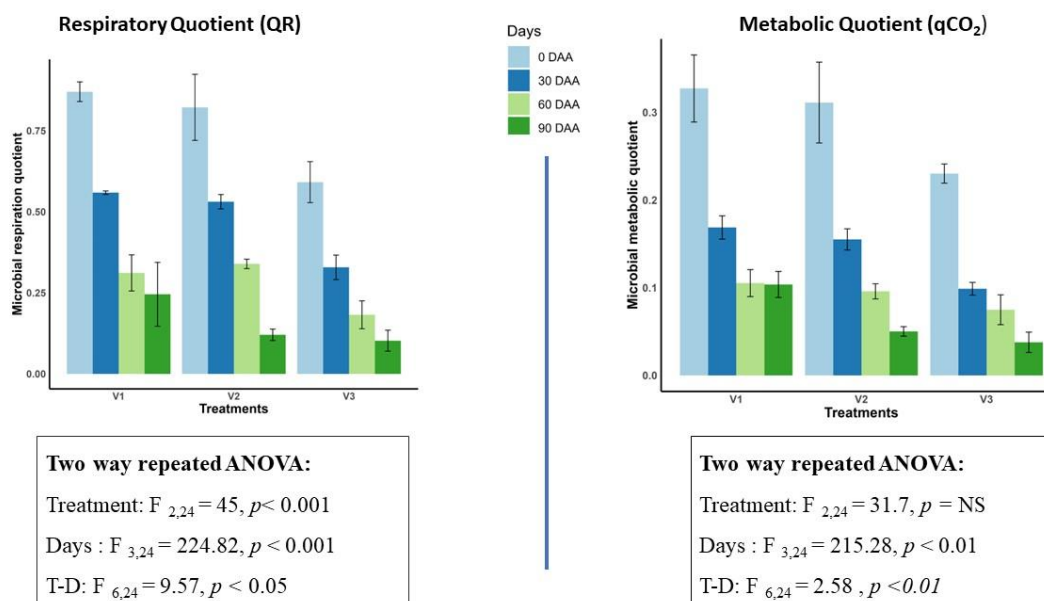
Fig 51. Analysing respiratory quotient (RQ) and metabolic quotient (QCO$_2$) from the MBC, BSR and SIR at 0, 30, 60 and 90 days of vermicomposting

Another important ratio that could predict the stress intensity in composting systems is respiratory quotient or QR. In all three of our experimental vermicomposting systems, a steady and significant temporal decline ($F_{3,24} = 224.88$, $p < 0.001$) was noted in this ratio or the ratio of BSR to SIR. An increase in the value of QR signifies a depression in the number of metabolically active species and an increase in population of the autochthonous population (Tripathy et al., 2014). It has a positive relationship with the events of soil perturbations and its decrease thus indicates lower stress factors in a system. V3 or cow dung vermicompost system with no added contaminant source, thus showed the lowest value of QR, indicative of lowest stress. While, on comparing the initial QR value of V1 and V2, the V1 with higher load of fluoride bearing biochar showed the highest QR. The change in QR values among the systems was also significant ($F_{2,24} = 45$, $p < 0.001$) showing composition of these composting systems can contribute to controlling stress towards microbial community. The overall decline supported successful vermi stabilisation in the experiments performed. A recent study by Charan et al., (2024), indicated that decrease in RQ and qCO_2 show the efficiency of earthworms in transforming an unfavourable feedstock to favourable by reducing contaminant induced stress during the vermi-sanitation. The enzymatic activities in any composting system are reflective of the resident microbial population within and an augmentation in the count of microflora has already been correlated to the enzymatic activities in earlier studies (Charan eta l., 2024). They had noted an increase in the FDA hydrolysing activity and DGH activity under vermicomposting and pointed out to the rapid hydrolysis occurring in the system. The presence of large amount of labile organic matter as referred by Diaz-Burgos et al in 1993, also aids the proliferation. The significant increase in FDA hydrolysis ($F_{3,24} = 98.86$, $p < 0.001$) and DGH activity ($F_{3,24} = 24.36$, $p < 0.001$) in all three vermi beds of our study, namely V1, V2 and V3 temporally, till the 60 days of earthworm mediated feedstock processing can thus also be a result of such microbial proliferations and reflect availability of mineralizable substrate. Under standard conditions of environmental factors, FDA can be hydrolysed successfully by diverse number of enzymes such as, esterase, lipases and proteases (Jha et al., 2024; Chakraborty et

al., 2022). All these enzymes are contributed by the microbial flora and they actively transport FDA within their cells and hydrolyse it by enzymatic action (Tripathy et al., 2014). Thus, based on these reports, the increase in these activities can again be correlated to proliferation of microflora in the system. However, a sudden drop in these enzymatic activities was observed after 60 days of study, as also observed in results of MBC, BSR and SIR. These together support the idea of a declining microbe population at that time and lack of mineralizable substrate from attainment of vermi-stabilisation. These results also indicate at a net improvement in total bacterial and fungal activity in the system (Chakraborty et al., 2022). DGH assays estimate the dehydrogenase enzymes in as composting bed that reflect the total oxidative activity of inhabitant micro flora, thus its increase may also be a contribution of the enhanced microflora in all three vermibeds. However, there was significant variation in these enzymatic activities among different vermi types ($F_{2,24, FDA}$ = 92.88, p< 0.001 and $F_{3,24, DGH}$ = 24.36, p < 0.001). V1 showed the least activity, which might be attributed to its extra load of fluoride as an contaminant that might affect microbial growth.
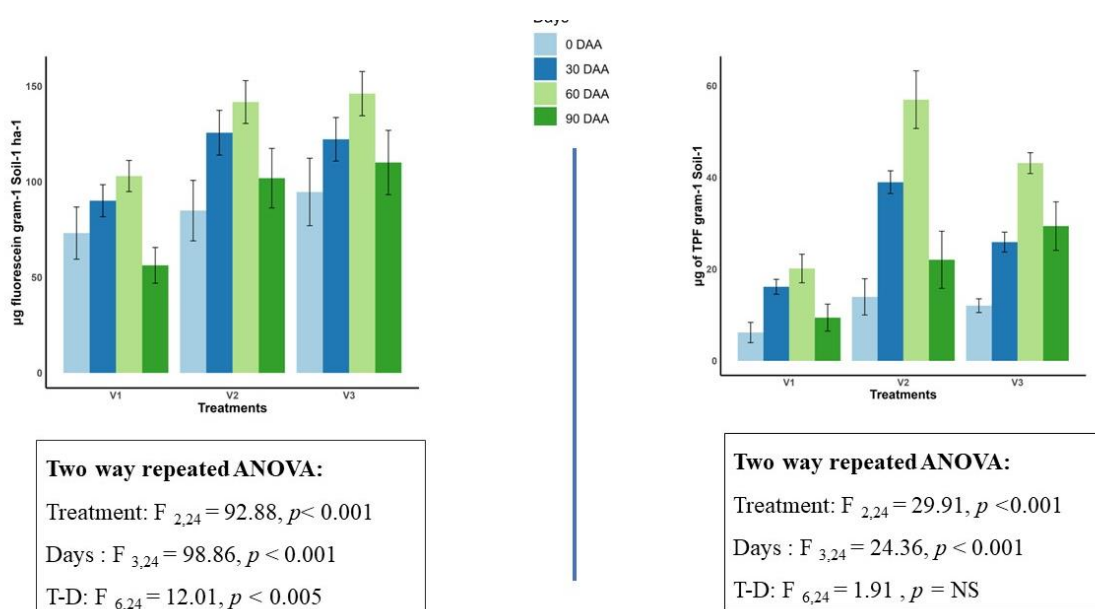
Fig 52. Analysing fluoroscein di acetate (FDA) and dehydrogenase (DHG) activity at 0, 30, 60 and 90 days of vermicomposting

4.4.2.6. Fate of fluoride and temporal changes in fluoride fraction in vermibed

In this study, a substantial fraction of fluoride was seen to be evidently transforming from its bio available water-soluble and exchangeable fractions to the more stabler fractions like the oxide bound, carbonate phase and most importantly the, organic matter bound form during the process of vermisanitation of different types of biochar-cow dung mixtures. Actually, the oxide, carbonate, organic matter bound and residual fraction of an element are potentially recognized as bio-unavailable in their nature and difficult to mineralise (Goswami et al., 2016). This earthworm mediated transformation is primarily possible because of two metal-binding mechanisms as reported by Dallinger in 1993, which simultaneously aid the survival of earthworms in contaminant enriched surroundings. Firstly, these engineers of soil, curb the efficiency of contaminant ions from influencing their regular biochemical cellular functioning by storing those ions as insoluble calcium phosphate granules or chloragosomes (Stürzenbaum et al., 1998. Next, these conjugates are chelated by a low molecular weight protein metallothionein. This protein enriched with sulphur donating cysteine residues, transport these chloragosomes to chloragogenous tissues present within the intestine of earthworm for neutralization (Dallinger, 1993). Additionally, the mineralisation process of labile organic matter in presence of these earthworms increase the humic acid level, which itself has a strong potential in immobilization of different heavy metals and metalloids stable metal-humus complex formations as stated by Dominguez and Edwards, (2011). A study by Tripathy et al., (2014) reported a negative collinearity between the total metal concentration in feedstock of a compost to the microbial activity reported in that vermi-pit and also shows that abundance of bioavailable forms of toxicants hinder microbial proliferation in a compost. The results we received from analysing the different fractions of fluoride in the composting systems after (90 days) and before maturity (0 days), was a sheer refection of all these prior findings and an interesting shift was noticed from the bio available water-soluble (WS) form of fluoride to the

more benign, stable and less bi-available organic matter (OM) bound form at the end of 90 days of processing. Both the reduction in WS ($F_{2,12} = 24.5$, $p < 0.001$) and OM ($F_{2,12} = 195.72$, $p < 0.001$) fluoride fraction over the days were significant when tested by two -way ANOVA. The results supported an efficient vermi sanitisation of fluoride saturated water hyacinth- based biochar.

Two way repeated ANOVA:

WS: Days : $F_{2,12} = 24.5$, $p < 0.001$

OM: Treatment: $F_{1,12} = 7.20$, $p < 0.01$

Days : $F_{2,12} = 195.72$, $p < 0.001$

RS: Treatment: $F_{1,12} = 22.52$, $p < 0.001$
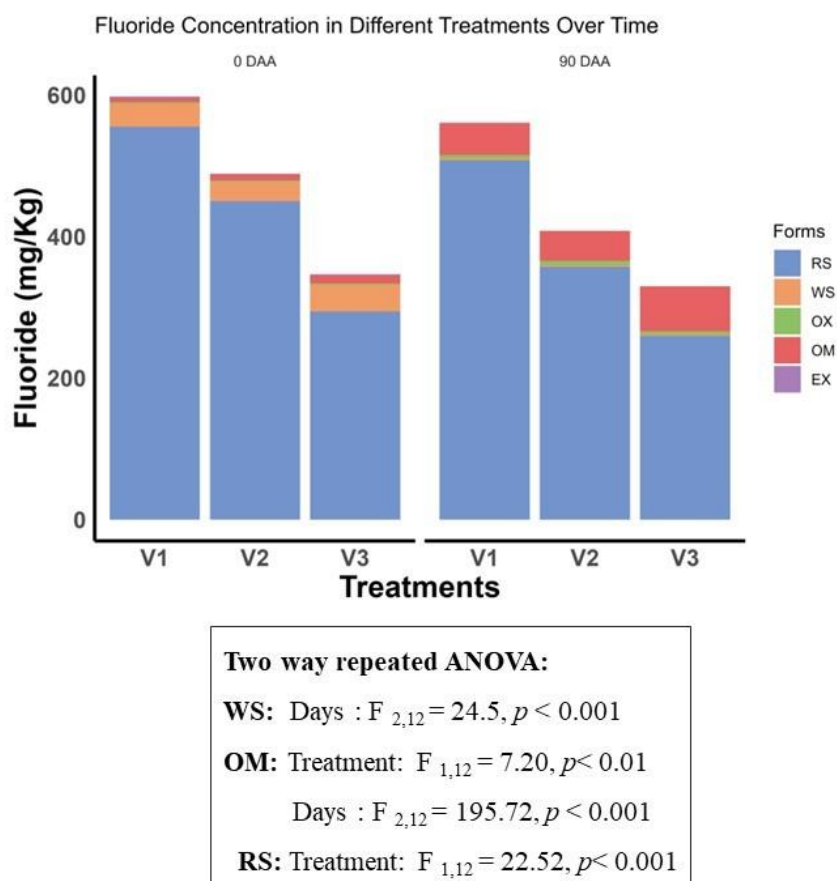
Fig 53. Fluoride fractionation study of samples collected at 0 and 90 days of vermicomposting

4.5. Effect of vermisanitised fluoride enriched biochar on tomato cultivation

Analyses were carried out throughout the growth stages of the tomato plants to get an in depth understanding of the changes in physicochemical and microbial properties of pot soil, the fate of fluoride, signs of fluoride bio accumulation etc.

183
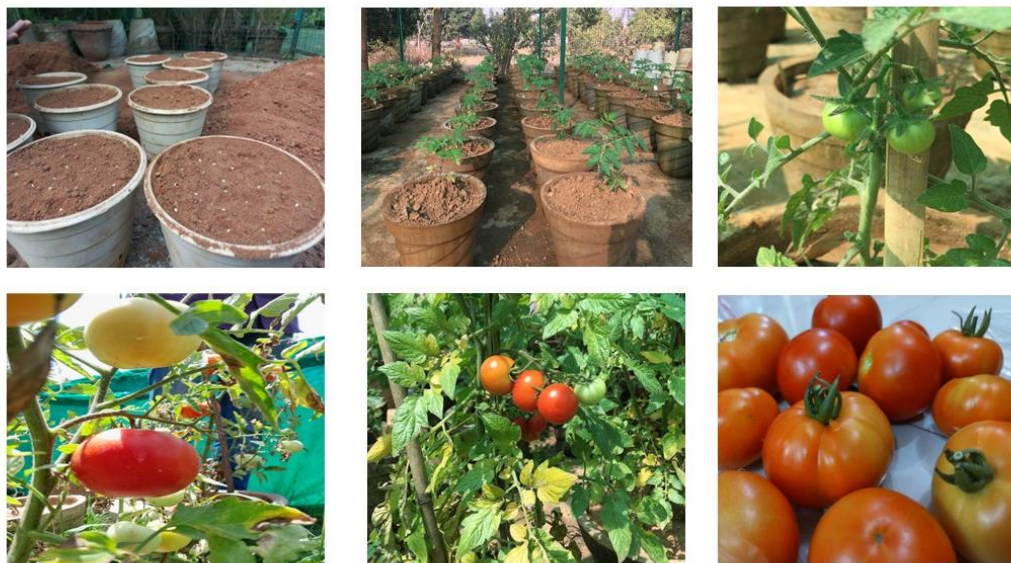
Fig 54. Photographs from different stages of growth of tomatoes in pot experiment for estimating the efficiency of prepared biochar-vermi.

4.5.1. Physico-chemical properties of tomato pot soil

Major physico-chemical parameters of soils collected from eight different treatment amended pots used for growing tomatoes were recorded at planting and post-harvest. The parameters were pH, EC, TOC (%), and available N- P-K. The microbial abundance and enzymatic activities in these soils were also recorded temporarily during different developmental stages of tomato sapling's growth (0. 30,60 and 90 days).

Initially the experimental soil pH of was recorded at near neutral range for all treatments used. But as the experiment proceeded there came alterations in the parameter and when recorded again at the end of 90 days, slight shift towards alkalinity was observed but was not found significant from results of two-way ANOVA. Thus, we could say the amendments did not perturb the soil pH and helped in maintaining the original conditions. The slight shifts towards alkalinity were evident in all treatments but T8 or recommended fertiliser dose amended pot.

However, the picture for EC was not the same. There were significant differences in the parameter across the treatments ($F_{7,32} = 21.78$, $p < 0.001$) and also over the days of application ($F_{1,32} = 266.27$, $p < 0.001$). This increase in EC might be from the incorporation of organic amendments to the pot soils and such increase were also observed in reports by Jha et al., 2023, where they tested the efficiency of a steel waste remediated vermicompost in sesame production. This could also be attributed to the activity of plant root and rhizospheric microbes who mineralised the soil organic matter during the time. The most significant changes were noticed in the soil TOC %. It showed significant enhancement ($F_{1,32} = 90.97$, $p < 0.001$) from 0 day to 90 days. It also varied significantly within the treatments ($F_{7,32} = 9.13$, $p < 0.001$). TOC% were higher in first six treatments (T1- T6) which could be attributed to the organic nature of amendments they received. T6, T5, T3 and T4 performed the best in this regard. However, interestingly, treatment T7 (absolute control) and T8 (fertiliser amended) with no organic amendments provided, also showed increase in TOC% which might have its sources in the dried plant parts that accumulated over time in the pots. The findings were in accord with Charan et al., 2023.
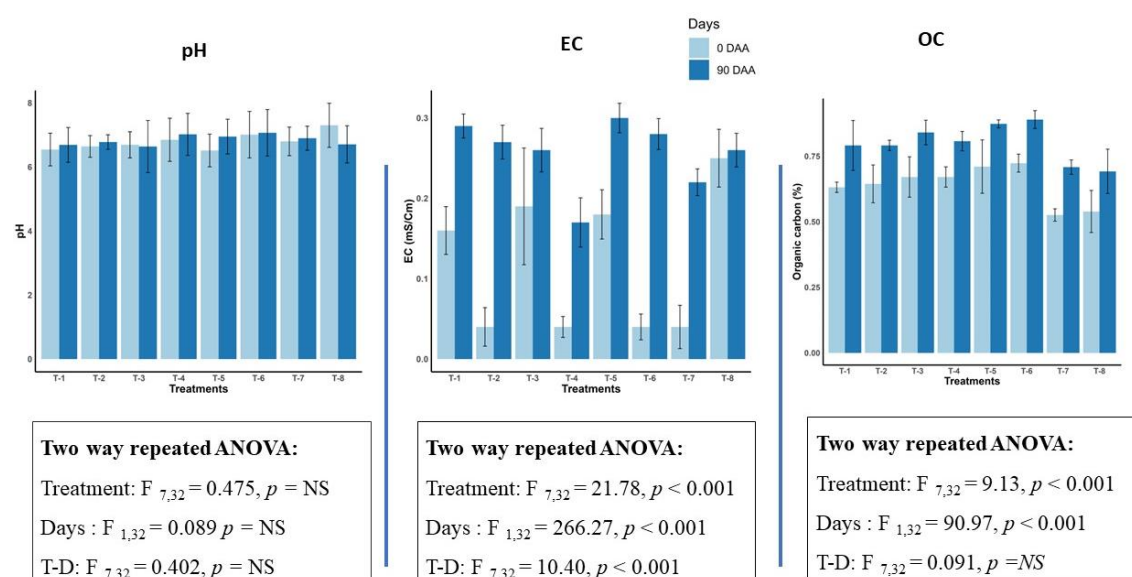
Fig 55. Analysis of physico-chemical attributes (pH, EC and TOC%) at the beginning (0 days) and end (90 days) of pot experiment with tomatoes

The soils were initially low in available N content when analysed at 0 day. But the results of soil analysis at harvest were strikingly different. A significant ($F_{1,32} = 10602$, $p < 0.001$) sharp increase in the parameter was noted in all the treatments. This feat could be attributed to the plant roots and rhizosphere inhabiting microflora who solubilised the N from the amendments and made them bio available. Another interesting observation was the lower N availability in the fertiliser treated pots in comparison to the organic amended ones, which could support the superiority of these organic treatments in agriculture. Similar increase was also reported by Jha et al., 2023 and Charan et al., 2023. We had seen in the vermi-remediation experiments that earthworm activity increased the net available P content in the vermicompost. Subsequent addition of such P enriched amended thus enhanced the available p content in the pot soils over the time. The soil resident phosphate solubilisers also aided in solubilising P. Beside the temporal increase in available P being significant ($F_{1,32} = 2330.2$, $p < 0.01$), the available P content in different treatment amended pot soils also varied significantly among each other. The highest available P was found in treatment T4, followed by T6, T5 and T3. The soil from controls showed least values of available phosphorus. Jha et al., 2024 reported similar findings in vermi amended sesame cultivation soils. The availability of potassium (K) in soils also went up with time from very low in the first phase (0 days) to harvesting (90 days). In this case, we find all the treatments have showed significant enhancement ($F_{1,32} = 10204$, $p < 0.001$) of available K. However, the parameter varied significantly ($F_{7,32} = 1907$, $p < 0.001$) among the treatments as well, with the highest coming from the treatment T8 or fertiliser amended one, closely being followed up by T5 and T3 respectively. The bedrocks in this region are often loaded with micaceous minerals which in itself are sources of potassium in unavailable form. Potassium solubilisers might have aided this release from bedrocks as well. An efficient mineralisation of nutrients by plants and microbes as well as enzymatic actions in soil may also be held responsible for the same (Jha et al., 2023).
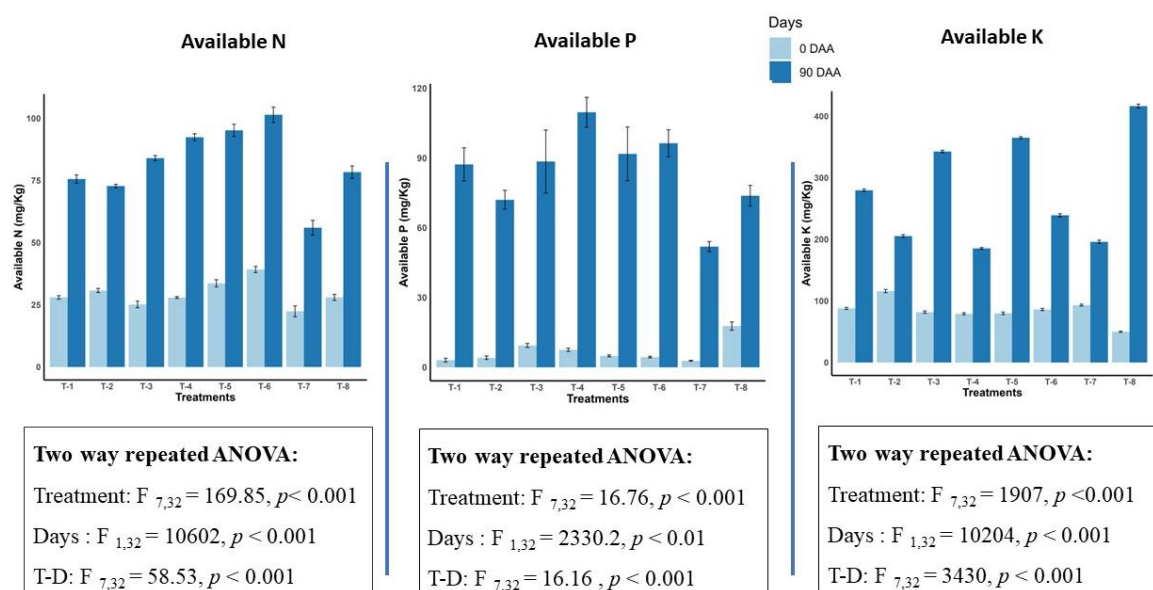
Fig 56. Analysis of physico-chemical attributes (Available N, P and K) at the beginning (0 days) and end (90 days) of pot experiment with tomatoes

4.5.2. Studying dynamics of microbial parameters

As stated by Nannipieri et al., 2003, the contribution of microbes in C and N cycling are potential soil health indicator. Tang et al., (2017) showed a reduced MBC value in soils over the time often exert negative effect on nutrient cycling. Soil MBC was recorded temporally during different stages of plant growth for all treatments. Diversity of observations were recorded. The MBC varied significantly over days ($F_{3,64}$ = 158.1, p< 0.001) and across treatments ($F_{7,64}$ = 1126.08, p< 0.001). After showing a good MBC value at 0 days right after addition of amendments, a gradual decline in MBC value was noted for most treatments in 0 days except for T3, T5 and T6. This could be due to the competition between soil microflora and soil for available nutrients. T3, T4 and T5 although could facilitate microbial enhancement in the first phase, their MBC values started to decline afterwards and reached the lowest at the end of 60 days. This period was parallel to the maturation phase for tomatoes and earlier literatures had mentioned similar observation at this phase. They had attributed it to the

growing competition for nutrient sources between plant roots and soil microflora for their survivals (Charan et al., 2023, Tripathy et al., 2014). However, the MBC value again reported an increase after the harvesting period (90days). The absence of competing crop, and addition of organic matter from the remaining plant residues in the soil might act as potential targets for decomposer community and aid their proliferation
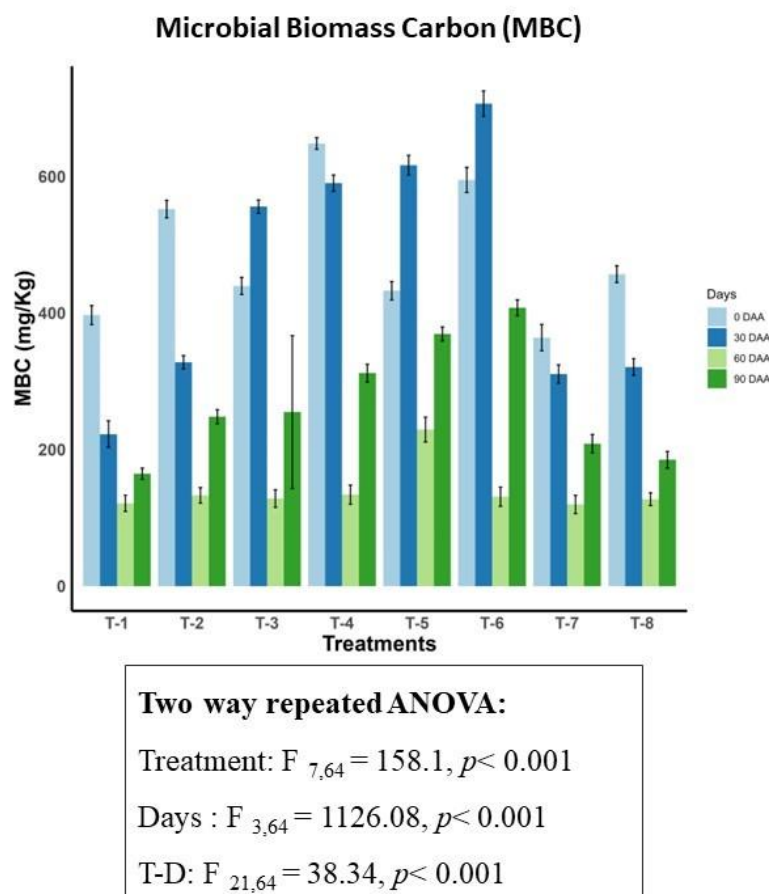
Fig 57. Temporal monitoring of microbial biomass carbon (MBC) at 0, 30, 60 and 90 days of pot experiment with tomatoes

The reflection of the alteration in this parameter over the time of cultivation could also be felt in results of other analysed microbial activities. Soil respiration studies, namely the BSR and SIR showed significant variations over time ($F_{3,64} = 1126.08$, $p < 0.001$ and $F_{3,64} = 3320$, $p < 0.001$). The lowest respiration rates were recorded in fertiliser amended soils while soils from

organic amendments performed the best with highest being in T6, T4 and T5. Basal soil respiration usually reflects the metabolically dormant population of microbes. It is dependent on the population dynamics of K strategist microbes or the autochthonous microbes, which are usually slow growers by nature. On the other hand, substrate-induced respiration reflects the metabolically active microbe populations of a sample. It depends on the fast-growing zymogenous population (Jha et al., 2024). Thus, improved respiration rates assure better soil microbial abundances. But again, both these parameters faced a recession in the 60-day soil analysis. This phase being the maturation phase of tomatoes invokes strong competition between microflora residing in the soil and plant roots for capturing nutrients essential for survival, which thereby reflects in the diminished microbial activity (Charan et al., 2023).
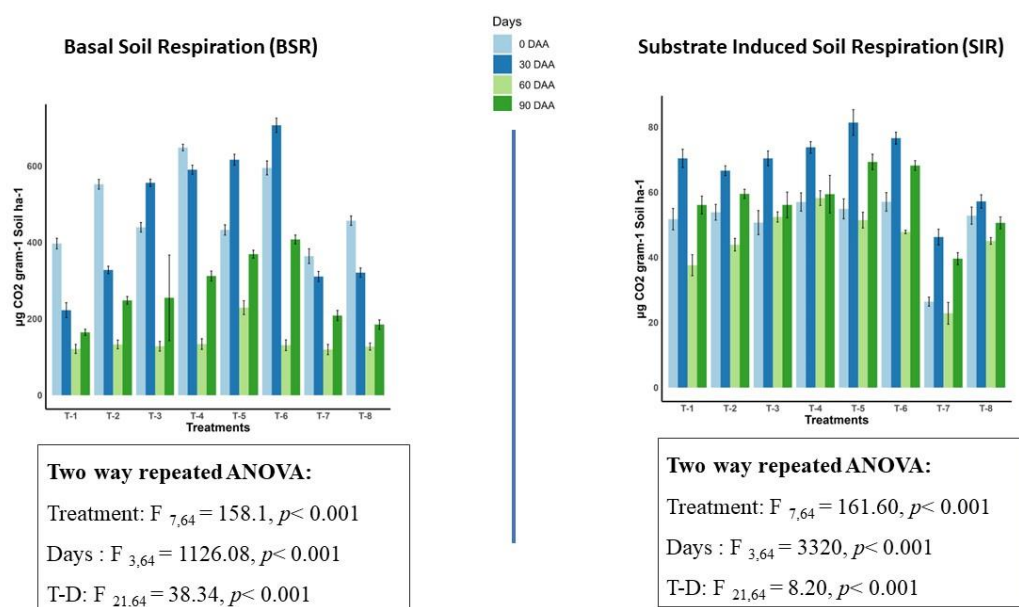
Fig 58. Analysis of basal soil respiration (BSR) and substrate induced respiration(SIR) temporally at 0, 30, 60, 90 days of pot experiment with tomatoes

Studies on enzymatic activities also provide important insights about soil health and quality. Two important enzymatic actions that have been recorded temporally during the study were FDA hydrolysis activity and DGH activity. The enzymatic activities in soil system are

reflective of the resident microbial population within the system and any increase in the count of microflora has positive relations to the enzymatic activities (Charan et al., 2024). FDA can be hydrolysed by different enzymes such as, esterase, lipases and proteases present in microflora (Jha et al., 2024; Chakraborty et al., 2022). Thus, an increase in these enzyme activities can again be correlated to proliferation of microflora in the system. But such enhancements in FDA activity were not visible until harvesting period for all treatment soils. They all reported a sharp decline, while hitting the lowest level at the time of tomatoes maturation. The microbe- plant competition for nutrients may also be held responsible here.
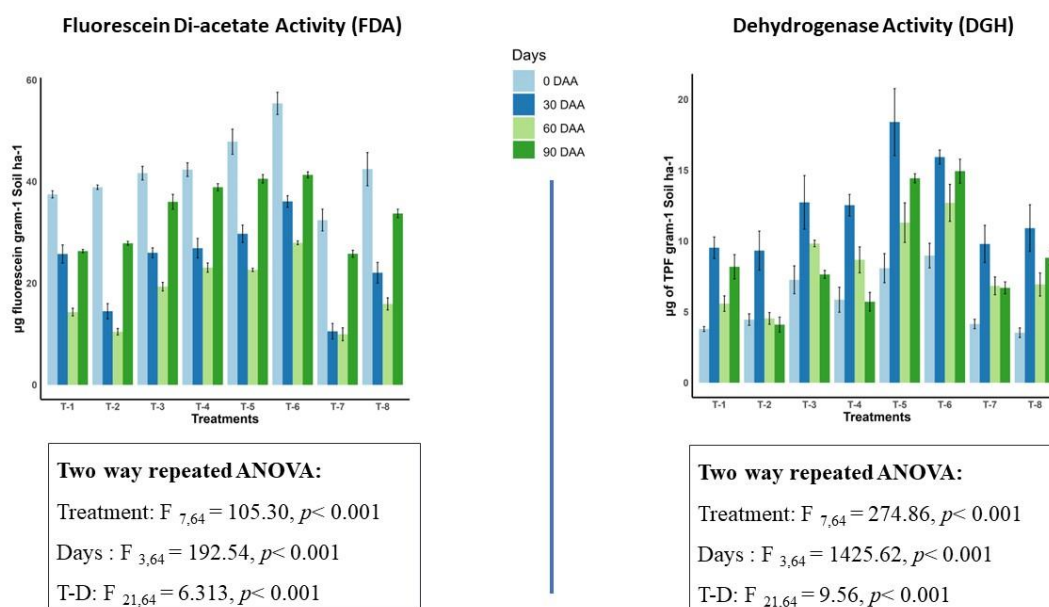
Fig 59. Analysing fluoroscein di acetate (FDA) and dehydrogenase (DHG) activity at 0, 30, 60 and 90 days of pot experiment with tomatoes

For dehydrogenase enzyme, there was an initial increase observed from 0 to 30 days. This initial increase in microbial activity supports the plant growth promotion by mineralising the provide organic amendments and supplying nutrition to the plant (Charan et al., 203). However, this parameter also faced a reduction on reaching 60 days from the discussed competition from maturing plants. Both FDA and DGH variations varied significantly over the time ($F_{3,64}$ =

190

192.54, p< 0.001 and F $_{3,64}$ = 1425.62, p< 0.001 respectively) and their values also had significant variations within treatments (F $_{7,64}$ = 105.30, p< 0.001 and F $_{7,64}$ = 274.86, p< 0.001). the highest enzymatic activities were observed in treatments T6, T5 and T4, showing their potential in protecting soil health and microflora.

4.5.3. Lycopene content of tomatoes and their yield

Plant agronomic parameters and yield are very important in adjudging the efficiency of a treatment provided to the plants. Thus, they were recorded with prudence after harvesting the fruits to picturise the efficiency of applied experimental organic amendments against the recommended fertiliser doses. Interestingly, no visible signs of fluoride toxicity were evident in any treatment provided and plant growth parameters, fruit yield, fruit colour were also better in both inorganic fertilizer and organic compost treated plants in comparison against plants grown in control soil. Presumably, the addition to synthetic fertilizer to plants acts as an immediate source of available macronutrients required during growth and directly facilitate plant growth. Whereas, the organic amendments nurture the soil, enhance the residing microflora and activate mineralisation of nutrients that could then be absorbed by crops and thus facilitate plant growth indirectly (Gaur et al., 1980). One essential agronomic trait of tomatoes is their bright red appearance. It is regulated by presence of pigment lycopene in them. This bright red carotenoid hydrocarbon is mainly found in tomato and other red fruits and vegetables and they have been reported to have huge benefits to human health (Stahl and Sies et al., 1996). A study by Chatterjee et al. (2013), demonstrated that the lycopene in tomatoes were often enhanced when the cropping system was organic and microbial amendments. Experiment. Another report from Avila-Juarez et al. (2015) recorded higher content of lycopene in tomatoes after applying cow-dung based vermicompost to the soil. In the current study, we have also used organic amendments to soils growing tomatoes and thus

we analysed the content of this carotenoid in our harvested fruits from individual treatments. However, no significant difference was found in this case ($F_{7,16} = 0.716$, p = NS) across the treatments. The lycopene content in all experimental vermi amended treatments gave results comparable to fertiliser treated ones thus being an ecofriendly alternative to synthetic fertilisers. Next, we moved on to compare the total yield of tomatoes for different treatments and in this case, we noticed a remarkable and significant ($F_{7,16} = 0.71$, p < 0.05) variation within the treatments. The lowest of yields were from the plants grown in absolute soil and the fertiliser supplemented plants gave the highest produce of about 1100 grams of fruit/ plant. The results from the organic amended treatments T3 and T4 were also remarkably high ascertaining the agricultural prospects of these amendments.

Treatment: $F_{7,16} = 0.716, p = NS$

Treatment: $F_{7,16} = 0.71, p < 0.05$
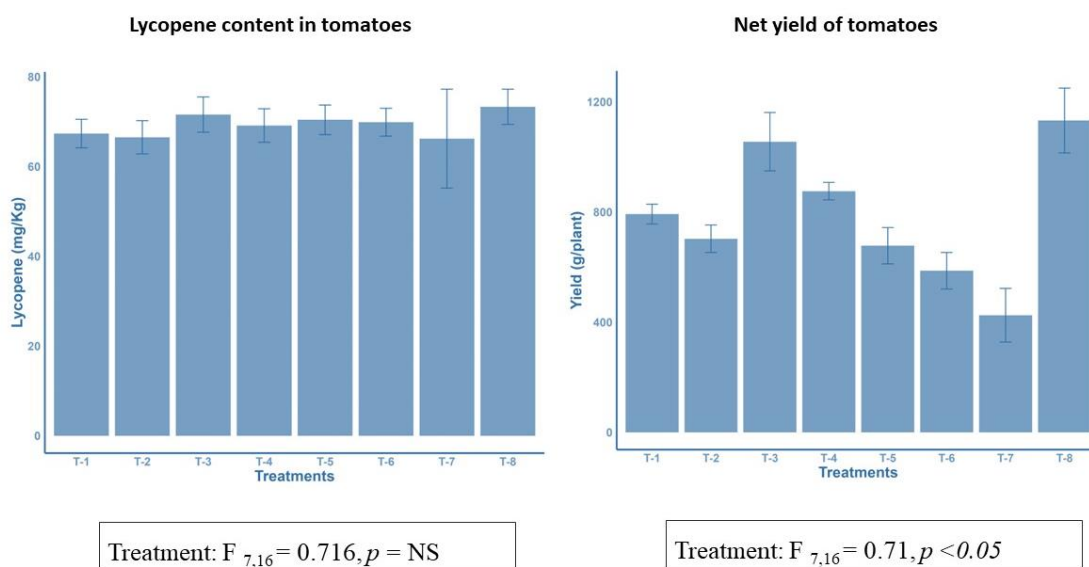
Fig 60. Analysing lycopene content and yield of tomatoes harvested from individual treatments

4.5.4. Estimating F⁻ bio-accumulation in plant parts

Alkali fusion method was used to estimate the total fluoride content present in different plant parts of tomato grown under different experimental treatments. This was necessary to find out whether there are chances of fluoride toxicity in crops grown using fluoride saturated biochar

sanitised vermicompost. From the analysed samples (roots, shoots and fruits) of each treatment, highest fluoride content was recorded from the roots of plants across all treatments involved. However, there was significant variations in fluoride found in roots across treatments (Treatment: $F_{7,16} = 108.3$, $p < 0.001$). The second highest accumulation was found in shoot part of the plants and again there existed significant differences among treatments (Treatment: $F_{7,16} = 73.59$, $p < 0.001$). But surprisingly, fluoride accumulation was also found in the plants grown in absolute control soils, indicating towards an inherent source of fluoride in the native soils. Fertiliser aided soils also showed fluoride accumulation and use of fluoride bearing phosphatic fertilisers may be one reason behind the event. But, to our expectations, very little and almost negligible amounts of fluoride were detected in the edible part or the fruit. Surprising enough, the highest fluoride content in fruits were found in treatment T8 or fertiliser amended soil grown tomatoes. This, therefore exposes a potential risk of using phosphatic fertilisers in food crops. Whereas, on the contrary, the fluoride content from experimental vermicompost amended soil grown fruits, were all lower than 2 mg/kg and thus can be tagged fluoride safe.

Fruit: Treatment: $F_{7,16} = 25.74$, $p < 0.001$
Shoot: Treatment: $F_{7,16} = 73.59$, $p < 0.001$
Root: Treatment: $F_{7,16} = 108.3$, $p < 0.001$
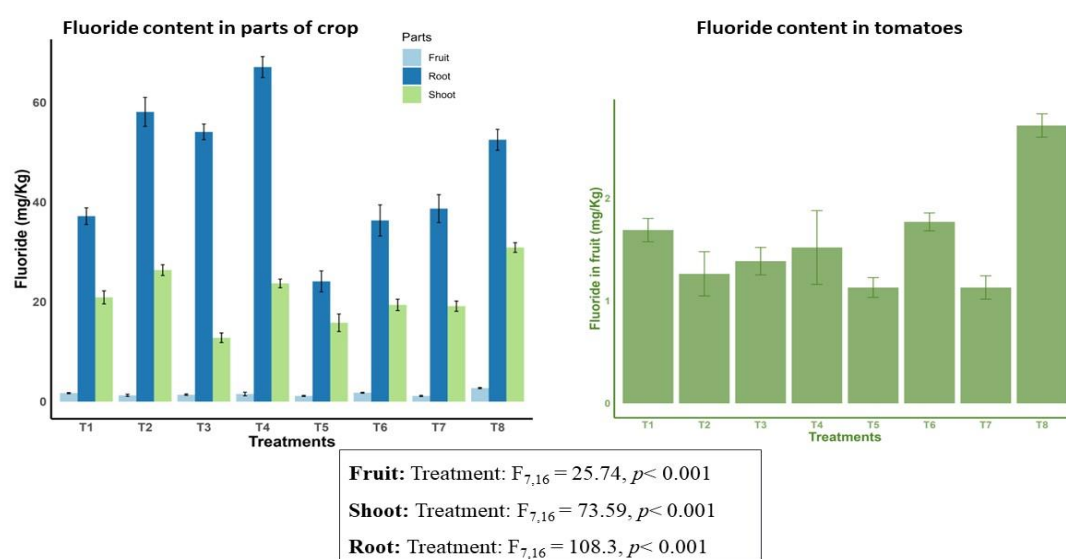
Fig 61. Analysing total fluoride content in plant parts (root, shoot and fruit) of harvested tomatoes to trace any possible bioaccumulation

To further ascertain the safety of these experimentally grown fruits, the bio concentration factor or BCF was calculated. BCF is calculated to find out the amount of desired contaminant accumulated in plant parts from soil. The BCF for fluoride in tomatoes produced in experiment was estimated with a formula used by Pal et al. (2012).

BCF= Fluoride in tomato (mg.kg^{-1} dry weight)/fluoride in soil (mg.kg^{-1} dry weight of soil)

This value when exceeds unity, indicates potential threat to human health from fluoride but to our satisfaction, none of the BCF values calculated from treatments used in this study exceeded unity and were therefore safe for human consumption.
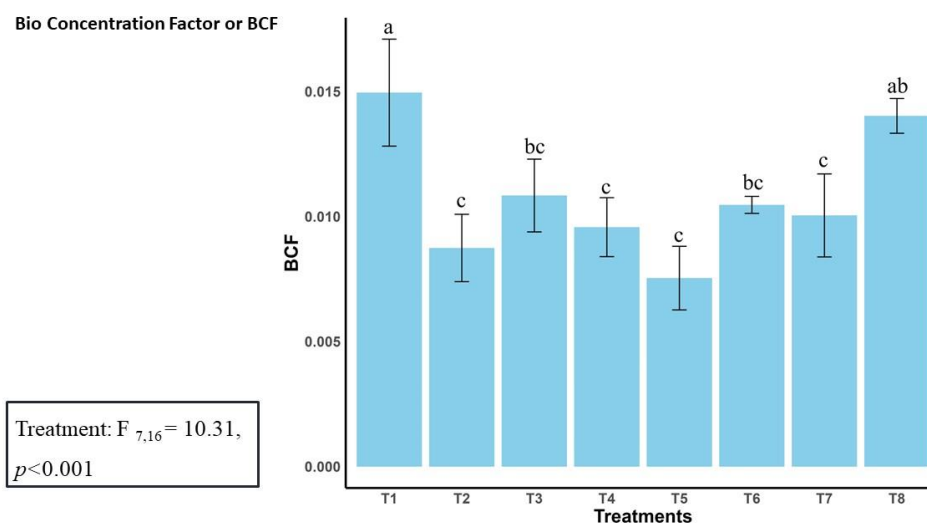
Fig 62 Analysing the bio concentration factor (BCF) in tomatoes harvested from different treatments to estimate any possible risks from bioaccumulation

4.6. Effect of vermisanitised fluoride enriched biochar on rice cultivation under field conditions

Analyses were carried out throughout the growth stages of the rice plants to get an in depth understanding of the changes in physicochemical and microbial properties of rice soil, the fate of fluoride, signs of fluoride bio accumulation etc.

194

Fig 63. Photographs from different stages of growth of rice in field experiment for estimating the efficiency of prepared biochar-vermi.

4.6.1. Physico-chemical properties of rice field soil

Major physico-chemical parameters of soils collected from ten different treatment amended plots used for growing rice (Variety- Sita) were recorded at planting and post-harvest. The parameters were pH, EC, TOC (%), and available N-P-K. The microbial abundance and enzymatic activities in these soils were also recorded temporarily during different developmental stages of crop growth (0. 30,60 and 90 days).

The experimental soil pH was recorded at slightly acidic (5.1-5.61) range for all treatments used during transplanting of seedlings. But as the experiment proceeded there came alterations in the parameter and when recorded again after the harvest end (90 days), slight shift towards alkalinity or acidity was observed in most parameters. But no significant change over the days were noted from results of two-way ANOVA (F $_{1,40}$ = 1.14, p =NS). Thus, we could say the amendments did not modify the soil pH and maintained the original conditions. However, there were significant differences across the treatments (F $_{9,40}$ = 3.63, p < 0.01). The soil EC, on contrary, also varied over the days of application (F $_{1,40}$ = 0.013, p = NS) and showed increase over time in some of the treatments (T2, T3, T4, T5). The rest of the treatments however, declined in EC. There were significant differences (F $_{9,40}$ = 4.25, p < 0.001) among the treatments as well. This increase in EC might be from the incorporation of organic matter rich amendments to the plot soils and such increase were also observed in reports by Jha et al., 2023. This could also be attributed to the activity of plant root and root zone residing microbes who helped in mineralising the soil organic matter during the time. The decline in EC, on the other hand could be attributed to leaching of salts during the rainfall and submerged conditions. The most significant changes were noticed in the soil TOC %. It showed significant enhancement (F $_{1,40}$ = 6.42, p < 0.001) from 0 day to 90 days. It also varied significantly within the treatments (F $_{9,40}$ = 7.99, p < 0.001). TOC% were higher in the eight treatments who

received organic amendments (T2- T8) which could be attributed to the carbonaceous nature of vermicompost and biochar they received. T9, T8, T3 and T2 performed the best in this regard. However, interestingly, treatment T7 (absolute control) and T8 (fertiliser amended) showed limited increase, despite receiving any organic supplments. This extra carbon might have its sources in the dried plant parts that perished in the plot during the study. The findings are in accord with Charan et al., 2023.
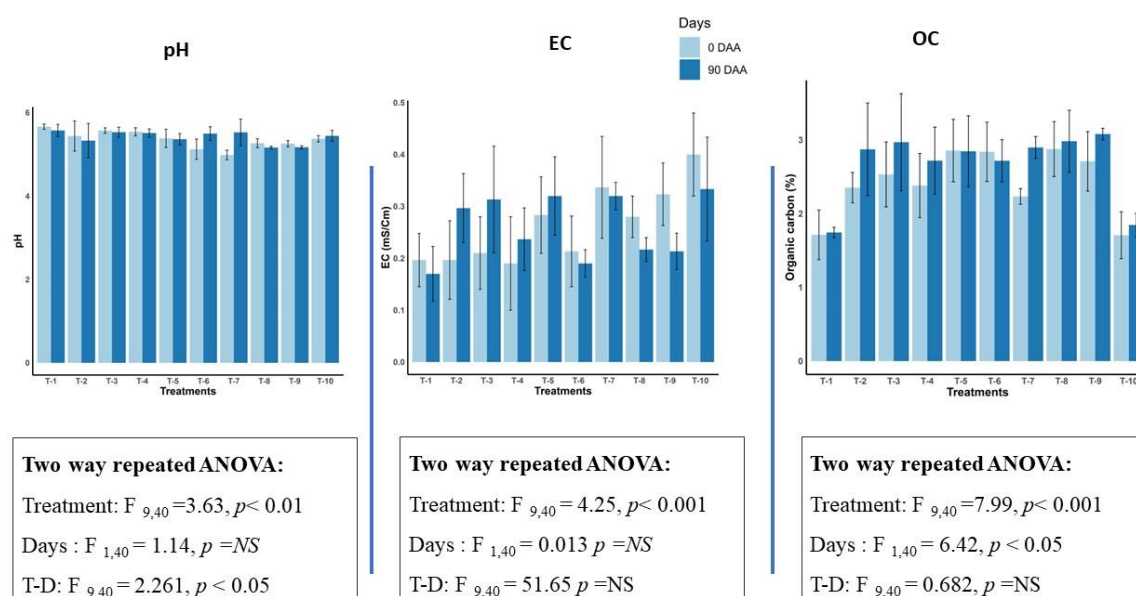
Fig 64. Analysis of physico-chemical attributes (pH, EC and TOC%) at the beginning (0 days) and end (90 days) of field experiment with rice

The soils were initially low in available N content when analysed at the beginning (0 day). But the results of soil analysis at harvest were strikingly different. A significant ($F_{1,40} = 712.73$, $p < 0.001$) sharp increase in the parameter was noted in all the treatments. This feat could be attributed to the plant roots and rhizosphere inhabiting microflora who solubilised the N from the amendments and made them bio available. Another interesting observation was the lower N availability in the fluoride saturated biochar treated plots (T8, T9) and absolute control (T1) plot in comparison to the compost amended ones. This could support the superiority of these organic composts treatments in agriculture. Similar increase was also reported by Jha et al.,

2023 and Charan et al., 2023. We had seen earlier in the vermi-remediation study that earthworm activity increased the content of total available P in the vermibed with time. Subsequent addition of such P enriched amendments thus enhanced the available P content in the experimental plot over the time. The soil residing phosphate solubilisers also aided in solubilising P. Beside the temporal increase in available P being significant ($F_{1,40} = 1191.17$, p < 0.001), the available P content in different treatment amended plot soils also varied significantly ($F_{9,40} = 6.42$, p < 0.001) among each other. The highest available P was found in treatment T4, followed by T6 and T5. The soil from controls showed least values of available phosphorus followed by T8 and T9. Jha et al., 2024 reported similar findings. Another reason behind this increase may be from the submerged condition in rice fields. The availability of potassium (K) in soils also went up with time from very low in the first phase (0 days) to appreciable amount harvesting (90 days). In this case, we find all the treatments have showed significant enhancement ($F_{1,40} = 1124.89$, p < 0.001) of available K.
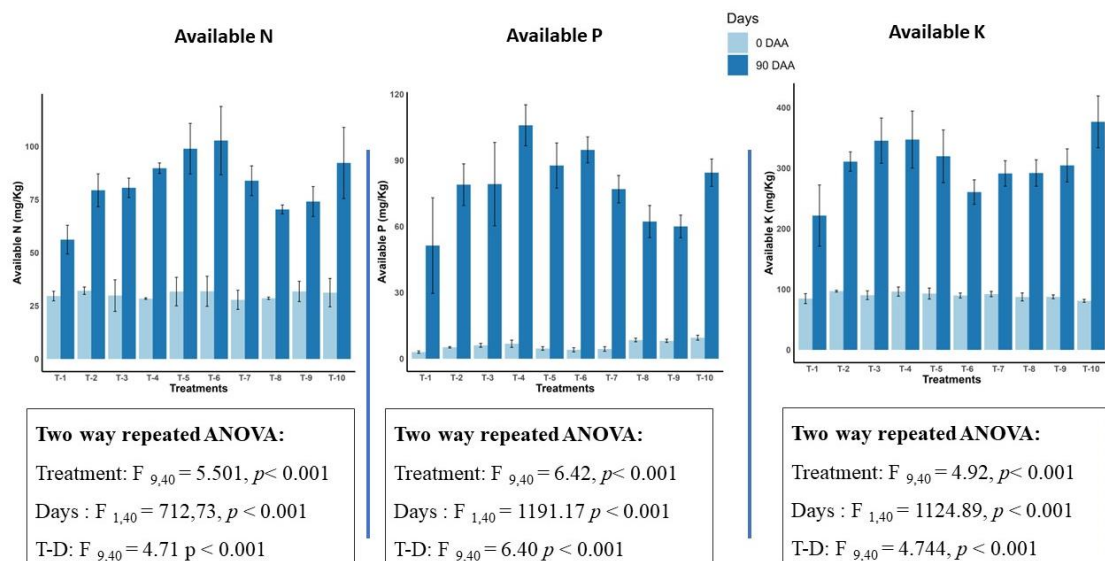
Fig 65. Analysis of physico-chemical attributes (Available N, P and K) at the beginning (0 days) and end (90 days) of field experiment with rice

However, the parameter varied significantly ($F_{9,40} = 1907$, p < 0.001) among the treatments as well, with the highest coming from the treatment T10 or fertiliser amended one, closely being

followed up by T4 and T3 respectively. The bedrocks in this region are often loaded with micaceous minerals which are sources of bio-unavailable potassium as reported in earlier literatures. Potassium solubilisers might have also aided K release from bedrocks in this scenario. An efficient mineralisation of nutrients by plants and microbes as well as enzymatic actions in soil also might have boosted it. (Jha et al., 2023).

4.6.2. Studying microbial activity in soils of experimental rice field

According to Nannipieri et al., 2003, the contribution of microbes in C and N cycling could be used as a potential soil health indicator. Tang et al., (2017) reported that a reduction in MBC value in soils over the time could exert negative impact on nutrient cycling of the system. Soil MBC was recorded temporally during different stages rice plant growth for all treatments. Diverse observations were recorded. The MBC varied significantly over days ($F_{3,80} = 822.74$, $p < 0.001$) and across treatments ($F_{9,80} = 178.86$, $p < 0.001$). After showing a satisfactory MBC value at the beginning of experiment (0 days), a gradual decline in MBC value was noted for most treatments when measured again at day 30, except for treatments T8, T9 and T10. These three treatments being amended with fluoride laden biochar and synthetic fertilisers, might have created some adverse effect on microflora disrupting their proliferation. Other treatments although could facilitate microbial enhancement in the first thirty days, their MBC values started to decline afterwards and reached the lowest point within the experimental time frame at the end of 60 days. This period was parallel to the maturation phase for rice and earlier literatures had mentioned similar observation at this phase (Charan et al., 2023, Tripathy et al., 2014). This could be due to the competition between soil microflora and soil for available nutrients at the time of crop maturation. However, the MBC value again reported an increase after the harvesting period (90days). The absence of competing crop, and addition of organic matter from the remaining plant residues in the soil might act as potential targets for decomposer community and aid their proliferation. However, the microflora in T8 and T9 could

not show satisfactory growth even at the after-harvest phase. The inorganic and toxicant bearing amendments perhaps prevent microbial growth in these plots.
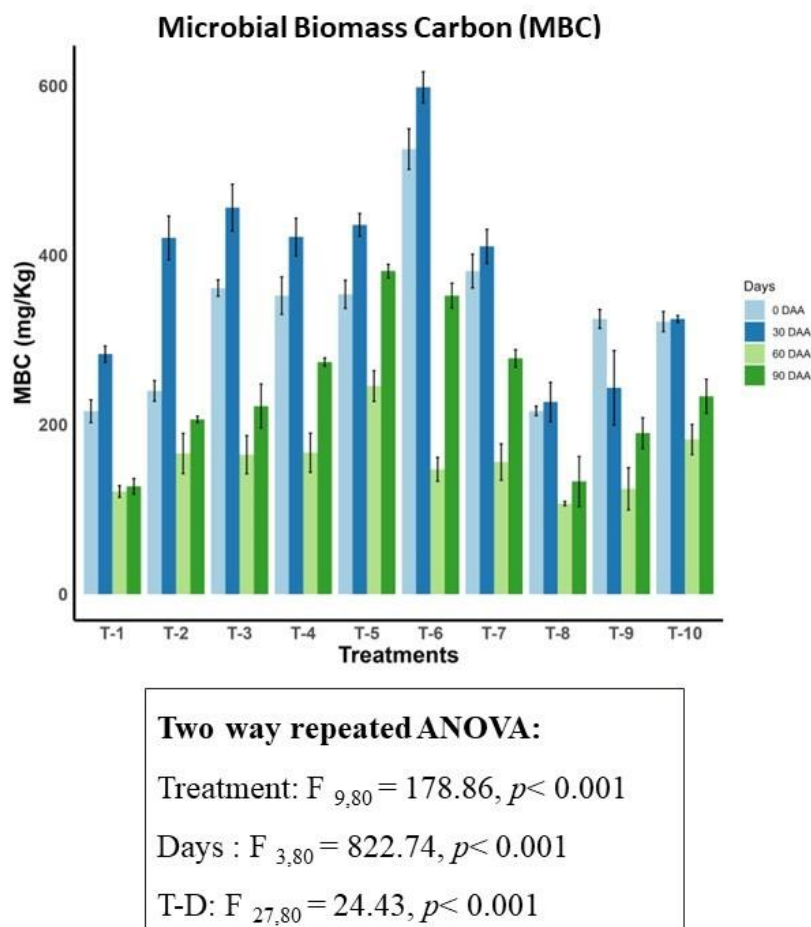
Fig 66. Temporal monitoring of microbial biomass carbon (MBC) at 0, 30, 60 and 90 days of field experiment with rice

The reflection of the alteration in this parameter over the time of cultivation could also be felt in results of other analysed microbial activities. Soil respiration studies, namely the BSR and SIR showed significant variations over time ($F_{3,80}$ = 322.11, p< 0.001 and $F_{3,80}$ = 402.05, p< 0.001). The lowest respiration rates were recorded in saturated biochar (T8, T9) and fertiliser amended soils while soils from organic amended plots performed the best with highest respiration rates being recorded in treatments T2, T5, T6 and T4. Basal soil respiration which usually reflects the metabolically dormant population of inhabiting microorganisms is

dependent on the population dynamics of the autochthonous microbes. On the other hand, substrate-induced respiration reflects the metabolically active, zymogenous populations of a sample (Jha et al., 2024). Thus, improved respiration rates correlate positively to better soil microbial abundances. But again, both these parameters faced a recession in the 60-day soil analysis. This phase being the maturation phase of rice invokes strong competition between microflora residing in the soil and plant roots for capturing nutrients essential for survival, which reflects in the diminished microbial growth (Charan et al., 2023).

Basal Soil Respiration (BSR)

Two way repeated ANOVA:

Treatment: $F_{9,80} = 122.81$, $p < 0.001$

Days : $F_{3,80} = 322.11$, $p < 0.001$

T-D: $F_{27,80} = 11.23$, $p < 0.001$

Substrate Induced Soil Respiration (SIR)

Two way repeated ANOVA:

Treatment: $F_{9,80} = 46.90$, $p < 0.001$

Days : $F_{3,80} = 402.05$, $p < 0.001$

T-D: $F_{27,80} = 3.864$, $p < 0.001$
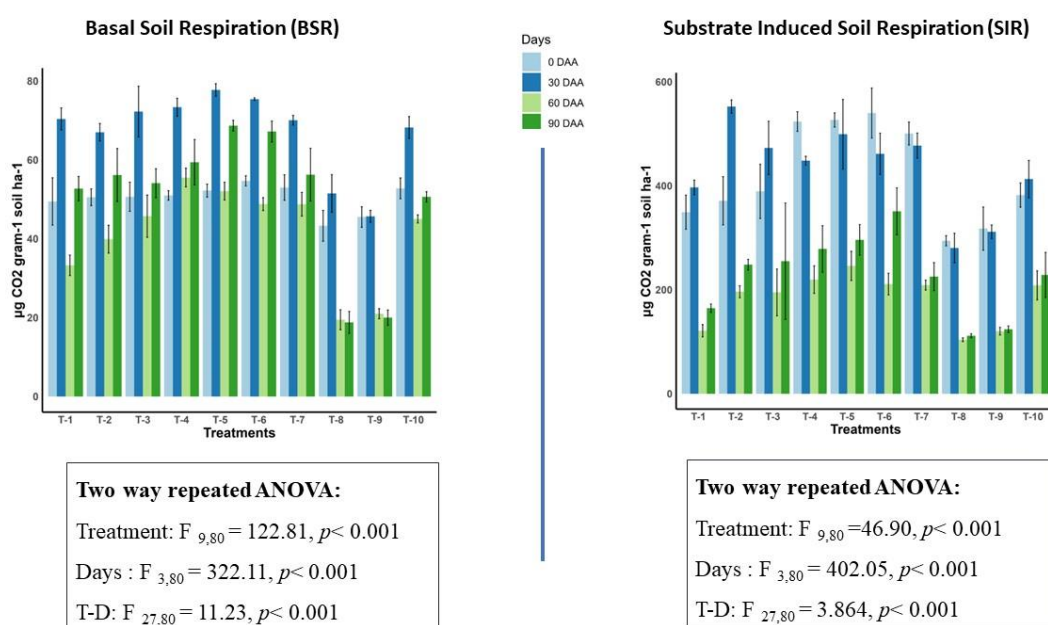
Fig 67. Analysis of basal soil respiration (BSR) and substrate induced respiration(SIR) temporally at 0, 30, 60, 90 days of field experiment with rice

Two important enzymatic actions have been recorded temporally during the study- FDA hydrolysis activity and DGH activity. The enzymatic activities in soil system are reflective of the resident microbial population within soil and any increase in their count has positive relations to the enzymatic activities (Charan et al., 2024). FDA can be hydrolysed by different enzymes present in microflora (Jha et al., 2024). Thus, an increase in these enzyme activities indicate the proliferation of microbes. But such enhancements in FDA activity were not visible

until harvesting period for all treatment soils. They all reported a sharp decline in first three days of study, while hitting the lowest level at the time of rice maturation or grain filling. The microbe- plant competition for nutrients might have been responsible here. Again, T8 and T9 did not show satisfactory results. For dehydrogenase enzyme, there was an initial increase observed from 0 to 30 days. This initial increase might be from the abundance of available nutrients from supplied amendments, and this supports the plant growth promotion by mineralising the provided organic amendments further and supplying nutrition to the plant (Charan et al., 2023). However, this parameter also faced a reduction on reaching 60 days from the discussed competition from maturing plants as discussed in earlier sections. Both FDA and DGH variations varied significantly over the time (F $_{3,80}$ = 186.25, p< 0.001 and F $_{3,80}$ = 81.81s, p< 0.001 respectively) and their values also had significant variations within treatments (F $_{9,80}$ = 5.98, p< 0.001 and F $_{9,80}$ = 16.32, p< 0.001). The highest enzymatic activities were observed in treatments T6, T5 and T7.
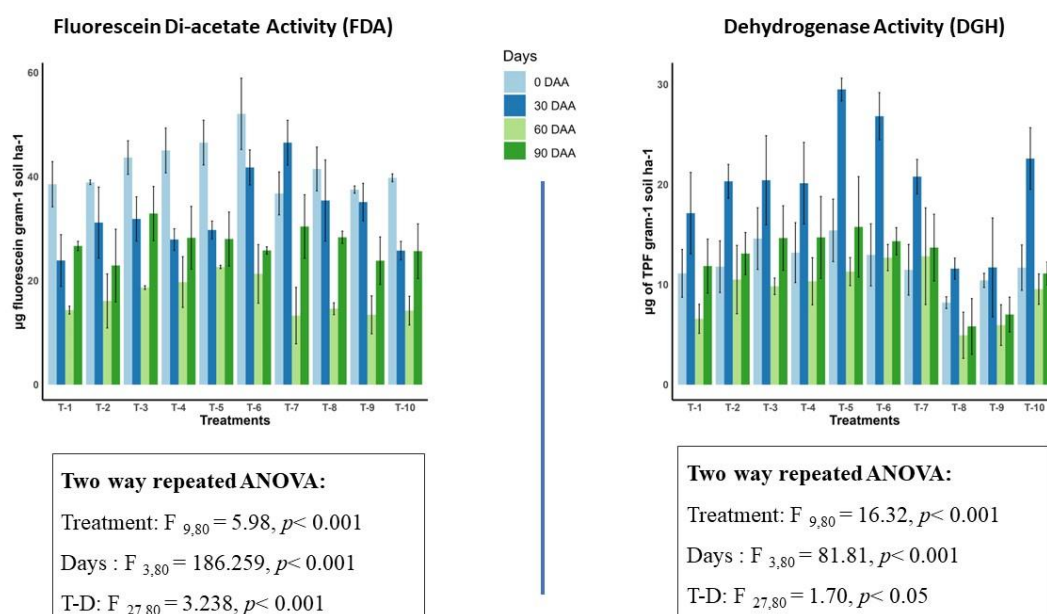
Fig 68. Analysing fluoroscein di acetate (FDA) and dehydrogenase (DHG) activity at 0, 30, 60 and 90 days of field experiment with rice

4.6.3. Agronomic parameters of harvested rice

Presumably, the addition to synthetic fertilizer to plants acts as an immediate source of available macronutrients required during growth and directly facilitate plant growth. Whereas, the organic amendments nurture the soil, enhance growth of microflora and activate effective mineralisation of nutrients and thus facilitate plant growth indirectly (Gaur et al., 1980).

Plant agronomic parameters and yield are very important in adjudging the efficiency of a treatment provided to the plants. Thus, they were recorded after harvesting the grain, from each of the ten treatments diligently, to judge the efficiency of applied experimental organic amendments against the recommended fertiliser doses. Interestingly, no visible signs of fluoride toxicity were evident in any treatment provided and plant growth parameters, grain yield, straw yield, test weight etc, were also better in organic compost treated plants in comparison against plants grown in control soil.

Significant differences were found when test weight or 100 grain weight was recorded from rice harvested from each of the ten experimental treatments ($F_{9,20} = 5.51$, $p < 0.001$). The highest test weights were recorded from treatments T10 (fertilise amended), T5 ,T4 (V2 amended) and T7 (cow dung vermi V3 amended) and no significant difference in these treatments were observed in terms of test weight, as perceived from shared same (a) notations. T8, T9 (fluoride saturated biochar laden) showed the least test weights showing incompetence of these treatments in terms of agricultural prospect. A similarity was encountered when number of panicles per plant was counted. The organic amended treatment T4, T5 and T7 competed with the highest performing T10 (recommended fertiliser dose amended) and no significant difference in the panicle numbers were noted here. However, some treatments (T1,T2, T8 and T9) showed poor tillering and less effective tillers or panicles. Thus, being significantly different from high performing ones ($F_{9,20} = 10.1$, $p < 0.001$).

Test weight or 1000 seed weight (gms)

Fluoride : F $_{9,20}$ = 5.51, p < 0.001

Panicles per plant

Fluoride : F $_{9,20}$ = 10.1, p < 0.001
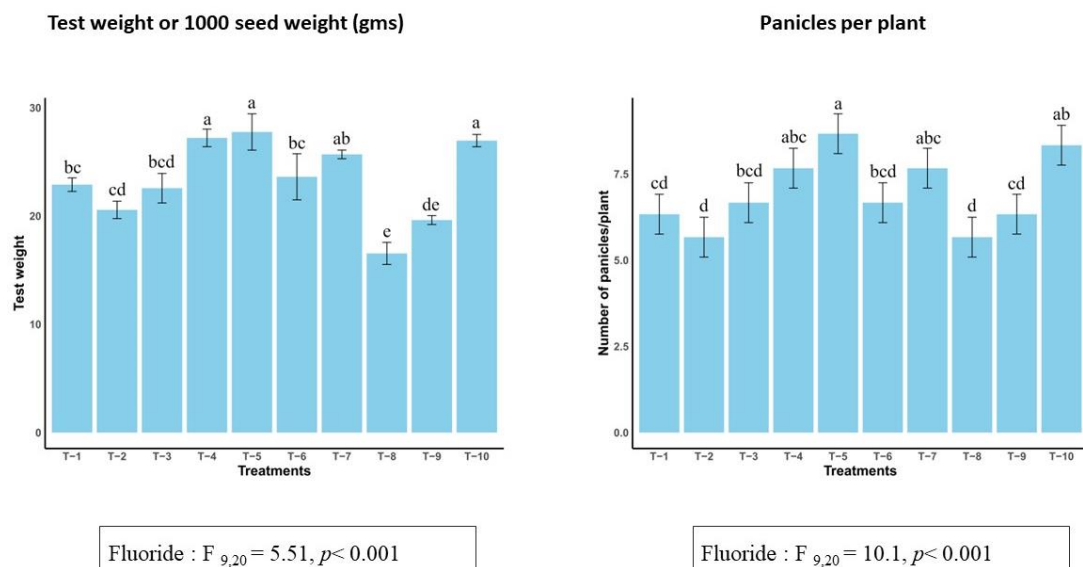
Fig 69. Analysing agronomic prospect from number of panicles/ plant and test weight (1000 seed weight) of rice harvested from expperimental field

Grain yield (T/ha)

Fluoride : F $_{9,20}$ = 5.472, p < 0.001

Straw yield (T/ha)

Fluoride : F $_{9,20}$ = 1.737, p=NS

Fig 70. Analysing grain yield and straw yield of rice harvested from experimental field

The next major agronomic parameters observed were grain yield (T/ ha) and straw yield (T/ha)

All experimental treatments performed satisfactorily and gave comparable yields to that from the recommended fertiliser dose treated one (T10) but T8 and T9. These treatments gave much lower yields and proved inefficiency in agricultural terms. This might be from the negative

impacts of the toxic fluoride that got mixed in the soil from the disposed saturated biochar. The differences in yields between these groups were thus significant ($F_{9,20}$ = 5.47, p <0.001). However, the straw yield had no significant difference among treatments ($F_{9,20}$ = 1.737, p =NS).

4.6.4. Estimating F⁻ bio-accumulation in rice grains

Alkali fusion method was used to estimate the total fluoride content present in edible plant parts of rice (grain) grown under different experimental treatments. This was necessary to find out whether there are chances of fluoride toxicity in crops grown using fluoride saturated biochar sanitised vermicompost. From the analysed samples, highest fluoride content was recorded from the grain of rice harvested from T8, T9 and T10 experimental plots. Fertiliser aided soils also showed fluoride accumulation and use of fluoride bearing phosphatic fertilisers may be one reason behind the event. But presence of fluoride in T8 and T9 indicates that disposal of fluoride saturated biochar directly to fields without proper remediation or sanitation (vermicomposting in this study) could develop chances of fluoride contamination in soil and subsequently crops growing in such locations could also get affected.

However, there was significantly low fluoride content in other treatments ($F_{9,20}$= 9.377, p <0.001). It was surprising to find minute fluoride accumulation in plants grown in absolute control soils which could indicate towards an inherent source of fluoride present in the native soil itself. The content of fluoride in other experimental vermi amended treatments (T2-T7) had no significant difference from that in control soil, thus allowing us to presume, that these amendments bring no chance of fluoride toxicity along with their use.

Total fluoride in grain

Bio concentration factor or BCF

Fluoride : $F_{9,20} = 9.3777$, $p < 0.001$

Fluoride : $F_{9,20} = 2.116$, $p = NS$
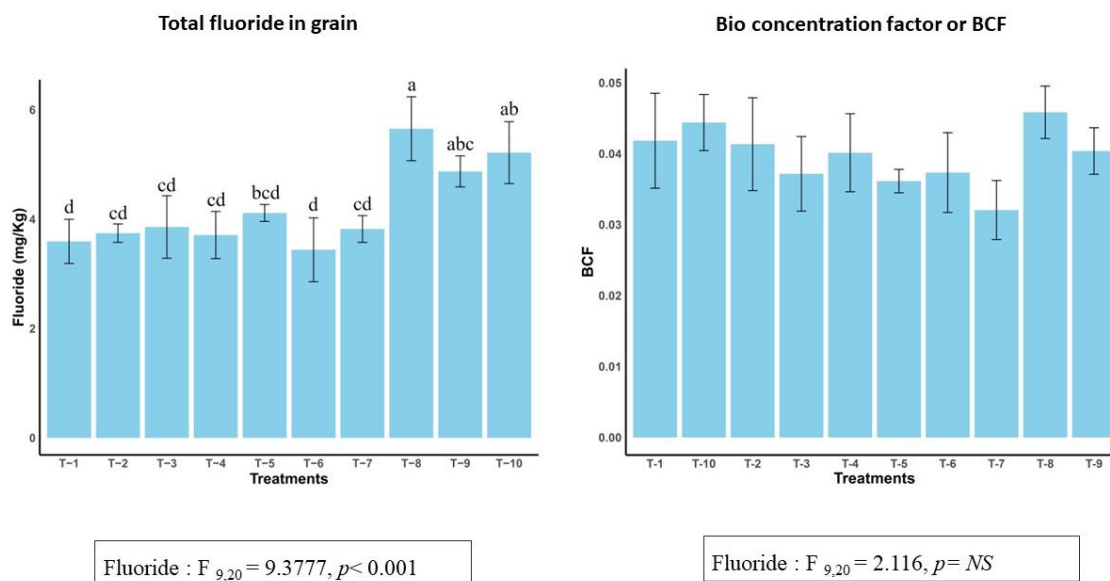
Fig 71. Analysing total fluoride content in edible plant part- the grains of harvested rice and the bio concentration factor (BCF) in grains from experimental field to trace any possible bioaccumulation

To further ascertain the safety of these experimentally grown grains, the bio concentration factor or BCF was calculated. The value of BCF when exceeds unity, indicates potential threat to human health from fluoride but to our satisfaction, none of the BCF values calculated from treatments used in this study exceeded unity and were therefore safe for human use. However, the grains with higher detectable fluoride, may cause potential threats if consumed for longer terms.

Conclusions

Chapter 5: Conclusions

The permissible limit for fluoride ions (F^-) in drinking water, as set by the WHO, is 1.5 ppm. Consuming water from sources that exceed this limit can lead to a range of health issues, including fluorosis, which has become a growing global menace. India is also severely affected by this problem. This study focused on fluoride pollution in groundwater from the less explored regions of Jharkhand, specifically investigating the sources, distribution, intensity, and dynamics of fluoride in the aquifers of this region. In the Dhanbad district (n = 283), 23% of the groundwater samples analyzed exceeded the permissible limit and were categorized as 'unsafe'. The elevated fluoride levels in this unsafe water were linked to higher concentrations of Na^+ and HCO_3^- ions, as illustrated by the Piper diagram. A positive correlation between F^- and pH, along with a negative correlation with Ca^{2+} ions, suggested that alkaline conditions and a deficiency of Ca^{2+} in the aquifers might facilitate the dissolution of F^- from the underlying bedrock. Additionally, bivariate plots of major ions indicated that calcite precipitation, silicate weathering, and carbonate dissolution could be responsible for the increase in fluoride concentrations. The logistic regression (LR) prediction model (AUC = 95.6%) successfully identified the key contributors to fluoride contamination. Physicochemical properties of groundwater, such as electrical conductivity (EC) and HCO_3^-, which showed the highest contribution in both LR and random forest (RF) models, could also be used to predict fluoride contamination, making this strategy especially useful in regions with limited resources and without fluoride measuring equipment. The unsuitability of fluoride-contaminated water for both domestic and agricultural use, as highlighted by the Fuzzy-TOPSIS analysis and various irrigation and health-risk indices, presents a significant concern. Moreover, unsampled areas at risk for fluoride contamination can be identified using the inverse distance weighting (IDW) surface maps generated in this study. Overall, this study provides valuable insights for

identifying high-risk zones for fluoride contamination and developing appropriate and sustainable management plans for fluoride mitigation.

Another region studied in the state was the mica mining areas, where significant findings contributed to understanding the fluoride problem. This study conducted an in-depth analysis of fluoride (F^-) contamination in groundwater within the mica mining regions of Tisri and Gawan blocks in Giridih district. A substantial portion (40%) of the groundwater samples exceeded the WHO and BIS permissible fluoride limit of 1.5 ppm, indicating F^- contamination primarily due to geogenic factors, such as silicate weathering and carbonate dissolution, exacerbated by unregulated mica mining activities. The findings revealed distinct differences between fluoride-contaminated (FC) and uncontaminated (FU) water samples. Significantly higher levels of sodium and bicarbonate in the contaminated samples highlighted the impact of prolonged rock-water interactions and mineral dissolution in the aquifers, supporting earlier findings from the Dhanbad district. The Health Risk Assessment (HRA) indicated non-carcinogenic risks from fluoride, particularly for children under 12, underscoring the urgent need for intervention. Advanced methodologies, including Self-Organizing Maps (SOM) and the Sobol sensitivity index (SSI), were effectively employed in the study. SOM predicted fluoride contamination with 80% accuracy, while the SSI identified key factors influencing fluoride contamination and associated health risks, notably fluoride concentration and body weight. The insights gained into the geochemical processes driving fluoride leaching in the mica mining regions provided critical information for local authorities, aiding the development and implementation of targeted groundwater management strategies to mitigate fluoride contamination. The predictive efficiency of SOM offers a useful tool for identifying fluoride-prone areas in other regions without extensive sampling. Expanding the study to other areas with similar geogenic and anthropogenic influences could further improve the understanding of fluoride contamination patterns.

Results obtained from analyzing water samples from both these regions were helpful in elucidating the fluoride dynamics better. This will also enable local authorities to prioritize high-risk areas and allocate resources efficiently to safeguard public health further. Once identified, these problems were then provided targeted mitigations.

In the next phase of this study, we successfully synthesized an efficient, low-cost, and sustainable green biosorbent from water hyacinth (*Pontederia crassipes*) to treat fluoride-contaminated drinking water. Batch experimental studies showed that the highest fluoride removal occurred at pH 4, using a biochar dose of 10 g/L in an adsorbate solution with a fluoride concentration of 10 mg/L, under a specific reaction temperature. However, a more optimized and practical scenario was achieved using response surface methodology (RSM). The optimized conditions identified by RSM included a pH of 6, a biochar dosage of 6.5 g/L, an initial fluoride concentration of 20 mg/L, and a reaction temperature of 32.98°C. The model showed good precision with an R^2 value of 0.83 and an insignificant lack-of-fit value. Further investigation revealed that the adsorption process followed the Langmuir adsorption isotherm model in its first linear form, along with pseudo-second-order kinetics. The adsorption mechanism involved both physisorption and chemisorption, forming an absolute monolayer on the homogeneous surface of the prepared biochar. The successful exfoliation achieved through nitric acid treatment was evident in the increased pore volume (0.037 cc/g) and specific surface area (147.722 m²/g) as determined by BET analysis. FTIR analysis identified the surface functional groups responsible for adsorption, while FESEM-EDS confirmed the morphological and spectral changes upon fluoride adsorption. This research highlights the potential of the invasive aquatic weed *Pontederia crassipes* as a promising biosorbent for fluoride removal and explores the underlying mechanisms. Future studies should focus on the lifespan of the adsorbent, its commercial-scale production, and the disposal of the saturated biochar.

After successfully removing fluoride using the biochar, the next step was to ensure its safe disposal. Contaminant-laden biochar cannot simply be discarded due to its biodegradable nature, which could lead to further contamination. To address this, vermitechnology—a sustainable pollution mitigation method using earthworms (*Eisenia fetida*)—was employed. Three types of experimental vermibeds (V1, V2, and V3) were produced and tested for fluoride safety through fractionation studies. Remarkably, the population of adult *E. fetida* in the vermibeds increased approximately threefold, indicating no signs of toxicity in the earthworms. A significant reduction in pH was observed, likely due to the production of HCO_3^-, NO_3^-, PO_4^-, and organic acids, suggesting effective organic matter mineralization. The decrease in electrical conductivity (EC) might have resulted from the insolubility, leaching, and microbial immobilization of salts during vermicomposting. The reduction in total organic carbon (TOC%) indicated accelerated microbial activity and CO_2 evolution during mineralization. Additionally, increases in available nitrogen (N), phosphorus (P), and potassium (K) further supported the mineralization process within the vermibeds. Key microbial activity indicators such as basal soil respiration (BSR), substrate-induced respiration (SIR), microbial biomass carbon (MBC), fluorescein diacetate (FDA) hydrolysis, and dehydrogenase activity (DHG) peaked around 60 days of vermicomposting, followed by a sharp decline, presumably signaling stabilization within the vermibed and increased competition among the microbial community. The declining qCO_2 and QR over time reflected reduced stress on the microbial flora. Importantly, the decrease in the water-soluble fraction of fluoride and the increase in the organically bound form over time indicated reduced bioavailability of fluoride in the compost, making it safe for further use. The earthworms likely contributed to the reduction in contaminant bioavailability by ingesting the toxic substances and binding them in their tissues through metal-binding proteins such as metallothioneins, which efficiently sequester toxic metals. Thus, effective vermisanitization of fluoride-saturated spent biochar was achieved.

The final phase of this study focused on assessing the agronomic potential of the biochar-sanitized vermicompost and evaluating any possible fluoride bioaccumulation in crops grown in soils amended with these products. Both tomato and rice experiments produced comparable yields to those from the recommended dose treatments. The addition of the experimental biochar-vermicompost improved soil quality, particularly in terms of available nitrogen (N), phosphorus (P), potassium (K), and total organic carbon (TOC), during both the pot experiments with tomatoes and field experiments with rice. Soil health remained stable, comparable to control conditions, as reflected by microbial activity in soils treated with vermi-amended compost. Negligible amounts of fluoride were detected in the edible parts of the food crops, supporting the suitability of this biochar-vermicompost for agricultural use and ruling out the possibility of fluoride contamination from the applied experimental biochar vermicompost. In contrast, treatment pots and plots that were directly amended with fluoride-saturated biochar (without vermicomposting) showed lower yields and hindered microbial activity, highlighting the potential risks of disposing fluoride-laden biochar directly without proper treatment. This study provided an in-depth understanding of fluoride aquifer chemistry and established a clear picture of the spatial distribution of fluoride in the study area. A biochar-based filter derived from water hyacinth was successfully developed to remove fluoride from the target solution, and the adsorption kinetics were also explored. Vermitechnology was efficiently employed to recycle the fluoride-contaminated, biodegradable biochar. The final compost product was applied to fields, where it proved to be a success in terms of both fluoride safety and agronomic benefits.

In summary, the study transformed what was considered waste-water hyacinth into a valuable biochar capable of removing fluoride. The fluoride-laden biochar was then remediated into a vermicompost suitable for agricultural use. This process, from identifying the problem to creating biochar and safely remediating it into a useful compost, exemplifies a true "*cradle to grave*" approach.

Bibliography

Abu Musa, Md., Chowdhury, S., Biswas, S., Nur Alam, S. M., Parvin, S., and Abdus Sattar, Md. 2024. Removal of aqueous methylene blue dye over Vallisneria Natans biosorbent using artificial neural network and statistical response surface methodology analysis. Journal of Molecular Liquids 393:123624. https://doi.org/10.1016/j.molliq.2023.123624.

Adeyeye, O. A., Xiao, C., Zhang, Z., Yawe, A. S., and Liang, X. 2021. Groundwater fluoride chemistry and health risk assessment of multi-aquifers in Jilin Qianan, Northeastern China. Ecotoxicology and Environmental Safety 211:111926. https://doi.org/10.1016/j.ecoenv.2021.111926.

Adimalla, N., and Qian, H. 2019. Groundwater quality evaluation using water quality index (WQI) for drinking purposes and human health risk (HHR) assessment in an agricultural region of Nanganur, south India. Ecotoxicology and Environmental Safety 176:153–161. https://doi.org/10.1016/j.ecoenv.2019.03.066.

Adimalla, N., and Venkatayogi, S. 2018. Geochemical characterization and evaluation of groundwater suitability for domestic and agricultural utility in semi-arid region of Basara, Telangana State, South India. Appl Water Sci 8:44. https://doi.org/10.1007/s13201-018-0682-1.

Adimalla, N., Vasa, S. K., and Li, P. 2018. Evaluation of groundwater quality, Peddavagu in Central Telangana (PCT), South India: an insight of controlling factors of fluoride enrichment. Model. Earth Syst. Environ. 4:841–852. https://doi.org/10.1007/s40808-018-0443-z.

Agalakova, N. I., and Nadei, O. V. 2020. Inorganic fluoride and functions of brain. Critical Reviews in Toxicology 50:28–46. https://doi.org/10.1080/10408444.2020.1722061.

Agbovi, H. K., and Wilson, L. D. 2021. Adsorption processes in biopolymer systems: fundamentals to practical applications. In Natural Polymers-Based Green Adsorbents for Water Treatment, Elsevier, pp. 1–51. https://doi.org/10.1016/B978-0-12-820541-9.00011-9.

Ahmad, I., Ghaffar, A., Zakir, A., Khan, Z. U. H., Saeed, M. F., Rasool, A., Jamal, A., Mihoub, A., Marzeddu, S., and Boni, M. R. 2022. Activated Biochar Is an Effective Technique for Arsenic Removal from Contaminated Drinking Water in Pakistan. Sustainability 14:14523. https://doi.org/10.3390/su142114523.

Ahmad, M., Rajapaksha, A. U., Lim, J. E., Zhang, M., Bolan, N., Mohan, D., Vithanage, M., Lee, S. S., and Ok, Y. S. 2014. Biochar as a sorbent for contaminant management in soil and water: A review. Chemosphere 99:19–33. https://doi.org/10.1016/j.chemosphere.2013.10.071.

Akhil, D., Lakshmi, D., Kartik, A., Vo, D.-V. N., Arun, J., and Gopinath, K. P. 2021. Production, characterization, activation and environmental applications of engineered biochar: a review. Environ Chem Lett 19:2261–2297. https://doi.org/10.1007/s10311-020-01167-7.

Alef, K. 1995. Soil respiration. In Methods in applied soil microbiology and biochemistry, Academic Press London, p. 222.

Ali, S., Shekhar, S., Bhattacharya, P., Verma, G., Chandrasekhar, T., and Chandrashekhar, A. K. 2018. Elevated fluoride in groundwater of Siwani Block, Western Haryana, India: A potential concern for sustainable water supplies for drinking and irrigation. Groundwater for Sustainable Development 7:410–420. https://doi.org/10.1016/j.gsd.2018.05.008.

Altaf, R., Lin, X., Zhuang, W., Lu, H., Rout, P. R., and Liu, D. 2021. Nitrilotrismethylenephosphonate sorption from wastewater on zirconium-lanthanum modified magnetite: Reusability and mechanism study. Journal of Cleaner Production 314:128045. https://doi.org/10.1016/j.jclepro.2021.128045.

Anazawa, K. 2006. Chapter 6: Fluorine and Coexisting Volatiles in the Geosphere: The Role in Japanese Volcanic Rocks. In Advances in Fluorine Science, Elsevier, pp. 187–224. https://doi.org/10.1016/S1872-0358(06)01006-2.

Annadurai, S. T., Rengasamy, J. K., Sundaram, R., and Munusamy, A. P. 2014. Incidence and effects of fluoride in Indian natural ecosystem: a review. Adv Appl Sci Res 5:173–185.

Aoba, T. 1997. The Effect of Fluoride On Apatite Structure and Growth. Critical Reviews in Oral Biology & Medicine 8:136–153. https://doi.org/10.1177/10454411970080020301.

Apambire, W. B., Boyle, D. R., and Michel, F. A. 1997. Geochemistry, genesis, and health implications of fluoriferous groundwaters in the upper regions of Ghana. Environmental Geology 33:13–24. https://doi.org/10.1007/s002540050221.

APHA., 2012. Standard methods for the examination of water and wastewater. Vol 10: American public health association Washington, DC.

Aravinthasamy, P., Karunanidhi, D., Subba Rao, N., Subramani, T., and Srinivasamoorthy, K. 2020. Irrigation risk assessment of groundwater in a non-perennial river basin of South India: implication from irrigation water quality index (IWQI) and geographical information system (GIS) approaches. Arab J Geosci 13:1125. https://doi.org/10.1007/s12517-020-06103-1.

Assefa, B. 2006. Defluoridation of Ethiopian rift valley region water using reverse osmosis membranes. Zede Journal 23:1–6.

Ávila-Juárez, L., Rodríguez González, A., Rodríguez Piña, N., Guevara González, R. G., Torres Pacheco, I., Ocampo Velázquez, R. V., and Moustapha, B. 2015. Vermicompost leachate as a supplement to increase tomato fruit quality. J. Soil Sci. Plant Nutr. 0–0. https://doi.org/10.4067/S0718-95162015005000005.

Ayers, R. S., and Westcot, D. W. 1985. Water quality for agriculture. Food and agriculture organization of the United Nations Rome.

Azeem, M., Shaheen, S. M., Ali, A., Jeyasundar, P. G. S. A., Latif, A., Abdelrahman, H., Li, R., Almazroui, M., Niazi, N. K., Sarmah, A. K., Li, G., Rinklebe, J., Zhu, Y.-G., and Zhang, Z. 2022. Removal of potentially toxic elements from contaminated soil and water using bone char compared to plant- and bone-derived biochars: A review. Journal of Hazardous Materials 427:128131. https://doi.org/10.1016/j.jhazmat.2021.128131.

Balajii, M., and Niju, S. 2019. Biochar-derived heterogeneous catalysts for biodiesel production. Environ Chem Lett 17:1447–1469. https://doi.org/10.1007/s10311-019-00885-x.

Bandara, A. Y., Weerasooriya, D. K., Bradley, C. A., Allen, T. W., and Esker, P. D. 2020. Dissecting the economic impact of soybean diseases in the United States over two decades ed. Binod Bihari Sahu. PLoS ONE 15:e0231141. https://doi.org/10.1371/journal.pone.0231141.

Banerjee, A., Banerjee, S., and Sarkar, P. 2016. Statistical design of experiments for optimization of arsenate reductase production by Kocuria palustris (RJB-6) and

immobilization parameters in polymer beads. RSC Adv. 6:49289–49297. https://doi.org/10.1039/C6RA00030D.

Banerjee, S., Banerjee, A., and Sarkar, P. 2018. Statistical optimization of arsenic biosorption by microbial enzyme via Ca-alginate beads. Journal of Environmental Science and Health, Part A 53:436–442. https://doi.org/10.1080/10934529.2017.1409009.

Barbier, O., Arreola-Mendoza, L., and Del Razo, L. M. 2010. Molecular mechanisms of fluoride toxicity. Chemico-Biological Interactions 188:319–333. https://doi.org/10.1016/j.cbi.2010.07.011.

Batabyal, A. K., and Gupta, S. 2017. Fluoride-contaminated groundwater of Birbhum district, West Bengal, India: Interpretation of drinking and irrigation suitability and major geochemical processes using principal component analysis. Environ Monit Assess 189:369. https://doi.org/10.1007/s10661-017-6041-0.

Batool, F., Akbar, J., Iqbal, S., Noreen, S., and Bukhari, S. N. A. 2018. Study of Isothermal, Kinetic, and Thermodynamic Parameters for Adsorption of Cadmium: An Overview of Linear and Nonlinear Approach and Error Analysis. Bioinorganic Chemistry and Applications 2018:1–11. https://doi.org/10.1155/2018/3463724.

Belhassan, H., Merzouki, M., El Mouhri, G., Amakdouf, H., Lamrani, O., Mehdi Haily, E., Massaoudi, Y., Boukir, A., and Benlemlih, M. 2023. High efficiency removal of heavy metals and organic pollutants from brassware using raw coal: Kinetic adsorption and optimized process. Results in Chemistry 5:100855. https://doi.org/10.1016/j.rechem.2023.100855.

Benmessaoud, A., Nibou, D., Mekatel, E. H., and Amokrane, S. 2020. A comparative study of the linear and non-linear methods for determination of the optimum equilibrium isotherm for adsorption of Pb2+ ions onto Algerian treated clay. Iranian Journal of Chemistry and Chemical Engineering (IJCCE) 39:153–171.

Bhattacharya, S. S., and Kim, K.-H. 2016. Utilization of coal ash: Is vermitechnology a sustainable avenue? Renewable and Sustainable Energy Reviews 58:1376–1386. https://doi.org/10.1016/j.rser.2015.12.345.

Bhattacharyya, P., Reddy, K. J., and Attili, V. 2011. Solubility and Fractionation of Different Metals in Fly Ash of Powder River Basin Coal. Water Air Soil Pollut 220:327–337. https://doi.org/10.1007/s11270-011-0757-1.

BIS., 2012. Indian Standard drinking water specifications IS 10500:2012. Bureau of Indian standards, New Delhi.

Boostani, H. R., Najafi-Ghiri, M., Hardie, A. G., and Khalili, D. 2019. Comparison of Pb stabilization in a contaminated calcareous soil by application of vermicompost and sheep manure and their biochars produced at two temperatures. Applied Geochemistry 102:121–128. https://doi.org/10.1016/j.apgeochem.2019.01.013.

Boyle, D. R., and Chagnon, M. 1995. An incidence of skeletal fluorosis associated with groundwaters of the maritime carboniferous basin, Gasp� region, Quebec, Canada. Environ Geochem Health 17. https://doi.org/10.1007/BF00188625.

Brassard, P., Godbout, S., Lévesque, V., Palacios, J. H., Raghavan, V., Ahmed, A., Hogue, R., Jeanne, T., and Verma, M. 2019. Biochar for soil amendment. In Char and Carbon Materials Derived from Biomass, Elsevier, pp. 109–146. https://doi.org/10.1016/B978-0-12-814893-8.00004-3.

Brindha, K., and Elango, L. 2011. Fluoride in groundwater: causes, implications and mitigation measures. Fluoride properties, applications and environmental management 1:111–136.

Brunauer, S., Emmett, P. H., and Teller, E. 1938. Adsorption of gases in multimolecular layers. Journal of the American chemical society 60:309–319.

Buentello-Montoya, D., Zhang, X., Li, J., Ranade, V., Marques, S., and Geron, M. 2020. Performance of biochar as a catalyst for tar steam reforming: Effect of the porous structure. Applied Energy 259:114176. https://doi.org/10.1016/j.apenergy.2019.114176.

Cai, S., Liu, Y., and Chen, J. 2020. FeCu-biochar enhances the removal of antibacterial sulfapyridine from groundwater by activation of persulfate. Environ Chem Lett 18:1693–1700. https://doi.org/10.1007/s10311-020-01026-5.

Casida Jr, L., Klein, D. A., and Santoro, T. 1964. Soil dehydrogenase activity. Soil science 98:371–376.

Castaño-Sánchez, A., Hose, G. C., and Reboleira, A. S. P. S. 2020. Salinity and temperature increase impact groundwater crustaceans. Sci Rep 10:12328. https://doi.org/10.1038/s41598-020-69050-7.

CGWB. 2009. Ground Water Year Book. .

CGWB., 2021.Ground water year book. Jharkhand. Ministry of Jalshakti. Mid Eastern
Region, Patna. Government of India.

CGWB., 2022. Aquifer mapping and management of groundwater resources. Ministry of
Jalshakti. Mid Eastern Region, Patna. Government of India.

Chakraborty, P., Sarkar, S., Mondal, S., Agarwal, B. K., Kumar, A., Bhattacharya, S.,
Bhattacharya, S. S., and Bhattacharyya, P. 2022. Eisenia fetida mediated vermi-
transformation of tannery waste sludge into value added eco-friendly product: An
insight on microbial diversity, enzyme activation, and metal detoxification. Journal of
Cleaner Production 348:131368. https://doi.org/10.1016/j.jclepro.2022.131368.

Chakraborty, S., Ghosh, S., Prajapati, J., Mandal, J., and Bhattacharyya, P. 2024. Dietary
Exposure of Arsenic Due to Mining Activities and the Plight to Human Health: an
Assessment Through Multimodal Statistical Approaches. Expo Health.
https://doi.org/10.1007/s12403-024-00639-3.

Chakraborty, V., and Das, P. 2023. Synthesis of nano-silica-coated biochar from thermal
conversion of sawdust and its application for Cr removal: kinetic modelling using
linear and nonlinear method and modelling using artificial neural network analysis.
Biomass Conv. Bioref. 13:821–831. https://doi.org/10.1007/s13399-020-01024-1.

Chander, K., Dyckmans, J., Joergensen, R., Meyer, B., and Raubuch, M. 2001. Different
sources of heavy metals and their long-term effects on soil microbial properties.
Biology and Fertility of Soils 34:241–247. https://doi.org/10.1007/s003740100406.

Chang, J. I., and Chen, Y. J. 2010. Effects of bulking agents on food waste composting.
Bioresource Technology 101:5917–5924.
https://doi.org/10.1016/j.biortech.2010.02.042.

Charan, K., and Bhattacharyya, P. 2023. Vermicomposted red mud-An up-and-coming
approach towards soil fertility and crop quality. Journal of Crop and Weed 19:36–51.

Charan, K., Bhattacharyya, P., and Bhattacharya, S. S. 2024a. Vermitechnology transforms
hazardous red mud into benign organic input for agriculture: Insights on earthworm-
microbe interaction, metal removal, and soil-crop improvement. Journal of
Environmental Management 354:120320.
https://doi.org/10.1016/j.jenvman.2024.120320.

Charan, K., Mandal, J., and Bhattacharyya, P. 2024b. Application of autochthonous extremophilic Bacillus xiamenensis in remediation of groundwater- A sorption-based metal cleaning approach. Groundwater for Sustainable Development 24:101063. https://doi.org/10.1016/j.gsd.2023.101063.

Chatterjee, R., Jana, J. C., and Paul, P. K. 2013. Vermicompost Substitution Influences Shelf Life and Fruit Quality of Tomato (Lycopersicon esculentum Mill.). AJAST. https://doi.org/10.7726/ajast.2013.1006.

Chen, J., Gao, Y., Qian, H., Ren, W., and Qu, W. 2021. Hydrogeochemical evidence for fluoride behavior in groundwater and the associated risk to human health for a large irrigation plain in the Yellow River Basin. Science of The Total Environment 800:149428. https://doi.org/10.1016/j.scitotenv.2021.149428.

Chen, L., Li, F., Wei, Y., Li, G., Shen, K., and He, H.-J. 2019. High cadmium adsorption on nanoscale zero-valent iron coated Eichhornia crassipes biochar. Environ Chem Lett 17:589–594. https://doi.org/10.1007/s10311-018-0811-y.

Chen, Z.-H., Hills, A., Lim, C. K., and Blatt, M. R. 2010. Dynamic regulation of guard cell anion channels by cytosolic free Ca 2+ concentration and protein phosphorylation. The Plant Journal 61:816–825. https://doi.org/10.1111/j.1365-313X.2009.04108.x.

Choi, A. L., Sun, G., Zhang, Y., and Grandjean, P. 2012. Developmental Fluoride Neurotoxicity: A Systematic Review and Meta-Analysis. Environ Health Perspect 120:1362–1368. https://doi.org/10.1289/ehp.1104912.

Choubisa, S. L., Choubisa, D., and Choubisa, A. 2023. Fluoride contamination of groundwater and its threat to health of villagers and their domestic animals and agriculture crops in rural Rajasthan, India. Environ Geochem Health 45:607–628. https://doi.org/10.1007/s10653-022-01267-z.

Choudhary, M., Jat, H. S., Datta, A., Yadav, A. K., Sapkota, T. B., Mondal, S., Meena, R. P., Sharma, P. C., and Jat, M. L. 2018. Sustainable intensification influences soil quality, biota, and productivity in cereal-based agroecosystems. Applied Soil Ecology 126:189–198. https://doi.org/10.1016/j.apsoil.2018.02.027.

Chowdhury, P., Mukhopadhyay, B. P., Nayak, S., and Bera, A. 2022. Hydro-chemical characterization of groundwater and evaluation of health risk assessment for fluoride

contamination areas in the eastern blocks of Purulia district, India. Environ Dev Sustain 24:11320–11347. https://doi.org/10.1007/s10668-021-01911-1.

Chubar, N. I., Samanidou, V. F., Kouts, V. S., Gallios, G. G., Kanibolotsky, V. A., Strelko, V. V., and Zhuravlev, I. Z. 2005. Adsorption of fluoride, chloride, bromide, and bromate ions on a novel ion exchanger. Journal of Colloid and Interface Science 291:67–74. https://doi.org/10.1016/j.jcis.2005.04.086.

Coyte, R. M., Singh, A., Furst, K. E., Mitch, W. A., and Vengosh, A. 2019. Co-occurrence of geogenic and anthropogenic contaminants in groundwater from Rajasthan, India. Science of The Total Environment 688:1216–1227. https://doi.org/10.1016/j.scitotenv.2019.06.334.

Dai, Y., Liang, Y., Xu, X., Zhao, L., and Cao, X. 2018. An integrated approach for simultaneous immobilization of lead in both contaminated soil and groundwater: Laboratory test and numerical modeling. Journal of Hazardous Materials 342:107–113. https://doi.org/10.1016/j.jhazmat.2017.08.023.

Dallinger, R. 1993. Strategies of metal detoxification in terrestrial invertebrates. Ecotoxicology of metals in invertebrates 245.

Das, A., Das, S. S., Chowdhury, N. R., Joardar, M., Ghosh, B., and Roychowdhury, T. 2020. Quality and health risk evaluation for groundwater in Nadia district, West Bengal: An approach on its suitability for drinking and domestic purpose. Groundwater for Sustainable Development 10:100351. https://doi.org/10.1016/j.gsd.2020.100351.

Das, S., Dash, H. R., and Chakraborty, J. 2016. Genetic basis and importance of metal resistant genes in bacteria for bioremediation of contaminated environments with toxic metal pollutants. Appl Microbiol Biotechnol 100:2967–2984. https://doi.org/10.1007/s00253-016-7364-4.

Davison, A., Takmaz-Nisancioglu, S., and Bailey, I. 1985. The dynamics of fluoride accumulation by vegetation. Fluoride toxicity 30–46.

Daw, R. K. 2004. Experiences with domestic defluoridation in India. .

D�az-Burgos, M. A., Ceccanti, B., and Polo, A. 1993. Monitoring biochemical activity during sewage sludge composting. Biol Fert Soils 16:145–150. https://doi.org/10.1007/BF00369417.

de Mendiburu, F., and de Mendiburu, M. F. 2019. Package 'agricolae.' R Package, version 1:1143–49.

Deka, H., Deka, S., Baruah, C. K., Das, J., Hoque, S., Sarma, H., and Sarma, N. S. 2011. Vermicomposting potentiality of Perionyx excavatus for recycling of waste biomass of java citronella - An aromatic oil yielding plant. Bioresource Technology 102:11212–11217. https://doi.org/10.1016/j.biortech.2011.09.102.

Dey, S., and Giri, B. 2016. Fluoride Fact on Human Health and Health Problems: A Review. Med Clin Rev 02. https://doi.org/10.21767/2471-299X.1000011.

Dhingra, R. S., and Shah, M. 2021. A holistic study on fluoride-contaminated groundwater models and its widespread effects in healthcare and irrigation. Environ Sci Pollut Res 28:60329–60345. https://doi.org/10.1007/s11356-021-16367-z.

Dilly, O. 2005. Microbial Energetics in Soils. In Microorganisms in Soils: Roles in Genesis and Functions, Soil Biology, eds. Ajit Varma and Francois Buscot. Berlin/Heidelberg: Springer-Verlag, pp. 123–138. https://doi.org/10.1007/3-540-26609-7_6.

Dominguez, J., and Edwards, C. A. 2011. Biology and ecology of earthworm species used for vermicomposting. Vermiculture technology: earthworms, organic waste and environmental management. CRC Press, Boca Raton 27–40.

Doneen, L. 1964. Water quality for agriculture. Department of Irrigation, University of California, California 48.

Dwivedi, S., Mondal, P., and Balomajumder, C. 2017. Bioremoval of Fluoride from Synthetic Water Using Gram-Negative Bacteria *Shewanella putrefaciens*. J. Hazard. Toxic Radioact. Waste 21:04016023. https://doi.org/10.1061/(ASCE)HZ.2153-5515.0000341.

Edmunds, W. M., and Smedley, P. L. 2012. Fluoride in natural waters. In Essentials of medical geology: Revised Edition, Springer, pp. 311–336.

Elovich, S. Y., and Larinov, O. 1962. Theory of adsorption from solutions of non electrolytes on solid (I) equation adsorption from solutions and the analysis of its simplest form,(II) verification of the equation of adsorption isotherm from solutions. Izv. Akad. Nauk. SSSR, Otd. Khim. Nauk 2:209–216.

Emenike, C. P., Tenebe, I. T., and Jarvis, P. 2018. Fluoride contamination in groundwater sources in Southwestern Nigeria: Assessment using multivariate statistical approach

and human health risk. Ecotoxicology and Environmental Safety 156:391–402. https://doi.org/10.1016/j.ecoenv.2018.03.022.

Epstein, E. 2017. The science of composting. CRC press.

Fito, J., Tibebu, S., and Nkambule, T. T. I. 2023. Optimization of Cr (VI) removal from aqueous solution with activated carbon derived from Eichhornia crassipes under response surface methodology. BMC Chemistry 17:4. https://doi.org/10.1186/s13065-023-00913-6.

Fordyce, F. M., Vrana, K., Zhovinsky, E., Povoroznuk, V., Toth, G., Hope, B. C., Iljinsky, U., and Baker, J. 2007. A health risk assessment for fluoride in Central Europe. Environ Geochem Health 29:83–102. https://doi.org/10.1007/s10653-006-9076-7.

Freundlich, H. M. F. 1906. Over the adsorption in solution. J. Phys. chem 57:1100–1107.

Galgali, P., Palimkar, S., Adhikari, A., Patel, R., and Routh, J. 2023. Remediation of potentially toxic elements -containing wastewaters using water hyacinth – a review. International Journal of Phytoremediation 25:172–186. https://doi.org/10.1080/15226514.2022.2068501.

Ganguli, S., Hosen Rifat, Md. A., Howlader, S., Hasan, Md. A., Islam, S., Alam, Md. N. E., and Islam, Md. N. 2022. Assessment of Bhatiari Lake water quality: Pollution indices, hydrochemical signatures and hydro-statistical analysis. Journal of the Indian Chemical Society 99:100585. https://doi.org/10.1016/j.jics.2022.100585.

Ganguly, P., Sarkhel, R., and Das, P. 2020. Synthesis of pyrolyzed biochar and its application for dye removal: Batch, kinetic and isotherm with linear and non-linear mathematical analysis. Surfaces and Interfaces 20:100616. https://doi.org/10.1016/j.surfin.2020.100616.

Gantait, A., Das, S., Ghosh, S., Bohra, G., and Mukhopadhyay, S. 2022. Hydrogeochemical evolution and quality assessment of groundwater of Ajmer district, Rajasthan, India. J Earth Syst Sci 131:236. https://doi.org/10.1007/s12040-022-01975-1.

Gaur, A., and Sadasivam, K. 1980. Recycling of organic wastes in agriculture. IARI, New Delhi.

Ghaeminia, M., and Mokhtarani, N. 2018. Remediation of nitrate-contaminated groundwater by PRB-Electrokinetic integrated process. Journal of Environmental Management 222:234–241. https://doi.org/10.1016/j.jenvman.2018.05.078.

Ghahramani, E., Kamarehie, B., Rezaiee, R., Jafari, A., Azimi, F., Darvishmotevalli, M., Faridan, M., Maleki, A., Zandsalimi, Y., and Karami, M. A. 2023. Fluoride content in drinking water of the rural areas of Divandarreh city, Kurdistan province, Iran: a non-carcinogenic risk assessment. International Journal of Environmental Analytical Chemistry 103:341–353. https://doi.org/10.1080/03067319.2020.1857752.

Giri, S., and Singh, A. K. 2024. Fluoride and Metals in the Agricultural Soils of Mica Mining Areas of Jharkhand, India: Assessing the Ecological and Human Health Risk. Soil and Sediment Contamination: An International Journal 33:393–415. https://doi.org/10.1080/15320383.2023.2208675.

Gogoi, A., Mazumder, P., Tyagi, V. K., Tushara Chaminda, G. G., An, A. K., and Kumar, M. 2018. Occurrence and fate of emerging contaminants in water environment: A review. Groundwater for Sustainable Development 6:169–180. https://doi.org/10.1016/j.gsd.2017.12.009.

Gopinath, K. P., Vo, D.-V. N., Gnana Prakash, D., Adithya Joseph, A., Viswanathan, S., and Arun, J. 2021. Environmental applications of carbon-based materials: a review. Environ Chem Lett 19:557–582. https://doi.org/10.1007/s10311-020-01084-9.

Goswami, L., Pratihar, S., Dasgupta, S., Bhattacharyya, P., Mudoi, P., Bora, J., Bhattacharya, S. S., and Kim, K. H. 2016. Exploring metal detoxification and accumulation potential during vermicomposting of Tea factory coal ash: sequential extraction and fluorescence probe analysis. Sci Rep 6:30402. https://doi.org/10.1038/srep30402.

Grandjean, P., and Landrigan, P. 2006. Developmental neurotoxicity of industrial chemicals. The Lancet 368:2167–2178. https://doi.org/10.1016/S0140-6736(06)69665-7.

Gunarathne, V., Ashiq, A., Ramanayaka, S., Wijekoon, P., and Vithanage, M. 2019. Biochar from municipal solid waste for resource recovery and pollution remediation. Environ Chem Lett 17:1225–1235. https://doi.org/10.1007/s10311-019-00866-0.

Gupta, P. K., Kumar, A., Simon, M., and Manisha. 2021. Arsenic Pollution in Groundwater and Its In Situ Microbial Remediation Technologies. In Fate and Transport of Subsurface Pollutants, Microorganisms for Sustainability, eds. Pankaj Kumar Gupta and Ram Naresh Bharagava. Singapore: Springer Singapore, pp. 183–197. https://doi.org/10.1007/978-981-15-6564-9_10.

Gupta, S. K., Deshpande, R. D., Agarwal, M., and Raval, B. R. 2005. Origin of high fluoride in groundwater in the North Gujarat-Cambay region, India. Hydrogeol J 13:596–605. https://doi.org/10.1007/s10040-004-0389-2.

Halim, M. A., Majumder, R. K., Nessa, S. A., Oda, K., Hiroshiro, Y., Saha, B. B., Hassain, S. M., Latif, Sk. A., Islam, M. A., and Jinno, K. 2009. Groundwater contamination with arsenic in Sherajdikhan, Bangladesh: geochemical and hydrological implications. Environ Geol 58:73–84. https://doi.org/10.1007/s00254-008-1493-8.

Handa, B. K. 1975. Geochemistry and Genesis of Fluoride-Containing Ground Waters in India. Groundwater 13:275–281. https://doi.org/10.1111/j.1745-6584.1975.tb03086.x.

Hanse, A., Chabukdhara, M., Gohain Baruah, S., Boruah, H., and Gupta, S. K. 2019. Fluoride contamination in groundwater and associated health risks in Karbi Anglong District, Assam, Northeast India. Environ Monit Assess 191:782. https://doi.org/10.1007/s10661-019-7970-6.

Hashemkhani, M., Rezvani Ghalhari, M., Bashardoust, P., Hosseini, S. S., Mesdaghinia, A., and Mahvi, A. H. 2022. Fluoride removal from aqueous solution via environmentally friendly adsorbent derived from seashell. Sci Rep 12:9655. https://doi.org/10.1038/s41598-022-13756-3.

He, J., An, Y., and Zhang, F. 2013. Geochemical characteristics and fluoride distribution in the groundwater of the Zhangye Basin in Northwestern China. Journal of Geochemical Exploration 135:22–30. https://doi.org/10.1016/j.gexplo.2012.12.012.

He, K., He, G., Wang, C., Zhang, H., Xu, Y., Wang, S., Kong, Y., Zhou, G., and Hu, R. 2020. Biochar amendment ameliorates soil properties and promotes Miscanthus growth in a coastal saline-alkali soil. Applied Soil Ecology 155:103674. https://doi.org/10.1016/j.apsoil.2020.103674.

Heidarinejad, Z., Dehghani, M. H., Heidari, M., Javedan, G., Ali, I., and Sillanpää, M. 2020. Methods for preparation and activation of activated carbon: a review. Environ Chem Lett 18:393–415. https://doi.org/10.1007/s10311-019-00955-0.

Heller, K. E., Eklund, S. A., and Burt, B. A. 1997. Dental Caries and Dental Fluorosis at Varying Water Fluoride Concentrations. J Public Health Dent 57:136–143. https://doi.org/10.1111/j.1752-7325.1997.tb02964.x.

Hem, J. D. 1985. Study and interpretation of the chemical characteristics of natural water. Department of the Interior, US Geological Survey.

Ho, Y. S., and McKay, G. 1998. Sorption of dye from aqueous solution by peat. Chemical Engineering Journal 70:115–124. https://doi.org/10.1016/S0923-0467(98)00076-1.

Hossain, S., Hosono, T., Yang, H., and Shimada, J. 2016. Geochemical Processes Controlling Fluoride Enrichment in Groundwater at the Western Part of Kumamoto Area, Japan. Water Air Soil Pollut 227:385. https://doi.org/10.1007/s11270-016-3089-3.

Houessionon, M. G. K., Ouendo, E.-M. D., Bouland, C., Takyi, S. A., Kedote, N. M., Fayomi, B., Fobil, J. N., and Basu, N. 2021. Environmental Heavy Metal Contamination from Electronic Waste (E-Waste) Recycling Activities Worldwide: A Systematic Review from 2005 to 2017. IJERPH 18:3517. https://doi.org/10.3390/ijerph18073517.

Hsu, T. H.-S., Lin, S.-Y., Lin, C.-C., and Cheng, W.-T. 2011. Preliminary feasibility study of FTIR microscopic mapping system for the rapid detection of the composited components of prostatic calculi. Urol Res 39:165–170. https://doi.org/10.1007/s00240-010-0316-z.

Hu, B., Song, X., Lu, Y., Liang, S., and Liu, G. 2022. Fluoride enrichment mechanisms and related health risks of groundwater in the transition zone of geomorphic units, northern China. Environmental Research 212:113588. https://doi.org/10.1016/j.envres.2022.113588.

Hu, H., Sun, L., Wang, T., Lv, C., Gao, Y., Zhang, Y.-F., Wu, H., and Chen, X. 2019. Nano-ZnO functionalized biochar as a superhydrophobic biosorbent for selective recovery of low-concentration Re(VII) from strong acidic solutions. Minerals Engineering 142:105885. https://doi.org/10.1016/j.mineng.2019.105885.

Huang, L., Luo, Z., Huang, X., Wang, Y., Yan, J., Liu, W., Guo, Y., Babu Arulmani, S. R., Shao, M., and Zhang, H. 2022. Applications of biomass-based materials to remove fluoride from wastewater: A review. Chemosphere 301:134679. https://doi.org/10.1016/j.chemosphere.2022.134679.

Huang, W.-H., Lee, D.-J., and Huang, C. 2021. Modification on biochars for applications: A research update. Bioresource Technology 319:124100. https://doi.org/10.1016/j.biortech.2020.124100.

Hussain, N., Chatterjee, S. K., Maiti, T. K., Goswami, L., Das, S., Deb, U., and Bhattacharya, S. S. 2021. Metal induced non-metallothionein protein in earthworm: A new pathway for cadmium detoxification in chloragogenous tissue. Journal of Hazardous Materials 401:123357. https://doi.org/10.1016/j.jhazmat.2020.123357.

Hussain, N., Singh, A., Saha, S., Venkata Satish Kumar, M., Bhattacharyya, P., and Bhattacharya, S. S. 2016. Excellent N-fixing and P-solubilizing traits in earthworm gut-isolated bacteria: A vermicompost based assessment with vegetable market waste and rice straw feed mixtures. Bioresource Technology 222:165–174. https://doi.org/10.1016/j.biortech.2016.09.115.

Hussain, S. T., Mahmood, T., and Malik, S. A. 2010. Phytoremediation technologies for Ni++ by water hyacinth. African journal of Biotechnology 9:8648–8660.

Inyang, M. I., Gao, B., Yao, Y., Xue, Y., Zimmerman, A., Mosa, A., Pullammanappallil, P., Ok, Y. S., and Cao, X. 2016. A review of biochar as a low-cost adsorbent for aqueous heavy metal removal. Critical Reviews in Environmental Science and Technology 46:406–433. https://doi.org/10.1080/10643389.2015.1096880.

Ismail, A. 1997. Vermicology: the biology of earthworms. Orient Longman.

Jacks, G., Bhattacharya, P., Chaudhary, V., and Singh, K. P. 2005. Controls on the genesis of some high-fluoride groundwaters in India. Applied Geochemistry 20:221–228. https://doi.org/10.1016/j.apgeochem.2004.07.002.

Jackson, M. 1973. Soil chemical analysis, pentice hall of India Pvt. Ltd., New Delhi, India 498:151–154.

Jacobson, J. S., Weinstein, L. H., Mccune, D. C., and Hitchcock, A. E. 1966. The Accumulation of Fluorine by Plants. Journal of the Air Pollution Control Association 16:412–417. https://doi.org/10.1080/00022470.1966.10468494.

Jandu, A., Malik, A., and Dhull, S. B. 2021. Fluoride and nitrate in groundwater of rural habitations of semiarid region of northern Rajasthan, India: a hydrogeochemical, multivariate statistical, and human health risk assessment perspective. Environ Geochem Health 43:3997–4026. https://doi.org/10.1007/s10653-021-00882-6.

Jenkinson, D. 1988. Determination of microbial biomass carbon and nitrogen in soil. Advances in nitrogen cycling in agricultural systems. Ed. JR Wilson. Wallingford: CABI 368–386.

Jha, P. K., and Tripathi, P. 2021. Arsenic and fluoride contamination in groundwater: A review of global scenarios with special reference to India. Groundwater for Sustainable Development 13:100576. https://doi.org/10.1016/j.gsd.2021.100576.

Jha, S., Banerjee, S., Ghosh, S., Verma, A., and Bhattacharyya, P. 2024. Eisenia fetida-driven vermitechnology for the eco-friendly transformation of steel waste slag into organic amendment: An insight through microbial diversity and multi-model approach. Environmental Research 251:118636. https://doi.org/10.1016/j.envres.2024.118636.

Jha, S., Verma, A., and Bhattacharyya, P. 2023. Assessing the Effectiveness of Vermicomposted Products and Predicting Potential Hazards From Metal Contaminated Steel Waste Through Multi-model Analysis. Water Air Soil Pollut 234:679. https://doi.org/10.1007/s11270-023-06687-w.

Jia, H., Qian, H., Zheng, L., Feng, W., Wang, H., and Gao, Y. 2020. Alterations to groundwater chemistry due to modern water transfer for irrigation over decades. Science of The Total Environment 717:137170. https://doi.org/10.1016/j.scitotenv.2020.137170.

Jia, Y., Shi, S., Liu, J., Su, S., Liang, Q., Zeng, X., and Li, T. 2018. Study of the Effect of Pyrolysis Temperature on the Cd2+ Adsorption Characteristics of Biochar. Applied Sciences 8:1019. https://doi.org/10.3390/app8071019.

Jolly, S., Oberoi, D., Sharma, R., and Ralhan, S. 1974. Fluoride balance studies in cases of endemic fluorosis.

Joon, V., Shahrawat, R., and Kapahi, M. 2017. The Emerging Environmental and Public Health Problem of Electronic Waste in India. Journal of Health and Pollution 7:1–7. https://doi.org/10.5696/2156-9614-7.15.1.

Kadam, A., Wagh, V., Patil, S., Umrikar, B., and Sankhua, R. 2021. Seasonal assessment of groundwater contamination, health risk and chemometric investigation for a hard rock terrain of western India. Environ Earth Sci 80:172. https://doi.org/10.1007/s12665-021-09414-y.

Kalderis, D., Tsuchiya, S., Phillipou, K., Paschalidou, P., Pashalidis, I., Tashima, D., and Tsubota, T. 2020. Utilization of pine tree biochar produced by flame-curtain pyrolysis in two non-agricultural applications. Bioresource Technology Reports 9:100384. https://doi.org/10.1016/j.biteb.2020.100384.

Kaminsky, L. S., Mahoney, M. C., Leach, J., Melius, J., and Jo Miller, M. 1990. Fluoride: Benefits And Risks of Exposure. Critical Reviews in Oral Biology & Medicine 1:261–281. https://doi.org/10.1177/10454411900010040501.

Karro, E., and Uppin, M. 2013. The occurrence and hydrochemistry of fluoride and boron in carbonate aquifer system, central and western Estonia. Environ Monit Assess 185:3735–3748. https://doi.org/10.1007/s10661-012-2824-5.

Kasera, N., Augoustides, V., Kolar, P., Hall, S. G., and Vicente, B. 2022. Effect of Surface Modification by Oxygen-Enriched Chemicals on the Surface Properties of Pine Bark Biochars. Processes 10:2136. https://doi.org/10.3390/pr10102136.

Kashyap, C. A., Ghosh, A., Singh, S., Ali, S., Singh, H. K., Chandrasekhar, T., and Chandrasekharam, D. 2020. Distribution, genesis and geochemical modeling of fluoride in the water of tribal area of Bijapur district, Chhattisgarh, central India. Groundwater for Sustainable Development 11:100403. https://doi.org/10.1016/j.gsd.2020.100403.

Kashyap, S. J., Sankannavar, R., and Madhu, G. M. 2021. Fluoride sources, toxicity and fluorosis management techniques – A brief review. Journal of Hazardous Materials Letters 2:100033. https://doi.org/10.1016/j.hazl.2021.100033.

Kaur, L., Rishi, M. S., and Siddiqui, A. U. 2020. Deterministic and probabilistic health risk assessment techniques to evaluate non-carcinogenic human health risk (NHHR) due to fluoride and nitrate in groundwater of Panipat, Haryana, India. Environmental Pollution 259:113711. https://doi.org/10.1016/j.envpol.2019.113711.

Keerthanan, S., Bhatnagar, A., Mahatantila, K., Jayasinghe, C., Ok, Y. S., and Vithanage, M. 2020. Engineered tea-waste biochar for the removal of caffeine, a model compound in pharmaceuticals and personal care products (PPCPs), from aqueous media. Environmental Technology & Innovation 19:100847. https://doi.org/10.1016/j.eti.2020.100847.

Keesari, T., Pant, D., Roy, A., Sinha, U. K., Jaryal, A., Singh, M., and Jain, S. K. 2021. Fluoride Geochemistry and Exposure Risk Through Groundwater Sources in Northeastern Parts of Rajasthan, India. Arch Environ Contam Toxicol 80:294–307. https://doi.org/10.1007/s00244-020-00794-z.

Kerdoun, M. A., Mekhloufi, S., Adjaine, O. E. K., Bechki, Z., Gana, M., and Belkhalfa, H. 2022. Fluoride concentrations in drinking water and health risk assessment in the south of Algeria. Regulatory Toxicology and Pharmacology 128:105086. https://doi.org/10.1016/j.yrtph.2021.105086.

Khan, A. F., Srinivasamoorthy, K., and Rabina, C. 2020. Hydrochemical characteristics and quality assessment of groundwater along the coastal tracts of Tamil Nadu and Puducherry, India. Appl Water Sci 10:74. https://doi.org/10.1007/s13201-020-1158-7.

Kim, J., Kim, R., Lee, J., Cheong, T., Yum, B., and Chang, H. 2005. Multivariate statistical analysis to identify the major factors governing groundwater quality in the coastal area of Kimje, South Korea. Hydrological Processes 19:1261–1276. https://doi.org/10.1002/hyp.5565.

Kim, K., and Jeong, G. Y. 2005. Factors influencing natural occurrence of fluoride-rich groundwaters: a case study in the southeastern part of the Korean Peninsula. Chemosphere 58:1399–1408. https://doi.org/10.1016/j.chemosphere.2004.10.002.

Kimambo, V., Bhattacharya, P., Mtalo, F., Mtamba, J., and Ahmad, A. 2019. Fluoride occurrence in groundwater systems at global scale and status of defluoridation – State of the art. Groundwater for Sustainable Development 9:100223. https://doi.org/10.1016/j.gsd.2019.100223.

Klut, M. E., Bisalputra, T., and Antia, N. J. 1981. Abnormal Ultrastructural Features of a Marine Dinoflagellate Adapted to Grow Successfully in the Presence of Inhibitory Fluoride Concentration 1. The Journal of Protozoology 28:406–414. https://doi.org/10.1111/j.1550-7408.1981.tb05311.x.

Kohonen, T. 2013. Essentials of the self-organizing map. Neural Networks 37:52–65. https://doi.org/10.1016/j.neunet.2012.09.018.

Kosheleva, R. I., Mitropoulos, A. C., and Kyzas, G. Z. 2019. Synthesis of activated carbon from food waste. Environ Chem Lett 17:429–438. https://doi.org/10.1007/s10311-018-0817-5.

Kouser, B., Bala, A., Verma, O., Prashanth, M., Khosla, A., and Pir, R. A. 2022. Hydrochemistry for the assessment of groundwater quality in the Kathua region, Jammu and Kashmir, India. Appl Water Sci 12:143. https://doi.org/10.1007/s13201-022-01673-9.

Krishan, G., Rao, M. S., Kumar, C. P., Kumar, S., Loyal, R. S., Gill, G. S., and Semwal, P. 2017. Assessment of Salinity and Fluoride in Groundwater of Semi-Arid Region of Punjab, India. Curr. World Environ 12:34–41. https://doi.org/10.12944/CWE.12.1.05.

Krishnakumari, B., Abhishek, V. M., Puneeth, T., Vignesh, S., Irfan, M. M., and Poonamallee, C. 2018. Removal of iron and manganese from ground water. International Journal of Engineering Research & Technology 6:1–4.

Kumar, M., Chaminda, T., Honda, R., and Furumai, H. 2019. Vulnerability of urban waters to emerging contaminants in India and Sri Lanka: Resilience framework and strategy. APN SCI BULL 9. https://doi.org/10.30852/sb.2019.799.

Kumar, P. S., Kirthika, K., and Kumar, K. S. 2008. Removal of Hexavalent Chromium Ions from Aqueous Solutions by an Anion-Exchange Resin. Adsorption Science & Technology 26:693–703. https://doi.org/10.1260/026361708788251402.

Kumar, R., Sharma, P., Sharma, P. K., Rose, P. K., Singh, R. K., Kumar, N., Sahoo, P. K., Maity, J. P., Ghosh, A., Kumar, M., Bhattacharya, P., and Pandey, A. 2023. Rice husk biochar - A novel engineered bio-based material for transforming groundwater-mediated fluoride cycling in natural environments. Journal of Environmental Management 343:118222. https://doi.org/10.1016/j.jenvman.2023.118222.

Kumar, S., and Singh, M. 2015. Effect of fluoride contaminated irrigation water on eco-physiology, biomass and yield in Gossypium hirsutum L. Trop Plant Res 2:134–142.

Kumar, S., Gupta, A., and Yadav, J. 2007. Fluoride removal by mixtures of activated carbon prepared from Neem (Azadirachta indica) and Kikar (Acacia arabica) leaves. .

Lacson, C. F. Z., Lu, M.-C., and Huang, Y.-H. 2021. Fluoride-containing water: A global perspective and a pursuit to sustainable water defluoridation management -An overview. Journal of Cleaner Production 280:124236. https://doi.org/10.1016/j.jclepro.2020.124236.

Lagergren, S. 1898. About the theory of so-called adsorption of soluble substances. .

Lall, U., Josset, L., and Russo, T. 2020. A Snapshot of the World's Groundwater Challenges. Annu. Rev. Environ. Resour. 45:171–194. https://doi.org/10.1146/annurev-environ-102017-025800.

Langmuir, I. 1918. The adsorption of gases on plane surfaces of glass, mica and platinum. Journal of the American Chemical society 40:1361–1403.

Lebioda, L., Zhang, E., Lewinski, K., and Brewer, J. M. 1993. Fluoride inhibition of yeast enolase: Crystal structure of the enolase–Mg 2+ –F − –P i complex at 2.6 Å resolution. Proteins 16:219–225. https://doi.org/10.1002/prot.340160302.

Lee, E., Rout, P. R., and Bae, J. 2021. The applicability of anaerobically treated domestic wastewater as a nutrient medium in hydroponic lettuce cultivation: Nitrogen toxicity and health risk assessment. Science of The Total Environment 780:146482. https://doi.org/10.1016/j.scitotenv.2021.146482.

Lee, Y., Lee, S. W., Tsang, Y. F., Kim, Y. T., and Lee, J. 2020. Engineered rice-straw biochar catalysts for the production of value-added chemicals from furan. Chemical Engineering Journal 387:124194. https://doi.org/10.1016/j.cej.2020.124194.

Li, S., Smith, K. D., Davis, J. H., Gordon, P. B., Breaker, R. R., and Strobel, S. A. 2013. Eukaryotic resistance to fluoride toxicity mediated by a widespread family of fluoride export proteins. Proc. Natl. Acad. Sci. U.S.A. 110:19018–19023. https://doi.org/10.1073/pnas.1310439110.

Li, Y., Pei, G., Qiao, X., Zhu, Y., and Li, H. 2018. Remediation of cadmium contaminated water and soil using vinegar residue biochar. Environ Sci Pollut Res 25:15754–15764. https://doi.org/10.1007/s11356-018-1762-3.

Lim, P. N., Wu, T. Y., Shyang Sim, E. Y., and Lim, S. L. 2011. The potential reuse of soybean husk as feedstock of Eudrilus eugeniae in vermicomposting. J Sci Food Agric 91:2637–2642. https://doi.org/10.1002/jsfa.4504.

Ling, L.-L., Liu, W.-J., Zhang, S., and Jiang, H. 2017. Magnesium Oxide Embedded Nitrogen Self-Doped Biochar Composites: Fast and High-Efficiency Adsorption of Heavy Metals in an Aqueous Solution. Environ. Sci. Technol. 51:10081–10089. https://doi.org/10.1021/acs.est.7b02382.

Liu, H., Liu, Y., Tang, L., Wang, J., Yu, J., Zhang, H., Yu, M., Zou, J., and Xie, Q. 2020. Egg shell biochar-based green catalysts for the removal of organic pollutants by activating persulfate. Science of The Total Environment 745:141095. https://doi.org/10.1016/j.scitotenv.2020.141095.

Liu, J., Ma, Y., Gao, Z., Zhang, Y., Sun, Z., Sun, T., Fan, H., Wu, B., Li, M., and Qian, L. 2022. Fluoride contamination, spatial variation, and health risk assessment of groundwater using GIS: a high-density survey sampling in Weifang City, North

China. Environ Sci Pollut Res 29:34302–34313. https://doi.org/10.1007/s11356-021-18443-w.

Liu, Y., and Zhu, W. H. 1991. Environmental characteristics of regional groundwater in relation to fluoride poisoning in North China. Environ. Geol. Water Sci 18:3–10. https://doi.org/10.1007/BF01704572.

Lopez, A. M., Wells, A., and Fendorf, S. 2021. Soil and Aquifer Properties Combine as Predictors of Groundwater Uranium Concentrations within the Central Valley, California. Environ. Sci. Technol. 55:352–361. https://doi.org/10.1021/acs.est.0c05591.

Lou, Z., Xing, S., Xiao, X., Shan, W., Xiong, Y., and Fan, Y. 2018. Selective adsorption of Re(VII) by chitosan modified with imidazolium-based ionic liquid. Hydrometallurgy 179:141–148. https://doi.org/10.1016/j.hydromet.2018.05.025.

Lu, J., Fu, Z., and Yin, Z. 2008. Performance of a water hyacinth (Eichhornia crassipes) system in the treatment of wastewater from a duck farm and the effects of using water hyacinth as duck feed. Journal of Environmental Sciences 20:513–519. https://doi.org/10.1016/S1001-0742(08)62088-4.

Lu, L., Shan, R., Shi, Y., Wang, S., and Yuan, H. 2019. A novel TiO2/biochar composite catalysts for photocatalytic degradation of methyl orange. Chemosphere 222:391–398. https://doi.org/10.1016/j.chemosphere.2019.01.132.

Madhnure, P., Sirsikar, D., Tiwari, A., Ranjan, B., and Malpe, D. 2007. Occurrence of fluoride in the groundwaters of Pandharkawada area, Yavatmal district, Maharashtra, India. Current Science 675–679.

Madima, N., Mishra, S. B., Inamuddin, I., and Mishra, A. K. 2020. Carbon-based nanomaterials for remediation of organic and inorganic pollutants from wastewater. A review. Environ Chem Lett 18:1169–1191. https://doi.org/10.1007/s10311-020-01001-0.

Magalong, J. R., DelaCruz, J., Bumatay, J., Deocaris, C., and Deocaris, M. C. 2022. Package 'PUPAK.'.

Maithani, P., Gurjar, R., Banerjee, R., Balaji, B., Ramachandran, S., and Singh, R. 1998. Anomalous fluoride in groundwater from western part of Sirohi district, Rajasthan and its crippling effects on human health. Current Science 773–777.

Malik, A. 2007. Environmental challenge vis a vis opportunity: The case of water hyacinth. Environment International 33:122–138. https://doi.org/10.1016/j.envint.2006.08.004.

Malik, L. A., Bashir, A., Qureashi, A., and Pandith, A. H. 2019. Detection and removal of heavy metal ions: a review. Environ Chem Lett 17:1495–1521. https://doi.org/10.1007/s10311-019-00891-z.

Mandal, J., Jain, V., Sengupta, S., Rahman, Md. A., Bhattacharyya, K., Rahman, M. M., Golui, D., Wood, M. D., and Mondal, D. 2023. Determination of bioavailable arsenic threshold and validation of modeled permissible total arsenic in paddy soil using machine learning. J of Env Quality 52:315–327. https://doi.org/10.1002/jeq2.20452.

Mandal, R., Das, A., Sudheer, A. K., Kumar, S., Verma, S., Gaddam, M., and Deshpande, R. D. 2021. Sources, controls, and probabilistic health risk assessment of fluoride contamination in groundwater from a semi-arid region in Gujarat, Western India: An isotope–hydrogeochemical perspective. Environ Geochem Health 43:4043–4059. https://doi.org/10.1007/s10653-021-00894-2.

Mapoma, H. W. T., Xie, X., Liu, Y., Zhu, Y., Kawaye, F. P., and Kayira, T. M. 2017. Hydrochemistry and quality of groundwater in alluvial aquifer of Karonga, Malawi. Environ Earth Sci 76:335. https://doi.org/10.1007/s12665-017-6653-2.

Maroušek, J., Kolář, L., Strunecký, O., Kopecký, M., Bartoš, P., Maroušková, A., Cudlínová, E., Konvalina, P., Šoch, M., Moudrý (Jr), J., Vaníčková, R., and Vrbka, J. 2020. Modified biochars present an economic challenge to phosphate management in wastewater treatment plants. Journal of Cleaner Production 272:123015. https://doi.org/10.1016/j.jclepro.2020.123015.

Maurya, J., Pradhan, S. N., Seema, and Ghosh, A. K. 2020. Evaluation of ground water quality and health risk assessment due to nitrate and fluoride in the Middle Indo-Gangetic plains of India. Human and Ecological Risk Assessment: An International Journal 27:1349–1365. https://doi.org/10.1080/10807039.2020.1844559.

McQuaker, N. R., and Gurney, M. 1977. Determination of total fluoride in soil and vegetation using an alkali fusion-selective ion electrode technique. Analytical Chemistry 49:53–56.

Medina-Sauza, R. M., Álvarez-Jiménez, M., Delhal, A., Reverchon, F., Blouin, M., Guerrero-Analco, J. A., Cerdán, C. R., Guevara, R., Villain, L., and Barois, I. 2019. Earthworms

Building Up Soil Microbiota, a Review. Front. Environ. Sci. 7:81. https://doi.org/10.3389/fenvs.2019.00081.

Meenakshi, and Maheshwari, R. C. 2006. Fluoride in drinking water and its removal. Journal of Hazardous Materials 137:456–463. https://doi.org/10.1016/j.jhazmat.2006.02.024.

Mezghani, I., Elloumi, N., Abdallah, F. B., Chaieb, M., and Boukhris, M. 2005. Fluoride accumulation by vegetation in the vicinity of a phosphate fertilizer plant in Tunisia. Fluoride 38:69–75.

Mishra, S., Das, M., and Dash, U. 2010. Review on adverse effects of water contaminants like arsenic, fluoride and phosphate and their remediation.

Mohan, D., Kumar, S., and Srivastava, A. 2014. Fluoride removal from ground water using magnetic and nonmagnetic corn stover biochars. Ecological Engineering 73:798–808. https://doi.org/10.1016/j.ecoleng.2014.08.017.

Mohan, D., Sharma, R., Singh, V. K., Steele, P., and Pittman, C. U. 2012. Fluoride Removal from Water using Bio-Char, a Green Waste, Low-Cost Adsorbent: Equilibrium Uptake and Sorption Dynamics Modeling. Ind. Eng. Chem. Res. 51:900–914. https://doi.org/10.1021/ie202189v.

Mohapatra, S., Padhye, L. P., and Mukherji, S. 2018. Challenges in Detection of Antibiotics in Wastewater Matrix. In Environmental Contaminants, Energy, Environment, and Sustainability, eds. Tarun Gupta, Avinash Kumar Agarwal, Rashmi Avinash Agarwal, and Nitin K. Labhsetwar. Singapore: Springer Singapore, pp. 3–20. https://doi.org/10.1007/978-981-10-7332-8_1.

Moirana, R. L., Mkunda, J., Perez, M. P., Machunda, R., and Mtei, K. 2021. The influence of fertilizers on the behavior of fluoride fractions in the alkaline soil. Journal of Fluorine Chemistry 250:109883. https://doi.org/10.1016/j.jfluchem.2021.109883.

Moller, P. F., and Gudjonsson, S. V. 1932. Massive Fluorosis of Bones and Ligaments. Acta Radiologica Original Series, Volume 13:269–294. https://doi.org/10.1177/028418513201300309.

Mondal, N. K., Bhaumik, R., Banerjee, A., Datta, J. K., and Baur, T. 2012. A comparative study on the batch performance of fluoride adsorption by activated silica gel and activated rice husk ash. International Journal of Environmental Sciences 2:1643–1661.

Mondal, N. K., Kundu, M., Das, K., Bhaumik, R., and Datta, J. K. 2013. Biosorption of fluoride from aqueous phase onto Aspergillus and its calcium-impregnated biomass and evaluation of adsorption kinetics. Fluoride 46:239–245.

Mondal, S., Khan, M. R., and Mukherjee, A. 2020. Spatial distribution and risk area assessment of Aphelenchoides besseyi using geostatistical approaches in Giridih district of Jharkhand, India. Journal of Nematology 52:1–16. https://doi.org/10.21307/jofnem-2020-033.

More, S., Dhakate, R., Ratnalu, G. V., and Machender, G. 2021. Hydrogeochemistry and Health Risk Assessment of groundwater and surface water in fluoride affected area of Yadadri-Bhuvanagiri District, Telangana State, India. Environ Earth Sci 80:262. https://doi.org/10.1007/s12665-021-09544-3.

Mridha, D., Priyadarshni, P., Bhaskar, K., Gaurav, A., De, A., Das, A., Joardar, M., Chowdhury, N. R., and Roychowdhury, T. 2021. Fluoride exposure and its potential health risk assessment in drinking water and staple food in the population from fluoride endemic regions of Bihar, India. Groundwater for Sustainable Development 13:100558. https://doi.org/10.1016/j.gsd.2021.100558.

Mudhoo, A., Gautam, R. K., Ncibi, M. C., Zhao, F., Garg, V. K., and Sillanpää, M. 2019. Green synthesis, activation and functionalization of adsorbents for dye sequestration. Environ Chem Lett 17:157–193. https://doi.org/10.1007/s10311-018-0784-x.

Mukate, S., Bhoominathan, S., and Solanky, V. 2022. Assessment of human health risk arising due to fluoride and nitrate in groundwater: a case study of Bhokardan tehsil of Maharashtra. Human and Ecological Risk Assessment: An International Journal 28:594–620. https://doi.org/10.1080/10807039.2022.2081837.

Mukherjee, I., and Singh, U. K. 2021. Characterization of groundwater nitrate exposure using Monte Carlo and Sobol sensitivity approaches in the diverse aquifer systems of an agricultural semiarid region of Lower Ganga Basin, India. Science of The Total Environment 787:147657. https://doi.org/10.1016/j.scitotenv.2021.147657.

Mukherjee, I., and Singh, U. K. 2022. Exploring a variance decomposition approach integrated with the Monte Carlo method to evaluate groundwater fluoride exposure on the residents of a typical fluorosis endemic semi-arid tract of India. Environmental Research 203:111697. https://doi.org/10.1016/j.envres.2021.111697.

Mukome, F. N. D., Buelow, M. C., Shang, J., Peng, J., Rodriguez, M., Mackay, D. M., Pignatello, J. J., Sihota, N., Hoelen, T. P., and Parikh, S. J. 2020. Biochar amendment as a remediation strategy for surface soils impacted by crude oil. Environmental Pollution 265:115006. https://doi.org/10.1016/j.envpol.2020.115006.

Nafouanti, M. B., Li, J., Mustapha, N. A., Uwamungu, P., and AL-Alimi, D. 2021. Prediction on the fluoride contamination in groundwater at the Datong Basin, Northern China: Comparison of random forest, logistic regression and artificial neural network. Applied Geochemistry 132:105054. https://doi.org/10.1016/j.apgeochem.2021.105054.

Naik, M. R., Barik, M., Jha, V., Sahoo, S. K., and Sahoo, N. K. 2021. Spatial distribution and probabilistic health risk assessment of fluoride in groundwater of Angul district, Odisha, India. Groundwater for Sustainable Development 14:100604. https://doi.org/10.1016/j.gsd.2021.100604.

Nandi, R., Mondal, S., Mandal, J., and Bhattacharyya, P. 2024a. Deciphering geochemical fingerprints and health implications of groundwater fluoride contamination in mica mining regions using machine learning tactics. Environ Geochem Health 46:400. https://doi.org/10.1007/s10653-024-02177-y.

Nandi, R., Mondal, S., Mandal, J., and Bhattacharyya, P. 2024b. From fuzzy-TOPSIS to machine learning: A holistic approach to understanding groundwater fluoride contamination. Science of The Total Environment 912:169323. https://doi.org/10.1016/j.scitotenv.2023.169323.

Nannipieri, P., Ascher, J., Ceccherini, M. T., Landi, L., Pietramellara, G., and Renella, G. 2003. Microbial diversity and soil functions. European J Soil Science 54:655–670. https://doi.org/10.1046/j.1351-0754.2003.0556.x.

Nannipieri, P., Gregos, S., Ceccanti, B., 1990. Ecological significance of the biological activity insoil.In: Smith,J.L., Paul, E.A.(Eds.), SoilBiochemistry, 6.Marcel Dekker, New York, NY, pp. 293–354

Nawaz, T., and Sengupta, S. 2019. Contaminants of Emerging Concern: Occurrence, Fate, and Remediation. In Advances in Water Purification Techniques, Elsevier, pp. 67–114. https://doi.org/10.1016/B978-0-12-814790-0.00004-1.

Niculescu-Mizil, A., and Caruana, R. 2005. Obtaining Calibrated Probabilities from Boosting. In , pp. 413–20.

Nizam, S., Virk, H. S., and Sen, I. S. 2022. High levels of fluoride in groundwater from Northern parts of Indo-Gangetic plains reveals detrimental fluorosis health risks. Environmental Advances 8:100200. https://doi.org/10.1016/j.envadv.2022.100200.

Olaka, L. A., Wilke, F. D. H., Olago, D. O., Odada, E. O., Mulch, A., and Musolff, A. 2016. Groundwater fluoride enrichment in an active rift setting: Central Kenya Rift case study. Science of The Total Environment 545–546:641–653. https://doi.org/10.1016/j.scitotenv.2015.11.161.

Onipe, T., Edokpayi, J. N., and Odiyo, J. O. 2021. Geochemical characterization and assessment of fluoride sources in groundwater of Siloam area, Limpopo Province, South Africa. Sci Rep 11:14000. https://doi.org/10.1038/s41598-021-93385-4.

Ostan, K. T., Manlapaz, P. A. C., Mesias, J. C. L., Deocaris, C. C., and Deocaris, M. C. C. 2022. Package 'PUPAIM.' Langmuir 8.

Page, A. L. 1982. Methods of soil analysis: chemical and microbiological properties. American Society of Agronomy.

Page, A. L., Miller, R. H., and Keenedy, D. R. 1982. Chemical and microbiological properties. In Methods of soil analysis, Madison, WI, USA: American Society of Agronomy.

Paixão, G. R., Camparotto, N. G., Brião, G. D. V., Oliveira, R. D. L., Colmenares, J. C., Prediger, P., and Vieira, M. G. A. 2022. Synthesis of mesoporous P-doped carbon and its application in propranolol drug removal: Characterization, kinetics and isothermal studies. Chemical Engineering Research and Design 187:225–239. https://doi.org/10.1016/j.cherd.2022.09.009.

Pal, K. C., Mondal, N. K., Bhaumik, R., Banerjee, A., and Datta, J. K. 2012. Incorporation of fluoride in vegetation and associated biochemical changes due to fluoride contamination in water and soil: a comparative field study. Annals of Environmental Science 6.

Panaskar, D. B., Wagh, V. M., Muley, A. A., Mukate, S. V., Pawar, R. S., and Aamalawar, M. L. 2016. Evaluating groundwater suitability for the domestic, irrigation, and industrial

purposes in Nanded Tehsil, Maharashtra, India, using GIS and statistics. Arab J Geosci 9:615. https://doi.org/10.1007/s12517-016-2641-1.

Patolia, P., and Sinha, A. 2017. Fluoride contamination in Gharbar Village of Dhanbad District, Jharkhand, India: source identification and management. Arab J Geosci 10:381. https://doi.org/10.1007/s12517-017-3164-0.

Paul, S., Das, S., Raul, P., and Bhattacharya, S. S. 2018. Vermi-sanitization of toxic silk industry waste employing Eisenia fetida and Eudrilus eugeniae: Substrate compatibility, nutrient enrichment and metal accumulation dynamics. Bioresource Technology 266:267–274. https://doi.org/10.1016/j.biortech.2018.06.092.

Paul, S., Goswami, L., Pegu, R., and Sundar Bhattacharya, S. 2020. Vermiremediation of cotton textile sludge by Eudrilus eugeniae: Insight into metal budgeting, chromium speciation, and humic substance interactions. Bioresource Technology 314:123753. https://doi.org/10.1016/j.biortech.2020.123753.

Peter, S., Le Provost, G., Mehring, M., Müller, T., and Manning, P. 2022. Cultural worldviews consistently explain bundles of ecosystem service prioritisation across rural Germany. People and Nature 4:218–230. https://doi.org/10.1002/pan3.10277.

Piearce, T. G., Oates, K., and Carruthers, W. J. 1990. A fossil earthworm embryo (Oligochaeta) from beneath a Late Bronze Age midden at Potterne, Wiltshire, UK. Journal of Zoology 220:537–542. https://doi.org/10.1111/j.1469-7998.1990.tb04732.x.

Pillai, K. S., and Stanley, V. A. 2002. Implications of fluoride--an endless uncertainty. J Environ Biol 23:81–87.

Plaimart, J., Acharya, K., Mrozik, W., Davenport, R. J., Vinitnantharat, S., and Werner, D. 2021. Coconut husk biochar amendment enhances nutrient retention by suppressing nitrification in agricultural soil following anaerobic digestate application. Environmental Pollution 268:115684. https://doi.org/10.1016/j.envpol.2020.115684.

Plaza, C., Nogales, R., Senesi, N., Benitez, E., and Polo, A. 2008. Organic matter humification by vermicomposting of cattle manure alone and mixed with two-phase olive pomace. Bioresource Technology 99:5085–5089. https://doi.org/10.1016/j.biortech.2007.09.079.

Podgorski, J., and Berg, M. 2022. Global analysis and prediction of fluoride in groundwater. Nat Commun 13:4232. https://doi.org/10.1038/s41467-022-31940-x.

Pontié, M., Dach, H., and Leparc, J. 2008. Nanofiltration as a sustainable water defluoridation operation dedicated to large scale pilot plants for the future. In , p. 4.

Pradhan, B., Chand, S., Chand, S., Rout, P. R., and Naik, S. K. 2023. Emerging groundwater contaminants: A comprehensive review on their health hazards and remediation technologies. Groundwater for Sustainable Development 20:100868. https://doi.org/10.1016/j.gsd.2022.100868.

Prasad, Y. S., and Rao, B. V. 2018. Monitoring and assessment of groundwater quality in a khondalitic terrain, Andhra Pradesh, India. Environ Monit Assess 190:426. https://doi.org/10.1007/s10661-018-6757-5.

Priyadarshini, A., Sahoo, M. M., Raut, P. R., Mahanty, B., and Sahoo, N. K. 2021. Kinetic modelling and process engineering of phenolics microbial and enzymatic biodegradation: A current outlook and challenges. Journal of Water Process Engineering 44:102421. https://doi.org/10.1016/j.jwpe.2021.102421.

Qasemi, M., Afsharnia, M., Farhang, M., Ghaderpoori, M., Karimi, A., Abbasi, H., and Zarei, A. 2019. Spatial distribution of fluoride and nitrate in groundwater and its associated human health risk assessment in residents living in Western Khorasan Razavi, Iran. Desalination and Water Treatment 170:176–186. https://doi.org/10.5004/dwt.2019.24691.

Qin, H., Shao, X., Shaghaleh, H., Gao, W., and Hamoud, Y. A. 2023. Adsorption of Pb2+ and Cd2+ in Agricultural Water by Potassium Permanganate and Nitric Acid-Modified Coconut Shell Biochar. Agronomy 13:1813. https://doi.org/10.3390/agronomy13071813.

Radha, K., Kalaivani, K., and Lavanya, R. 2009. A case study of biomedical waste management in hospitals. Global journal of health science 1:82–88.

Rahman, A. A., and Ravenscroft, P. 2003. Groundwater resources and development in Bangladesh. University ress.

Raj, D., and Shaji, E. 2017. Fluoride contamination in groundwater resources of Alleppey, southern India. Geoscience Frontiers 8:117–124. https://doi.org/10.1016/j.gsf.2016.01.002.

Rajor, A., Xaxa, M., Mehta, R., and Kunal. 2012. An overview on characterization, utilization and leachate analysis of biomedical waste incinerator ash. Journal of Environmental Management 108:36–41. https://doi.org/10.1016/j.jenvman.2012.04.031.

Ramdani, A., Kadeche, A., Adjdir, M., Taleb, Z., Ikhou, D., Taleb, S., and Deratani, A. 2020. Lead and cadmium removal by adsorption process using hydroxyapatite porous materials. Water Practice and Technology 15:130–141. https://doi.org/10.2166/wpt.2020.003.

Ranjbar, E., Ghiassi, R., and Akbary, Z. 2017. Lead removal from groundwater by granular mixtures of pumice, perlite and lime using permeable reactive barriers. Water & Environment J 31:39–46. https://doi.org/10.1111/wej.12223.

Rao, K. N., and Latha, P. S. 2019. Groundwater quality assessment using water quality index with a special focus on vulnerable tribal region of Eastern Ghats hard rock terrain, Southern India. Arab J Geosci 12:267. https://doi.org/10.1007/s12517-019-4440-y.

Rao, N. S., Dinakar, A., and Kumari, B. K. 2021. Appraisal of vulnerable zones of non-cancer-causing health risks associated with exposure of nitrate and fluoride in groundwater from a rural part of India. Environmental Research 202:111674. https://doi.org/10.1016/j.envres.2021.111674.

Rao, N. S., Rao, P. S., Dinakar, A., Rao, P. V. N., and Marghade, D. 2017. Fluoride occurrence in the groundwater in a coastal region of Andhra Pradesh, India. Appl Water Sci 7:1467–1478. https://doi.org/10.1007/s13201-015-0338-3.

Rashid, A., Farooqi, A., Gao, X., Zahir, S., Noor, S., and Khattak, J. A. 2020. Geochemical modeling, source apportionment, health risk exposure and control of higher fluoride in groundwater of sub-district Dargai, Pakistan. Chemosphere 243:125409. https://doi.org/10.1016/j.chemosphere.2019.125409.

Rasool, A., Farooqi, A., Xiao, T., Ali, W., Noor, S., Abiola, O., Ali, S., and Nasim, W. 2018. A review of global outlook on fluoride contamination in groundwater with prominence on the Pakistan current situation. Environ Geochem Health 40:1265–1281. https://doi.org/10.1007/s10653-017-0054-z.

Rasoulzadeh, H., Dehghani, M. H., Mohammadi, A. S., Karri, R. R., Nabizadeh, R., Nazmara, S., Kim, K.-H., and Sahu, J. N. 2020. Parametric modelling of Pb(II) adsorption onto chitosan-coated Fe3O4 particles through RSM and DE hybrid

evolutionary optimization framework. Journal of Molecular Liquids 297:111893. https://doi.org/10.1016/j.molliq.2019.111893.

Ravindra, B., Subba Rao, N., and Dhanamjaya Rao, E. N. 2023. Groundwater quality monitoring for assessment of pollution levels and potability using WPI and WQI methods from a part of Guntur district, Andhra Pradesh, India. Environ Dev Sustain 25:14785–14815. https://doi.org/10.1007/s10668-022-02689-6.

Rawat, K. S., Singh, S. K., and Gautam, S. K. 2018. Assessment of groundwater quality for irrigation use: a peninsular case study. Appl Water Sci 8:233. https://doi.org/10.1007/s13201-018-0866-8.

Refat Nasher, N. M., and Humayan Ahmed, Md. 2021. Groundwater geochemistry and hydrogeochemical processes in the Lower Ganges-Brahmaputra-Meghna River Basin areas, Bangladesh. Journal of Asian Earth Sciences: X 6:100062. https://doi.org/10.1016/j.jaesx.2021.100062.

Rezania, S., Ponraj, M., Talaiekhozani, A., Mohamad, S. E., Md Din, M. F., Taib, S. M., Sabbagh, F., and Sairan, F. M. 2015. Perspectives of phytoremediation using water hyacinth for removal of heavy metals, organic and inorganic pollutants in wastewater. Journal of Environmental Management 163:125–133. https://doi.org/10.1016/j.jenvman.2015.08.018.

Roberts, S. K. 2006. Plasma membrane anion channels in higher plants and their putative functions in roots. New Phytologist 169:647–666. https://doi.org/10.1111/j.1469-8137.2006.01639.x.

Robinson, W. O., and Edgington, G. 1946. Fluorine in soils: Soil Science 61:341–354. https://doi.org/10.1097/00010694-194605000-00001.

Rout, P. R., Bhunia, P., and Dash, R. R. 2014. Modeling isotherms, kinetics and understanding the mechanism of phosphate adsorption onto a solid waste: Ground burnt patties. Journal of Environmental Chemical Engineering 2:1331–1342. https://doi.org/10.1016/j.jece.2014.04.017.

Rout, P. R., Bhunia, P., and Dash, R. R. 2017a. Assessing Possible Applications of Waste Organic Solid Substances as Carbon Sources and Biofilm Substrates for Elimination of Nitrate Toxicity from Wastewater. J. Hazard. Toxic Radioact. Waste 21:04016027. https://doi.org/10.1061/(ASCE)HZ.2153-5515.0000350.

Rout, P. R., Bhunia, P., and Dash, R. R. 2017b. Evaluation of kinetic and statistical models for predicting breakthrough curves of phosphate removal using dolochar-packed columns. Journal of Water Process Engineering 17:168–180. https://doi.org/10.1016/j.jwpe.2017.04.003.

Rout, P. R., Dash, R. R., and Bhunia, P. 2016. Nutrient removal from binary aqueous phase by dolochar: Highlighting optimization, single and binary adsorption isotherms and nutrient release. Process Safety and Environmental Protection 100:91–107. https://doi.org/10.1016/j.psep.2016.01.001.

Rout, P. R., Shahid, M. K., Dash, R. R., Bhunia, P., Liu, D., Varjani, S., Zhang, T. C., and Surampalli, R. Y. 2021. Nutrient removal from domestic wastewater: A comprehensive review on conventional and advanced technologies. Journal of Environmental Management 296:113246. https://doi.org/10.1016/j.jenvman.2021.113246.

Routroy, S., Harichandan, R., Mohanty, J. K., and Panda, C. R. 2013. A Statistical appraisal to hydrogeochemistry of fluoride contaminated ground water in Nayagarh district, Odisha. J Geol Soc India 81:350–360. https://doi.org/10.1007/s12594-013-0045-3.

Roy, S., Sengupta, S., Manna, S., and Das, P. 2018. Chemically reduced tea waste biochar and its application in treatment of fluoride containing wastewater: Batch and optimization using response surface methodology. Process Safety and Environmental Protection 116:553–563. https://doi.org/10.1016/j.psep.2018.03.009.

Sadhu, M., Bhattacharya, P., Vithanage, M., and Padmaja Sudhakar, P. 2021. Adsorptive removal of fluoride using biochar – A potential application in drinking water treatment. Separation and Purification Technology 278:119106. https://doi.org/10.1016/j.seppur.2021.119106.

Sahariah, B., Goswami, L., Farooqui, I. U., Raul, P., Bhattacharyya, P., and Bhattacharya, S. 2015. Solubility, hydrogeochemical impact, and health assessment of toxic metals in municipal wastes of two differently populated cities. Journal of Geochemical Exploration 157:100–109. https://doi.org/10.1016/j.gexplo.2015.06.003.

Sahariah, B., Sinha, I., Sharma, P., Goswami, L., Bhattacharyya, P., Gogoi, N., and Bhattacharya, S. S. 2014. Efficacy of bioconversion of paper mill bamboo sludge and lime waste by composting and vermiconversion technologies. Chemosphere 109:77–83. https://doi.org/10.1016/j.chemosphere.2014.02.063.

Sahoo, P. K., Ray, S. B., Kerketta, A., Behera, P., Neogi, G., and Sahoo, H. B. 2022. Geogenic enrichment of fluoride in groundwater of hard rock aquifer in fluorosis prevalent area of Balangir district, Odisha, India. Groundwater for Sustainable Development 19:100830. https://doi.org/10.1016/j.gsd.2022.100830.

Sahoo, T. R., and Prelot, B. 2020. Adsorption processes for the removal of contaminants from wastewater. In Nanomaterials for the Detection and Removal of Wastewater Pollutants, Elsevier, pp. 161–222. https://doi.org/10.1016/B978-0-12-818489-9.00007-4.

Sahu, B. L., Banjare, G. R., Ramteke, S., Patel, K. S., and Matini, L. 2017. Fluoride Contamination of Groundwater and Toxicities in Dongargaon Block, Chhattisgarh, India. Expo Health 9:143–156. https://doi.org/10.1007/s12403-016-0229-3.

Samadder, S. R., Prabhakar, R., Khan, D., Kishan, D., and Chauhan, M. S. 2017. Analysis of the contaminants released from municipal solid waste landfill site: A case study. Science of The Total Environment 580:593–601. https://doi.org/10.1016/j.scitotenv.2016.12.003.

Santana, N. A., Ferreira, P. A. A., Tarouco, C. P., Schardong, I. S., Antoniolli, Z. I., Nicoloso, F. T., and Jacques, R. J. S. 2019. Earthworms and mycorrhization increase copper phytoextraction by Canavalia ensiformis in sandy soil. Ecotoxicology and Environmental Safety 182:109383. https://doi.org/10.1016/j.ecoenv.2019.109383.

Sarma, G. K., and Rashid, Md. H. 2018. Synthesis of Mg/Al Layered Double Hydroxides for Adsorptive Removal of Fluoride from Water: A Mechanistic and Kinetic Study. J. Chem. Eng. Data 63:2957–2965. https://doi.org/10.1021/acs.jced.8b00242.

Schn�rer, J., and Rosswall, T. 1982. Fluorescein Diacetate Hydrolysis as a Measure of Total Microbial Activity in Soil and Litter. Appl Environ Microbiol 43:1256–1261. https://doi.org/10.1128/aem.43.6.1256-1261.1982.

Shahid, M. K., Kashif, A., Rout, P. R., Aslam, M., Fuwad, A., Choi, Y., Banu J, R., Park, J. H., and Kumar, G. 2020. A brief review of anaerobic membrane bioreactors emphasizing recent advancements, fouling issues and future perspectives. Journal of Environmental Management 270:110909. https://doi.org/10.1016/j.jenvman.2020.110909.

Shaji, E., Bindu, Viju, J., and Thambi, D. 2007. High fluoride in groundwater of Palghat District, Kerala. Current Science 240–245.

Shaji, E., Sarath, K. V., Santosh, M., Krishnaprasad, P. K., Arya, B. K., and Babu, M. S. 2024. Fluoride contamination in groundwater: A global review of the status, processes, challenges, and remedial measures. Geoscience Frontiers 15:101734. https://doi.org/10.1016/j.gsf.2023.101734.

Sharma, K., and Garg, V. K. 2017. Management of food and vegetable processing waste spiked with buffalo waste using earthworms (Eisenia fetida). Environ Sci Pollut Res 24:7829–7836. https://doi.org/10.1007/s11356-017-8438-2.

Sharma, S., Pradhan, K., Satya, S., and Vasudevan, P. 2005. Potentiality of earthworms for waste management and in other uses–A review. The Journal of American Science 1:4–16.

Siciliano, A. 2016. Removal of Cr(VI) from Water Using a New Reactive Material: Magnesium Oxide Supported Nanoscale Zero-Valent Iron. Materials 9:666. https://doi.org/10.3390/ma9080666.

Singh, C. K., Rina, K., Singh, R. P., Shashtri, S., Kamal, V., and Mukherjee, S. 2011. Geochemical Modeling of High Fluoride Concentration in Groundwater of Pokhran Area of Rajasthan, India. Bull Environ Contam Toxicol 86:152–158. https://doi.org/10.1007/s00128-011-0192-4.

Singh, G., Kumari, B., Sinam, G., Kriti, Kumar, N., and Mallick, S. 2018. Fluoride distribution and contamination in the water, soil and plants continuum and its remedial technologies, an Indian perspective– a review. Environmental Pollution 239:95–108. https://doi.org/10.1016/j.envpol.2018.04.002.

Singh, G., Rishi, M. S., Herojeet, R., Kaur, L., Priyanka, and Sharma, K. 2020. Multivariate analysis and geochemical signatures of groundwater in the agricultural dominated taluks of Jalandhar district, Punjab, India. Journal of Geochemical Exploration 208:106395. https://doi.org/10.1016/j.gexplo.2019.106395.

Sinha, R. K., Chauhan, K., Valani, D., Chandran, V., Soni, B. K., and Patel, V. 2010. Earthworms: Charles Darwin's 'unheralded soldiers of mankind': protective & productive for man & environment. Journal of environmental protection 1:251.

Skórka-Majewicz, M., Goschorska, M., Żwierełło, W., Baranowska-Bosiacka, I., Styburski, D., Kapczuk, P., and Gutowska, I. 2020. Effect of fluoride on endocrine tissues and their secretory functions -- review. Chemosphere 260:127565. https://doi.org/10.1016/j.chemosphere.2020.127565.

Smith, L. A. 1995. Remedial options for metals-contaminated sites. (No Title).

Smolik, B., Telesiński, A., Szymczak, J., and Zakrzewska, H. 2011. Assessing of humus usefulness in limiting of soluble fluoride content in soil. Ochr Środ Zas Nat 49:202–208.

Sobol′, I. M. 2001. Global sensitivity indices for nonlinear mathematical models and their Monte Carlo estimates. Mathematics and Computers in Simulation 55:271–280. https://doi.org/10.1016/S0378-4754(00)00270-6.

Son, E.-B., Poo, K.-M., Chang, J.-S., and Chae, K.-J. 2018. Heavy metal removal from aqueous solutions using engineered magnetic biochars derived from waste marine macro-algal biomass. Science of The Total Environment 615:161–168. https://doi.org/10.1016/j.scitotenv.2017.09.171.

Sreedevi, P. D., Ahmed, S., Made, B., Ledoux, E., and Gandolfi, J. M. 2006. Association of hydrogeological factors in temporal variations of fluoride concentration in a crystalline aquifer in India. Environ Geol 50:1–11. https://doi.org/10.1007/s00254-005-0167-z.

Srivastava, S., and Flora, S. J. S. 2020. Fluoride in Drinking Water and Skeletal Fluorosis: a Review of the Global Impact. Curr Envir Health Rpt 7:140–146. https://doi.org/10.1007/s40572-020-00270-9.

Srivastava, V., De Araujo, A. S. F., Vaish, B., Bartelt-Hunt, S., Singh, P., and Singh, R. P. 2016. Biological response of using municipal solid waste compost in agriculture as fertilizer supplement. Rev Environ Sci Biotechnol 15:677–696. https://doi.org/10.1007/s11157-016-9407-9.

Stahl, W., and Sies, H. 1996. Lycopene: A Biologically Important Carotenoid for Humans? Archives of Biochemistry and Biophysics 336:1–9. https://doi.org/10.1006/abbi.1996.0525.

Stockbridge, R. B., Robertson, J. L., Kolmakova-Partensky, L., and Miller, C. 2013. A family of fluoride-specific ion channels with dual-topology architecture. eLife 2:e01084. https://doi.org/10.7554/eLife.01084.

Stürzenbaum, S. R., Höckner, M., Panneerselvam, A., Levitt, J., Bouillard, J.-S., Taniguchi, S., Dailey, L.-A., Khanbeigi, R. A., Rosca, E. V., Thanou, M., Suhling, K., Zayats, A. V., and Green, M. 2013. Biosynthesis of luminescent quantum dots in an earthworm. Nature Nanotech 8:57–60. https://doi.org/10.1038/nnano.2012.232.

Stürzenbaum, S. R., Kille, P., and Morgan, A. J. 1998. The identification, cloning and characterization of earthworm metallothionein. FEBS Letters 431:437–442. https://doi.org/10.1016/S0014-5793(98)00809-6.

Subba Rao, N., Marghade, D., Dinakar, A., Chandana, I., Sunitha, B., Ravindra, B., & Balaji, T. (2017). Geochemical characteristics and controlling factors of chemical composition of groundwater in a part of Guntur district, Andhra Pradesh, India. Environmental earth sciences, 76, 1-22. https://doi.org/10.1007/s12665-017-7093-8

Subramaniyan, A., Karthikeyan, B., and Lakshmanan, E. 2022. Geochemical evaluation of fluoride and groundwater quality for drinking and irrigation purposes in a weathered gneissic rock aquifer of southern penisular India. Environ Earth Sci 81:273. https://doi.org/10.1007/s12665-022-10395-9.

Suneetha, M., Sundar, B. S., and Ravindhranath, K. 2015. Removal of fluoride from polluted waters using active carbon derived from barks of Vitex negundo plant. J Anal Sci Technol 6:15. https://doi.org/10.1186/s40543-014-0042-1.

Suthar, S. 2007. Nutrient changes and biodynamics of epigeic earthworm Perionyx excavatus (Perrier) during recycling of some agriculture wastes. Bioresource Technology 98:1608–1614. https://doi.org/10.1016/j.biortech.2006.06.001.

Suthar, S., Garg, V. K., Jangir, S., Kaur, S., Goswami, N., and Singh, S. 2008. Fluoride contamination in drinking water in rural habitations of Northern Rajasthan, India. Environ Monit Assess 145:1–6. https://doi.org/10.1007/s10661-007-0011-x.

Tadda, M. A., Altaf, R., Gouda, M., Rout, P. R., Shitu, A., Ye, Z., Zhu, S., and Liu, D. 2021. Impact of Saddle-Chips biocarrier on treating mariculture wastewater by moving bed

biofilm reactor (MBBR): Mechanism and kinetic study. Journal of Environmental Chemical Engineering 9:106710. https://doi.org/10.1016/j.jece.2021.106710.

Tan, X., Liu, Y., Zeng, G., Wang, X., Hu, X., Gu, Y., and Yang, Z. 2015. Application of biochar for the removal of pollutants from aqueous solutions. Chemosphere 125:70–85. https://doi.org/10.1016/j.chemosphere.2014.12.058.

Tang, Y., Yu, L., Guan, A., Zhou, X., Wang, Z., Gou, Y., and Wang, J. 2017. Soil mineral nitrogen and yield-scaled soil N2O emissions lowered by reducing nitrogen application and intercropping with soybean for sweet maize production in southern China. Journal of Integrative Agriculture 16:2586–2596. https://doi.org/10.1016/S2095-3119(17)61672-1.

Temkin, M. 1940. Kinetics of ammonia synthesis on promoted iron catalysts. Acta physiochim. URSS 12:327–356.

Teng, Y., and Chen, W. 2019. Soil Microbiomes—a Promising Strategy for Contaminated Soil Remediation: A Review. Pedosphere 29:283–297. https://doi.org/10.1016/S1002-0160(18)60061-X.

Thapa, P., Aryal, K. K., Mehata, S., Vaidya, A., Jha, B. K., Dhimal, M., Pradhan, S., Dhakal, P., Pandit, A., Pandey, A. R., Bista, B., Pokhrel, A. U., and Karki, K. B. 2016. Oral hygiene practices and their socio-demographic correlates among Nepalese adult: evidence from non communicable diseases risk factors STEPS survey Nepal 2013. BMC Oral Health 16:105. https://doi.org/10.1186/s12903-016-0294-9.

Thapa, R., Gupta, S., Kaur, H., and Baski, R. 2019. Assessment of groundwater quality scenario in respect of fluoride and nitrate contamination in and around Gharbar village, Jharkhand, India. HydroResearch 2:60–68. https://doi.org/10.1016/j.hydres.2019.09.002.

Tognetti, C., Mazzarino, M. J., and Laos, F. 2007. Improving the quality of municipal organic waste compost. Bioresource Technology 98:1067–1076. https://doi.org/10.1016/j.biortech.2006.04.025.

Tran, N. H., Reinhard, M., and Gin, K. Y.-H. 2018. Occurrence and fate of emerging contaminants in municipal wastewater treatment plants from different geographical regions-a review. Water Research 133:182–207. https://doi.org/10.1016/j.watres.2017.12.029.

Tripathi, B. D., and Upadhyay, A. R. 2003. Dairy Effluent Polishing by Aquatic Macrophytes. Water, Air, and Soil Pollution 143:377–385. https://doi.org/10.1023/A:1022813125339.

Tripathy, S., Bhattacharyya, P., Mohapatra, R., Som, A., and Chowdhury, D. 2014. Influence of different fractions of heavy metals on microbial ecophysiological indicators and enzyme activities in century old municipal solid waste amended soil. Ecological Engineering 70:25–34. https://doi.org/10.1016/j.ecoleng.2014.04.013.

Umar, R., and Alam, F. 2012. Assessment of hydrogeochemical characteristics of groundwater in parts of Hindon–Yamuna interfluve region, Baghpat District, Western Uttar Pradesh. Environ Monit Assess 184:2321–2336. https://doi.org/10.1007/s10661-011-2120-9.

Vázquez-Vuelvas, O. F., Chávez-Camacho, F. A., Meza-Velázquez, J. A., Mendez-Merino, E., Ríos-Licea, M. M., and Contreras-Esquivel, J. C. 2020. A comparative FTIR study for supplemented agavin as functional food. Food Hydrocolloids 103:105642. https://doi.org/10.1016/j.foodhyd.2020.105642.

Vieira, R. H., and Volesky, B. 2000. Biosorption: a solution to pollution? International microbiology 3:17–24.

Vieira, W. T., De Farias, M. B., Spaolonzi, M. P., Da Silva, M. G. C., and Vieira, M. G. A. 2020. Removal of endocrine disruptors in waters by adsorption, membrane filtration and biodegradation. A review. Environ Chem Lett 18:1113–1143. https://doi.org/10.1007/s10311-020-01000-1.

Vithanage, M., and Bhattacharya, P. 2015. Fluoride in Drinking Water: Health Effects and Remediation. In CO2 Sequestration, Biofuels and Depollution, Environmental Chemistry for a Sustainable World, eds. Eric Lichtfouse, Jan Schwarzbauer, and Didier Robert. Cham: Springer International Publishing, pp. 105–151. https://doi.org/10.1007/978-3-319-11906-9_4.

Vorland, C. J., Stremke, E. R., Moorthi, R. N., and Hill Gallant, K. M. 2017. Effects of Excessive Dietary Phosphorus Intake on Bone Health. Curr Osteoporos Rep 15:473–482. https://doi.org/10.1007/s11914-017-0398-4.

Wagh, V., Mukate, S., Muley, A., Kadam, A., Panaskar, D., and Varade, A. 2020. Study of groundwater contamination and drinking suitability in basaltic terrain of Maharashtra,

India through PIG and multivariate statistical techniques. Journal of Water Supply: Research and Technology-Aqua 69:398–414. https://doi.org/10.2166/aqua.2020.108.

Walkley, A., and Black, I. A. 1934. An examination of the Degtjareff method for determining soil organic matter, and a proposed modification of the chromic acid titration method. Soil science 37:29–38.

Wan Mahari, W. A., Waiho, K., Azwar, E., Fazhan, H., Peng, W., Ishak, S. D., Tabatabaei, M., Yek, P. N. Y., Almomani, F., Aghbashlo, M., and Lam, S. S. 2022. A state-of-the-art review on producing engineered biochar from shellfish waste and its application in aquaculture wastewater treatment. Chemosphere 288:132559. https://doi.org/10.1016/j.chemosphere.2021.132559.

Wang, J., and Guo, X. 2023. Adsorption kinetics and isotherm models of heavy metals by various adsorbents: An overview. Critical Reviews in Environmental Science and Technology 53:1837–1865. https://doi.org/10.1080/10643389.2023.2221157.

Wang, M., Lan, X., Xu, X., Fang, Y., Singh, B. P., Sardans, J., Romero, E., Peñuelas, J., and Wang, W. 2020. Steel slag and biochar amendments decreased CO2 emissions by altering soil chemical properties and bacterial community structure over two-year in a subtropical paddy field. Science of The Total Environment 740:140403. https://doi.org/10.1016/j.scitotenv.2020.140403.

Wang, P., Verin, A. D., Birukova, A., Gilbert-McClain, L. I., Jacobs, K., and Garcia, J. G. N. 2001. Mechanisms of sodium fluoride-induced endothelial cell barrier dysfunction: role of MLC phosphorylation. American Journal of Physiology-Lung Cellular and Molecular Physiology 281:L1472–L1483. https://doi.org/10.1152/ajplung.2001.281.6.L1472.

Wang, Y.-Y., Lu, H.-H., Liu, Y.-X., and Yang, S.-M. 2016. Ammonium citrate-modified biochar: An adsorbent for La(III) ions from aqueous solution. Colloids and Surfaces A: Physicochemical and Engineering Aspects 509:550–563. https://doi.org/10.1016/j.colsurfa.2016.09.060.

Wickham, H. 2011. ggplot2. Wiley interdisciplinary reviews: computational statistics 3:180–185.

World Health Organisation. 2004. Guidelines for drinking water quality (Vol.1). World Health Organisation, Geneva.

World Health Organisation. 2011. Guidelines for drinking water quality. World Health Organisation, Geneva.

World Health Organization. 2020. Chromium in drinking-water. World Health Organization.

World Health Organization. 2021. A global overview of national regulations and standards for drinking-water quality.

Xiang, W., Zhang, X., Chen, J., Zou, W., He, F., Hu, X., Tsang, D. C. W., Ok, Y. S., and Gao, B. 2020. Biochar technology in wastewater treatment: A critical review. Chemosphere 252:126539. https://doi.org/10.1016/j.chemosphere.2020.126539.

Xie, X., Shi, J., Pi, K., Deng, Y., Yan, B., Tong, L., ... & Jiang, G. (2023). Groundwater quality and public health. Annual Review of Environment and Resources, *48*(1), 395-418.

Xu, Y., Bai, T., Yan, Y., Zhao, Y., Yuan, L., Pan, P., and Jiang, Z. 2020. Enhanced removal of hexavalent chromium by different acid-modified biochar derived from corn straw: behavior and mechanism. Water Science and Technology 81:2270–2280. https://doi.org/10.2166/wst.2020.290.

Yadav, A., and Garg, V. K. 2019. Biotransformation of bakery industry sludge into valuable product using vermicomposting. Bioresource Technology 274:512–517. https://doi.org/10.1016/j.biortech.2018.12.023.

Yakout, S. M. 2017. Physicochemical Characteristics of Biochar Produced from Rice Straw at Different Pyrolysis Temperature for Soil Amendment and Removal of Organics. Proc. Natl. Acad. Sci., India, Sect. A Phys. Sci. 87:207–214. https://doi.org/10.1007/s40010-017-0343-z.

Yapo, N. S., Aw, S., Briton, B. G. H., Drogui, P., Yao, K. B., and Adouby, K. 2022. Removal of fluoride in groundwater by adsorption using hydroxyapatite modified Corbula trigona shell powder. Chemical Engineering Journal Advances 12:100386. https://doi.org/10.1016/j.ceja.2022.100386.

Yousefi, M., Ghoochani, M., and Hossein Mahvi, A. 2018. Health risk assessment to fluoride in drinking water of rural residents living in the Poldasht city, Northwest of Iran. Ecotoxicology and Environmental Safety 148:426–430. https://doi.org/10.1016/j.ecoenv.2017.10.057.

Yuan, J. -H., and Xu, R. -K. 2011. The amelioration effects of low temperature biochar generated from nine crop residues on an acidic Ultisol. Soil Use and Management 27:110–115. https://doi.org/10.1111/j.1475-2743.2010.00317.x.

Zhang, P., Liu, S., Tan, X., Liu, Y., Zeng, G., Yin, Z., Ye, S., and Zeng, Z. 2019. Microwave-assisted chemical modification method for surface regulation of biochar and its application for estrogen removal. Process Safety and Environmental Protection 128:329–341. https://doi.org/10.1016/j.psep.2019.06.009.

Zhang, Q., Xu, P., Qian, H., and Yang, F. 2020. Hydrogeochemistry and fluoride contamination in Jiaokou Irrigation District, Central China: Assessment based on multivariate statistical approach and human health risk. Science of The Total Environment 741:140460. https://doi.org/10.1016/j.scitotenv.2020.140460.

Zhang, X.-C., Gao, H.-J., Yang, T.-Y., Wu, H.-H., Wang, Y.-M., Zhang, Z.-Z., and Wan, X.-C. 2016. Anion Channel Inhibitor NPPB-Inhibited Fluoride Accumulation in Tea Plant (Camellia sinensis) Is Related to the Regulation of Ca2+, CaM and Depolarization of Plasma Membrane Potential. IJMS 17:57. https://doi.org/10.3390/ijms17010057.

Zhao, B., Xu, X., Xu, S., Chen, X., Li, H., and Zeng, F. 2017. Surface characteristics and potential ecological risk evaluation of heavy metals in the bio-char produced by co-pyrolysis from municipal sewage sludge and hazelnut shell with zinc chloride. Bioresource Technology 243:375–383. https://doi.org/10.1016/j.biortech.2017.06.032.

Zou, Q., An, W., Wu, C., Li, W., Fu, A., Xiao, R., Chen, H., and Xue, S. 2018. Red mud-modified biochar reduces soil arsenic availability and changes bacterial composition. Environmental Chemistry Letters 16:615–622. https://doi.org/10.1007/s10311-017-0688-1.